DEPARTMENT OF ELECTRONIC & ELECTRICAL ENGINEERING

University of Strathclyde Engineering

AGEING OF LIQUID INSULATION SYSTEMS INCLUDING NANOPARTICLE SUSPENSIONS

A thesis presented in fulfilment of the requirement for the degree of

Doctor of Philosophy

Guanduo Chen

2016

Department of Electronic and Electrical Engineering

University of Strathclyde

Glasgow, UK

DECLARATION OF AUTHENTICITY AND AUTHOR'S RIGHTS

This thesis is the result of the author's original research. It has been composed by the author and has not been previously submitted for examination which has led to the award of a degree.

Signed:

Date:

ACKNOWLEDGEMENTS

The author wishes to express his sincere gratitude to Dr. Marin J Given for his valuable guidance, support and supervision. Thanking him for giving me this opportunity for this study. In the preparation of this thesis, he helped me through all the stages of the writing of this thesis. Without his patient and illuminating instruction, the completion of this thesis would not have been possible.

Thanks also go to the members of the HVT group and all my friends in University of Strathclyde for their valuable discussions and ideas.

The author is indebted to his parents for their encouragement, help and patience. This will always be remembered with thanks.

LIST OF SYMBOLS

Symbol	Meaning
$\mathbf{E}_{internal}$	Internal energy
H	Enthalpy
k	Chemical reaction rate constant
n_p	Number of molecules of product
n_r	Number of molecules of reactant
p	Pressure
$\mathbf{R}_{gas}$	Universal gas constant
V	Volume
T	Temperature / Time of flight
$\mathbf{E}_a$	Activation energy
A	Pre-exponential factor/ frequency factor in Arrhenius equation
T_{life}	Lifetime of oil samples
θ	Hot spot temperature
μ_a	Mobility of a positive ion A^+
μ_b	Mobility of a negative ion B^-
σ	Conductivity / Debye length
φ	Electrostatic potential
ρ	Charge density / Density
ε_0	Vacuum permittivity

$\boldsymbol{\varepsilon_r}$	Relative permittivity
$\boldsymbol{C_x}$	Number of ions per unit volume at position x in Boltzmann distribution
$\boldsymbol{C_\infty}$	Number of ions per unit volume at infinity in Boltzmann distribution
W	Electrostatic energy of ion
$\boldsymbol{k_B}$	Boltzmann constant
Q or q	Charge of a charge carrier
$\boldsymbol{e}$	Electron charge
$\boldsymbol{z_i}$	Valence of the ion
$\boldsymbol{\varphi_0}$	Electric potential at the electrode surface
$\boldsymbol{C_i}$	Number of ions per unit volume at a potential φ_0
J	Current density / Charge carrier flux
I	Current
V	Voltage
E	Electric field strength
$\boldsymbol{\overline{E}}$	Average electrical field
$\boldsymbol{\omega}$	Angular frequency
$\mathbf{V}_{\boldsymbol{drift}}$	Velocity of a charge carrier
$\boldsymbol{d}$	Distance / gap between two electrodes
TOF	Time of flight

I_{peak}	Peak current
I_{dc}	DC current
$\overline{v}$	Velocity of charge carrier
U	Magnitude of the applied voltage
m	Mass
h	Planck's constant
∅	Work function for electron emission
φ_{image}	Image potential
EHD	Electrohydrodynamic
v_{liquid}	Speed of the liquid flow
$v_{apparent}$	Apparent velocity of charge carriers in a flowing liquid
μ_{ion}	Actual mobility of charge carrier
F_d	Frictional force or Stokes' drag force
η	Dynamic viscosity
r	Radius
v_{ion}	Velocity of a charged particle
N	Charge carriers density
μ	Mobility
D	Diffusion coefficient
C	Concentration of charge carriers
μ'	Mean or expectation of the normal distribution

σ'	Standard deviation for the normal distribution
τ	Relaxation time / time constant for fit
F_V	Van der Waals attractive force between the two particles
F_R	Repulsion force between the two particles
G_{Cell}	Conductance of the test cell
G_c	Conductance of the cylindrical component of the test cell
G_h	Conductance of the hemispherical component of the test cell
γ_c	Geometric parameters for cylindrical section of the test cell
γ_h	Geometric parameters for the hemispherical section of the test cell
γ_{Cell}	Geometric parameters for the test cell
r_i	Radius of the inner conductor of the test cell
r_o	Radius of the outer conductor of the test cell
Q_{nano}	Charge carried by nanoparticle
v_{nano}	Velocity of nanoparticles
μ_{nano}	Mobility of nanoparticles
Q_s	Saturation value of charge carried by nanoparticle

ABSTRACT

Liquid based insulation systems in the Electrical Power Industry will suffer a reduction in their dielectric performance over time because of ageing. Changes due to ageing effects include reduction in breakdown strength and increases in the conductivity of the liquid leading to larger losses in the system. In recent years, adding nanoparticles have been discovered to be a possible way of improving the properties of the liquid insulating material by increasing breakdown strength and thermal conductivity. It is therefore important to investigate whether the presence of nanoparticles can affect the mechanisms or rates at which ageing occurs.

The research presented in this thesis focuses on the influence of ageing on the conductivity of Shell Diala S3 ZX-IG mineral insulation oil and the number and mobility of charge carriers present in the system. The conductivity and mobility have been derived from current transients produced under bipolar conditions at relatively low electric fields (0.3 to 0.7 kV/cm).

Background material on ageing processes and reaction kinetics and possible diagnostic measurements; conductivity, mobility and how they can be measured and the nature properties of nanoparticles are provided.

The techniques used to accelerate the ageing of the insulating liquids are then discussed with some broad estimates of the degree of acceleration. The development of the measurement system used to record the current transients and the interpretation of these transients in terms of mobility and conductivity is then described. Three sets of aged samples have been considered: samples that were thermally aged without nanoparticles (to act as a reference); samples that were thermally aged then had EFH1 magnetite nanoparticles added and samples that had Sigma magnetite nanoparticles added prior to thermal ageing.

Current transients were measured for each sample over a range of voltages and these measurements were repeated over 5 successive days. Changes were observed in the current transients over this 5 day period. Possible reasons for these changes are discussed and the fitting techniques developed to determine the initial values and the equilibrium values of the parameters are described.

For oil samples without nanoparticles added, thermal ageing resulted in a monotonic increase of the conductivity. Changes were also observed in the mobility of charge carriers. The mobility of charge carriers initially decreases in the first 48 hours of ageing and then increases with further ageing time. Increase of the density of charge carriers was observed as a result of thermal ageing.

The samples with EFH1 nanoparticles added post ageing had significantly higher values of conductivity. This again increased monotonically with ageing time. The higher conductivities appear to be due to a higher mobility of charge carriers in the samples with EFH1 nanoparticles added. Again there is no simple relationship between mobility and ageing time.

The study using the Sigma nanoparticles indicates that adding a relatively low concentration of nanoparticles to an unaged sample or to a sample after ageing does not change the conductivity of the liquid and the mobility of charge carriers significantly. However if the same concentration is added prior to thermal ageing significant changes in both the conductivity and the mobility of charge carriers is observed. This suggests that the rate of ageing or the ageing mechanism is affected by the presence of the nanoparticles.

Although the addition of nanoparticles provides an approach of improving the dielectric properties of insulating oil, special attention needs to be paid on the drawbacks caused by the presence of nanoparticles. Using the insulating oil modified by nanoparticles can lead to an increase of the energy losses. In addition, the thermal ageing rate of the insulating oil could also be increased by the presence of nanoparticles. Further investigation of the effect of nanoparticles on ageing is required before the nanofluid can be used as alternative of the traditional insulating oil.

Key words: Aging, liquid insulating material, nanoparticles, time-of-flight measurement, conductivity, mobility.

CONTENTS

1. INTRODUCTION

With the development of modern economy, in many parts of the world the demand for electricity is increasing. The increased emphasis on renewable energy requires the long-distance transmission of electrical energy. The required improvement of high voltage technology puts forward higher requirements for the performance of insulation materials. The study of new insulation materials is attracting more and more attention.

A transformer is one of the most important devices in the power system; if it fails, it will lead to local breakdown of power grid, bringing huge economic losses. In the world, the oil-paper insulation structure is widely used in many large power transmission and distribution transformers. The deterioration of insulation system due to ageing of an insulation material is considered as one of the main reasons for transformer failure. During the actual operation of transformer, due to many factors such as electric stress, heating, moisture, oxygen, ageing will occur to the insulating paper and transformer oil. The mechanism of ageing of an insulating material typically involves many complex physical and chemical processes. Both the physical and chemical characteristics of the insulating oil in transformers deteriorates with the ageing and the impacts on the electrical characteristics had been analyzed in earlier studies [**1**] [**2**] [**3**]. The study of the ageing of insulating material is required to accurately determining the degree of ageing of insulation system inside the transformer and to assess the possibility of faults. Also, the study of ageing of insulating material is helpful to monitor the operating conditions of transformer and correctly predict its remaining life.

For the investigation of the insulating property of liquid insulating material, the conductivity of the liquid and the mobility of charge carriers in the liquid are two parameters of significance. Time of flight measurement method on liquid insulating materials has been established and proved to be an effective approach to measure the liquid's conductivity and the mobility of charge carriers in the liquid [**4**].

In recent years, a new kind of nanofluid insulating materials has been manufactured by adding different kinds of nanoparticles into the general insulating oil. This new kind of insulating fluid is regarded as a substitute of the traditional insulating oil as they exhibit better dielectric properties. It has been suggested that the breakdown strength of insulating liquids under both AC and impulse conditions can be significantly improved by adding nanoparticles [**5**]. Reduction in the breakdown behaviour of the insulating oil which occurs as a result of contamination with particles or with water, could also in part be reversed by such nanoparticles. In addition, the performance of insulating oil with nanoparticles added after accelerated ageing were also investigated in an earlier study [**6**] and it was found that the nanofluid still showed a higher breakdown strength than the general insulating liquid without nanoparticles added. However, the influence of presence of nanoparticles on the ageing of mineral oil and its impact on conductivity and the mobility of charge carriers is still not well understood. Therefore it is interesting to investigate the ageing effects on the insulating material with nanoparticles suspension through the Time of flight measurement method.

1.1. THESIS STRUCTURE

The subsequent sections of this thesis are organized as follows:

Chapter 2 covers the background of ageing of liquid insulation looking at some basic chemical kinetics and the Arrhenius equation. Two possible kinds of ageing methods: electrical ageing and chemical ageing are then described with some diagnostic mechanisms used for determining the ageing degree of insulating oil.

Chapter 3 describes the basis of the measurement methods which were used in this project. Two parameters: the conductivity of a liquid and the mobility of charge carriers are introduced along with the concept of time of flight measurement. Simple modeling of the charge carrier motion expected during the measurement will be described and discussed.

Chapter 4 reviews the reported effects of adding nanoparticles to an insulating liquid. The effects of nanoparticles on breakdown voltage and conductivity will be discussed.

Chapter 5 describes the ageing methods used in this project. Ultraviolet–visible spectroscopy results indicating the changes observed in the oil as a method of characterizing the ageing will be presented. The expected acceleration of the ageing under the conditions used is discussed.

Chapter 6 describes the development of the time-of flight measurement system in detail. The problems encountered in the development of the measurement system and the solutions developed are discussed.

In Chapter 7~9, results on the conductivity and the mobility of charge carriers in three different classes of sample that have undergone thermal ageing are reported. The sample types are:

1. Unaged and aged oil samples **without** nanoparticles in Chapter7
2. Unaged and aged oil samples with EFH1 nanoparticles added **post** ageing in Chapter 8
3. Unaged and aged oil samples with Sigma nanoparticles added **before** ageing in Chapter 9

The preparation of each type of sample is described at the beginning of the relevant chapter. The behaviours of the current transients and the conductivity and mobility parameters are reported. Comparisons between sample types 1 and 2 are discussed in section 8.7. Similar comparison between sample types 1 and 3 is discussed in section 9.7.

Chapter 10 summarizes the findings and key achievements of this research project and suggests future work which is required to determine the impact of nanoparticles on the ageing of insulating liquids.

2. AGEING

2.1. INTRODUCTION

This chapter includes some previous researches and background knowledge about ageing of insulating materials which refer to this project. The significance of ageing of insulation systems has been described in the introduction. This chapter will give a more detailed description of the processes involved in the ageing of insulation. Some basic methods relating to chemical reaction will be introduced. The Arrhenius equation which is commonly used for analysis of the relation between temperature and the chemical reaction rate, will be reviewed. Several diagnostic measurement methods of ageing of insulating materials will be introduced.

2.2. CHEMICAL KINETICS AND REACTION RATES

The ageing process is essentially a chemical reaction. Therefore, a brief review of some basic related chemical knowledge is necessary. Chemical kinetics deals with the rates of chemical reactions and factors that influence these rates. It is concerned with the quantitative determination of rate of chemical reactions.

2.2.1. CHEMICAL REACTION RATE

The rate of different chemical reactions varies widely. For example, the formation of coal will take hundreds or even thousands of years to complete, while some reactions such as a combustion reaction or a neutralization reaction take place almost instantaneously. Chemical reaction rate represents the velocity of a chemical reaction. It is usually defined as the change, in terms of amount of any one of the product formed or any one of the reactants consumed per unit time, which can be defined as [**7**]:

$$\text{Rate of reaction} = -\frac{dn_r}{d_t}, \text{Rate of reaction} = \frac{dn_p}{dt} \qquad \textbf{2-1}$$

Where, n_r is number of molecules of reactant and n_p is the number of molecules of product. There are several environmental factors (temperature, pressure, catalysts, etc.) that can influence the chemical reaction rate. However, the most important determining factor is the chemical characteristics of the reactants and products. If the

reactants molecules have relatively strong chemical bonds, it usually means the chemical reaction will require more energy or take a longer time. In other word, the chemical reaction rate will be relatively low.

In thermodynamics, there are two significant parameters which are usually used to describe the state of a physical system [**8**]:

- **Enthalpy:** Enthalpy is a measure of the total energy of a thermodynamic system which can be simply expressed by:

$$\mathrm{H} = \mathrm{E}_{internal} + \mathrm{p}V \qquad \textbf{2-2}$$

  Where H is the enthalpy of a system, $\mathrm{E}_{internal}$ is the internal energy, p is the pressure of the system with a unit of Pascal (Pa) and V is the volume of the system. It is a state function with a unit of joules. Note that, the enthalpy of a system cannot be measured directly therefore change of enthalpy is more widely used to represent the energy change of an isolated system. During the thermal ageing process of a liquid insulation system for instance, the enthalpy of the system will increase since increasing the temperature leads to an increase of the internal energy.

- **Entropy:** In a thermodynamic system, all differences in environmental factors such as pressure, temperature and density tend to zero over time. The entropy of a system can be defined by the number of microscopic conditions possible within an externally defined state. It also defines the thermal energy in a system that is unavailable to perform mechanical work. For any isolated system, entropy can only increase and never decrease. The system will tend to reach a thermodynamic equilibrium where the system has its maximum entropy. The concept of entropy provides a reasonable explanation of why some processes in reality are irreversible and why endothermic reactions can take place. For example in this project, the ageing of the liquid insulation cannot be a reversible reaction since the entropy of the system will keep increasing with time.

2.2.2. ACTIVATION ENERGY

Collision between the reactant molecules is the fundamental precondition which leads to a chemical reaction taken place. However, not all collisions will result in a reaction, only when the reactant molecules collide with enough energy to break the chemical bonds between the atoms in the molecules and allow recombination to form new product molecules will a reaction occur. The minimum energy necessary for a chemical reaction is called the activation energy [**8**]. The activation energy represents the energy barrier for transformation between reactants and products. In other words, the activation energy describes how difficult it is for a reaction to take place. If the reactant molecules do not have enough energy to overcome the energy barrier, then the reaction will never happen. Reactant molecules with enough energy to overcome the energy barrier are normally known as activated molecules. For a specific reaction, the reaction rate will depend on the total quantity of activation molecules per unit volume. If there are more activation molecules in a unit volume, then the reaction rate will be larger. Activation energy also plays a role in the Arrhenius equation which will be introduced in section 2.3.1.

2.3. AGEING IN LIQUID

It is known that the insulating oil is commonly used with paper in many transformers in the electric power transfer system. The cellulose paper-mineral oil combined insulation system is one of the most widely used insulating systems in transmission and distribution transformers. This kind of insulating system is usually expected to keep an acceptable dielectric insulating property for 40 years [**9**]. However, the degradation of the insulating oil which occurs during service is one of the major concerns for a transformer. The rate of degradation depends on many factors such as temperature, water content, characteristics of the materials and the availability of oxygen. According to the study of H. William and P.E. Bartley who investigated the failures which occurred in transformers rated (25 MVA or above) since 1997 till 2001, the main reason that leads to a transformer failure is the breakdown of the insulation system [**10**] which might be a result of the degradation of insulating system due to ageing effects.

2.3.1. INFLUENCE OF TEMPERATURE: ARRHENIUS EQUATION

For the effect of temperature on chemical reaction rate, the Netherlands' chemist Van't Hoff developed the Van't Hoff's equation based on experimental results in 1884. In 1889, the Swedish chemist Arrhenius further analyzed the relationship between the reaction rate and temperature proposed by Van't Hoff, and explained this equation's principle relative to the concept of activation energy and the existence of energy barrier in the reaction, and proposed the "Arrhenius equation" [**11**]. The equation is used to express the relation between temperature and chemical reaction rate in a chemical reaction.

The general expression of Arrhenius equation is:

$$\mathrm{k} = \mathrm{A} \cdot e^{\left(\frac{-E_a}{R_{gas}T}\right)} \qquad \textbf{2-3}$$

Where, k is the rate constant, R_{gas} is universal gas constant which is equal to 8.314J/K.mol, T is thermodynamic temperature in kelvin, E_a is the activation energy in joules, A is a pre-exponential factor (also known as frequency factor), which generally depends on intermolecular impact frequency.

The Arrhenius equation gives a generalized rule: For the majority of general chemical reactions at room temperature, the chemical reaction rate will double if the temperature is increased by 10℃. This approach is generally valid to many situations for small change in temperature as in this case, both A and E_a do not significantly change. If the change in temperature is large, changes are possible in the values of both A and E_a and the reaction rate will deviate from the prediction.

The logarithmic form of the Arrhenius equation is written as:

$$\ln k = \ln A - \frac{E_a}{R_{gas}T} \qquad \textbf{2-4}$$

From the logarithmic form, the rate of change of $\ln k$ associated with $\frac{1}{T}$ is proportional to the activation energy E_a. For chemical reactions performed at different temperatures, if the activation energy of a chemical reaction is higher, then its reaction rate will rise quickly when the temperature rises as compared to a chemical reaction with lower activation energy. In other word, the chemical reaction is more sensitive to changes in temperature as the activation energy increases.

As in the logarithmic expression of Arrhenius equation, $\ln k$ has a linear relation with the reciprocal of the temperature. A plot of $\ln k$ vs. $\frac{1}{T}$ will be a straight line, and the slope of the straight line should be equal to the value of $-\frac{E_a}{R_{gas}}$ with an intercept of lnA.

Assuming A is constant, differentiation of equation 2-4 with respect to T gives:

$$\frac{d(lnk)}{dT} = \frac{E_a}{R_{gas}} T^{-2} \qquad \textbf{2-5}$$

A relationship between the reaction rate k_1 at temperature T_1 and reaction rate k_2 at temperature T_2 can be determined by integrating equation 2-5 over the temperature range of T_1 to T_2:

$$\ln\left(\frac{k_2}{k_1}\right) = \frac{E_a}{R_{gas}}\left(\frac{1}{T_1} - \frac{1}{T_2}\right) \qquad \textbf{2-6}$$

This is valid if the variation of temperature is in a small range, where the value of E_a can be approximately considered as constant.

Assuming that for a known oil sample, the time spent at a particular temperature to reach a specified degradation level was known as the oil sample's 'lifetime'. It is expected that this 'lifetime' should be inversely proportional to the chemical reaction rate of the ageing process. The larger the reaction rate is, the shorter lifetime the oil sample will have. This allows the Arrhenius relationship to be used to provide a way of estimating the changes in lifetime associated with temperature.

The earliest study of life estimation can be traced back to 1930 [**12**] when an empirical expression was given to show the relation between the lifetime of insulation and the thermal stresses. In 1948, Dakin produced a new expression for lifetime estimation of thermal ageing based on the Arrhenius equation [**13**]. In 1990, Cygan and Laghari suggested combined models for thermal and electrical ageing of insulation [**12**].

This Arrhenius law based lifetime estimation assumes that the values of *A*, E_a and R_{gas} are constant. In this case, Arrhenius equation 2-3 can be rewritten as:

$$\ln T_{life} = A' + B' \frac{1}{T} \qquad \textbf{2-7}$$

Where, T_{life} represent the 'lifetime' of the oil sample, A' and B' are constant parameters which depends on the reacting materials and the reaction conditions. Equation 2-7 indicates that if the ageing of an oil sample follows the Arrhenius behaviours, there will be a linear relationship between the logarithm of the 'lifetime' of the sample and the temperature of thermal ageing which is suggested by [**2**] [**14**]. This approach provides a way to estimate the 'lifetime' of the oil sample at a specified temperature. The expected acceleration of ageing in this project will be introduced in section 5.5.

2.3.2. ELECTRICAL AGEING

Electrical ageing is one of the most important causes of the degradation of insulation system. Partial discharge is the main cause of electrical ageing. Generally, partial discharge means discharge occurring at some part in an insulation system under the effect of electric field without voltage collapse or complete breakdown of the insulation system [**15**].

Taking the oil-paper insulation system used in many transformers for instance, partial discharge may occur to the insulating paper inside the transformer under the applied electric field, which is one of the main factors affecting the ageing of transformer's insulation system. During operation, in some area of the solid insulator, electric field strength may be significantly higher, reaching the breakdown field strength of the insulation, causing a discharge in a local area. Partial discharge generally occurs to regions where the insulation is weak for example in air filled voids and other defects, or where the electric field strength is high such as wiring connection or metal protrusions or inclusions. The degree of electrical ageing of a transformer oil-paper insulation structure depends on the accumulation of damage due to partial discharges. Partial discharge usually depends on the electric field distribution and some environmental parameters such as temperature, moisture, etc. Free electrons produced by the partial discharge can be accelerated by the electric field and when they collide with molecules of the insulation material, they may have sufficient energy to break bonds between molecules and within molecules. Therefore,

the degradation of insulation material can occur. If repeated partial discharges occur in a region the accumulation of damage increase the probability of a breakdown occurring under over voltage conditions. If the partial discharge activity occurs for long periods, the accumulated damage may result in failure under normal operating voltages. Therefore, partial discharge is a slow process for damage to the insulation equipment. In addition, partial discharge is also often accompanied by temperature rise of insulating material which further increases the degree of ageing of insulation material [**16**].

2.3.3. CHEMICAL AGEING

Chemical ageing mainly means the oxidation reaction of molecules in the insulating material under the influence of a series of environmental factors such as heat, light, moisture, oxygen and catalysts to form a new product. The insulating properties of insulator will degrade during this process. This oxidation reaction is generally irreversible. Common transformer oils such as mineral oil are manufactured from crude oil by distillation relating to the different boiling points of components. Insulating mineral oil commonly consists of alkanes, cycloalkanes, aromatic hydrocarbons and other hydrocarbons [**17**]. During the chemical aging process, the molecules in the insulating oil will be oxidized to possible product such as: aldehydes, alcohols, ketones, and various acidic compounds.

Usually, at room temperature, the chemical ageing of insulating oil is a very slow process. Its insulating properties will therefore not change significantly over time. However, as previously described, during the operation of many transformers, especially for large high-voltage transformers, the temperature near the core is generally much higher than the ambient. Therefore, the chemical ageing rate of insulation material will be greatly accelerated in the area close to the windings. According to IEEE guide C57.91-2011 [**18**], when 100MVA transformer runs over the rated load of nameplate, its hotspot temperature can reach 120℃-130℃. Therefore, in this project, the thermal ageing temperature is selected as 120℃ relating to the lower temperature in the range given by [**18**].

The ageing process can be considered as a series of chemical reactions and the reaction rate can be increased in the presence of a catalyst which decreases the effective activation energy or increases the probability of collision. Previous studies [**19**] indicate that copper can be used as the catalyst during the ageing of insulating oil as it exhibits an obvious effect on accelerating the ageing process. Copper was selected in [**19**] as it was a metal likely to be present in transformers due to its use as a conductor in transformer windings.

2.4. DIAGNOSTIC MEASUREMENTS:

The dielectric performance of the insulating oil is of great significance in a dielectric insulation system. Many previous researches of the insulating oil especially relating to the high voltage transformers have been made, attempting to find a reliable way to estimate, indicate and monitor the ageing state of the transformer oil. In fact lifetime is not the time to electrical failure but rather as the time when a property of the insulating system reaches a specified value such as: the breakdown voltage, the acid number, etc. Different diagnostic techniques for the insulation system in aged transformers have been reviewed by previous researchers [**20**] [**21**] [**22**]. Different kinds of diagnostic techniques have been established. Typical chemical and physical diagnostic techniques on samples of liquid insulation include：Dielectric properties, high voltage breakdown test, water content test, ultra-violet/infra-red spectroscopy and dissolved gas analysis. However, although many diagnostic methods have been investigated and discussed, no single technique has been shown to provide a consistent indicator to accurately predict the time to a failure of an insulating system. Therefore, combinations of the results from different diagnostic methods are used to determine any possible problems in the insulating system [**20**].

Since the most common liquid insulation system is the oil-paper insulation system in the transformer, in this section, some common methods for determining and testing the aging of oil-paper insulation system in the transformer will be briefly introduced.

2.4.1. UV/VIS/IR SPECTROSCOPY

Ultraviolet/Visible/Infrared (UV/VIS/IR) spectroscopy is a common test method for assessing the aging of insulating oil. A series of papers relating to the effect of ageing on liquid insulation based on (UV/VIS/IR) spectroscopy has been published by I. L. Hosier [**23**] [**24**] [**25**]. For most insulating oils, the ageing often makes the colour of insulating oil liquid darker. The light transmission of insulating oil as a function of wavelength can be obtained by measuring and analyzing the UV/VIS spectra of insulating oil, therefore the darkening can be quantified. The degree of ageing of insulating oil can be determined conveniently and the lifetime of insulating oil can be estimated approximately. In addition, the presence of particular molecular bonds in the insulating oil can be determined through infrared spectroscopy. Changes in the spectra can be related to changes in the bonds present and therefore changes in molecular structure. This can allow the approximate degree of oxidation of the insulating oil to be determined. However, due to the wide range of insulating oils, different initial distributions of molecules and therefore bonds will be present in different oils. Even for the same insulating oil differences will occur due to manufacture. Therefore, the relative degree of ageing of two samples of insulating oil cannot be accurately determined by the use of these two optical methods alone. However it has been suggested [**19**]**,** that the degree of ageing in insulating oil can be estimated using the wavelength when the transmittance is equal to 50%.

2.4.2. DIELECTRIC SPECTROSCOPY

Measurement of the dielectric spectrum of an insulation material is also a common method of assessing the insulator ageing. This method is to determine the degree of ageing of the insulating oil by measuring a series of dielectric parameters (dielectric loss factor $\tan\delta$, relative permittivity and resistance etc.) within a certain range of frequency or time. These dielectric parameters can be changed due to the ageing process. The dielectric loss of a liquid insulator, for instance, depends on its complex permittivity. Ageing will lead to changes in chemical composition of a liquid insulator and consequently affects its complex permittivity; therefore, the degree of

ageing of a liquid insulator can be evaluated by measuring its dielectric loss [**1**] [**26**] [**27**].

2.4.3. BREAKDOWN VOLTAGE TEST

AC or pulse breakdown measurement is also a common way of investigating the ageing degradation of insulating oils which has been used in many studies [**1**] [**28**] [**29**] [**30**]. The popularity of this approach is that the breakdown voltage is a key parameter which exhibits the insulating performance of insulating oil during operation. Generally, aged insulating oil is expected to have a lower breakdown voltage compared with the unaged oil. However, the breakdown measurement result can be influenced by the water content in the oil sample. Unaged insulating oil may have a lower breakdown voltage than aged insulating oil due to the reduction of water content that occurs during the thermal ageing process. Therefore as mentioned above, breakdown tests cannot accurately estimate the ageing degree of insulating oil.

2.4.4. OTHER METHODS

Furanic derivatives analysis, dissolved gas analysis and acid value analysis will be briefly reviewed in this section as they are suggested to be effective method for investigating the ageing of the oil-paper insulating system in transformer. Note that, although these methods could reasonably estimate the degradation of insulating oil in transformers due to ageing effects, some key evidence parameters used in this approach relate to the degradation of cellulose in the paper that is used together with insulating oil as paper-oil insulating structures. Therefore, these approaches may not be suitable for investigating the ageing behaviours of insulating oil in isolation.

2.4.4.1. Furanic derivatives analysis

Although Furanic derivative analysis is commonly used to assess ageing in paper-oil insulation studies [**31**] [**32**] [**33**] [**34**] [**35**], the Furanic gases such as Furfural (C_4H_3OCHO), come from the decomposition of the cellulose chains in the insulation paper. Therefore this approach is not relevant to the ageing of a liquid.

2.4.4.2. Dissolved gas analysis

During the degradation of the insulation system of a transformer, different gases, such as hydrogen (H_2), methane (CH_4), ethane (C_2H_6) and ethylene (C_2H_4) can also be generated and dissolved into the transformer oil. Therefore, investigation of the concentration of key gases gives information on both the types of fault in the transformer and its severity.

The three main causes of fault gas generation are:

- Corona or partial discharge
- Thermal heating
- Arcing

Previous study [**36**] indicates that the hydrogen gas is expected to be generated due to the corona occurring in the oil and cellulose. Hydrocarbon vapours such as methane, ethylene and ethane are likely generated due to the overheating of transformer oil. Acetylene can be produced with the presence of arc at low temperature. Carbon dioxide (CO_2) and carbon monoxide (CO) can be generated as well due to the thermal decomposition of cellulose in the paper in a transformer's insulation system. According to the IEEE guide C57.104 [**37**], the ratio of CO_2/CO can be used as an effective indicator that shows the thermal decomposition of cellulose.

2.4.4.3. Acid value analysis

As mentioned earlier, in the chemical ageing process of insulating oil, the products may include some acids such as oleic acid, and these acidic components may reduce the oil insulating properties. These acidic substances typically include organic acids, esters, phenolic compounds etc. Some acidic substances may also further react with alcohols to form viscous substances with higher molecular weights so that the viscosity of transformer oil may be changed. Therefore, measurement of acid value is a conventional test method for transformer oil. The common measurement method for acid value is to use ethanol to extract acidic substances from the oil and then use potassium hydroxide (KOH) solution for titration to determine the content of acidic substances in the sample oil [**38**]. The acid value of transformer oil can therefore represent the degree of contamination and degradation of transformer oil.

2.5. SUMMARY

In this chapter, some basic concepts relating to the chemical kinetics have been reviewed, including: chemical reaction rate, enthalpy, entropy and activation energy. Arrhenius equation in different forms relative to the estimation of lifetime of insulating oil were introduced and discussed. Relationship between the chemical reaction rate and the temperature was shown using Arrhenius equation.

Both the electrical ageing and chemical ageing of the insulating materials associated with partial discharge and oxidation reaction was discussed, respectively. The presence of copper as a catalyst during the thermal ageing process could increase the chemical reaction rate which can enhance the ageing degree of insulating oil.

Diagnostic measurement methods using UV/VIS/IR spectroscopy, dielectric spectroscopy and breakdown measurement were reviewed since they could provide useful information about the ageing of liquid insulation.

Furanic derivatives analysis, dissolved gas analysis and acid value analysis were also briefly reviewed. Although these three techniques do not investigate the parameters only caused by the ageing of oil, these approaches are commonly adopted to predict the lifetime of paper-oil insulating system in transformers. In this project, UV/VIS spectroscopy was used to quantify the changing of the oil colour due to thermal ageing. Furanic derivatives analysis, dissolved gas analysis and acid values analysis were not adopted as these methods are strongly related to the degradation of the cellulose in the insulating paper commonly used together with insulating oil rather than the degradation simply caused by the ageing of the insulating oil.

3. CONDUCTIVITY AND MOBILITY MEASUREMENTS

3.1. INTRODUCTION

This chapter will introduce the methods used to measure the conductivity of highly insulating liquids and the mobility of the charge carriers it contains. Related background knowledge will be reviewed. The theoretical basis for the measurement of insulating oil conductivity and its charge carrier mobility, the significant parameters, as well as physical quantities that can be directly measured, such as the d.c. current I_{dc}, the peak current I_{peak} and time of flight will be described in this section. In addition, the derivation and calculation method of charge carriers' mobility will be introduced and discussed.

3.2. CONDUCTIVITY AND ITS MEASUREMENT:

3.2.1. ABOUT CONDUCTIVITY

The conductivity is one of the crucial parameters used to describe the electrical characteristic of an insulating liquid. The different methods used to measure liquid conductivity over 50 years was reviewed in the 1970s by M. Hilaire [**39**].

Generally, the study of the conductivity of insulating oil relates to the purity, the degree of ionization and the concentration of conductive ions in the insulating liquid. The study of conductivity contributes to the selection and improvement of liquid insulating materials. In addition, measurement of conductivity of insulating oil could provide a monitoring approach for the ageing of liquid insulation during the service life which is helpful to avoid apparatus failure and reduce risks to the insulating system [**40**].

Electric conduction of electrolyte solution

Many of the ideas used when discussing conduction in insulating liquids come from the principles developed to explain the behaviour of more conductive electrolytic solutions. Electric conduction of an electrolyte solution depends on the migration of ions in the liquid under the influence of the electric field and their charge. It is assumed that the liquid is electrically neutral with equal quantities of total charge carried by the positive and negative ions. In the absence of an electric field, the ions in the electrolyte solution will have a random thermal motion. Within unit time, the

total displacement of an ion will be approximately zero. When an external electric field is applied the forces acting on the ions add a drift velocity to their random motion. The direction of the drift velocity will depend on the polarity of the ions. This net movement of charge leads to a current. For the current to be maintained in the electrolyte charge transfer between the electrodes and the electrolyte must also occur. Electrons must be transferred from the negative electrode or cathode into the electrolyte by either creating new negative ions or neutralizing positive ions. At the positive electrode electrons must be transferred from the electrolyte to the anode through neutralization of negative ions or the creation of new positive ions. Therefore, when the electrolyte solution conducts, the directional migration of ions in the liquid and the electrochemical reaction in the electrode must occur at the same time, both of which are indispensable.

Conductive situation of dielectric fluid between parallel metal plate electrodes

After a step voltage is applied to a dielectric fluid between plain parallel conducting electrodes, it is seen that the current flowing through the liquid reduces slowly with the time of measurement. Generally, it will take a time of the order of hundreds of minutes to obtain a quasi-static current.

There are two major processes causing a current to flow in the liquid:

1. The first is that the liquid will contain ions which are affected by the electric field and move, transporting charge through the liquid. Therefore, the conductivity of the insulating liquid is related to the ionization of molecules in the liquid. The following chemical equation expresses the process where a neutral molecule is resolved into two ions in a thermodynamic equilibrium.

$$\mathrm{AB} = A^{+} + B^{-} \qquad \textbf{3-1}$$

   Then, the resulting conductivity caused by the molecule resolved into ions can be expressed by the following equation:

$$\sigma' = \mu_a q_a + \mu_b q_b \qquad \textbf{3-2}$$

   Where σ' is the conductivity; μ_a, μ_b represents the mobility of A^{+} and B^{-}, respectively and q_a, q_b represents the charge concentration of A^{+} and B^{-},

respectively. These ions, which will always be present in the liquid, are sometimes referred to as residual ions and arise due to dissociation within the liquid and may also be due to impurities. This current associated with these ions is usually called the residual current [**41**].

2. The second process is due to new ions generated at the electrodes. New ions can be injected into the liquid from the metal plate, or neutral entities close to the electrode can lose or gain electrons. These new ions then move towards the electrode with opposite polarity, transferring charge across the liquid. This kind of current is generally called the injection current [**42**].

These two mechanisms can occur at the same time and it can be difficult to separate their effects on the measured currents. With long term measurements some of the residual ions will be swept out of the system and the current will decrease. However this lower value of current is not purely an injection current as new residual ions will be generated by dissociation and ionization in the bulk of the liquid.

When the electric field across the liquid is increased, the resulting d.c. current will increase due to a higher drift velocity of the ions. In addition the injection of charge at the electrodes and dissociation can be enhanced by the increase in the applied electric field leading an increase in the total number of charge carriers in the bulk of the liquid which could also increase the current flow through the liquid.

Electric double layer and Poisson-Boltzmann equation

When a solid electrode is in contact with a liquid insulator, for example, a metal electrode in contact with the insulating oil, a double layer structure can be formed at the interfacial region due to the change of physicochemical variables such as electrical potential and electrolyte concentration between the two phases [**43**]. This double layer was first found in 1853 by Hermann von Helmholtz. The situation at interfacial region between a negative charged metal electrode and insulating oil can be represented by Figure 3-2 [**44**]. A layer of positive ions will be strongly adsorbed to the surface of the metal to balance the negative electron cloud associated with the surface of the metal. This layer is commonly known as the Helmholtz inner layer. Beyond the inner layer, negatively charged particles are present as a result of the positive charge in the Helmholtz inner layer. This region is known as the Helmholtz

outer layer. Moving further away from the interface, beyond the Helmholtz double layer, there is a diffuse region which is usually known as the Gouy-Chapman layer which was observed by Louis Georges Gouy in 1900's [**45**]. The length of the Gouy-Chapman layer depends on the concentration of charge carriers in the bulk of the liquid where equilibrium of the potential difference between the electrode and the dielectric liquid can be obtained. The change of potential of negative ions in the bulk of liquid associated with the distance away from the interface is illustrated in Figure 3-2. The origin here represents the position of the Helmholtz inner layer.

The number of positive and negative charges per volume should be equal at a distance relatively far away from the electrodes since the system has to be electrically neutral. However in the region close to the surface, because positive charges tend to balance the surface negative charges in the metal, some positive ions in the liquid will be attracted and adsorbed at the electrode surface which will lead to an increase of the positive charge density. For example, in the situation of a negative electrode immersed in a solution, positive ions in the bulk of liquid are known as Counter-ions and negative ions are Co-ions. Near the electrode surface, the concentration of counter-ions would be higher than that of the co-ions.

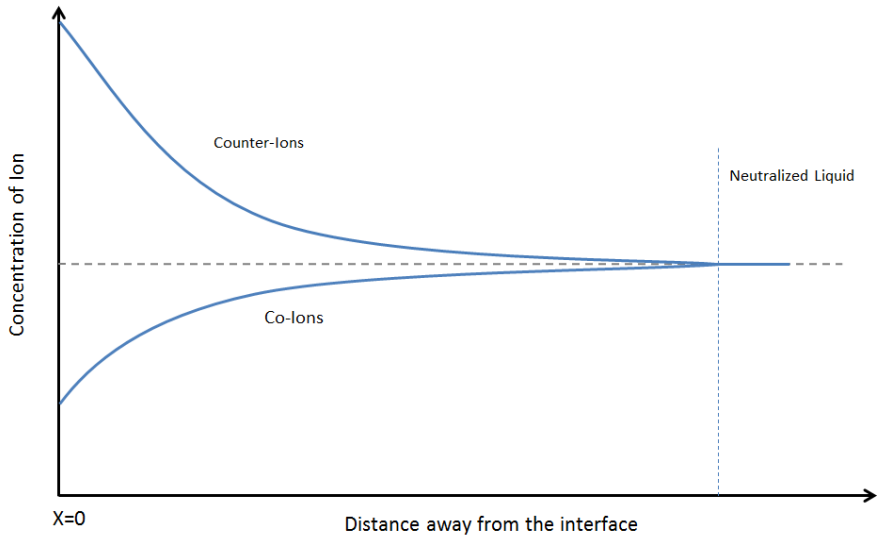

Figure 3-1 Concentration of Ions close to the electrode surface

Figure 3-1 plots the number of ions of these two types per unit volume, ion concentration, with the distance away from the electrode surface. If a certain potential value can be assigned to the electrode surface, then, the effective surface

potential as a function of the distance away from the surface can be calculated. Again, with the assumption that the liquid is electrically neutral, at the position that is sufficiently far from the surface, the potential should be zero.

A characteristic parameter known as the Debye length can be defined by analyzing this double layer using the Poisson-Boltzmann equation.

The Poisson-Boltzmann equation relates the variation of potential from the Poisson equation with the distribution of ions which are assumed to follow the Boltzmann Distribution.

The left side part of the Poisson-Boltzmann equation is based on Poisson equation (equation 3-3), which describes the relationship between the electric potential of ions and the charge local density.

$$\nabla^2\varphi = -\frac{\rho}{\varepsilon_0} \qquad \textbf{3-3}$$

Where: $\nabla^2\varphi$ is the second derivative of the electrostatic potential; ρ is the charge density in unit of C/m^3 and ε_0 is the permittivity of vacuum.

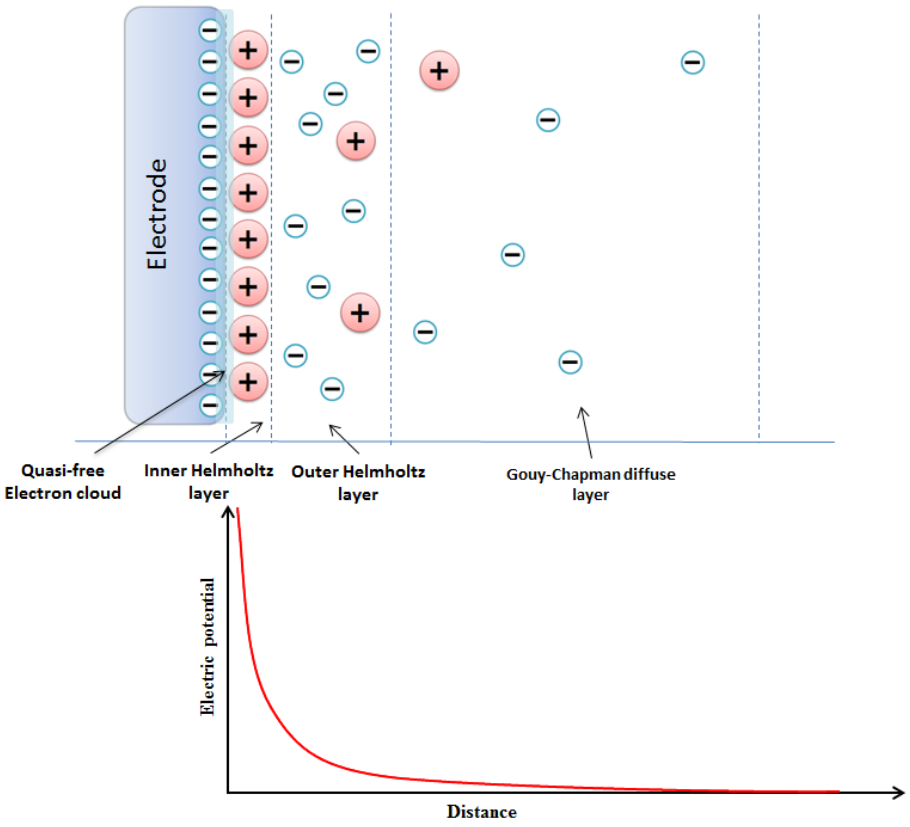

Figure 3-2 Schematic model and the potential distribution of the electric double layer

For a double layer in an electrically neutral liquid, the Poisson equation can be simplified by considering the geometry to be one dimensional and it can be then written as:

$$\frac{d^2\varphi}{d\,x} = -\frac{\rho(x)}{\varepsilon_0 \cdot \varepsilon_r} \qquad \textbf{3-4}$$

Where ε_r is the relative permittivity which depends on the material (the liquid which holds the electric field). The charge density $\rho(x)$ now varies only as a function of the distance away from the electrode x now is one-dimensional. The potential resulting from the charge distribution is assigned as:

1. The potential at the surface of the electrode is an assigned surface potential $\varphi(0) = \varphi_0$
2. The potential at an infinite or sufficiently far away distance from the electrode surface is equal to zero $\varphi(\infty) = 0$

The right side part of the Poisson-Boltzmann equation is based on Boltzmann statistics. It is assumed that the ions in the solution obey the Boltzmann distribution that gives the probability that a system will be in a certain state as a function of that state's energy and the temperature of the system [**46**]**.** The Boltzmann distribution provides a way of calculating the probability that an ion will have certain energy which allows the local charge density of the double layer to be calculated. The ion concentration at a particular location can be expressed as:

$$C_x = C_\infty \exp\left(\frac{-W}{k_B T}\right) \qquad \textbf{3-5}$$

Where C_x is the number of ions per unit volume at position x, C_∞ is the number of ions per unit volume at infinity, the average concentration of ions in the solution. W is the electrostatic energy of ions in joule which equal to the work required to move this ion from infinity to location x. k_B is the Boltzmann constant and T is the temperature in kelvin. The term $\exp\left(\frac{-W}{k_B T}\right)$ represents the probability of an ion to have energy W following the Boltzmann distribution.

With the assumption that the electrostatic potential at infinite distance from the electrode φ_∞ is equal to zero, the relationship between a charged particle's electric potential φ_x and its electric energy could be written as:

$$\varphi_x = \frac{W}{Q} \qquad \textbf{3-6}$$

Where the Q is the charge of the particle and W is the work required to move this particle from infinity to its location, x.

Assuming the electric potential at the electrode surface is φ_0, the concentration of a particular type of ion at the electrode surface can be expressed as:

$$C_i = C_\infty \exp\left(\frac{-z_i e \varphi_0}{k_B T}\right) \qquad \textbf{3-7}$$

Where C_i is the number of ions per unit volume at a potential φ_0, z_i is the valence of the ion and e is the charge of an electron.

Equation 3-7 describes the relationship between the local concentration of ions and the relative electric potential. For each population of ions, the charge density can be calculated based on the total number of ions per unit volume.

$$\rho = \mathrm{z}_i \, \mathrm{e} \, \mathrm{C}_i \qquad \textbf{3-8}$$

Therefore, the charge density can be expressed as:

$$\rho = \mathrm{z}_i \, \mathrm{e} \, \mathrm{C}_i = \mathrm{z}_i e C_\infty exp\left(\frac{-\mathrm{z}_i e \varphi_0}{k_B T}\right) \qquad \textbf{3-9}$$

Since there can be multiple populations of ions in the bulk of liquid:

$$\rho = \sum_i \mathrm{z}_i \, \mathrm{e} \, \mathrm{C}_i = \sum_i z_i e C_\infty exp\left(\frac{-z_i e \varphi_0}{k_B T}\right) \qquad \textbf{3-10}$$

Combined Equation 3-4 and Equation 3-10 leads to the Poisson-Boltzmann equation 3-11.

$$\frac{d^2\varphi}{d\,x} = -\frac{\rho(x)}{\varepsilon_0 \cdot \varepsilon_r} = -\frac{1}{\varepsilon_0 \cdot \varepsilon_r} \sum_i z_i e C_\infty exp\left(\frac{-z_i e \varphi_0}{k_B T}\right) \qquad \textbf{3-11}$$

Assuming that the surface potential is lower that the thermal energy:

$$z_i e \varphi_0 \ll k_B T$$

Equation 3-11 can be expanded into a Taylor series and a linearized equation can be obtained by neglecting the higher power terms in the series:

$$-\varepsilon_0 \cdot \varepsilon_r \cdot \frac{d^2\varphi}{d\,x} = \sum_i z_i e\, C_\infty \left(1 + \frac{-z_i e \varphi_0}{k_B T}\right) \qquad \textbf{3-12}$$

Rearranging this equation gives:

$$-\varepsilon_0 \cdot \varepsilon_r \cdot \frac{d^2\varphi}{d\,x} = \sum_i z_i e\, C_\infty - \sum_i \frac{{z_i}^2 e^2 C_\infty}{k_B T} \varphi_0 \qquad \textbf{3-13}$$

Away from the double layer, the number of positive charges and negative charges is equal. So the term $\sum z_i e\, C_\infty$ must be equal to zero. So Equation 3-13 can be simplified as:

$$\varepsilon_0 \cdot \varepsilon_r \cdot \frac{d^2\varphi}{d\,x} = \varphi_0 \cdot \sum_i \frac{{z_i}^2 e^2 C_\infty}{k_B T} \qquad \textbf{3-14}$$

This is a simple second order differential equation for the potential distribution close to the surface. The decay of the surface potential therefore follows an exponential function:

$$\varphi = \varphi_0 \exp -\frac{x}{\sigma} \qquad \textbf{3-15}$$

Where,

$$\sigma^{-1} = \sqrt{\sum_i \frac{{z_i}^2 e^2 C_\infty}{\varepsilon_0 \varepsilon_r k_B T}} \qquad \textbf{3-16}$$

σ, known as the Debye length, gives the thickness of the Debye layer which is defined as:

"The distance over which the potential developed by separating a charge density from the background charge of the opposite polarity is equal to the thermal voltage [**47**]*"*

The Debye length reflects the screening of the charge in the inner Helmholtz layer and indicates where the potential has dropped to $1/e$ of its maximum value. Within the Debye length, the effect of the changing ion concentration is very important leading to significant changes in potential. Beyond the Debye length, the changes in potential are much lower as the distribution of Co-ions and Counter-ions leads to approximate neutrality. The Debye length controls the minimum separation between

two electrodes used in a conductivity measurement which must be longer than the related Debye length as if the two layers of ions caused by two electrodes interpenetrate the measured conductivity of the liquid will be increased [**4**] [**48**].

By knowing the concentration of ions in the liquid, the related Debye length can be calculated. However, in this project as insulating oil was used, the concentration of ions is not known but is expected to be small due to the low conductivity observed in insulating liquids. According to [**49**], the typical thickness of the double layer in practice is approximately in the order of 10 nm, other researchers suggest that the expected Debye length for insulating liquid should be in the order of $10^{-6} \sim 10^{-5}$ m [**50**] [**51**] . These values are significantly smaller than the separation of electrodes in the test cell used in this project (1mm) which allowed measurements to be made with confidence.

3.2.2. MEASUREMENT OF CONDUCTIVITY

As previously mentioned the conductivity of a liquid is a physical quantity that represents the capacity of the liquid to transmit current. The conductivity is the inverse of electrical resistivity, the units of conductivity is Sm^{-1}. A background to the conductivity measurement of insulating oil has been provided by Schober along with some experimental results [**52**]. When a voltage is applied to an insulating liquid, charge carriers inside the liquid will migrate in a specific direction under the force due to the electric field which leads to current. Assuming the thermodynamic equilibrium is not changed significantly by the applied field, the most commonly known expression of conductivity σ is related to the current density J and the field strength E which can be shown as:

$$\sigma = \frac{J}{E} \qquad \textbf{3-17}$$

The measurement of conductivity of insulating liquids is usually based on international standards. In accordance with the standards issued by ASTM, the electric field intensity used for conductivity measurement should be in a range of 200-1200 V/mm, and the distance between the electrode plates should be between 1-2.5mm. Standards issued by IEC are similar. The only difference is the voltage strength adopted is 250V/mm [**53**]. According to [**54**], by using these standards to

measure the conductivity, the current is time-dependent. Therefore there is still discussion at what time in point the current value should be used to calculate the conductivity of insulating liquid.

Another approach to find the conductivity of an insulating liquid is to measure the dissipation factor $\tan\delta$ of the insulating liquid under a.c. conditions and use:

$$\tan\delta = \frac{\sigma}{\varepsilon\omega} \qquad \textbf{3-18}$$

Where ε is the permittivity of the liquid and $\omega = 2\pi f$ is the angular frequency used during the measurement. For highly insulating liquid ($\sigma < 10^{-11}\mathrm{S}\cdot m^{-1}$), the accuracy of bridge measurement of $\tan\delta$ is low and the liquid conductivity calculated has a larger deviation than that found in d.c. measurements. This problem has been addressed by increasing the liquid temperature which increases its conductivity allowing the loss tangent of the sample to be determined more accurately [**53**]. This approach then requires the calculated conductivity to be corrected to the value expected at the required temperature.

3.2.3. MOBILITY AND ITS MEASUREMENTS

The mobility of charge carriers is a parameter that describes how fast charged particles move through the liquid medium as a result of an applied field. Previous studies and experiments of mobility measurement in dielectric liquid were reported in [**55**] [**56**] [**57**] [**58**]. Mobility plays an important role in studies of breakdown in insulating liquid, especially for HVDC transformers [**59**]. The mobility measurement of charge carriers in the insulating oil is usually carried out by a time of flight (TOF) method. In TOF measurements, the time required for charge carriers to drift through a certain distance is measured directly and used to calculate the velocity. It should be noted that in general the mobility derived from TOF measurements is referred to as an apparent mobility in the literature. An increase of measured electron drift velocity with the applied field in butane and cyclopentane was observed and presented in [**58**] which suggests that, for liquid with low mobility of charge carriers ($\leq 0.1 cm^2V^{-1}s^{-1}$), the electrons spend most of their lifetime in a localized state. The lifetime of free electrons in the liquid is lower than 10^{-4} second; therefore the

transmission of charge carriers is either due to the electrons hopping process or due to the movement of the ions under Coulomb force. The typical apparent mobility of positive ions and negative ions in insulating oil at ambient temperature regarding to literature was expected to be of the order of 10^{-9} m^2/Vs [**60**] [**61**]

There are two techniques of measuring the mobility of charge carriers in insulating liquid using the TOF method: monopolar polarization and bipolar polarization which are also known as single polarity method and reversal polarity method [**4**]. In either technique, the time of flight values is determined from the current transient. The basic principle of these two techniques is the same:

$$V_{drift} = \frac{d}{t} \qquad \textbf{3-19}$$

Where, V_{drift} is the velocity of a charge carrier, d is the distance and t is the period of required time for a charge carrier to transfer through the distance d.

3.3. WHAT CAN BE MEASURED FROM CURRENT TRANSIENT

In this section, three key parameters (TOF, peak current and d.c. current) that can be measured directly from the current transient measured using monopolar or bipolar polarization will be presented. TOF values can be used to calculate the mobility of charge carriers in insulating oil. Peak current values provide information about the maximum flux of charge carriers. DC current will be used to calculate the d.c. conductance of the oil which is proportional to the conductivity.

3.3.1. MONOPOLAR POLARIZATION

For the monopolar polarization method, a step voltage is applied to the insulating liquid between two electrodes. A "surge of current" due to the migration of ions towards the electrode with opposite sign is expected under the effect of applied electric field. The potential difference relative to the electric field between two electrodes leads to the charge carriers (either anions or cations) being swept across the bulk of the oil, and being collected in the area near the opposite electrode. Such a "surge of current" would decay quickly as when ions are neutralized at the electrodes. This would results a layer of ions forming very close to the electrode. Figure 3-3 is a

measured current transient from the experiment performed in this project. The value of TOF, I_{peak} and I_{dc} that can be obtained from this transient curve are indicated.

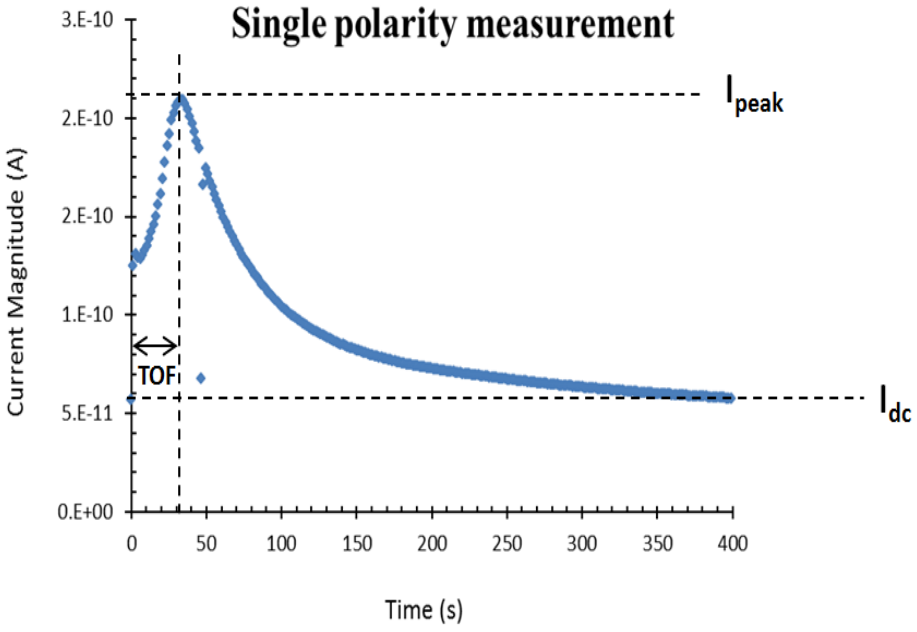

Figure 3-3 Current transient for monopolar polarization

However, the reproducibility of this method is poor. According to [**4**], the measured TOF value strongly depends on previous measurements of mobility. For example, a clear peak can be observed when a positive polarity measurement was taken after a previous monopolar measurement under negative polarity, while no peak can be observed when two negative polarity measurements are taken in succession. This may be due to the residual ions aggregation near electrodes as a result of earlier polarizations. Experimental results presented in [**4**] indicate that a relatively long time (over 120min) is necessary to eliminate the effects of pervious polarizations and achieve consistent results. Figure 3-4 is a transient behaviour of a monopolar measurement performed in this project which illustrates the expected current transient measured with a uniform ion distribution.

In this situation, [**54**] suggests that for plane parallel electrodes, the TOF value can be obtained from the interception of the linear regression line calculated from the current values before the current reaches the inflection point. In Figure 3-4, the blue curve is a measured current transient curve, and the red straight line is the linear regression of the initial current data. In practice the initial current does not truly

behave in a linear manner, therefore the intercept of the regression line on the t axis is sensitive to the selection of data points used to calculate the linear behaviour. In addition, measurements of the TOF using the bipolar method below resulted in smaller and more self-consistent values for the TOF.

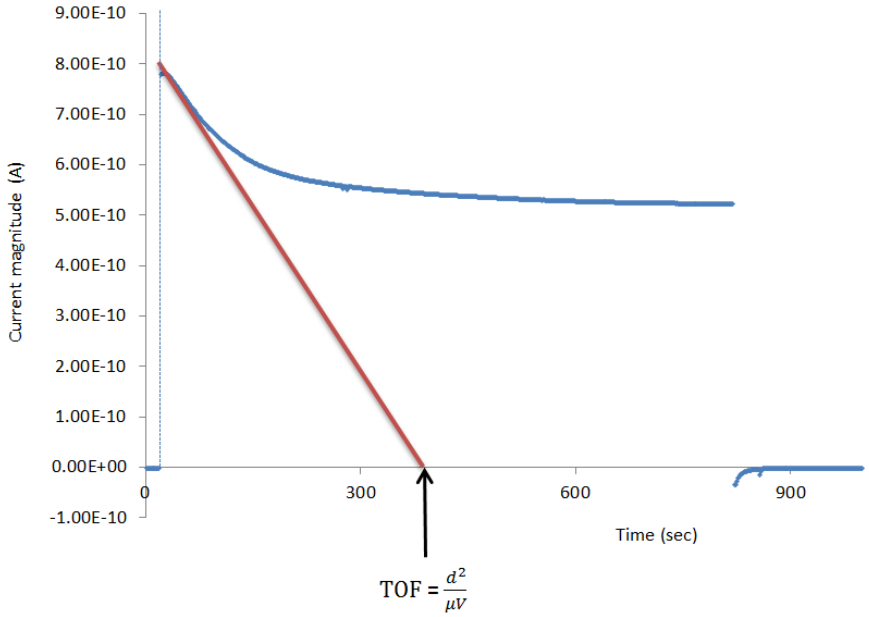

Figure 3-4 Monopolar polarization with uniform ion distribution (from measurements in section 6.7.1.1)

3.3.2. BIPOLAR POLARIZATION

For bipolar polarization method which has been used by previous research [**62**], a step field is initially applied to the insulating liquid in one direction for a period of time. During this initial polarization, the transient behaviour would be similar to the monopolar polarization process. After the measured current reaches a quasi-steady state indicating that the distribution of charge carriers has reached an equilibrium in the gap, sometimes assumed to indicate that the ions have been swept from the gap, the polarity of the applied field is reversed. In this case, the layers of ions close to the electrodes due to the initial polarization will be forced to move towards the opposite electrodes. A peak is observed in the current which is assumed to be caused by the arrival of the peak of the distribution of ions at the opposite electrode having crossed the gap. TOF is defined in the bipolar polarization method as the time interval between the moment when the applied voltage is reversed and the moment when the

measured current reaches a maximum value. Figure 3-5 is the general current transient behaviour during a bipolar polarization performed in this project. This includes a very short depolarization region observed when the applied voltage is finally reduced to zero. The TOF, peak current and d.c. current values which can be measured are also shown in Figure 3-5. Note that the value of peak current can be obtained directly from the recorded current transient and in this project the d.c. current was calculated from the average value of the last 20 recorded data points in the reverse polarization transient.

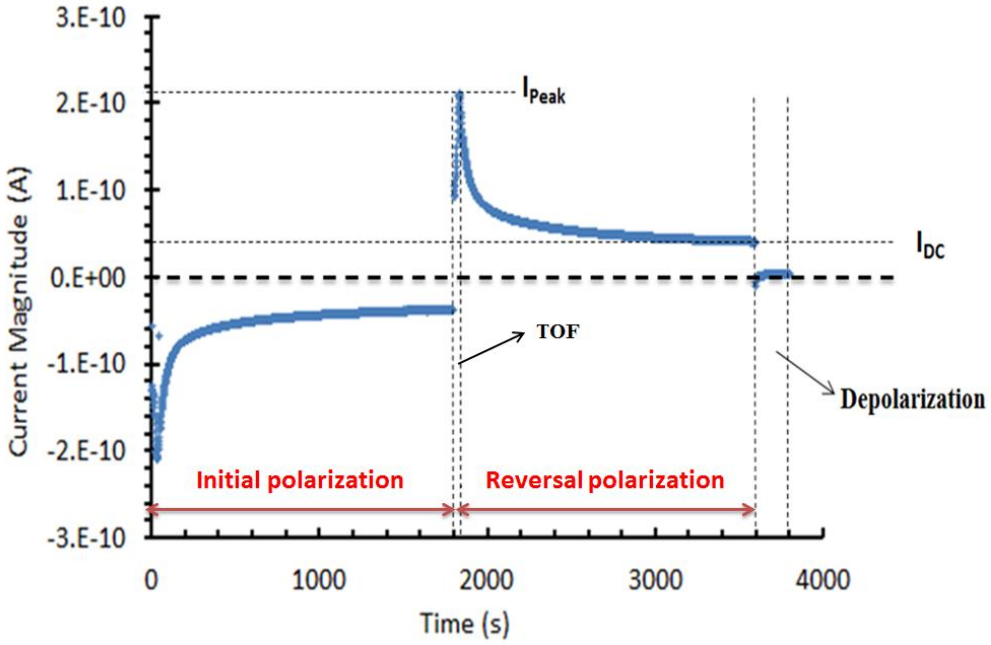

Figure 3-5 Current transient for bipolar polarization (from measurements in section 6.7.1.1)

An average velocity $\bar{v}$ of the charge carriers in the liquid can be calculated from the time of flight using:

$$\bar{v} = \frac{d}{TOF} \qquad \textbf{3-20}$$

Where d is the separation between two electrodes. The mobility μ can be derived from the velocity using:

$$\mu = \frac{\bar{v}}{\bar{E}} \qquad \textbf{3-21}$$

Where, $\bar{E}$ is the average electrical field between the electrodes. It is assumed that: $\bar{\mathrm{E}} = U/\mathrm{d}$, where U is the magnitude of the applied voltage. Equation 3-21 also assumes that the mobility μ is independent of electric field *E*. Combining equation 3-20 and equation 3-21 leads to an expression for the mobility in terms of the separation between electrodes the applied voltage and the TOF.

$$\mu = \frac{d^2}{U \cdot TOF} \qquad \textbf{3-22}$$

Equation 3-22 gives the method of calculating the apparent mobility of charge carriers in the insulating liquid. Due to its advantages over the monopolar approach the bipolar polarization method was adopted for measuring the TOF in this project and the expected mobility of charge carriers was derived using equation 3-22.

3.4. FACTORS AFFECTING CONDUCTIVITY AND MOBILITY

The conductivity of the insulating liquid and the mobility of charge carriers in the insulating liquid are the two main parameters investigated in this project. It was expected that the d.c. conductivity measurements would be strongly related to the charge injection process and the measurement of mobility of charge carrier might be influenced by electrohydrodynamic effects. Therefore the theory associated with charge injection and the electrohydrodynamic effects has been reviewed.

3.4.1. CHARGE INJECTION

As mentioned in section 3.2, the d.c. electric conduction of the insulating oil measured in this project is due to either charge injection or the residual conduction caused by the dissociation of molecules. As the insulating oil is a non-polar liquid the number of ions due to molecular dissociation is expected to be small. Therefore, the electric conduction behaviour of insulating oil should be dominated by the injection current once it reaches quasi-static state.

During the bipolar polarization measurement, when the d.c. current reaches a steady state, the process of charge injection may be similar to Schottky emission which is a thermionic emission enhanced by the electric field which lowers the energy barrier due to the image force. An expression for the modified Schottky emission model suggested by Forster can be used to express the field-assisted thermionic emission process for electrons [**63**] :

$$\mathrm{J} = \frac{4\pi me(k_B T)^2}{h^3} exp\left[\frac{-(\emptyset - e^{1.5}E^{0.5})}{k_B T}\right] \qquad \textbf{3-23}$$

Where: m is the mass of electron; e is the electron charge; T is the absolute temperature; k_B is the Boltzmann constant; h is Planck's constant and $\emptyset$ is the work function for electron emission.

Based on equation 3-23, there should be a linear relationship between logarithmic function of the charge injection related current density and the square root of the applied electric field if the behaviour of charge injection in this project follows this modified Schottky emission method.

The Schottky emission process deals specifically with the injection of electrons into a liquid. An alternative mechanism is that when an electric field is applied to the insulating liquid between two electrodes, ions can be created in the liquid. The mechanism of ion creation was investigated by A. Alj who provided evidence to suggest that ions can be created either in the bulk of the liquid or at the metal-liquid interface, depending on the strength of the applied electric field [**64**]. With a strong enough electric field applied, an ionic-dipole is able to form and become separated under the effect of electric force leading a creation of charge carriers in the liquid. If the applied field is relatively weak, charge carriers are more likely to be created at the metal-liquid interface due to electrochemical reactions and be extracted away from the metal by overcoming the image-force in a similar manner to the Schottky emission of electrons. This injection process in insulating liquid can be commonly separated into two steps. In the first step, ions will be generated on the electrodes. In the second step the generated ions overcome the image force and are injected to the bulk of the liquid. In this project, as the electrodes are made of stainless steel, electrons are readily available and therefore the creation of charge carriers at the

electrode should be very fast. This implies that although the ion creation process at the electrode remains unknown its rate will be higher than the rate of charge carriers overcoming the image forces and escaping from the electrodes. Therefore, the injection current is expected to be determined by the second step, the ion escaping process [**65**].

When a singly charged ion tends to leave a metal electrode, the image force caused by the apparent induced positive charge region tends to pull the ion back to the metal. Ignoring the effects of any space charge, the image potential φ_{image} due to the attracting image force as a function of the distance x from the electrode can be expressed as:

$$\varphi_{image}(x) = \frac{-e}{16\pi\varepsilon x} \qquad \textbf{3-24}$$

Where, e is the charge of electron and ε is the permittivity relating to the liquid. It is assumed that the potential at infinity ($x = \infty$) is equal to zero. When an electric field is applied, the potential distribution in the vicinity of the metallic electrode can be illustrated in Figure 3-6.

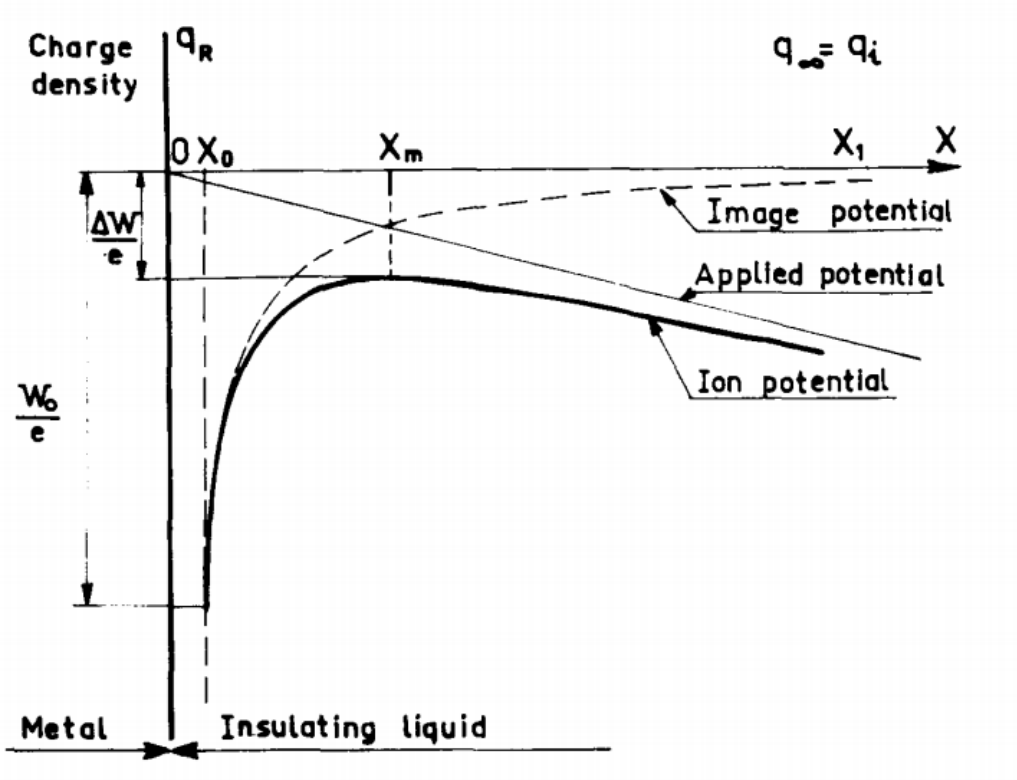

Figure 3-6 Change of potential due to the presence of electric field [42**]**

As shown in Figure 3-6, the applied electric field acts to lower the energy barrier due to the image potential, and therefore more ions with relatively lower energies could overcome the image force and escape from the region close to the electrode into the bulk of the liquid. This would lead to an enhancement of the charge injection process. Larger charge injection currents would be expected with a higher electric field applied. However, the formation of injected charge carriers in the liquid can lead to the presence of space charge close to the electrode. If the injected charge carriers clear the region of the electrode rapidly due to their mobility under the influence of the applied field little space charge will form. However if the applied electric field is relatively weak then the injection related current from the electrode dominates the mobility current away from the region of the electrode. More injected charges stay in the region close to the electrode which will lead to an imbalance of the distribution of positive charges and negative charges, forming a space charge region. In this case, the presence of space charge is of significance since it will reduce the local electric field strength and reduce the probability of further charges being injected into the liquid. An equilibrium steady state can be obtained when the rate of injection of charges is equal to the rate at which they are removed from the electrode area due to their mobility. This is known as the space charge limited condition (SCL) [**66**]. Under SCL conditions, the charge carriers' injection is actually limited by the ability of the system to transport ions away from the space charge region. Further increase of the applied electric field leads to a new equilibrium as charge moves more rapidly from the electrode area balanced by increased injection from the electrode. Convection and other movement in the liquid can also have a positive effect on the injection rate by sweeping ions away from the space charge region.

Ignoring space charge effects, the effective barrier height depends only on the image force potential and the change in potential caused by the applied field. In terms of these potentials the nature of the charge carrier (electron or ion) does not matter. Therefore it is expected that for ionic injection the behaviour of the exponential term in equation 3-23, which relates to the potential barrier and the energy distribution of the charge carriers, will take the same form. The pre-exponential term will be different, as in equation 3-23 it directly relates to the velocity distributions of

electrons. It is therefore expected that the ion injection mechanism should also result in a linear Schottky plot of $\ln I$ vs $\sqrt{V}$.

3.4.2. ELECTROHYDRODYNAMIC EFFECTS

The electrohydrodynamic (EHD) effect is related to systems that exhibit moving charged liquid media as a result of electric forces. It is also known as electroconvection in some literature [**47**]. When an external electric field is applied to a liquid material that contains some kind of charge carriers, those charge carriers will experience a Coulomb force which adds an acceleration component to their random Brownian motion. When the charge carriers collide with liquid molecules the motion of the carrier is re-randomized. This process leads to a net velocity in the direction of the electric field being superimposed on the random motion of the charge carriers, which therefore tend to drift through the liquid. The collisions tend to transfer kinetic energy and momentum to the liquid molecules from the charge carriers. This applies a net force to the liquid molecules in the direction of charge carrier drift causing a flow in the liquid.

The net flow of the liquid molecules and the drift of the charge carriers in the direction of the field can reduce the momentum transfer between the charge carriers and the liquid molecules in the direction of the field. An equilibrium state will be achieved when the drift velocities of the charge carriers and liquid molecules are such that no net momentum transfer occurs. At this point the relative velocity between the charge carriers and the liquid molecules would correspond to the drift velocity of the charge carriers in the absence of the EHD effect. The actual velocity of the ions will be equal to this drift velocity plus the velocity of the liquid. This leads to the measured actual mobility of charge carriers being greater than the value measured without the EHD effect. Earlier research suggests that such an effect is considerable even for a pulse input that contains only a few pC of total ion charges [**67**]. However, Felici suggest that the presence of ions in fluid does not necessarily mean the fluid is “electrified” [**68**]. Only when an imbalance of positive and negative charge carriers is present is EHD of significance.

The simplest model of the liquid motion can be established based on the assumption that the velocity of charge carriers in a flowing liquid is related to its actual mobility and the speed of the liquid flow.

$$v_{apparent} = \mu_{ion} E + v_{liquid} \quad \textbf{3-25}$$

If it is assumed that, in an incompressible and isothermal liquid system, there is a spherical volume of liquid associated with a charge Q moving over a specific distance d at a constant velocity v_{liquid} as a result of the EHD effect caused by an electric field E, then the upper limit of the speed of this volume of liquid v_{liquid} can be obtained through energy conservation by assuming that the reduction in the electrostatic potential energy of the charge Q is equal to the increased kinetic energy of the liquid:

$$\frac{1}{2}\left(\frac{4}{3}\pi r^3 \rho\right) v_{liquid}^2 = Q \cdot E \cdot d \quad \textbf{3-26}$$

Where, r is the radius of the sphere of liquid and ρ is the density of the liquid

Equation 3-26 provides an expression of the maximum speed of the liquid at a distance d from the electrode Equation 3-27:

$$v_{liquid} = \sqrt{\frac{3QdE}{2\pi r^3 \rho}} \quad \textbf{3-27}$$

Equation 3-27 only gives a maximum velocity of liquid in theory which can never be achieved. In fact, the reduced electrostatic potential energy cannot be completely transformed into the increased kinetic energy due to the damping friction of the liquid. During electroconvection, the speed of directional motion will be related to the viscosity of liquid. Assuming that the charge carriers in the liquid are spheres and the interaction between the charged particles can be neglected, according to Stokes' law, the viscous resistance of an ion moving in a homogeneous liquid can be expressed by the equation:

$$F_d = 6\pi\eta r v_{ion} \quad \textbf{3-28}$$

Where, F_d is the frictional force or Stokes' drag force in Newtons; η is the dynamic viscosity in $P_a \cdot s$; r is the radius of the spherical particle in meters and v_{ion} is the velocity of particle in m/s.

The charged particle will move with a specific constant speed in the liquid when the magnitude of frictional force F_d and electrostatic force F_e that the charged particle suffers are equal and opposite:

$$F_e = \frac{\mathrm{q} \cdot \mathrm{V}}{d} = 6\pi\eta R v_{ion} \quad \textbf{3-29}$$

Where, V is the applied voltage; q is the total charge of the charge carrier and d is the distance between two parallel electrodes. This gives an expression of the velocity of charge carriers in the liquid as:

$$v_{ion} = \frac{\mathrm{q} \cdot \mathrm{V}}{6\pi\eta R d} \quad \textbf{3-30}$$

At equilibrium steady state when charge carriers are moving at a constant speed in the liquid, the reduction in electrostatic potential energy is no longer transformed into the kinetic energy of the particles but is instead transformed either into heat energy increasing the temperature of the liquid or into an increase in the kinetic energy of the liquids in the form of liquid flow.

In reality, EHD is a more complicated process. The water heating process can be taken as an illustration. A fluid will stay at rest when the gravitational force is balanced by the pressure gradient. If a non-uniform heating source is applied at the bottom of the bulk of a liquid, convective motion will take place. A very slight heating of the fluid in the region of the heat source leads to a small change of density due to the change of temperature. As a result, the pressure gradient changes and the fluid will tend to move away from the heat source. As the warmer fluid moves away from the heat source cooling may take place and the density of the liquid increases. This leads to convection with liquid flowing upwards from the heat source, cooling and flowing back down. Regular hexagonal cells tend to be formed by the combination of upwards and downward flows in the liquid for small increases of

temperature. Further increases in the temperature will increase the convection and the hexagonal cell become less stable and ultimately the system converts to a turbulent flow. Investigations performed by Atten [**69**] and Felici [**68**] observed that the convective performance of electrified fluid can be similar to this classical example of heating of fluid. When a slight but strong enough electric field is applied to an "electrified" fluid initially at rest, forces will act on the bulk of the fluid, which can also lead to convection in the form of hexagonal cells. Similar to the previous description of fluid heating, further increase of the electric field would lead to instability of the cells and finally a transition into turbulent behaviour. A more significant EHD motion of the liquid is expected as a result of a stronger applied electric field.

The EHD motion of a liquid can help to move the injected charge carriers away from the electrode. As a result, the concentration of charge carriers close to the injecting electrode is reduced and consequently weakens the space charge effect. The charge injection process is expected to be enhanced by the EHD motion for this reason [**54**].

In general, increase of electric field will lead to a larger measured conductivity by increasing not only in the speed of charge carriers due to their mobility and the influence of EHD on mobility but also in the total number of charge carriers in the bulk of liquid due to increased carrier injection.

3.5. WHY THERE IS A PEAK IN THE CURRENT TRANSIENT

In the second reverse polarization of the bipolar measurements, a "peak" of the measured current can be observed [**4**]. A brief analysis of this peak position relative to the distribution of the concentration of charge carriers will be given in the following section which will be helpful for understanding the charge carriers' performance during bipolar measurement.

3.5.1. EINSTEIN'S RELATIONSHIP

Before analyzing the behaviour of ions in the gap between electrodes and the peak position of the observed current, a review of Einstein's relationship between Mobility and Diffusion is useful. This relationship was named after Albert Einstein who first reported it in 1905 simultaneously with other researchers [**70**].

If a DC voltage is applied to a dielectric liquid, charge carriers in the liquid will tend to migrate in a common direction under the effect of the electrostatic force. This common motion of the ions leads to a net current. Generally, this motion of the charge carrier is known as a drift.

If a concentration gradient of charge carriers exists, the charge carriers will tend to move from the regions with high concentration of charge carriers to the regions with low concentration. This kind of motion is based on the random movement related to the internal energy of charge carriers. This process is usually known as charge carrier diffusion.

Einstein's relationship shows that the relationship between the mobility of charged particle and diffusion coefficient D is:

$$\mu = \mathrm{D} \cdot \frac{q}{k_B T} \qquad \textbf{3-31}$$

Equation 3-31 shows that the mobility of charge carriers in a liquid is proportional to the diffusion constant *D*. The larger the value of the diffusion constant *D* is, the larger the mobility of charge carriers is. In theory, the diffusion constant *D* will increase with the applied field. However, M. Hilaire suggested that, when the field is below 1kV/cm, this field enhanced diffusion can be considered negligible [**71**].

In this project, for all the TOF measurements, only one peak could be observed after the applied voltage reversed. However, there might be more than one kind of charge carriers in the insulating oil and the sign of charge carriers can be different (either anions or cations). If the mobility of anions is significantly different from the mobility of cations, the current transient may have two peaks. By reviewing the literature, no multiple peaks can be found in the published data when using the bipolar polarization method to investigative the mobility of charge carriers in the liquid. One possible explanation for the single peak observed is that, the mobility of positive charge carriers is close to the mobility of negative charge carriers. In this case, the peak position actually represents an average mobility for both kinds of charge carriers. Another possible explanation could be that, the migration of either positive charge carriers or negative charge carriers is significantly larger than the other one which means the measured charge carriers' mobility may be dominated by

only one kind of charge carriers. In this case, the measured peak position represents the mobility of the more mobile charge carriers.

3.5.2. SIMULATION OF THE IONS FLOW

To understand the influence of diffusion on the distribution of ions moving under the influence of an applied field, a simple model for ion motion was developed. The following assumptions were made: only one kind of charge carriers is considered as the cause of the peak appearing in the current transient curve; the geometry is semi-infinite and plane parallel; the initial ion distribution is a Dirac delta close to a blocking electrode and the ion distribution moves under the influence of the electric field into an unbounded space. The current is calculated by considering the flux of ions through a plane parallel to the blocking electrode separated from it by a distance *x*. System has an ideally blocking electrode which means the transient behaviour will depend on the distribution of charge at the electrode as shown in equation 3-32.

3.5.2.1. For infinite system: no reflection

A system with infinite space will be considered as a beginning for analysis. The flux of carriers moving in this infinite system is made up of a field driven mobility component depending on concentration and a diffusive component depending on concentration gradient. *J* can be calculated using:

$$J = J_{Mob} + J_{Dif} = \mu EC - D\nabla C \qquad \textbf{3-32}$$

Where μ is the mobility, E is the applied field, D is the diffusion constant and *C* is the concentration of charge carriers.

Initially at the moment when the applied voltage reversal occurs at the beginning of the reversal polarization part, the charge distribution in the vicinity of the electrode is described by a Dirac Delta function. By definition, the area of a Dirac Delta function must equation to 1, to be physically realistic, this Dirac Delta must be：

$$C = 1/d \qquad \textbf{3-33}$$

Where, the *d* is the diameter of a charge carrier which gives the practical limit on the concentration. The general expression of the development of concentration profile can be obtained by solving the behaviour of an initial Dirac Delta concentration

distribution in an infinite parallel plane system at x = 0, t = 0 using the Fick's second law. This expression can be written as [**72**]**:**

$$C(x,t) = A_0 \frac{1}{\sqrt{4\pi Dt}} \exp\left(-\frac{x^2}{4Dt}\right) \qquad \textbf{3-34}$$

Where, x represents distance away from the initial location of a Dirac Delta distribution at specific time t, $-\infty < x < \infty$ in an infinite system; *D* is the diffusion constant; t is the time; A_0 is a coefficient since the total area for a Dirac Delta function is normally set to be equal to 1.

In the case of the charge carriers' diffusion, the total number of carriers in the system at any time is constant and given by:

$$\int_{-\infty}^{\infty} C dx = N_0 \qquad \textbf{3-35}$$

Where, N_0 is the total number of charge carrier present in the system. Equation 3-34 can be rewritten as:

$$C(x,t) = N_0 \frac{1}{\sqrt{4\pi Dt}} \exp\left(-\frac{x^2}{4Dt}\right) \qquad \textbf{3-36}$$

Considering a one-dimensional diffusion model in an infinite system and taking a cross section, equation 3-36 can be written as:

$$C(x,t) = \frac{N_0}{A} \frac{1}{\sqrt{4\pi Dt}} \exp\left(-\frac{x^2}{4Dt}\right) \qquad \textbf{3-37}$$

Where, A is a cross sectional area relative to the one-dimensional model which can be set equal to 1 for simplification. Equation 3-37 provides a model for the distribution of charge carriers with time considering only diffusive processes. The concentration distribution in this case will be symmetrically centred on the position $x = 0$.

The partial differential expression of equation 3-37 with respect to x can be obtained:

$$\frac{dC}{dx} = -\frac{x}{2Dt}\frac{N_0}{\sqrt{4\pi Dt}}\exp\left(-\frac{x^2}{4Dt}\right) \quad \textbf{3-38}$$

According to the Fick's first law, the diffusion flux can be calculated by:

$$J_{Dif} = -D \times \frac{dC}{dx} \quad \textbf{3-39}$$

The flux due to the diffusion of ions is described by equation 3-40.

$$J_{Dif} = \frac{x}{2t}\frac{N_0}{\sqrt{4\pi Dt}}\exp\left(-\frac{x^2}{4Dt}\right) \quad \textbf{3-40}$$

When an electrical field is applied to the system, a drift velocity v_d will be added onto the charged particles and the central position of the concentration distribution will move across the system with the time. To account for the effect of drift velocity, the parameter x can be rewritten as: $x - v_d t$ which models the displacement of the centre of the concentration profile with time due to the applied electric field.

Therefore, the expression of the concentration distribution as a function of time becomes:

$$C(x,t) = N_0\frac{1}{\sqrt{4\pi Dt}}\exp\left(-\frac{(x-v_d t)^2}{4Dt}\right) \quad \textbf{3-41}$$

Note that equation 3-41 is actually showing the behaviour of a concentration distribution under an applied field with a known mobility of charge carriers.

The drift velocity due to the applied electric field can be expressed as:

$$v_d = \mu E$$

The Einstein's relationship equation 3-31 gives the relation between mobility and the diffusion constant μ and the diffusion constant D:

$$\mu = \frac{q}{k_B T}D$$

Combination of these two equations gives:

$$v_d = \frac{q}{k_B T} DE \qquad \textbf{3-42}$$

Substituting equation 3-42 to equation 3-41 gives a general equation of the behaviour of the concentration of charge carriers as a function of distance, time and electric field.

$$C(x,t,E) = N_0 \frac{1}{\sqrt{4\pi Dt}} \exp\left(- \frac{\left(x - \frac{q}{k_B T} DEt\right)^2}{4Dt} \right) \qquad \textbf{3-43}$$

To calculate the flux associated with equation 3-43 the flux due to mobility and to diffusion must be calculated (equation 3-32). Therefore, the partial derivative with respect to x must be calculated. Equation 3-43 can be rearranged as:

$$C(x) = \frac{\alpha}{\sqrt{t}} \exp\left(- \frac{(x - \beta(E)t)^2}{4Dt} \right), \qquad \alpha = \frac{N_0}{\sqrt{4\pi D}}, \beta(E) = \frac{qD}{k_B T} E \qquad \textbf{3-44}$$

Therefore, the partial differential expression of equation 3-44 with respect to x can be calculated as:

$$\nabla C = \frac{dC_{(x)}}{dx} = \frac{\alpha}{\sqrt{t}} \left(- \frac{2(x - \beta(E)t)}{4Dt} \right) exp\left(- \frac{(x - \beta(E)t)^2}{4Dt} \right) \qquad \textbf{3-45}$$

Substituting equation 3-44 and equation 3-45 into equation 3-32 gives the total flux passing through a unit area at a particular distance x at a specific time t:

$$J = D \frac{\alpha}{\sqrt{t}} \exp\left(- \frac{(x - \beta(E)t)^2}{4Dt} \right) \left(\frac{qE}{k_B T} + \frac{2(x - \beta(E)t)}{4Dt} \right) \qquad \textbf{3-46}$$

Replacing α and β leads to a final expression for the flux in terms of the initial number density of charge carriers, the diffusion constant and the applied field, Equation 3-47.

$$J = D\frac{N_0}{\sqrt{4\pi Dt}}\exp\left(-\frac{\left(x-\frac{qDt}{k_BT}E\right)^2}{4Dt}\right)\left(\frac{qE}{k_BT}+\frac{2\left(x-\frac{qDt}{k_BT}E\right)}{4Dt}\right) \quad \textbf{3-47}$$

3.5.2.2. For semi-infinite system

In a more realistic system the initial ion distribution will not be at the electrode position (x =0) but instead at a position close to the electrode x_0. A basic equation based on equation 3-37 modified by the initial position of the layer of charge carriers can be derived as:

$$C_T(x,t) = \frac{N_0}{\sqrt{4\pi Dt}}\exp\left(-\frac{(x-x_0)^2}{4Dt}\right) \quad \textbf{3-48}$$

Where, x_0 represents the expected distance between the Dirac Delta concentration distribution and the electrode,

In addition, for simplicity, the electrode is regarded as blocking. And as a result, the flux at the boundary at $x = 0$ must be zero:

$$J(0,t) = 0 \quad \textbf{3-49}$$

As all the charge carriers are assumed to remain within the system, therefore:

$$\int_0^\infty C dx = N_0 \quad \textbf{3-50}$$

The above conditions can be satisfied by assuming that the flux of ions moving towards the barrier at $x = 0$ is totally reflected. By symmetry, the reflected concentration profile $C_R(x,t)$ required can be derived from a second distribution of N_0 ions centred at $-x_0$ with the initial form of a Dirac delta:

$$C_R(x,t) = C_I(-x,t) = \frac{N_0}{\sqrt{4\pi Dt}}\exp\left(-\frac{(x+x_0)^2}{4Dt}\right) \quad \textbf{3-51}$$

Equation 3-51 gives the concentration distribution due to the charge carriers reflected at the electrode at $x = 0$ associated with a Dirac Delta initial present at x_0. Again, similar to the previous approach, where mobility was considered by displacing the

centre of the concentration distribution, the reflected concentration for the displacing distribution at the blocking electrode can be modelled by displacing the centre of the second distribution from its original position at $x = -x_0$ in the negative x direction. This leads to two equations describing the concentration the first equation 3-52 dealing with the transfer flux:

$$C_T(x,t) = \frac{N_0}{\sqrt{4\pi Dt}} \exp\left(-\frac{\left(x - x_0 - \frac{qDt}{k_B T}\right)^2}{4Dt} \right) \quad \textbf{3-52}$$

And the second describing the reflected flux equation 3-53:

$$C_R(x,t) = \frac{N_0}{\sqrt{4\pi Dt}} \exp\left(-\frac{\left(x + x_0 + \frac{qDt}{k_B T}\right)^2}{4Dt} \right) \quad \textbf{3-53}$$

The total concentration distribution in the system can be expressed by combining the initial concentration profile and the reflected concentration profile:

$$C_{Total}(x,t) = C_T(x,t) + C_R(x,t) \quad \textbf{3-54}$$

Therefore, substituting equation 3-52 and equation 3-53 to equation 3-54 gives the general expression of concentration distribution associated with distance, time and the field. α and β given by equation 3-44 will be used again to simplify the following expressions.

$$C_{Total}(x,t,E) = \frac{\alpha}{\sqrt{t}} \left[\exp\left(-\frac{(x - x_0 - \beta(E)t)^2}{4Dt} \right) + \exp\left(-\frac{(x + x_0 + \beta(E)t)^2}{4Dt} \right) \right] \quad \textbf{3-55}$$

According to a common relationship based on Euler's formula:

$$\cosh x = \frac{e^x + e^{-x}}{2} \quad \textbf{3-56}$$

Equation 3-55 can be re-written as:

$$C_{Total}(x,t,E) = \frac{\alpha}{\sqrt{t}}\exp\left(-\frac{x^2}{4Dt}\right)\exp\left(-\frac{(x_0+\beta(E)t)^2}{4Dt}\right) \times 2\cosh\left(\frac{2x(x_0+\beta(E)t)}{4Dt}\right) \quad \textbf{3-57}$$

The partial differential expression with respect to x of equation 3-57 is:

$$\nabla C_{Total} = 2\frac{\alpha}{\sqrt{t}}\exp\left(-\frac{(x_0+\beta(E)t)^2}{4Dt}\right)\exp\left(-\frac{x^2}{4Dt}\right)\left[-\frac{2x}{4Dt}\cosh\left(\frac{2(x_0+\beta(E)t)x}{4Dt}\right) + \frac{2(x_0+\beta(E)t)}{4Dt}\sinh\frac{2(x_0+\beta(E)t)x}{4Dt}\right] \quad \textbf{3-58}$$

In this case, the initial net flux expression 3-32 can be calculated from the partial derivative of the total concentration distribution with respect to x.

$$J_{Total} = \mu E C_{Total} - D\nabla C_{Total} = D\left(\frac{q}{kT}EC_{Total} - \nabla C_{Total}\right) \quad \textbf{3-59}$$

Substituting equation 3-57 and equation 3-58 into equation 3-59 provides the final expression of the flux of ions in a semi-infinite system associated with distance *x*, time t and electric field E.

$$J_{Total} = \frac{qDE}{KT}\frac{\alpha}{\sqrt{t}}\exp\left(-\frac{x^2}{4Dt}\right)\exp\left(-\frac{(x_0+\beta(E)t)^2}{4Dt}\right)\times 2\cosh\left(\frac{2x(x_0+\beta(E)t)}{4Dt}\right) - D2\alpha\exp\left(-\frac{(x_0+\beta(E)t)^2}{4Dt}\right)\exp\left(-\frac{x^2}{4Dt}\right)\left[-\frac{2x}{4Dt}\cosh\left(\frac{2(x_0+\beta(E)t)x}{4Dt}\right) + \frac{2(x_0+\beta(E)t)}{4Dt}\sinh\frac{2(x_0+\beta(E)t)x}{4Dt}\right] \quad \textbf{3-60}$$

3.5.2.3. Simulation results

The behaviour predicted by equation 3-60, taking into account both mobility and diffusion driven fluxes, is complex. Therefore a simple numerical simulation was developed in Maple. The simulation used equation 3-57 to calculate the concentration profile in the system as a function of time. The concentration gradient

at a particular position and time $\nabla C(x,t)$was derived from the concentration profile $C(x,t)$:

$$\nabla C(x,t) = \frac{C(x+\Delta x,t) - C(x,t)}{\Delta x} \qquad \textbf{3-61}$$

The total flux was then calculated using equation 3-59.

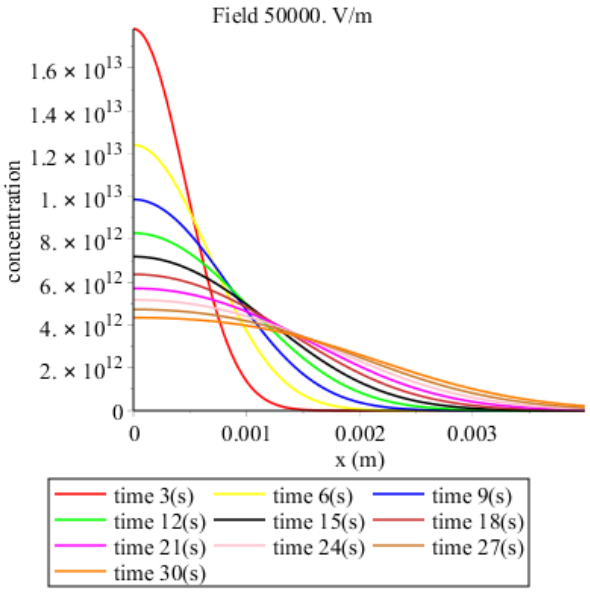

Figure 3-7 Development of concentration profile with time E=50kV/mm

In the model it was assumed that the initial Dirac delta concentration distribution was located at a distance of 1μm from the electrode and the flux values were calculated for the plane located 1mm away from the electrode. A value of the diffusion constant was selected to produce a mobility drift velocity of $2 \times 10^{-5} ms^{-1}$ for an applied field of $50 kV m^{-1}$ which should have lead to a TOF value of $50 s$.

The values of these parameters were selected based on the range of fields and values of TOF reported in the literature [4]. It might be expected that the peak in the flux would occur when the peak in the concentration profile passed the plane of interest. However the modelling showed that this straightforward assumption is not valid in a low field regime when the drift velocities in the system are low.

Figure 3-7 shows the development of the concentration profile in the first 30 seconds. The value of N was equal to10^{10}. It can be seen that the presence of diffusive fluxes has a significant effect on the development of the concentration profile. Rather than

seeing the narrow profile associated with the Dirac delta, after 3 seconds considerable broadening of the profile has occurred. The effect of the flux reflected by the boundary at $x = 0$ means that the maximum in the concentration profile is always close to its original position despite the displacement due to mobility. This reflected flux is occurring due to the presence of the diffusive processes in the system.

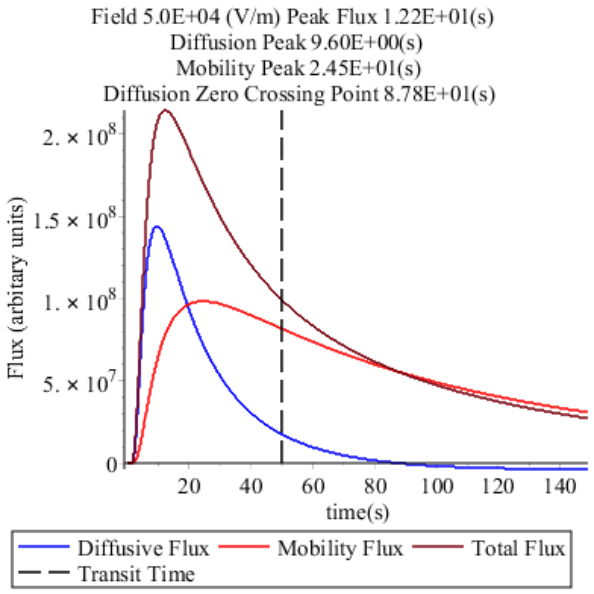

Figure 3-8 Behaviour of the flux components at $x = 1mm$ as a function of time E=50V/mm

Figure 3-8 shows the calculated total flux passing through the plane at $x = 1mm$ as a function of time with the separate mobility and diffusive fluxes. The peak in the total flux occurs at 12.2 s. which is much shorter than the expected value of 50 s based on mobility and time of flight shown as the vertical dashed line in the figure. This peak is made up of a peak in the diffusive flux component occurring at 9.6 seconds and the peak in the mobility flux component at 24.5 s. It can be seen that the diffusive flux becomes zero after 87.8s after which the value becomes negative. This indicates that a peak in the concentration profile $\nabla C = 0$ is passing through the plane. This time is larger than the value expected from the drift velocity defined for the model. A peak can also be observed in the mobility driven flux which occurs after approximately 24.5s. Again this does not correspond to the expected transit time for the ions from the electrode to the plane at x = 1mm. This is due to the broadening of the

concentration profile due to the diffusive component in the fluxes and their reflection at the boundary.

Initially the concentration at the plane of interest increases under the influence of both the mobility and diffusion driven fluxes with the diffusive flux dominating at short times. Up to 24.5s the concentration at the plane of interest is increasing leading to an increase in the mobility driven flux. However as the concentration profile broadens, the overall concentration values fall and this leads to the concentration at the plane of interest beginning to fall, despite the fact that the peak position has yet to reach the plane of interest. Neither the peaks in the flux components nor the time at which the peak concentration crosses the plane of interest correspond to the actual time for an ion to transit the system.

To understand the behaviour of the fluxes with time it is necessary to consider the behaviour of the concentration distribution with time, as diffusive and other processes leads to a broadening of the distribution reducing the values of concentration and concentration gradient in the system which affects both the mobility and diffusive components of the flux.

Figure 3-9 shows the initial effects of diffusion on the Dirac delta over the first 1μs of the simulation. It can be seen that the peak broadens and the maximum value of the concentration falls with time as the total number of charge carriers within the peak is constant. No significant displacement of the centre of the distribution occurs in this first μs as $v_d = 2 \times 10^{-5}\, ms^{-1}$.

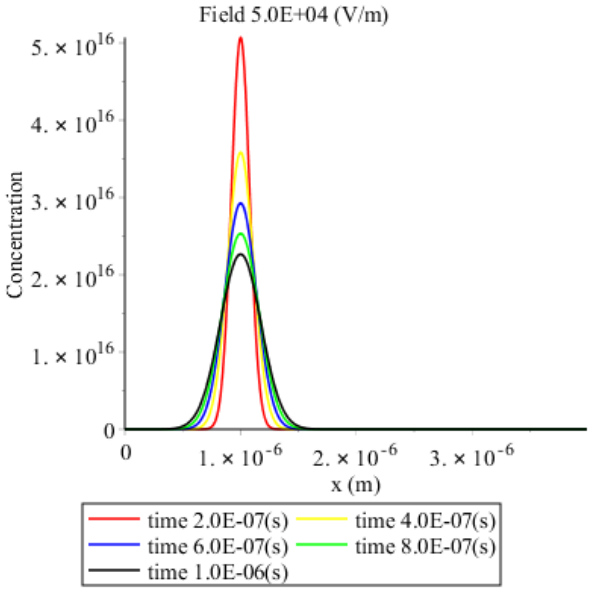

Figure 3-9 Development of the concentration distribution in 1μs

Within 10 μs the concentration distribution has spread sufficiently that it encounters the blocking electrode the reflected flux at this barrier causes the concentration at the barrier to increase while the peak concentration continues to fall, as shown in Figure 3-10

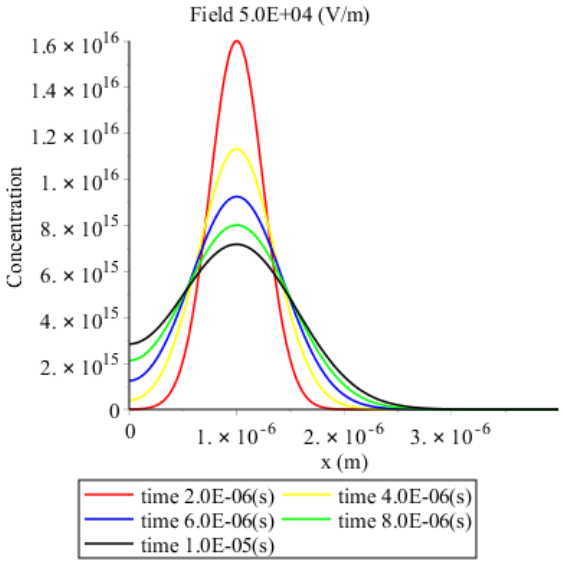

Figure 3-10 Development of the concentration distribution in 10μs

By 50 μs, Figure 3-11, the distribution has effectively become one sided with the concentration maximum occurring at the electrode boundary.

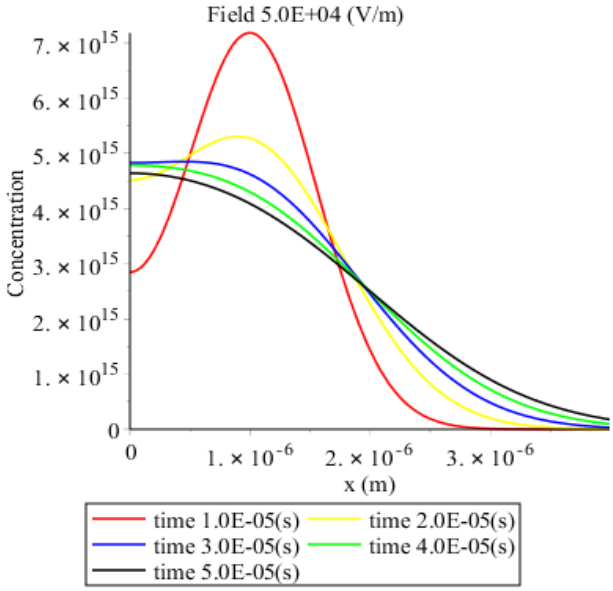

Figure 3-11 Development of the concentration distribution in 10μs

At times associated with the appearance of the peaks in both the mobility and diffusive flux components the distribution is still one sided with its maximum value close to the electrode.

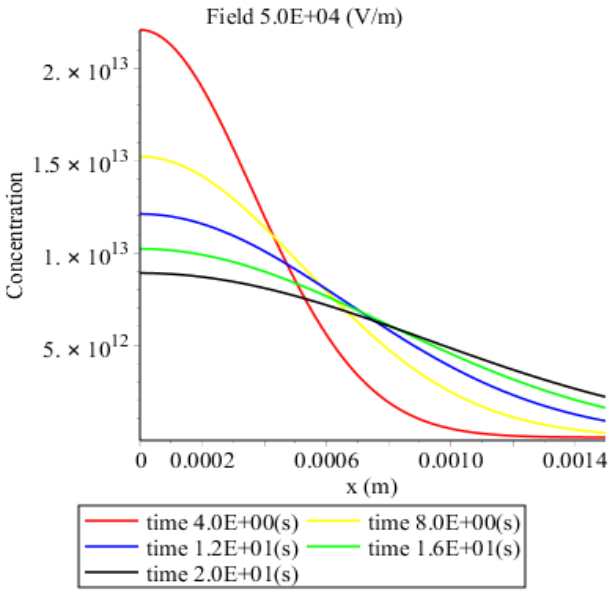

Figure 3-12 Development of the concentration distribution in 20s

Only at much longer times, 80 to 100s the effect of the mobility in the system lead to sufficient displacement of the charge carriers so that a peak in the concentration

distribution is observed. In Figure 3-13 after 100s a clear peak in concentration can be seen at approximate 2mm from the origin electrode.

Generally speaking, simulation results presented in Figure 3-9 to Figure 3-13 imply that the concentration distribution based on a Dirac delta function close to the electrode would broaden rapidly. The reflected flux occurring at the blocking electrode has a strong influence on the concentration distribution within a very short period of time. These simulation results also provide evidence that the use of the Dirac delta distribution rapidly leads to a distribution ($10^{-4}s$) which appears to be similar to that for the behaviour of an ion layer described in section 3.2.

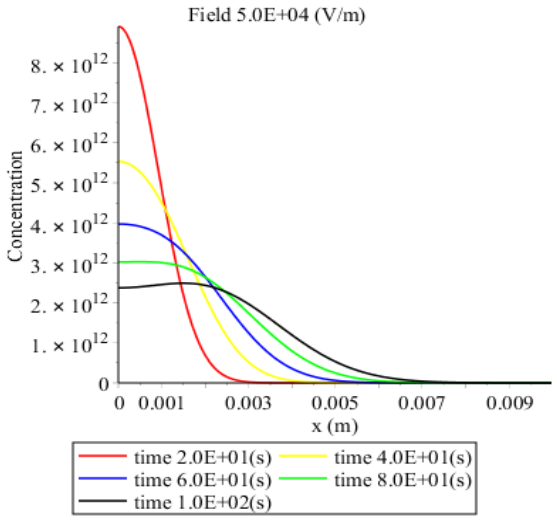

Figure 3-13 Development of the concentration distribution in 100s

It is now possible to explain the behaviour of the peaks in the diffusive and mobility fluxes. When looking at the concentration profiles at the plane of interest,1mm from the electrode. Figure 3-14 below shows the changing behaviour of concentration profiles with times in the range of 3.5 to 9.5 s and from 9.5 to 21.5 s. In this case, the applied field was $50\mathrm{kV/m}$. Figure 3-14(a),(b) shows the behaviours of concentration distribution profile as the diffusive flux component approaches its maximum value. As the peak broadens at the plane of interest, the concentration and the concentration gradient initially increase, increasing the value of the diffusive flux.

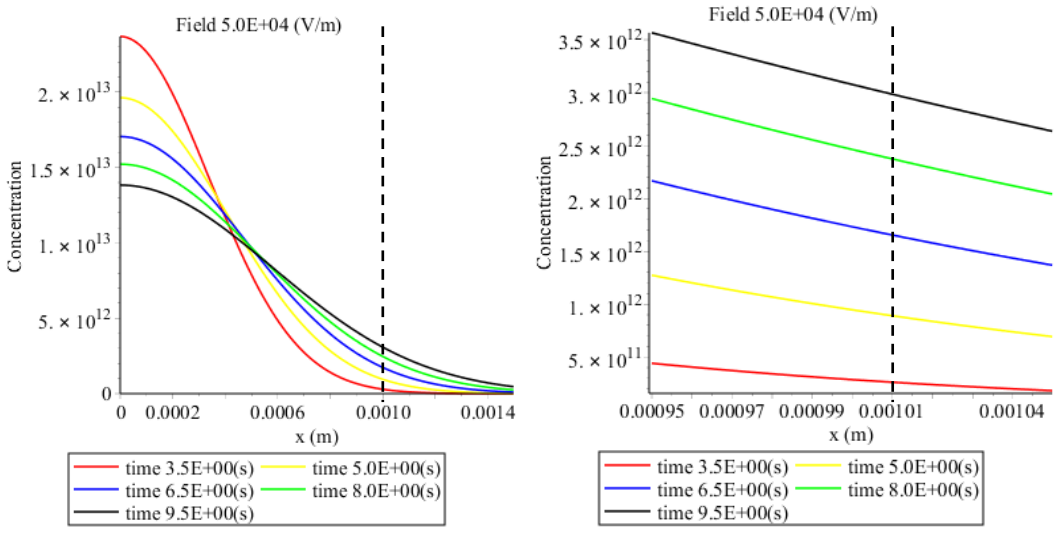

(a) (b)

Figure 3-14 (a) (b) Concentration profiles at the plane of interest associated with diffusion flux

At longer times, as shown in Figure 3-14(c),(d), although the broadening of the distribution is still causing the concentration to increase at the plane of interest, the concentration gradient starts to fall with time. Therefore the diffusive flux component starts to decrease.

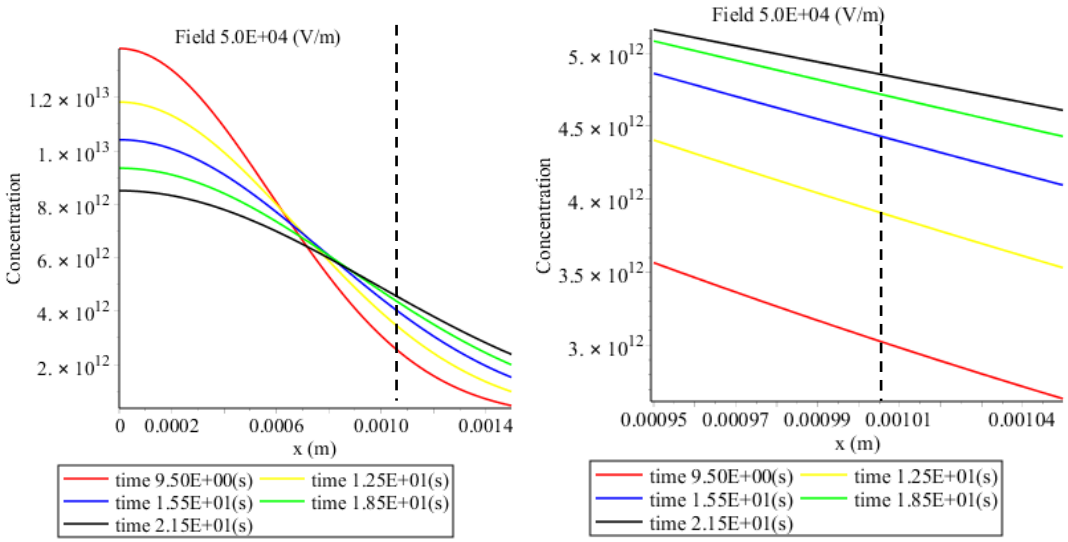

(c) (d)

Figure 3-14 (c) (d) Concentration profiles at the plane of interest associated with diffusion flux

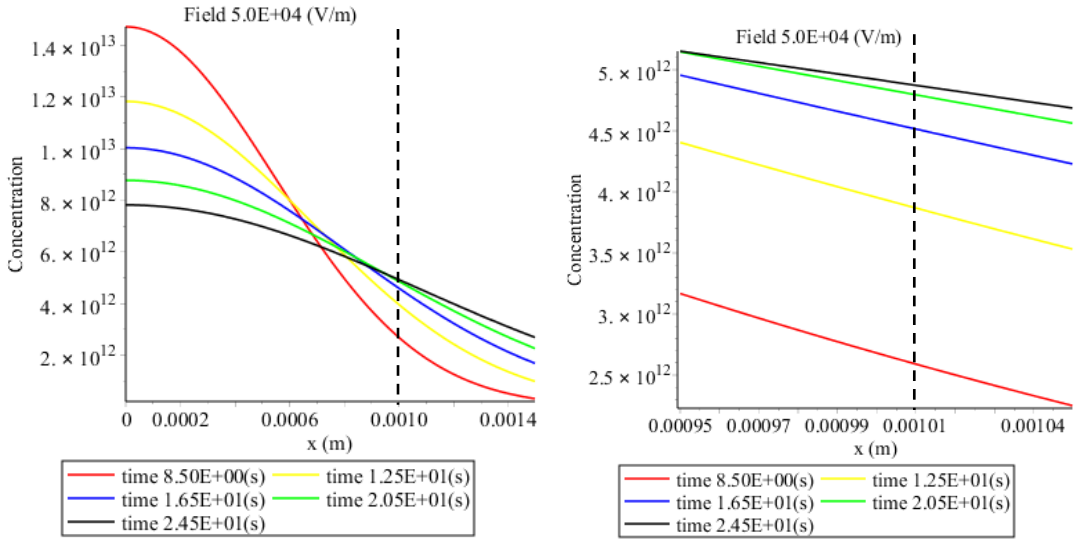

(a) (b)

Figure 3-15 (a) (b) Concentration profiles at the plane of interest associated with mobility flux

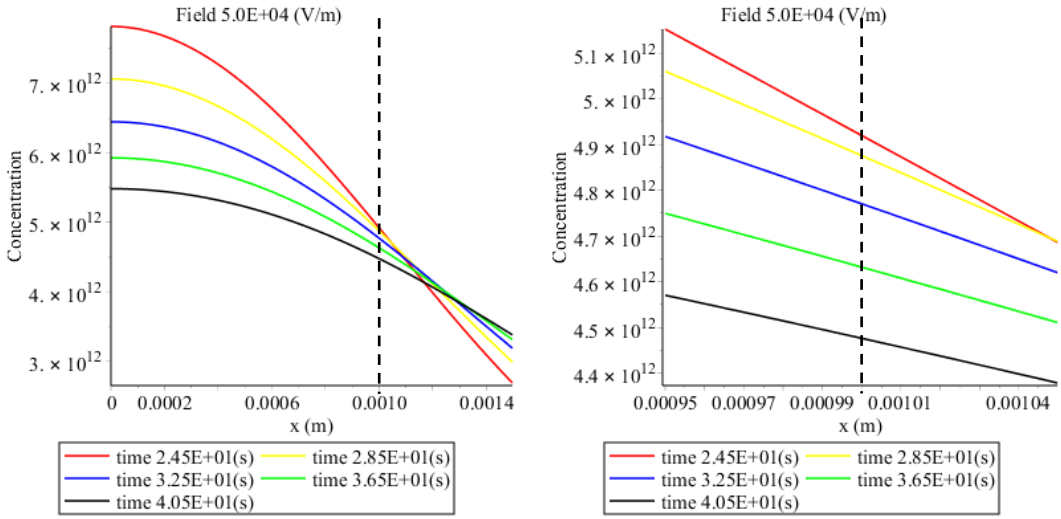

(c) (d)

Figure 3-15(c) (d) Concentration profiles at the plane of interest associated with mobility flux

Figure 3-15(a),(b) shows the behaviour of the concentration distribution profile as the mobility component reaches its maximum value. Again as the peak broadens at the plane of interest the concentration continues to increase, which in term increases the value of the flux component due to the field driven mobility. At longer times the broadening of the peak due to both diffusion and the reflected flux components leads

the concentration at the plane of interest to fall, Figure 3-15(c),(d). Therefore the mobility flux component starts to decrease. This does not mean that the maximum value of concentration in the distribution is crossing the plane of interest. The peak in the total flux is formed from the peaks of the diffusive and mobility flux components and tends to occur at a point in time between these two peaks. The size and position of these peaks depends on the applied field. The simulation was run for applied voltages in the range of 10 to 1000V (corresponding to average fields of 10 to 1000 kV/m) The simulated behaviour of the fluxes are shown in Figure 3-16 and the times associated with the peaks in the total flux, the diffusive flux component, the mobility flux component and the peak in the concentration profile crossing the plane of interest are shown in Table 3-1. This indicates that both the behaviour of the mobility and the diffusion flux are affected by the applied field. As the field increases the peaks in the flux components appear earlier. The behaviours of the flux at the plane of interest for different values of the applied electric field is shown in Figure 3-16

Electric field (kV/m)	Time of Peak Total flux (s)	Time of Peak Diffusion flux (s)	Time of Peak Mobility flux (s)	Time of Peak Concentration distribution (s)
10	11.3	10.7	31.8	> 400
20	11.8	10.5	30.4	> 250
30	12.1	10.3	28.5	225
40	12.2	9.96	26.5	131
50	12.2	9.6	24.5	87.8
60	12.1	9.22	22.7	64.0
70	11.9	8.84	21	49.7
80	11.7	8.46	19.6	40.3
90	11.4	8.12	18.3	33.8
100	11.1	7.8	17.1	29.1
200	8.26	5.6	10.3	12.6
500	4.26	3.12	4.62	5.0
1000	2.3	1.82	2.4	2.5

Table 3-1 Peak position under different applied field

In Figure 3-16 and Table 3-1 shifts are observed in the peak position of the mobility flux component and the diffusion flux component and therefore in the total flux as a result of applied field but in every case their peaks appear at a much shorter time than that predicted by the peak in the concentration profile. The influence of the change of electric field strength on the mobility flux component appears to be more significant than that of the diffusion flux component. For example, changing the field strength from 10kV/m to 100kV/m would shorten the time required for the peak of mobility flux component to reach maximum at the plane of interest from 31.8s to 17.1s. However, for diffusion flux component, this time interval was only reduced from 10.7s to 7.8s.

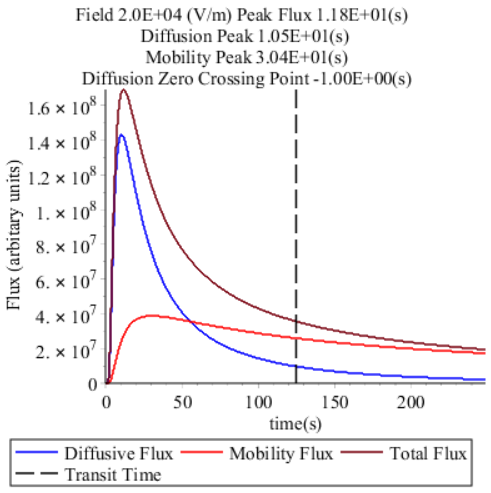

(a) E=10kV/m

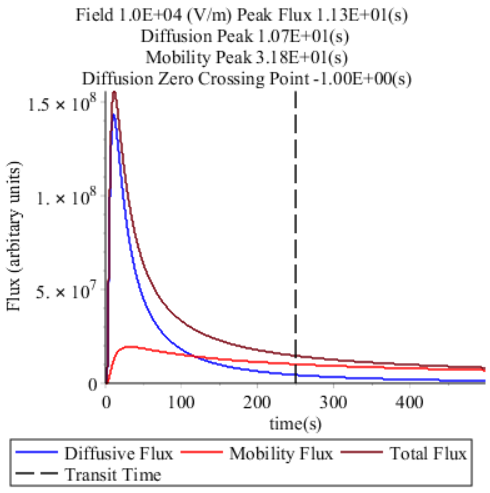

(b) E=20kV/m

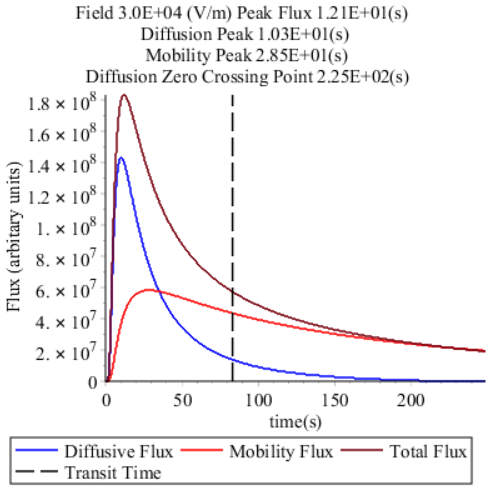

(c) E=30kV/m

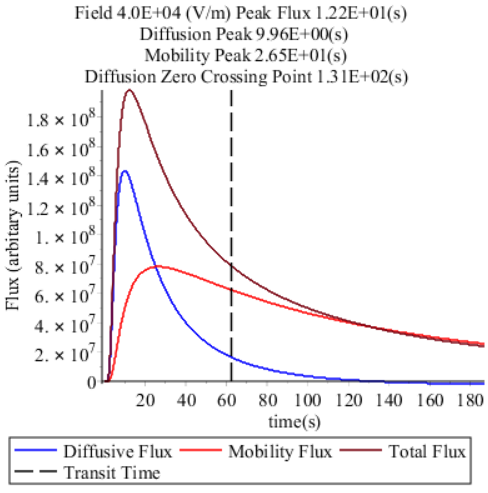

(d) E=40kV/m

Figure 3-16 (a)-(d) Development of total flux profile with time

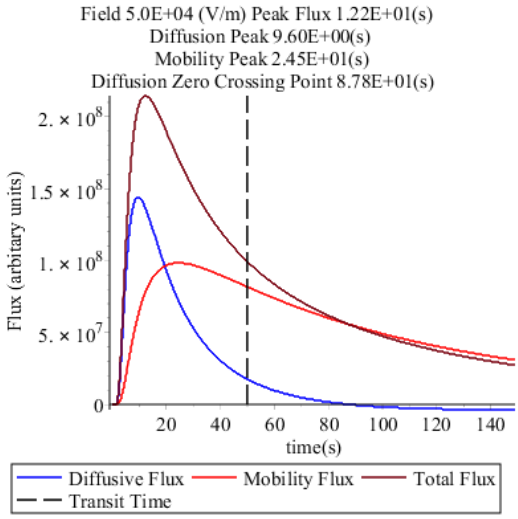

(e) E=50kV/m

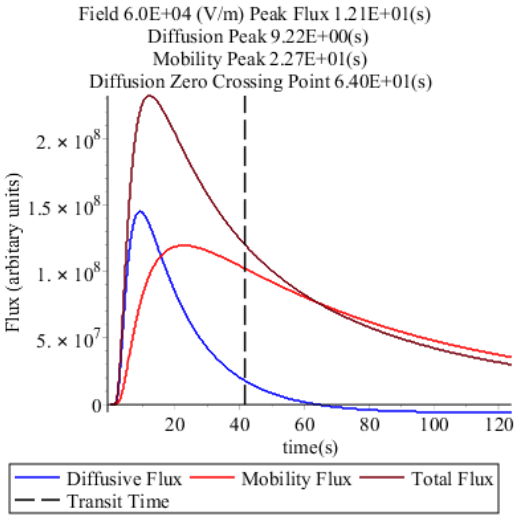

(f) E=60kV/m

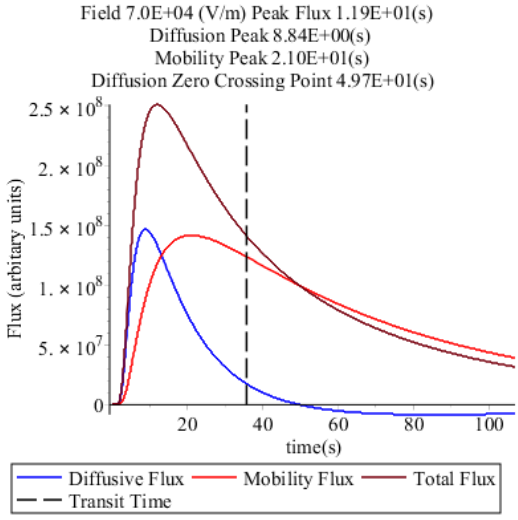

(g) E=70kV/m

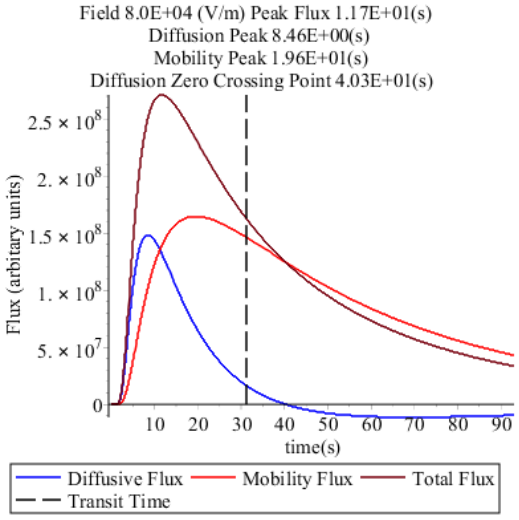

(h) E=80kV/m

Figure 3-16 (e)-(h) Development of total flux profile with time

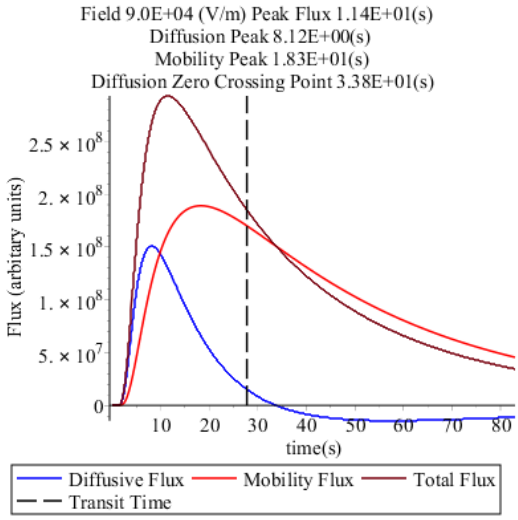

(i) E=90kV/m

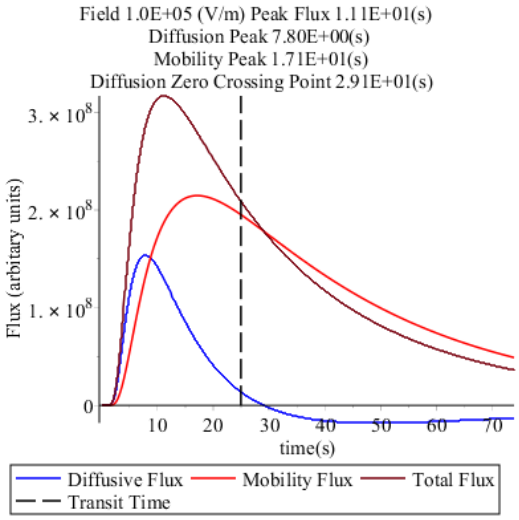

(j) E=100kV/m

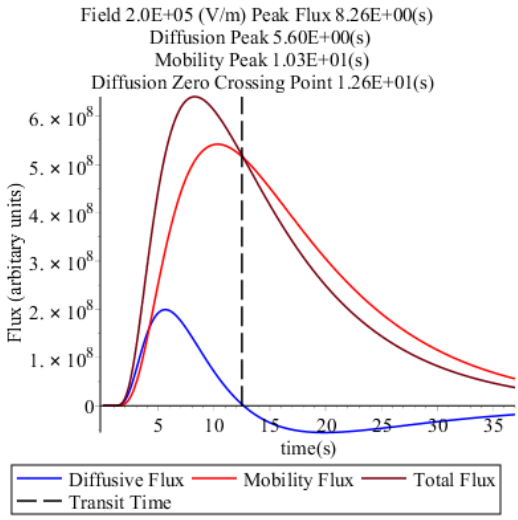

(k) E=200kV/m

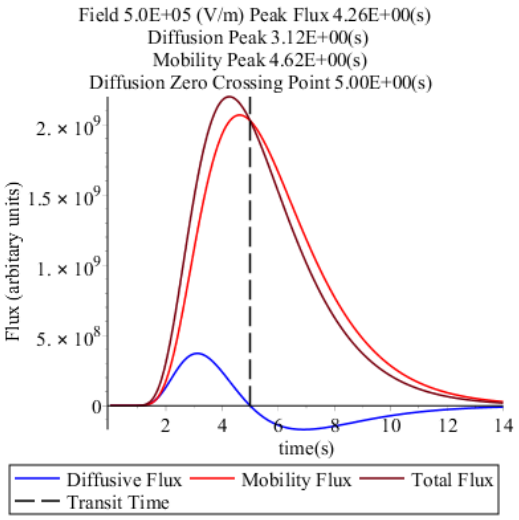

(l) E=500kV/m

Figure 3-16 (i)-(l) Development of total flux profile with time

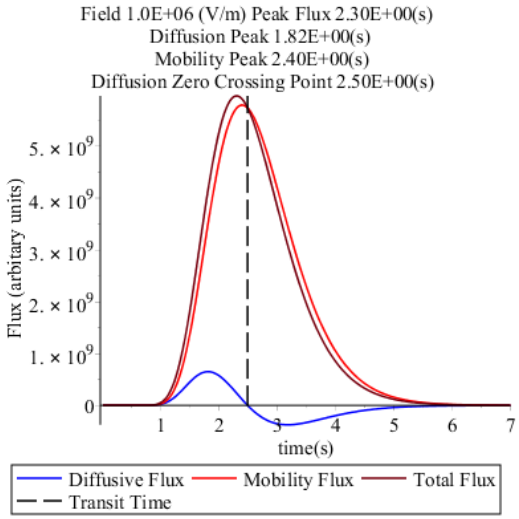

(m) E=1000kV/m

Figure 3-16 (m) Development of total flux profile with time

When a relatively low electric field (below 30kV/m) was applied to the system, the total flux passing through the plane of interest was dominated by the diffusion flux which is shown in Figure 3-16 (a) and Figure 3-16 (b). The peak position of the total flux was therefore close to that of the diffusion flux. When the applied field strength is increased above of 30kV/m, which is shown in Figure 3-16 (c) to Figure 3-16 (m), the influence of the mobility flux on the total flux increases and starts to become dominant at fields above 80Kv/m. When the applied field was increased to a range of 200kV/m to 1000kV/m, shown in Figure 3-16 (k) to Figure 3-16 (m), the total flux is almost entirely dominated by the mobility flux component. In this situation, the peak of the concentration distribution profile would be expected to pass through the plane of interest quickly within a short time.

From Figure 3-16, the peak of the diffusion flux always reaches the plane of interest earlier than the concentration at the plane of interest reaching its maximum value. Since the total flux is the combination of the two components the peak in the total flux will appear between the peaks of the diffusion flux component and the mobility flux component. As mentioned above, the time for both the peak of the mobility flux component and the peak of the diffusion flux component decrease with the increase of the electric field, therefore the predicted time for the peak in the total flux should also decrease with the increase in applied field. This is the case for fields above 60kV/m. However, as shown in Table 3-1, at lower fields the peak position

seems to increase slightly with increasing field reaching a maximum value. This is due to the increasing effect of the mobility flux component. The peak of the total flux can be "dragged" backward by the peak of the mobility flux component, moving relatively closer to this longer peak time. Therefore a peak of the time of total flux could be observed with the increase of electric field due to the interaction between mobility flux component and the diffusion flux component.

Behaviours of the concentration distribution profile with an applied field of 200kV/m to 1000kV/m are plotted in Figure 3-17 with the purpose to investigate the motion of charge carriers in a high field scenario.

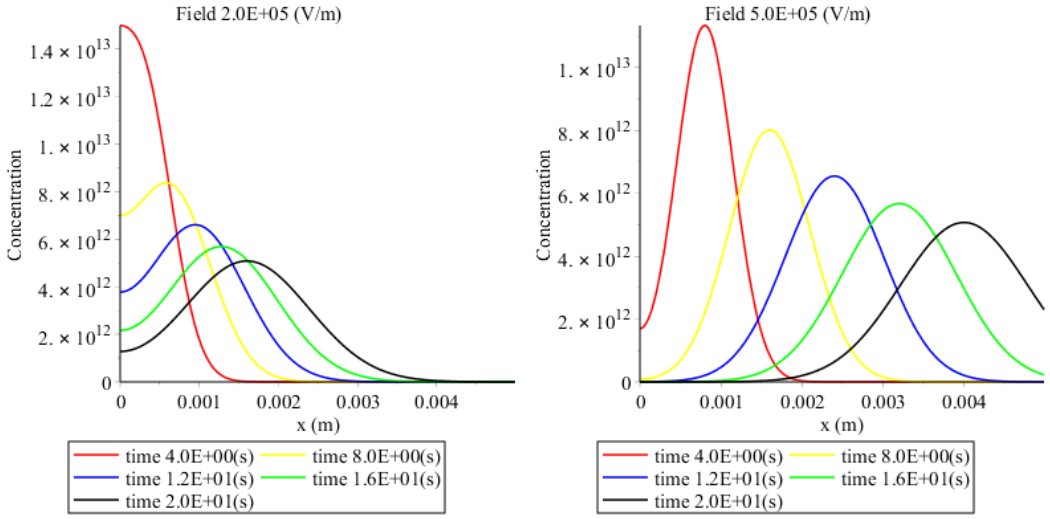

(a) E=200kV/m **(b) E=500kV/m**

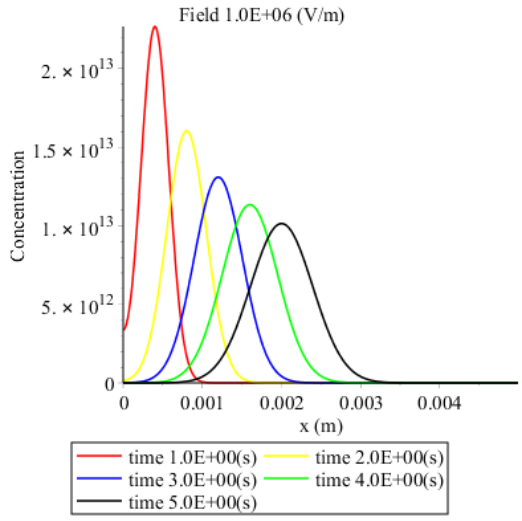

(c) E=1000kV/m

Figure 3-17 Concentration distribution profiles at high field

Figure 3-17 indicates that with a relatively stronger field applied, the concentration profiles move past the plane of interest with more obvious peak position. In addition, the influence caused by the reflection flux is reduced since charge carriers were swept away from the electrode quickly due to the high electric field. Therefore, less charge carriers would be expected to be able to be blocked and reflected by the electrode.

It is interesting to note that the expression of solution for one dimensional diffusion of Dirac delta concentration distribution is identical to the normal distribution, which from the author's understanding is logically reasonable.

Comparing Equation 3-43 with the equation for the normal distribution with mean μ and standard deviation σ Equation 3-60

$$C(x,t,E) = N\frac{1}{\sqrt{4\pi Dt}}\exp\left(-\frac{\left(x-\frac{q}{kT}DEt\right)^2}{4Dt}\right) \qquad \textbf{3-43}$$

$$\mathrm{f}(x) = \frac{1}{\sqrt{2\sigma'^2\pi}}\exp\left(-\frac{(x-\mu')^2}{2\sigma'^2}\right) \qquad \textbf{3-62}$$

It can be seen that the equations take essentially identical forms with the following correspondences:

$$\sigma' \widehat{=} \sqrt{2Dt}$$
$$\mu' \widehat{=} \frac{q}{kT}DEt \qquad \textbf{3-63}$$

The term $\sqrt{2Dt}$ therefore gives information about the degree by which the initial distribution of charge carriers has become spread over time t while the term $\frac{q}{kT}DEt$ represents the distance that the centre of the distribution has moved under the influence of the applied field E in the same time interval.

Applying a criteria that for an acceptable measurement the spread in the distribution of charge carriers at time t should be a fraction λ of the displacement of the centre of the distribution, the terms in Equation 3-61 can be used to determine acceptable experimental conditions.

$$\sqrt{2Dt} = \lambda \frac{q}{kT} DEt$$

$$2Dt = \lambda^2 \left(\frac{q}{kT}\right)^2 D^2 E^2 t^2 \quad \textbf{3-64}$$

Equation 3-64 can be simplified into the form:

$$\frac{2}{\lambda^2} = \left(\frac{q}{kT}\right)^2 DE^2 t \quad \textbf{3-65}$$

Using Einstein's relationship, Equation 3-65 can be rewritten in terms of the mobility.

$$\frac{2}{\lambda^2} = \frac{q}{kT} \mu E^2 t \quad \textbf{3-66}$$

Substituting the expected distance d travelled by the centre of the distribution in time t:

$$d = \mu E t \quad \textbf{3-67}$$

Into Equation 3-66 gives:

$$\frac{2}{\lambda^2} = \frac{q}{kT} Ed \quad \textbf{3-68}$$

And if it is assumed that d represents the distance between the electrodes the measurement voltage required to satisfy the condition in Equation 3-64 can be then defined as:

$$V = \frac{2}{\lambda^2} \frac{kT}{q} \quad \textbf{3-69}$$

This simple model indicates that the connection between the apparent mobility measured from the time of flight of the current transient and the actual mobility of the charge carriers may be weak and should be approached with caution. An approach to calculate appropriate voltages that can be applied to the system to achieve results where the diffusive effects on the moving ion distribution do not play a major role has been suggested. More detailed analysis including the presence of a second blocking electrode is required. The presence of this electrode will tend to

reduce the concentration gradients in the system and increase the concentration values in the system. The effect of a second blocking electrode cannot be modeled realistically by adding further distributions to the system obeying Fick's second law modified by mobility. Alternative numerical modeling approaches are therefore required to explore the behaviour of the system.

3.6. SUMMARY

Some of the background about the measurement of conductivity and mobility of charge carriers has been reviewed. The possible effects of Schottky charge injection processes has been briefly introduced and the possible effects of Electrohydrodynamic liquid motion on the mobility and conductivity has been discussed. A simple analytical model based on Fick's second law modified to include mobility has been developed to examine the influence of diffusion on TOF mobility measurements. This indicates that the apparent mobility measured from the time of flight does not necessarily relate to the actual mobility of the charge carriers. A possible criteria to determine the conditions for the time of flight methods to be a valid and accurate method for the investigation of the mobility of charge carriers is suggested based on the model.

4. NANO PARTICLES

4.1. INTRODUCTION

Background knowledge about the nature and characteristics of nanoparticles will be briefly reviewed in this chapter. The development of the methods of modification of insulating oil by adding nanoparticles will be introduced. Effects of nanoparticles on breakdown strength and the conductivity of liquid will be discussed. Some earlier related studies with different kinds of nanoparticles will be introduced.

4.2. REVIEW OF NANO PARTICLES IN GENERAL

Nanometre is one of the units of measurement of length, and 1nm equals 10^{-9}m. In a broad sense, nanomaterial is a material where at least one dimension of the size in microstructure is within a range of 0.1-100nm. There are different kinds of nanomaterial such as: metallic materials, inorganic non-metallic materials or polymer materials. There are a lot of nanoparticles in nature, such as soot particles and atmospheric dust. Its size is between molecular or atomic particles and macroscopic objects. When a substance has dimensions of the order of a nanometre, because of quantum effects, surface effects and interface effects, qualitative change will occur to the properties of such a substance, showing many special phenomena that are different from a macroscopic object or a single microscopic atom and molecule [**73**]. Taking a lotus leaf for instance, the surfaces of the lotus leaf and lotus flower have special micron-scale protuberances and nano-scale burrs so that they exhibit a macroscopic hydrophobicity; when a water droplet falls to the surface, it will not spread out, but form a ball under the surface tension [**74**]. Figure 4-1 shows the Protuberances on the leaf surface of lotus under a microscope.

These changes of properties as a result of nanoscale structures make research on nanotechnology and nanocomposites of great value to the development of new materials. It is widely believed that nanotechnology originated in a speech delivered by Richard Phillips Feynman, a physicist from the United States, in December 1959 gave the idea of “maneuvering things atom by atom”. Later, Norio Taniguchi, a professor from Tokyo, proposed the term nanotechnology formally in 1974 [**75**]. In 1994, T.J Lewis first proposed the concept of nanometric dielectrics [**44**]. In 1993, Choi et al. in the US Argonne National Laboratory proposed the concept of nanofluid

as a new class of heat transfer fluids [**76**]. Nanofluid means a suspension formed by adding nanoparticles to a liquid medium through a certain way. As nanoparticles have a relatively larger specific surface area, transmission of heat through the interface between particle and liquid will be accelerated by adding nanoparticles to a liquid. Therefore, the nanofluid usually shows good thermal conductivity.

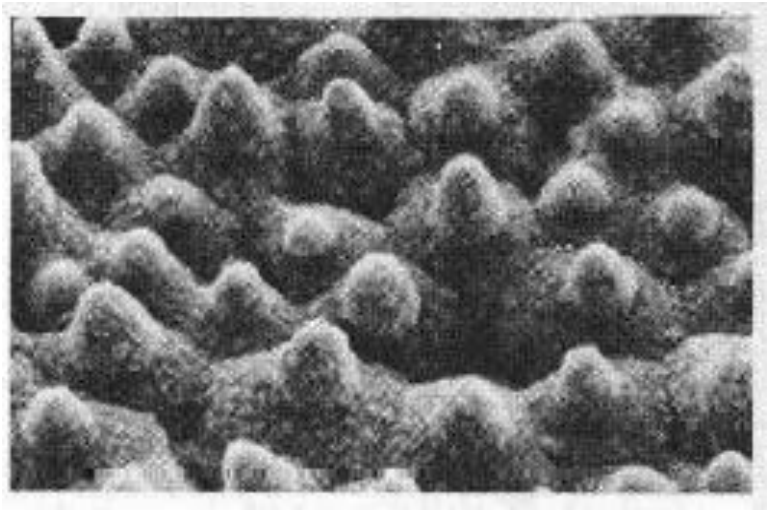

Figure 4-1 Protuberances on the leaf surface of lotus [74**]**

4.3. REVIEW OF NANO COMPOSITES (SOLID)

Composite materials are widely used in various fields due to their excellent overall performance. A nanoparticle composite material consists of a common material (such as resin, rubber, ceramic, metal, etc.) as the matrix with nano-sized materials added in an appropriate method so that the nano components can separate uniformly in the original matrix material.

In 1990, Y. Kojima, et al. from Tokyo successfully developed the first nanoparticle composite material [**77**].This material was originally developed in order to improve the mechanical and thermal properties of timing belt covers. Subsequently, T.J Lewis published a series of articles [**44**] [**78**] [**79**] [**48**] introducing the concept of nano dielectrics and suggesting that the nanocomposite has its unique properties mainly due to its interface effects. Generally, for nanocomposite materials, the smaller the size of a particle added, the more significant the impact of the interface effects. In 2001, the definition of nanodielectric was given by [**80**] :

"In the context, a nanodielectric would consist of a multi component dielectric possessing nanostructures, the presence of which lead to changes of one or several of its dielectric properties."

In the 21st century, T. Imai showed that adding a small amount of nano-fillers into an organic matrix (epoxy) can also improve the thermal and mechanical properties of the composite material [**81**]. Later, J.K Nelson discovered by studying the resin containing TiO_2 nanoparticles that adding TiO_2 nanoparticles changed the dielectric constant and dielectric loss of a material significantly [**82**]. Afterwards, nanocomposites became an important direction for the development of dielectric materials with modified and improved properties.

4.4. CHARACTERISTICS OF NANOMATERIAL

With the development of nanotechnology, many characteristics of nanometre material were found, such as: small dimension effect, quantum dimension effect, surface effect, macroscopic quantum tunnel effects and so on [**83**] [**84**]. A brief introduction of two main effects relating to this project will be given in this section.

4.4.1. SURFACE EFFECT

The surface effect of a nanomaterial means the change in nature after the ratio of number of surface atoms and total number of atoms in a nanoparticle increases sharply as the radius of particle decreases. For a nanoparticle, when the particle size is 10nm or less, reducing the particle size can significantly increase the proportion of surface atoms; when the particle size is reduced to 1nm, the proportion of surface atoms can reach more than about 90% [**85**]. Most atoms are concentrated on the surface of a nanoparticle. The presence of the surface atoms gives a high chemical activity to the particle leading to stronger interactions with their surroundings. Therefore nanoparticles usually have a high surface energy.

4.4.2. SMALL DIMENSION EFFECT

The small dimension effect means significant changes in macroscopic physical and chemical properties on a substance when a particle of the substance is reduced to the nanometre scale. This effect makes the material show in a variety of aspects such as mechanics, optics and magnetism, special properties different from a macroscopic

material, one example is enhanced absorption of light; when a particle of a metallic material is reduced to the nanometre scale, it will lose its original colour and showing a black colour. Using this property can produce high-efficiency solar collection equipment. It is also found that, the melting points of many solid materials in nano-scale are significantly lower than those of macroscopic objects due to this small dimension effect, e.g. some silver nanoparticles have a very low melting point (about 373K) [**84**].

4.5. NANO PARTICLES IN LIQUIDS

Before the discussion of the behaviour of Nanoparticles in liquids, it is useful to have a brief description about the liquid insulation materials. Liquid insulation materials are commonly used in many dielectric devices in combination with solid insulation materials as they can easily fill up any spaces which form weak regions in the insulation system. Insulating oil for instance is one of the most widely known liquid insulating materials and has been used in many transformers in the electric transmission system. The convective phenomenon of the insulating oil can help to dissipate the heat generated by the transformers during their service time.

Another advantage of using liquid insulation is its self-healing capability. For solid insulation, once a breakdown happens, the insulation is unlikely to recover its electrical strength. For liquid insulation, fresh insulating oil can move into the region of breakdown so that the overall electrical breakdown strength after the discharge event doesn't change significantly.

The initial aim of adding nanoparticles into insulating oil was to improve the thermal conductivity of insulating oil so that the temperature of the core and coil parts of the transformer can be reduced during operation. Early in 1990s, Segal et al investigated the effect of dispersing magnetite nanoparticles in to the insulating oil and found that the breakdown strength was increased by 50% from the initial pure mineral insulating oil with a positive impulse voltage applied [**86**]. Their research results suggest that the nanofluid made by adding nanoparticles suspensions into insulating oils might be an effective alternative material to traditional transformer oil with improved thermal and dielectric characteristics. Since then, insulating oils with nanoparticles suspension are an area of research interest.

As the diameter of the nanoparticles is very small, atoms at the surface of the nanoparticle have a very high chemical activity. For this reason, when adding a nanoparticle material to a liquid, nanoparticles in a liquid will tend to aggregate. Once nanoparticle aggregate, the size of the particles formed may reach the micron level. As a result, the special properties of nanoparticle will disappear and the particles themselves may leave suspension and form a precipitate. Appropriate modification to the surface of the nanoparticles to improve the dispersibility of nanoparticles so that they can exist stably in liquid is a key field of nanoparticles science and technology.

4.6. DISPERSION: SURFACE TREATMENTS AND SURFACTANTS.

As mentioned above, since the surface area of a nanoparticle is large, atoms with high chemical activity are likely to combine with other particles in the liquid, consequently lead to the aggregation of nanoparticles. Van der Waals and Coulomb force or other chemical bonding processes such as hydrogen bonding may be the causes of nanoparticle aggregation. For nanofluid manufacture, the nanoparticles must be well dispersed and prevented from aggregating. This is commonly addressed with the following methods:

- **Mechanical stirring/agitation:**

This is a conventional method to disperse a liquid or solid into another liquid. A rotary magnetic stirrer, for instance, is commonly used for stirring and mixing in the lab. This approach is useful to disperse the nanoparticles in the fluid.

- **Ultrasonic treatment:**

The cavitation due to ultrasonic waves can produce tiny bubbles in a liquid, and the energy from the collapse of bubbles can cause the nanoparticles to overcome the attraction force, preventing their aggregation. This method may also break any existing nanoparticle aggregation due to Van der Waals attraction force so that they can uniformly disperse in the liquid.

- **Surfactant:**

However, once the nanoparticles have been dispersed, the aggregation of nanoparticles can still occur. The long term stability of a nanofluid is mainly related

to the surface properties of nanoparticles. These can be modified by adding a surfactant into the nanoparticle suspension which has been shown to be an effective way to prevent the nanoparticles aggregation [**87**]. Surfactant molecules attach to the surface of a nanoparticle forming a layer on the surface of the nanoparticle due to intermolecular forces (Van der Waals force, Hydrogen bonding, etc.) [**88**]. This layer of surfactant molecules prevents the aggregation between nanoparticles so that the nanoparticles can uniformly disperse in a liquid. The common way of selecting surfactant follows the principle of similarity and intermiscibility. Oleic acid, a hydrocarbon based organic acid is similar to and therefore miscible with oils and is the common surfactants associated with the nanofluid in this project. Previous research made by Li Jian et al [83] indicate that oleic acid modified Fe_3O_4 nanoparticles suspension in vegetable oil shows a much better stability compared with vegetable oil with unmodified Fe_3O_4 nanoparticles added.

4.7. EFFECTS OF NANO PARTICLES ON BREAKDOWN BEHAVIOURS

It was originally believed that adding a conductive substance into a dielectric would increase its conductivity and that impurities and contamination of an insulating oil lead to a reduction in its insulating properties. However, in 1998, V. Segal et al. found that the addition of Fe_3O_4 nanoparticles to insulating oil can significantly improve its impulse breakdown strength [**86**]. However, the influence of adding nanoparticles to the insulating oil on its breakdown strength cannot be simply judged. In 2004, Kopwansky et al. indicate that the separation of magnetic nanoparticles is strongly dependent on the distribution of the external magnetic field. If the external magnetic field is parallel to the electric field, the magnetic nanoparticles will gather together to form a path between the two electrodes. In this case, the breakdown strength will be decreased [**89**].

Streamer propagation is used to explain the breakdown mechanism in liquids is reviewed and discussed by Lewis in [**90**]. The streamer is a gas cavity generated in the liquid which contains large numbers of ions and electrons and regions of space charge at the tip and tail. The presence of free charges in the high field region generated by the space charge plays an important role during the propagation of the streamer. Generally, the development of a streamer in transformer oil is caused by a

strong local electric field due to the injection of electrons and accumulation of space charge near the electrode. Therefore, the charge migration is also an important factor in determining the initiation and development of the streamer. In insulating oil, the free electrons can make the molecules polarize or combine with the molecules to form negatively charged ions. Under the influence of the applied electric field, these ions may migrate. During the process of migration, an electron can separate from an ion and move to a new liquid molecule to form a new ion. Through this continuous movement, the electrons can jump between the molecules of liquid moving more rapidly than the ions. In this process, Electron traps that capture free electrons are present around the liquid molecules, and the depths of such traps depend on the structures of liquid molecules and interaction between them [**91**]. Once a streamer is created in the insulating liquid, a space charge region will be formed at the "head" of the streamer which will enhance the local electric field. More free electrons will be accelerated, resulting further ionization at the head of the streamer. After adding nanoparticles to insulating oil, the nanoparticles in insulating oil could provide more electron traps. Free electrons produced by ionization will be captured by these traps [**92**]. These electron traps would reduce the migration rate and the energy of free mobile electrons for the streamer propagation mechanism. This would consequently, improve the dielectric strength of the liquid. Studies made by Chen Yilong et al [**93**] suggest that the density of electron traps per unit volume in the insulating oil can be increased by adding semiconducting TiO_2 nanoparticles. The adding of TiO_2 nanoparticles improved the insulating oil's ability to capture free ions significantly. Experiments made by Wenxia Sima et al. [**92**] also indicates that potential wells can be formed at the surface of different kinds of nanoparticles in the insulating oil. The presence of potential well could trap free charges passing through the area close to the nanoparticle so that the breakdown strength of the liquid can be improved.

On the other hand, the nanoparticles in insulating oil can also move freely. The flow of insulating oil liquid and Brownian movement of insulating oil molecules may result in changes of distance between nanoparticles. The electrons in insulating oil will continue to be captured by the electron traps and then released. During this electron capture and escape, a part of the energy of the electron will be lost in the form of heat radiation. The average energy of an electron will be reduced, therefore,

high-energy electrons which are able to lead to electron avalanche are less likely to be formed and the development of streamers will be inhibited.

A possible explanation for the behaviour of adding a conductive contaminant to an insulating liquid increasing its breakdown strength was made by Hwang et al [**94**] [**95**]who considered the charge relaxation time constant and electron trapping by conductive nanoparticles. This approach was extended to semiconducting and insulating nanoparticles by studies made by Takada et al. [**96**], Du et al. [**5**] [**91**] [**97**] [**98**] and Zhou et al. [**99**]. Hwang et al [**94**] put forward a theory for electron capture and constructed an electrodynamic model to explain the change mechanism for breakdown characteristics of transformer oil after adding nanoparticles. According to this theory, the impact of nanoparticles on the performance of insulating oil depends mainly on the relaxation time of the nanoparticles. This relaxation time gives the information of the time interval between the moment when an electric field is applied and the moment when the nanoparticles is "fully charged" (no more free charges can be captured by the traps generated by the nanoparticles).

A model for the deviation of electric field distribution relating to the presence of the nanoparticle in insulating oil under d.c electric field stress was introduced in [**100**] as illustrated in Figure 4-2.

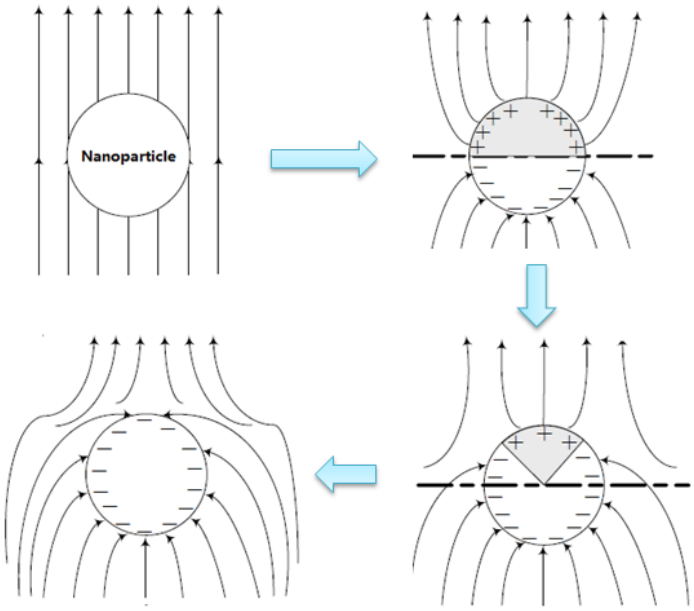

Figure 4-2 Polarization of nanoparticles under d.c. electric field [92**]**

Consider a nanoparticle of an arbitrary material with radius R, permittivity ε_2 and conductivity σ_2, immersed in the insulating oil, which has a permittivity ε_1 and conductivity σ_1. Ignoring the effect of any appreciable space charge, the relaxation time constant for a transformer oil-nanoparticle system can generally be expressed as:

$$\tau = \frac{2\varepsilon_1 + \varepsilon_2}{2\sigma_1 + \sigma_2} \qquad \textbf{4-1}$$

This relaxation time is obtained based on the electric field distribution outside the nanoparticle which is calculated by analysis of the electrostatic potential with the boundary conditions. The derivation procedure of this theory is not included in this thesis, but can be found in [**100**].

The polarization of the nanoparticle leads to an electric field distribution where electrons will be attracted to the nanoparticle and be trapped. This process continues until the charge on the nanoparticle is such that no further electrons can be captured. If the relaxation time of a nanoparticle is smaller than the insulating oil streamer growing time the nanoparticle will become polarized and be able to capture the fast-moving free electrons in the insulating oil and form anions with slower migration rate, thereby effectively reducing the movement speed of electrons, and inhibiting the development of the streamer. This leads to an increase in the breakdown voltage of liquid. If the time constant of the particle is larger than the streamer growth time, the polarization of the nanoparticle cannot develop in time to attract and trap the electrons to prevent them from contributing to streamer development. It is therefore expected that with longer time constants that the nanoparticles would not increase the breakdown strength.

Their studies suggest that the charges relating to the polarization in the semi-conducting or insulating nanoparticles suspension could trap the free electrons during the development of streamer, which gives an explanation of why these kinds of nanoparticles could increase the insulating oil's breakdown strength. In these mechanisms the charge relaxation time constant must be smaller than the time associated with streamer growth in the liquid to allow the nanoparticles to capture free electrons before they can take part in the streamer propagation process. However work performed by Chiesa et al. in 2009 [**101**], showed that adding silicon carbide

(SiC) conductive nanoparticles with a very short relaxation time constant ($\tau = 1.1 \times 10^{-12}$s) did not increase the insulating oil's breakdown strength. Later experiments performed by Zhou Yuanxiang in 2010 [**99**] showed that adding nanoparticles with a relatively long relaxation time constant (τ =42.5s) could increase the breakdown strength of transformer oil. In addition, experiments made by Du et al also suggested that by adding TiO_2 semiconductive nanoparticles with long relaxation time (τ =77s), the AC and impulse breakdown strength of transformer oil can be improved [**5**]. These results are inconsistent with the theories originating with Hwang et al [**94**] but the presence of electron traps close to the nanoparticle proposed by [**93**] and [**92**] provides an alternative mechanism for the change in breakdown strength observed in the long relaxation time nanoparticles [**99**].

4.8. EFFECT OF NANO PARTICLES ON CONDUCTIVITY

It was found that the conductivity of insulating oil could be changed by adding nanoparticles [**102**]. In this project, nanoparticles were added into the insulating oil samples during the measurements. Therefore the influence of nanoparticles presence on the conductivity measurements requires to be considered. It has been shown that nanoparticles have attractive interaction for free electrons leading to charge trapping which has been discussed in section 4.7 [**92**] [**94**] [**95**]. Free electrons become trapped so as to be bound around the nanoparticle. Figure 4-3(a) illustrates the situations without any electric field being applied to a nanofluid. Space traps formed between nanoparticles in the insulting liquid perform like "seats of free charges" where free electron could stay stably. In the absence of electric field, the electrons with sufficient energy could overcome the energy barrier between "seats" and transfer through the liquid in either direction. The possibility of electrons hopping towards either side would be equal. When an electric field is applied to the nanofluid, as illustrated in Figure 4-3(b), the energy potential of free electrons was changed. Application of an electric field leads to a voltage drop across the electrodes. This means that the probability of an electron transferring between traps in the direction of the field is reduced while the probability of transfer in the opposite direction is increased, Figure 4-3 (b).

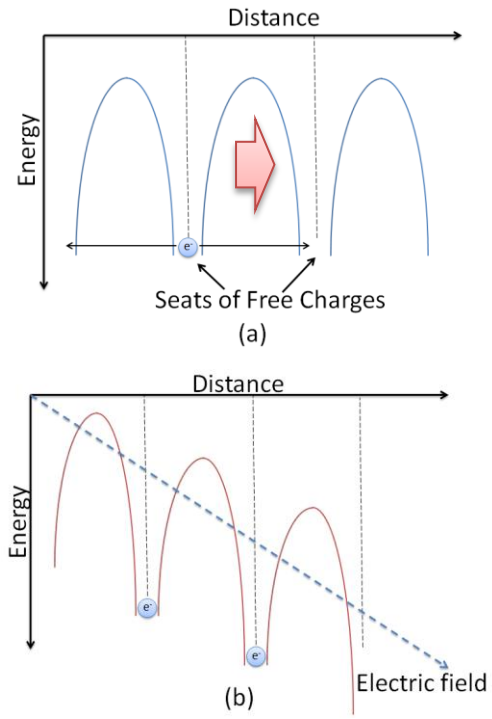

Figure 4-3 Transfer of free electrons (a): without electric field; (b): electric field applied

The effect of increasing the concentration of nanoparticles on the conductivity of an insulating liquid can be analyzed from two aspects that are closely related to equation 4-2.

$$\mathrm{J} = N \cdot q \cdot \mu \cdot \mathrm{E} \qquad \textbf{4-2}$$

Where: J is the current density; N is the total number of charge carriers per unit volume; q is the charge of electron; μ is the mobility of charge carriers and E is the electric field.

Increasing the concentration of nanoparticles leads to an increase in the number of free electron traps. In another words, the "seats" for free charges in the liquid per unit volume are increased due to the presence of nanoparticles. This could increase the opportunities for charge injection into the system effectively increasing the value of N in equation 4-2. Recently, a study performed by Lv indicates that adding TiO_2 nanoparticles into aged mineral oil could lead to a higher trap density and shallower trap energy level, which could allow the charge carriers to transfer more rapidly through the liquid material [**103**].

In addition, the average separation of the "seats" for free charge is also reduced as the concentration of nanoparticles increases. This means that a bonded electron has more opportunities to transfer from one trap to another, so as to increase the diffusion effect of charge carriers. From the discussion of Einstein's relationship in section 3.5.1, the diffusion effect of charge carriers is proportional to the mobility of charge carrier, therefore, the mobility of charge carriers μ in equation 4-2 can be increased by the increase of the concentration of nanoparticles.

With constant electric field strength, increasing the concentration of nanoparticles leads to an increase of both number of charge carriers N and mobility of charge carriers μ. This should lead to a higher current density and a higher conductivity of the liquid insulating materials and consequently leading to more energy losses in the power system.

4.9. STABILITY OF A COLLOIDAL SUSPENSION

When nanoparticles are added to an insulating liquid, a double layer structure similar to that described in section 3.2.1 is formed. This double layer structure is related to the stability of a colloidal suspension. When a nanoparticle is immersed into a liquid, the electro double layer can be formed at the surface of the particle. Ions will be attracted to move towards the particles under the effect of the coulomb force. The concentration of counter-ions around the particle will be higher than that in the bulk of liquid away from the particle. When two particles in the liquid approach each other, the concentration of counter-ions between the two electric double layers will be relatively higher than the equilibrium value. More liquid molecules will tend to flow into the region between the particles to reduce the concentration. This leads to a repulsive osmotic force between these two particles which increases as the particles approach each other. In addition, the force due to the interaction between the two double layers surrounding the particles also contributes a part of the total repulsive force.

In spite of the drag force which would prevent the movement of particles in the liquid, the force balance for one immersed particles can be written as:

$$F_V + F_R = 0$$

Where, F_V stands for the Van der Waals attractive force between the particles and the F_R stands for the total repulsion force between the two particles. If the relative position of these two particles changes, the potential energy of the particles will change as well. Therefore the potential energy distribution can be qualitatively analysed associated with the separation distance between two particles. Figure 4-4 below shows the potential energy distribution associated with the separation distance between two particles immersed in a liquid.

There are three possible scenarios that depend on the interaction between Van der Waal force and the repulsive force [**104**]. The potential energy under the effect of the repulsive force and the potential energy under the effect of Van der Waal force as a function of distance from the surface of a spherical particle are plotted as dashed line in Figure 4-4.

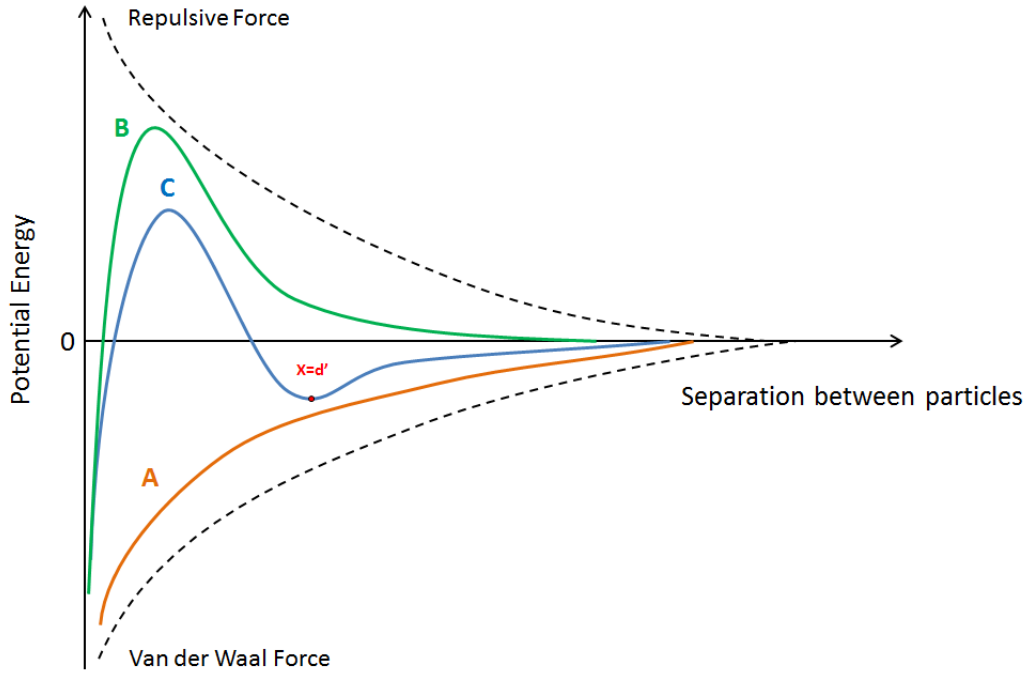

Figure 4-4 Potential energy distribution

Three possible combinations of the two opposite potentials are plotted as solid lines name by A, B and C, respectively. At infinity, the van der Waals potential and electrostatic potential should be zero. An absolute minimum of potential energy occurs at the distance very close to the surface due to the van der Waals force.

1. Scenario A represents the situation when the Van der Waal attractive force is always significantly larger than the repulsive force over different positions. In this case, the particles in liquid are likely to aggregate together since particles tend to stay at lower potential region. Aggregation of nanoparticles can be observed definitely in the liquid.
2. Scenario B represents the case that the Van der Waal force is much larger than the repulsive force when the separation reduces and particles are quite close to each other. However, the attractive force decreases very rapidly with the increase of separation. In this case, once the separation between particles is sufficiently long enough, the electrostatic repulsive force dominates the van der Waals force between particles and particles tend to "push away" the other particles. The maximum in the potential energy is known as repulsive barrier. If the barrier is significantly greater than the thermal energy of the particles that the Brownian motion cannot overcome this barrier, the aggregation of particles will not be able to occur. Particles can form a stable suspension in the liquid if their thermal energy is lower than the potential barrier.
3. Scenario C represents the situation that might happen in some nanoparticle suspensions, when the Van der Waal force has the same order as the repulsive force. In this case, there will be a maximum and a second minimum in the potential energy. At the point of the maximum potential energy, the net force will be zero. However, the particles will be most unlikely to stay in this position. Particles would either tend to aggregate with each other to reach the absolute minimum or tend to move away from each other until they reach a stable stage where the potential energy is equal to the second minimum value.

4.10. NANO PARTICLES IN LIQUIDS: WHAT HAS BEEN USED

In theory, many different types of nanoparticles can be added to a liquid insulator to improve its insulation performance. Nanoparticles commonly used in liquid include: Fe_3O_4, TiO_2, Al_2O_3, ZnO [**105**] [**102**], Silica (SiO_2) [**106**] and Boron nitride (BN) [**107**]

Among these nanoparticles, metal oxide nanoparticles (such as Al_2O_3, Fe_3O_4, and TiO_2) are the most widely used. This is probably because their prices are relatively low, and they are stable at ambient temperatures which make them relatively easy to prepare compared to other types of nanoparticles. Since it was observed that adding nanoparticles to insulating oil can improve the insulating properties, many studies have been performed, adding various types of nanoparticles to different types of insulating oil in order to be able to find suitable nanofluid with improved properties to replace the conventional insulating oil.

- **Fe_3O_4**

  As mentioned previously, the study of Fe_3O_4 magnetite nanoparticles started in 1998 by Segal et al who investigated the improvement of both AC and impulse breakdown strength by adding Fe_3O_4 nanoparticles to insulating oil. After that, many studies of Fe_3O_4 Ferrofluid associated with different type of insulating oils have been done [**108**] [**109**] [**110**] [**111**] [**112**]. Generally speaking, consistent with the research of Segal, these studies suggest that the breakdown properties of insulating oil can be modified by adding Fe_3O_4 nanoparticles added in many different conditions. It is worth mentioning that, with the increasing concentration of Fe_3O_4 nanoparticles, the viscosity of the nanoparticle suspension also increases.

- **TiO_2**

  The effects of adding titanium dioxide (TiO_2) nanoparticles to insulating oil on its breakdown strength has been investigated in [**5**] [**29**] [**91**] [**97**] [**98**] [**113**] [**114**] [**115**] [**116**]. Unlike the Fe_3O_4 magnetic nanoparticles, the TiO_2 nanoparticles show a better stability in the insulating oil in the presence of magnetic fields. These studies indicate that addition of TiO_2 nanoparticles could enhance the insulating oil's AC and impulse dielectric strength. However, compared with the Fe_3O_4 based nanofluids the enhancement of breakdown strength was less significant. Also, it was noted that the surfactant used to modifying the TiO_2 nanoparticles may also affect the insulating oil's dielectric performance. For example, TiO_2 nanoparticles modified by silicone oil could decrease the breakdown strength of the insulating oil [**116**] .

- **Al_2O_3**

Both the positive and negative impulse breakdown of aluminium oxide (Al_2O_3) based nanofluid were investigated by [**117**]. According to their experiment results, adding Al_2O_3 nanoparticles to the mineral oil enhance the insulating oil's positive impulse breakdown strength. However, for negative impulse test, the pure insulating oil appears to have a higher breakdown strength compared with the Al_2O_3 nanofluid.

- **ZnO**

  The dielectric properties of insulating oil based zinc oxide nanofluid were investigated by [**105**] [**102**]. These researches suggested that the presence of ZnO nanoparticles could enhance the breakdown strength of the insulating oil. However, if the concentration of ZnO nanoparticles in the insulating oil was over 0.05vol%, a decrease of breakdown voltage was observed which might be caused by the agglomeration of nanoparticles in the insulating oil. Also, [**105**] suggested that the conductivity of insulating oil can be increased by adding ZnO nanoparticles. Possible explanation for this was given in detail in section 4.8.

- **SiO_2**

  AC breakdown strength test for silicon dioxide (SiO_2) based nanofluid was performed by Muhammad Rafiq et al [**106**]. The breakdown strength of insulating oil can be increased by adding high concentration of SiO_2 nanoparticles. As with ZnO, the measured conductivity of the insulation oil was observed to increase when the nano particles were added.

- **BN**

  A boron nitride (BN) based nanofluid was prepared by adding BN nanoparticles to vegetable oil in the study of B. X. Du [**107**]. An improvement in the breakdown strength due to the presence of BN nanoparticles was observed. However, for conductivity measurement, in contrast with the ZnO and SiO_2 based nanoparticles [**105**], [**106**], the conductivity of insulating oil exhibited a decrease by adding BN nanoparticles.

4.11. SUMMARY

This chapter has covered some basic concepts of nano technology. A brief introduction of the nanomaterial was given. Some background about nanofluid was

also introduced. Methods related to the dispersion of nanoparticles in liquid were reported. The effects of the presence of nanoparticles, in terms of electron trapping, on the liquid insulating materials especially for breakdown behaviours have been reviewed associated with the polarization of nanoparticles. Double layer structure associated with nanoparticles in liquid has also been introduced and discussed corresponding to the stability of a colloidal suspension. Basic concept of Einstein's relationship is introduced. Some previous studies of nanofluid prepared with different types of nanoparticles have been reviewed.

Generally speaking, nano-components can be added into liquid or solid insulating materials in order to modify their dielectric properties. Nanofluid exhibits a possibility to be used as substations of conventional transformer oils since the presence of nanoparticles could improve the breakdown strength and thermal conductivity of the insulating oil under many situations. However, more researches are necessary to complete the theoretical understanding of the influence of nanoparticles presences on liquid insulating properties and to investigate the effects of nanoparticles on the liquid insulating materials during ageing process.

5. AGEING TECHNIQUES

5.1. INTRODUCTION

In this chapter, the ageing processes used will be introduced. A liquid insulator, especially insulating oil, will be frequently subject to two types of ageing during normal operation, namely, thermal ageing and electric ageing. For most transformers, especially the high-voltage transformers, the average temperature of the insulating liquid is generally far above the ambient temperature during operation [**18**]. The operation temperature has been reported to reach over 100℃ around some key components such as low-voltage winding or the high-voltage winding a 154kV transformer [**118**]. A high temperature can speed up ageing of the insulating oil, change electric features of the insulating oil and increase the rate of degeneration of its insulation performance. Possibility of accidents due to aged insulating oil will increase greatly, so how to deeply study ageing features of the insulating oil is significant for the safety and stability of a liquid insulation system.

The background to ageing processes and the rates at which ageing will occur has been introduced in the Chapter 2. In this work only thermal stressing has been used. Initially, to accelerate the ageing process, copper was included with the liquid samples as it has been shown that it increases the ageing rate [**23**]. In later work the ageing rate was found to be sufficient so that copper was not needed to produce a suitably aged sample within a reasonable timescale. The degree of ageing was monitored by examining changes in the optical transmission properties of the samples. Estimates are also made using the Arrhenius relationship on the degree of acceleration of the ageing process that occurred.

5.2. INSULATING LIQUID

The elementary background knowledge on the liquid insulator has been introduced in the Chapter 2 [**119**]. Several different oils were considered as test materials including: Shell Diala S3 ZX-I insulating oil [**120**], a recycled mineral oil (EOS ltd L10b) and vegetable based oils. Shell Diala and the EOS mineral oil are colourless and transparent liquids while the vegetable oil is a pale yellow in colour. The properties and makeup of the Shell Diala and the EOS recycled oil are defined by the

manufacturers, for the vegetable oils the properties and makeup is not necessarily well defined depending on the source of the oil and any treatments or processing that has occurred. Vegetable based oils are attracting more and more attention as insulating oil [**121**] [**19**] [**28**]. They have acceptable insulating properties and have the advantage that they are renewably sourced and unlike mineral oils are biodegradable. The refining and production process of the vegetable oils have a lower environmental impact than those for mineral oils and the flash point is also higher, reducing fire risks. However, the oxidation stability of vegetable oil is not as good as petroleum-based oils [**122**]. At present vegetable oils are not extensively used as insulating oil as more work is required to characterize their insulation behaviour.

It was decided to use Shell Diala oil in this series of tests as a quantity of pure oil was available within the research group and the uncertainty of the consistency of vegetable oil samples existed.

5.3. AGEING METHODS USED

Samples of the Shell Diala insulation oil were poured into 250mL borosilicate glass reagent bottles. The lid of the bottle was placed over the top but not completely tightened. This prevented contamination of the oil but allowed access to air. The samples were then placed in an oven and the temperature was set to 120°C. Samples were generally aged for between 2 and 8 days.

In some initial ageing experiments copper was also added to oil specimen as it had been shown that this catalyzed ageing processes in oil [**19**] [**23**] [**123**] [**124**]. The copper came from the braiding of a coaxial cable and the mass of copper used was calculated from the surface area expected. A similar surface area as reported in [**19**] was used. Figure 5-1 shows samples of unaged oil and samples that have been aged for 2 days, 4 days and 8 days with and without copper present. Samples of oil that were not exposed to the high temperature are also shown. It can be seen that clear changes in the appearance of the oil have happened because of ageing with the samples becoming darker in appearance. At any ageing time the sample which contained copper is darker.

Figure 5-1 Aged Samples: Sample 1 and Copper 1 unaged; Sample 2 and Copper 2 aged for 2 days at 120°C; Sample 3 and Copper 3 aged for 4 days at 120°C; Sample 4 and Copper 4 aged for 8 days at 120°C.

5.4. AGEING DIAGNOSTICS UV/VIS SPECTROSCOPY

In general, a change of colour during the ageing process could be observed which is thought to be related to the oxidation of some components of the insulating oil [**19**]. A more quantitative measurement of the colour change due to ageing can be obtained through the Ultraviolet/ visible spectroscopy (Section 2.4.1.) In this project, the spectroscopy was carried out using a BioMate 5 using 3.5 ml plastic cuvettes. The transmission rate of unaged, 2 day aged, 4 day aged 6 day, 8 day aged and 16 day aged oil samples were measured in the wavelength range from 380 nm to 780 nm in steps of 1nm. Pure water was used as a reference during the light transmission measurements. The measured spectra for oil samples are shown in Figure 5-2. The results for samples aged with copper are not included in this section as it was decided not to use copper in the ageing process as described later in this section.

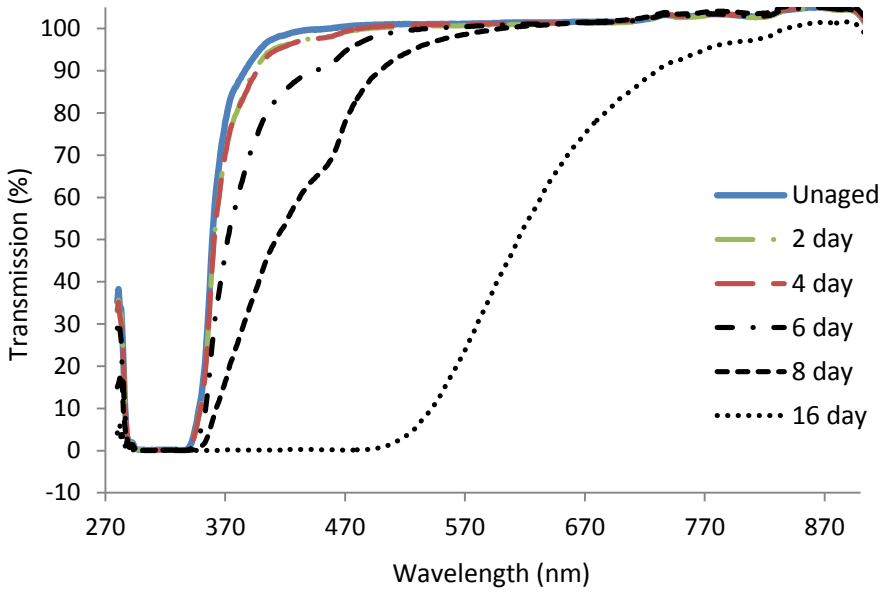

Figure 5-2 Change in transmission spectra for unaged and aged oil samples

A change of transmission at different wavelengths due to the darkening of the insulating oil can be observed from Figure 5-2. The broad transmission edge shifts from the ultraviolet side to UV/VIS side as the ageing time increased. The available spectral range using plastic cuvettes is in the range of 380 to 780 nm (visible spectrum).

Looking at the wavelength at which transmission is 20%, 50% and 80% provides an indicator of the extent of ageing, Figure 5-3.

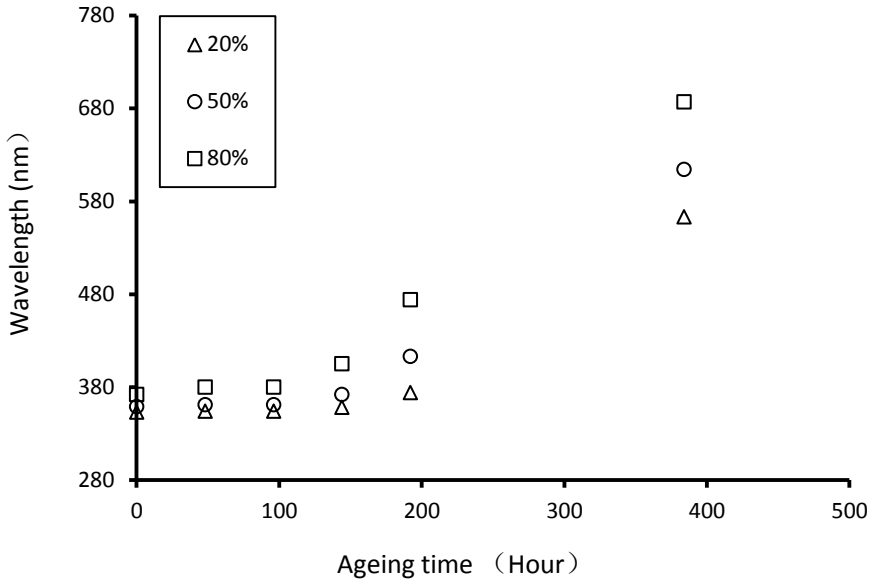

Figure 5-3 Cut off wavelengths for insulating oil samples

The thermal ageing process of insulation oil clearly leads to a reduction of light transmittance and shifts in the wavelength associated with 20%, 50% and 80% transmission. However a quantitative analysis of the degree of ageing is difficult as the measured cut off wavelength appears to have an upward trend with the increase of ageing time and the possible maximum value of cut off wavelength cannot be obtained. More samples aged for longer periods might be helpful to obtain a degradation criterion limit which can be used to estimate the degree of ageing. By knowing this criterion limit, relationship between the change of the colour and the change of some other key dielectric parameters (breakdown voltage, conductivity, etc.) can be established which could be used to further estimation the lifetime of the insulating oil.

After 6 days of ageing a precipitate was observed in samples aged with copper. This was also seen in samples without copper after 8 days and 16 days of ageing. Such precipitates have also been observed when a dodecyl benzene cable fluid was thermal aged for 840 hours at 105℃ with copper present [**23**]. This was taken as a suitable endpoint for the ageing process. As the presence of copper had only reduced this maximum ageing time by two days, there was no major advantage to using it in the ageing protocol. So subsequent ageing of samples was performed without copper present. This had the advantage of removing a factor from the ageing protocol.

5.5. EXPECTED ACCELERATION OF AGEING

As mentioned in 2.2.3, the accelerating thermal ageing temperature used in this project is 120°C relating to the hotspot temperature of 100MVA transformer given by IEEE guide C57.91-2011 [**18**]. Some analysis was performed to estimate the rate of accelerated ageing in this project and the ageing rate under normal operation condition.

Initially, the expected relation between lifetime and temperature was calculated based on [**125**]. According to [**125**], the life test protocol specified in ANSI/IEEE C 57.100-1986 defines the lifetime using equation 5-1. This protocol is used to estimate the lifetime of a insulation system under operation at elevated temperature in a transformer.

$$\log_{10} lifetime\ (h) = \frac{6328.8}{(273+\theta)} - 11.269 \qquad \textbf{5-1}$$

Here, θ is the hot spot temperature in centigrade of the winding in the transformer. The predicted lifetime as a function of temperature derived from equation 5-1 is shown in Figure 5-4. The lifetime axis is in logarithmic scale. The values of estimated lifetime at some specific temperatures are shown in Table 5-1.

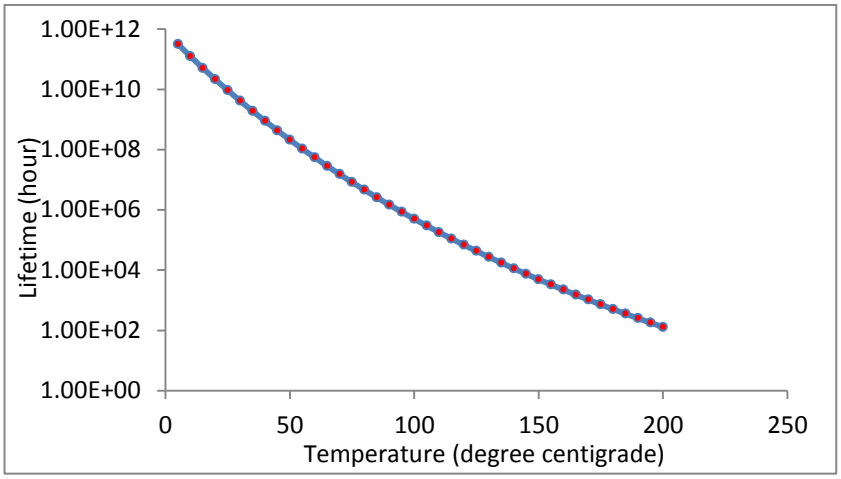

Figure 5-4 Estimated lifetime as a function of temperature based on equation 5-1

However, as it deals with a hot spot temperature, this method is likely to be based on the ageing of the cellulose based insulation rather than that of the oil alone. In 2008, Mohammad R. Meshkatoddini [**2**] provided an equation to predict the lifetime of naphthenic-based mineral oil associated with temperature based on his experimental results and Arrhenius equation.

Temperature (℃)	Estimated lifetime (hour)	Acceleration Factor
40	8.93E+08	1
80	4.57E+06	1.95E+02
120	6.84E+04	1.31E+04
160	2.22E+03	4.02E+05
200	1.29E+02	6.92E+06

Table 5-1 Lifetime predicted at specific temperature based on equation 5-1

In Mohammad's study, Acidity number measured with KOH neutralization method mentioned in 2.4.4 was adopted as a key indicator. The measured acidity number from a 230kV, 18 years old power transformer was set to be the degradation criterion limit. The relationship between lifetime and temperature suggested by [**2**] is:

$$t = 0.5374 \times e^{\left(\frac{782.9}{T}\right)} \qquad \textbf{5-2}$$

Where, t is the expected lifetime in hour, T is the temperature in degree of centigrade.

Again, the derived lifetime associated with temperature based on equation 5-2 is shown in Figure 5-5 and the estimated lifetimes at specific temperatures are shown in Table 5-2.

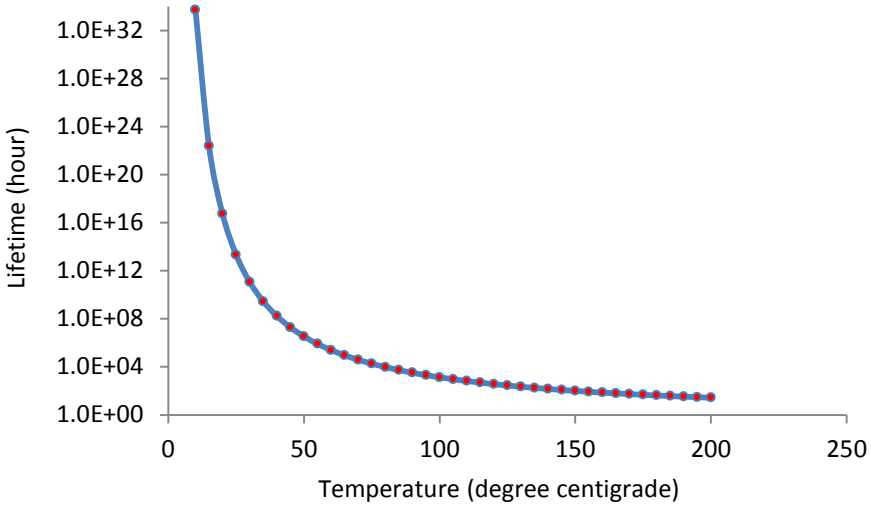

Figure 5-5 Estimated lifetime as a function of temperature based on equation 5-2

In reality, the temperature of insulating oil in an operating transformer cannot be simply estimated since it can be influenced by many factors such as the load of transformer, environmental temperature, etc. The temperature of insulating oil in a transformer also varies in different regions. For example, the temperature of oil is expected to be relatively higher at the region close to the core wiring. Therefore, it is difficult to give the real value of normal operation temperature for insulating oil used in different transformers.

Temperature (℃)	Estimated lifetime (hour)	Acceleration Factor
40	1.70E+08	1
80	9.56E+03	1.78E+04
120	3.66E+02	4.64E+05
160	7.17E+01	2.37E+06
200	2.69E+01	6.32E+06

Table 5-2 Lifetime predicted at specific temperature based on equation 5-2

For the sake of simplifying the estimation approach, the effective normal working temperature of the insulating oil is assumed to be 80℃ as used by Mohammad R. Meshkatoddini [**2**]. Using equation 5-2, the estimated lifetime of mineral oil thermally aged at 120℃ is equal to 3.8% of the estimated lifetime of mineral oil at the nominal working temperature of 80℃ which provides an acceleration factor of 26.12. This assumes that the kinetic constant related to thermal ageing is temperature independent. Table 5-3 has been derived to show the expected equivalent ageing time of insulating oil under normal working temperature by using this approximately equivalent based on equation 5-2.

Thermal aged at 120℃ (Days)	Normal working at 80℃ (Days)
2	52.24
4	104.48
8	208.96

Table 5-3 Equivalent ageing time relative to normal working temperature based on [2]

Another option is an approach based on equation 2-6 discussed in section 2.3.1 along with the Arrhenius equation and published values for the activation energy for the ageing of oil to estimate the degree of ageing which has occurred in the oil samples used in this project.

The activation energy of six different types of mineral and synthetic oils associated with the thermal ageing process has been investigated by Václav Mentlík et al using the thermogravimetric analysis [**126**]. According to their experimental results, for most of the mineral oils, the activation energy for the ageing process did not change significantly during the thermal ageing treatment. All the measured values of activation energy from the six oil samples stressed by thermal ageing were in a range of 60 kJ/mol to 90kJ/mol. Therefore, it is reasonable to assume that the activation energy of Shell Diala insulating oil used in this project would also lie in this range. A constant value of 75kJ/mol was used and it was assumed that ageing followed a first order chemical kinetic. Calculated results based on equation 2-6 indicate that, by increasing the temperature of thermal ageing from 80℃ to 120℃, the acceleration

factor relating to ageing is 13.5 which is approximately equal to half of the value calculated based on equation 5-2. Again the expected equivalent ageing time can be calculated and is shown in Table 5-4, assuming this reaction rate is constant during thermal ageing process.

Thermal aged at 120℃ (Days)	Normal working at 80℃ (Days)
2	26.955
4	53.91
8	107.82

Table 5-4 Equivalent ageing time related to normal working temperature based on [126**]**

Apart from the uncertainty over the actual activation energy for samples used in this project, this approach is weak because it assumes that the frequency factor A in the Arrhenius equation is constant. However, in reality, A and therefore the rate of reaction is a temperature dependent parameter.

There are some earlier publications providing ways of evaluating the ageing status of insulating oil based on the Arrhenius equation. Research performed by Hu et al. on mineral oil (25# Karamay) and TiO_2 nanofluid suggests that the lifetime of insulating material decreases by half as the ageing temperature is increased by 6 ℃ over a reference temperature of 80 ℃ [**127**]. In [**128**] [**129**] for mineral or synthetic oils it is suggests that the lifetime would decrease by half as the ageing temperature was increased by 7 ℃ over a reference temperature of 60 ℃ .

Therefore, the equivalent service time corresponding to this project can be evaluated in the Table 5-5 and Table 5-6.

Thermal aged at 120℃ (Days)	Normal working at 80℃ (Days)
2	203.19
4	406.37
8	812.71

Table 5-5 Equivalent ageing time relative to normal working temperature based on [127**]**

Thermal aged at 120℃ (Days)	Normal working at 60℃ (Days)
2	760.08
4	1520.15
8	3040.30

Table 5-6 Equivalent ageing time relative to normal working temperature based on [128] [129]

A relatively longer equivalent ageing time has been obtained using the two approaches mentioned above. Although none of the approximate approaches discussed above can give an accurate acceleration of the ageing process these estimations are still useful as they provide a general indication between the accelerated thermal ageing in this project and the ageing in a real working transformer.

5.6. SUMMARY

Shell Diala oil was selected to be used as experimental sample in this series of tests. Thermal ageing was performed on the Shell Diala oil samples at a temperature of 120℃. Aged samples will be used for experiments introduced in later sections. The effect of copper as a catalyst during the thermal ageing process was investigated. From the changes in the appearance of the oil, it is found that the rate of thermal ageing could be increased due to the copper presence.

UV/Vis spectra was measured from unaged oil and oils aged for 2 day, 4 day, 6 day, 8 day and 16 day, in range of wavelength from 380 nm to 780 nm. A change of absorption of at different wavelength due to the ageing of insulating oil can be observed. However, since a reasonable saturation value cannot be obtained when using the cut off wavelength as an indicator, the expected acceleration of ageing is difficult to investigate by using spectroscopy method.

The rate of accelerated thermal ageing at 120℃ was discussed with several approach based on the presented data and Arrhenius relationship. An initial link between thermal ageing in the laboratory in this project and the ageing under real operation could be established approximately. Estimates of the rate of ageing of the insulating

in real transformer could be performed based on the experimental data from the oil samples that have undergone accelerated thermal ageing. Environmental factors which can affect the ageing mechanism can also be investigated by comparing the difference between the oil samples aged in the lab and the oil samples aged in a real working transformer.

6. DEVELOPMENT OF CURRENT MEASUREMENT TECHNIQUES

6.1. INTRODUCTION TO EXPERIMENTAL TECHNIQUES

In this chapter, a general description of the development of the experimental system for measurement of the conductivity and mobility of charge carriers in an insulating liquid will be given. The experimental setup will be described along with the equipment used. Test results from the initial experimental systems will be reported and discussed along with the problems revealed. The final temperature-controlled system using a water bath is then described.

6.2. GENERAL ARRANGEMENT

In general, there are four main parts of the monopolar/bipolar measurement system for liquid insulating materials:

- Test cell: A test cell was used to contain the test samples and perform the electric measurements on the sample. (section 6.3)
- Voltage supply and current measurement device: These functions were performed by a Keithley 617 electrometer. (section 6.4)
- Control system: The electrometer was controlled by a PC through a standard IEEE-488 interface by using a GPIB-USB controller. (section 6.5)
- Screening system: A Faraday cage was used in initial measurements. In the final system screening was provided by using the water bath within a screened room. (section 6.6)

6.3. TEST CELL

6.3.1. DESCRIPTION OF STRUCTURE

The test cell used to perform the electrical measurements on the samples, followed the IEC 60247:2004 standard [**53**]. When a voltage is applied, a near uniform electromagnetic field is generated inside the test cell. A schematic of the test cell is shown in Figure 6-1. The individual components of the test cell are described below.

1. This is the container for the oil which also acts as one of the electrodes in the system. It is made of polished stainless steel. The inner profile is shown in

Figure 6-1 and is a cylinder of radius 14 mm ending in a hemisphere of the same radius.

2. Inner Electrode: This is again manufactured in stainless steel. Its outer profile is also cylindrical terminated at its lower end with a hemisphere. The radius of the cylinder and the hemisphere is 13 mm. There is a central cavity which is intended to allow a thermometer to be inserted to measure the temperature of the test cell. The top of this cavity has a cylindrical profile which allows a friction fit to be made with part 5.
3. Metal ring to support the inner electrode assembly. This has conical profiles on both its inner and outer surfaces. There is also a groove which allows excess oil to escape from the test cell during assembly. The outer surface forms a friction fit with component 1 while the inner surface forms a fit with component 4.
4. Insulation Spacer: This is formed from Polymethyl methacrylate (PMMA) and again has conical profiles to its outer surface and the central hole. The outer cone matches the corresponding inner cone on component 3. The inner cone matches that on component 5.
5. Inner electrode support. This is made of stainless steel and has an outer profile to form a friction fit with components 2 and 4. There is a hole through the centre of this component to allow a thermometer to be inserted into the recess in component 2. The top of this part has a screw terminal to allow an electrical connection to be made through this component to the inner electrode 2.

The test cell design is such that the separation of the inner and outer electrodes is much smaller than the separation between the inner electrode support (5) and the outer electrode. This means that any excess oil in the region between the support and the outer electrode is subjected to a much lower field and therefore should not significantly affect the current measured.

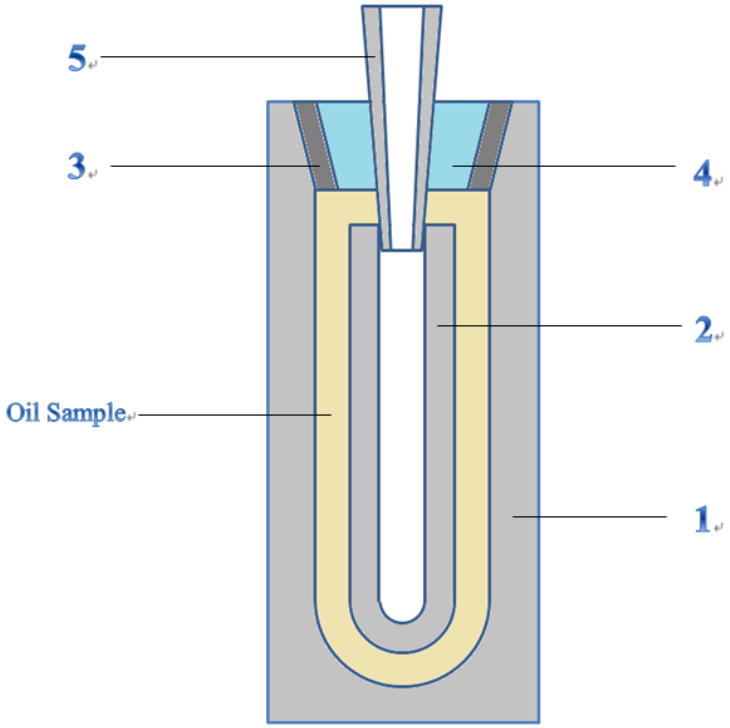

Figure 6-1 Schematic Cross Section of Test Cell

6.3.2. EXPECTED FIELD DISTRIBUTION

Considering that the behaviour of the conduction will be dominated by the field distribution in the cylindrical region of the test cell the field distribution was calculated as follows:

For a coaxial cylindrical geometry the electric field is given by:

$$E(r) = \frac{V}{\ln\frac{r_o}{r_i}}\frac{1}{r} \qquad 6\text{-}1$$

Where r_i is radius of the inner conductor, r_o is radius of the outer conductor and V is the voltage applied across the system. This is valid as long as r lies between the two radii. For an applied voltage of 1 volt the expected field at the inner conductor (r=0.013m) is 1.038 V/m and at the outer conductor (r=0.014m) is 0.964 V/m. This means that there is an approximate ± 3% variation in the electric field across the active volume of the test cell.

6.3.3. GEOMETRICAL FACTOR

It can be useful to relate the measured currents in the test cell to bulk parameters of the liquid such as resistivity or conductivity. An estimate of the geometrical factor for the test cell is therefore needed. The active region of the test cell is made up of two sections: the first is a pair of coaxial cylinders while the second part is a pair of concentric hemispheres. In the test cell used the radius of the inner cylinder and hemisphere r_i is 13mm. and the internal radius of the outer cylinder and hemisphere r_o is 14mm. The effective separation of the conductors, d is 1 mm. The length of the cylinder l is 87mm.

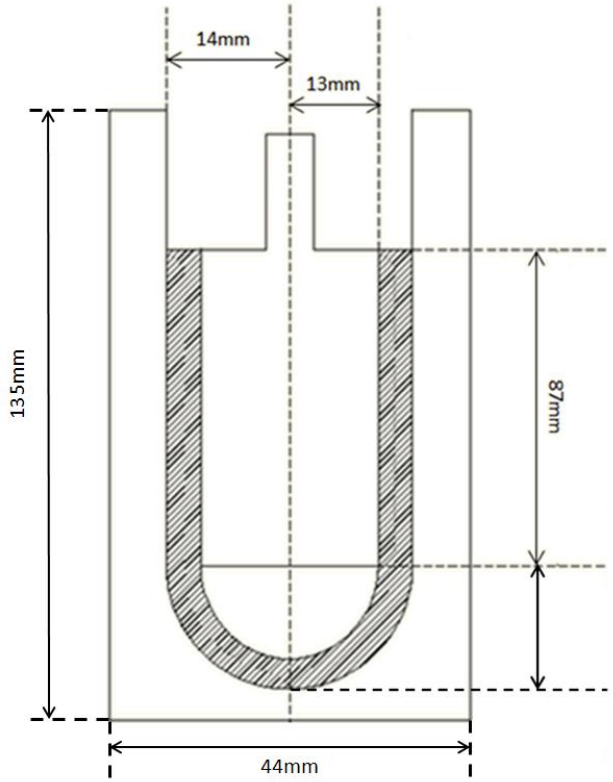

Figure 6-2 Dimensions of Test Cell

The total conductance of the test cell G_{Cell} is the sum of the conductances associated with the cylindrical $G_c$and hemispherical sections G_h.

$$\mathrm{G_{Cell}} = \mathrm{G_c} + \mathrm{G_h} = (\gamma_c + \gamma_h)\sigma = \gamma_{\mathrm{Cell}}\sigma \qquad 6\text{-}2$$

Where γ_c and γ_h are the geometric parameters for the cylindrical and hemispherical sections of the cell and γ_{Cell} is the effective geometric parameter of the complete test

cell. The standard expression for the conductance of a coaxial cylindrical system of length *l* is

$$G_c = \frac{2\pi\sigma l}{\ln\left(\frac{r_o}{r_i}\right)} \Rightarrow \gamma_c = \frac{2\pi l}{\ln\left(\frac{r_o}{r_i}\right)} \qquad 6\text{-}3$$

For a concentric hemispherical system it can be shown that the conductance is

$$G_h = \frac{\sigma 2\pi}{\frac{1}{r_i} - \frac{1}{r_o}} \Rightarrow \gamma_h = \frac{2\pi}{\frac{1}{r_i} - \frac{1}{r_o}} \qquad 6\text{-}4$$

The effective geometrical parameter for the test cell is therefore

$$\gamma_{Cell} = \frac{2\pi l}{\ln\left(\frac{r_o}{r_i}\right)} + \frac{2\pi}{\frac{1}{r_i} - \frac{1}{r_o}} \qquad 6\text{-}5$$

Using equation 6-5 and the dimensions of the test cell the effective geometric parameter has been calculated as:

$$\gamma_{Cell} = 8.519\ [m] \qquad 6\text{-}6$$

Conductance through the area above the cylindrical inner electrode has been ignored. The calculated geometrical parameter for this region is $\gamma_0 = 0.1147$m which will make little difference to the effective geometrical parameter for the cell.

6.3.4. TEST CELL CLEANING PROCESS

The test cell is made of polished stainless steel. After each experiment, traces of oil will remain on the electrode surface of the test cell. These traces could affect the measured behaviour of the next sample particularly if the oil has been aged or contains nanoparticles. It was therefore necessary to carefully clean the test cell before each experiment. A consistent approach to cleaning was used and is described below.

1. The test cell was disassembled and cleaned using hot water and detergent to remove the oil from the surfaces.
2. The detergent was then rinsed from the test cell components using tap water.
3. The cell was then reassembled and filled with distilled water which was then poured away. This process was repeated three times.

4. The test cell was then filled with ethanol which was then poured away.

The test cell was then placed in a well-ventilated place for at least 12 hours to allow the alcohol to evaporate before it was used. The final rinsing and cleaning of the test cell with distilled water and alcohol was performed on the assembled test cell to avoid contamination of the surfaces during assembly.

6.4. ELECTROMETER + CIRCUIT

An Electrometer (Keithley 617) was used as the DC voltage supply and to measure the currents in the project [**130**] [**131**]. It is capable of measuring currents below 1pA with a quoted resolution of 1fA. When the current range is between 2pA and 200pA, the permitted error should be less than 1.6%. When the current range is between 2nA and 200nA, the error should be less than 0.25%. As a voltage source, its output is adjustable between -102.35V and +102.4V in 50mV increments. The maximum output current of the voltage supply is 2mA. During the measurements performed in this project the measured currents fell in the range of 1 pA to 100nA indicating that the electrometer was an appropriate instrument. The positive terminal of the electrometer voltage source was connected to the inner electrode of the test cell. The negative terminal of voltage source was connected to ground. The outer electrode of the test cell is connected to earth through the electrometer current sensing circuitry and is at a virtual ground potential.

According to the manual for the electrometer it is usable when the power is first turned on. However, for extremely accurate measurement, it suggests that the instrument should be warm up for two hours. Considering the range of the currents measured in this project, the electrometer was allowed to warm up for at least one hour before the start of a measurement sequence. Typically a single measurement would last for one hour and at least 5 measurements would be made in sequence (Chapter 7) and the electrometer was not switched off in the intervals between measurements in a sequence. Before each measurement in a sequence was made the zero check and zero correction functions were used to remove any offsets in the instrument.

6.5. EXPERIMENTAL CONTROL

The Keithley 617 electrometer uses a standard IEEE-488 interface, so the instrument can be controlled from and data logged to a PC using a GPIB-USB controller (Prologix GPIB-USB controller). The recording data can be transferred through the Prologix controller and stored in the PC's hard drive. Programs were developed in Labview to control the electrometer and to record the data.

Although it is possible for the electrometer to take 3 measurements per second to achieve reliable data logging without missing measurements one sample was taking every 1.5s initially. Later modification to the control programme allowed the measurement interval to be reduced to 1s (section 6.7.2).

6.6. SCREENING OF MEASUREMENT SYSTEM

A screening system is necessary since the measurement of current through insulating material is relatively sensitive to possible electromagnetic interference. Two screening systems used in this project will be introduced in this section:

- **Faraday Cage in laboratory**

  For initial measurements mentioned in section 6.7.1, a grounded metal box was used as a Faraday cage with the purpose to shield the test cell from possible noise caused by the environment. The test cell was set upon an insulating slab inside the metal box. As the outer electrode act as a virtual ground potential, any current flowing through the insulating slab was expected to be much smaller than the current through the test cell.

- **Screened room**

  For temperature controlled measurements described in section 6.7.2, the whole measurement system was placed in a grounded screened room which acts as a Faraday cage.

6.7. ESTABLISHMENT OF MEASUREMENT SYSTEM

Initially, a system for insulating oil bipolar measurement was established at ambient temperature within a Faraday cage. A brief description of the measurement system will be reported. Several measurements were made in order to test its performances. Problems of initial measurements with the Faraday cage are discussed. Then, a

modified temperature-controlled measurement system with a water tank was established and its performance is reported.

6.7.1. INITIAL WORK AT AMBIENT TEMPERATURE IN FARADAY CAGE

6.7.1.1. Monopolar vs. bipolar measurements

As described in section 3.3 there are two possible methods for measuring TOF: monopolar and bipolar polarization. Initial tests were performed to check whether the monopolar method was suitable. The test cell was filled with an unaged oil sample, and the electrometer was used to apply a voltage of 40V across the cell. The current was measured every 1.5s. The current transient obtained is shown in Figure 6-3.

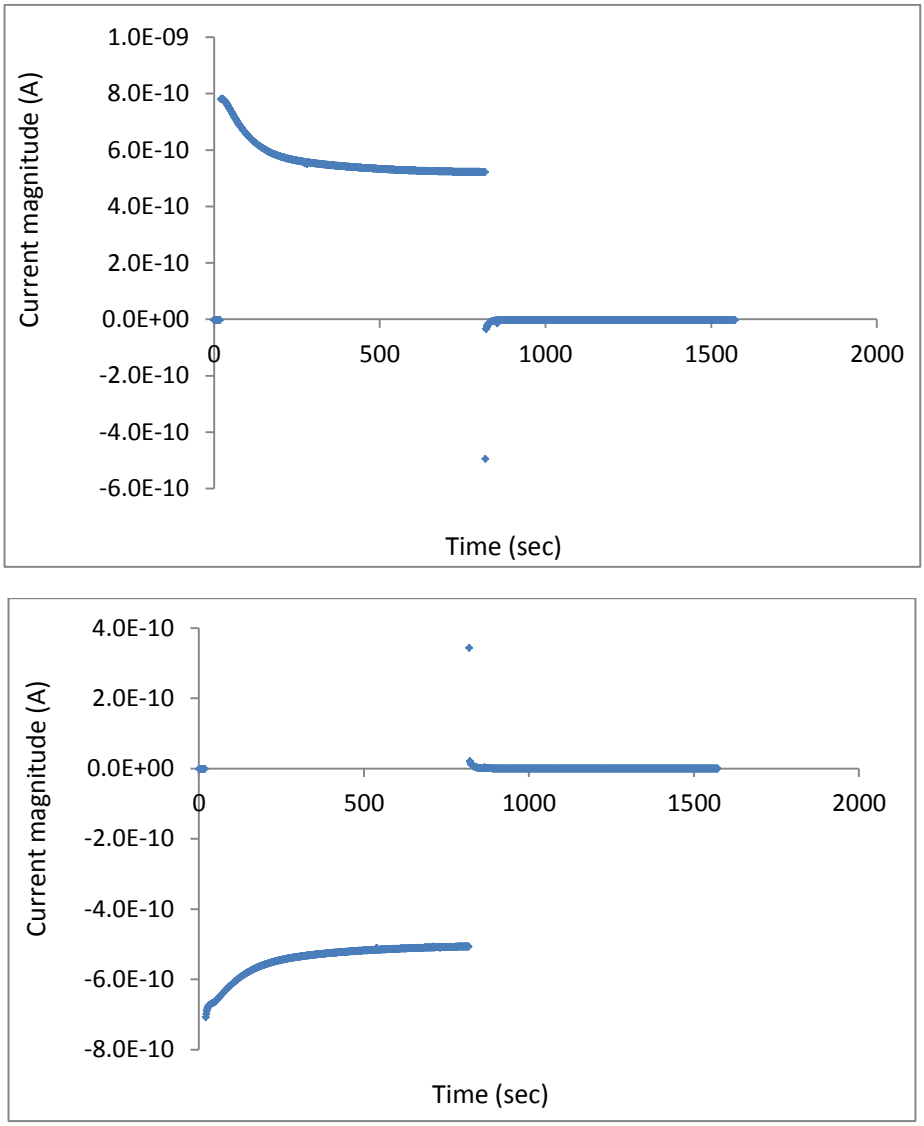

Figure 6-3 Monopolar Measurement: Upper graph positive polarization; lower graph negative polarization.

The current measurements were started 10s before the voltage was applied for 800s and then reduced to zero. A transient current with a peak value of the order of 780pA was observed which decayed to a steady value of 520pA after approximately 550s. When the voltage was reduced to zero a short lived transient in the reverse direction occurred. Broadly similar behaviours were observed under both positive and negative voltages, however no obvious peak value associated with a time of flight was observed in this process. This behaviour is in agreement with that reported in [**4**]. This indicates that although the current values were within the range that the electrometer can measure either the time of flight was very small or that the monopolar measurement method is not appropriate as the previous measurement may have a strong influence on the measured results.

The performance under bipolar conditions was then checked to see if peaks could be observed as discussed in section 3.3.2. In the bipolar polarity measurement, a step voltage of one polarity is first applied to the test cell for a period of time. At longer time, a d.c. current is observed which will depend on the rate at which charge carriers are injected into the system and the rate at which intrinsic carriers are generated in the liquid due to ionization processes. When the electric field is reversed, the rate at which charge is injected from the electrodes will increase as the space charge is now hetero-charge rather than homo-charge, increasing the local field and reducing the barrier height to charge injection. This leads to a local increase in the population of charge carriers close to the electrode. These processes have the effect of introducing a “pulse” of charge carriers into the liquid which then drift between the electrodes under the influence of the field. Ionic carriers which have been swept towards the electrodes during the first polarization may also contribute to the peak in the current.

In the trial of the bipolar measurement the test cell was filled with fresh unaged oil. A negative voltage of 40V was applied across the test cell while the current was measured with the electrometer. After 800s when the current transient had come close to its equilibrium d.c. value the voltage was reversed with a positive voltage of 40V applied to the test cell. The behaviour of the current is shown in Figure 6-4.

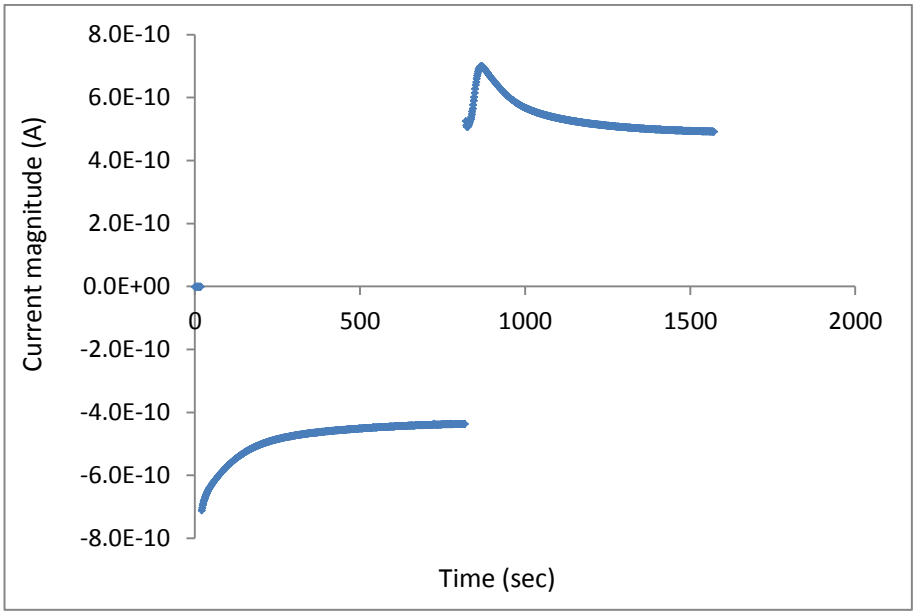

Figure 6-4 Bipolar Measurement

Using the bipolar method a clearly defined peak in the current can be seen approximately 50s after the voltage is reversed. The magnitude of this peak is 699pA. The d.c. current value under negative polarization was 437pA and under positive polarization was 491pA. These results showed that with the bipolar measurement method, the peak position and peak current value can be observed and determined clearly and therefore this was used for all measurements reported in this thesis.

6.7.1.2. Repeatability of measurements in fresh oil, (Measurements were broadly stable).

To test if the sample inside the test cell is changed during the measuring process a single sample of fresh oil was subjected to repeated bipolar measurements. The sample was exposed to a negative voltage of 30V for 800s then the polarity was reversed to positive 30V for a further 800s. The voltage across the test sample was then reduced to zero for 2minutes to allow any depolarization currents to be observed. The sample was then left under zero voltage for a period of one hour. Then the measurement was repeated 5 times. The experimental results are shown as the following Figure 6-5.

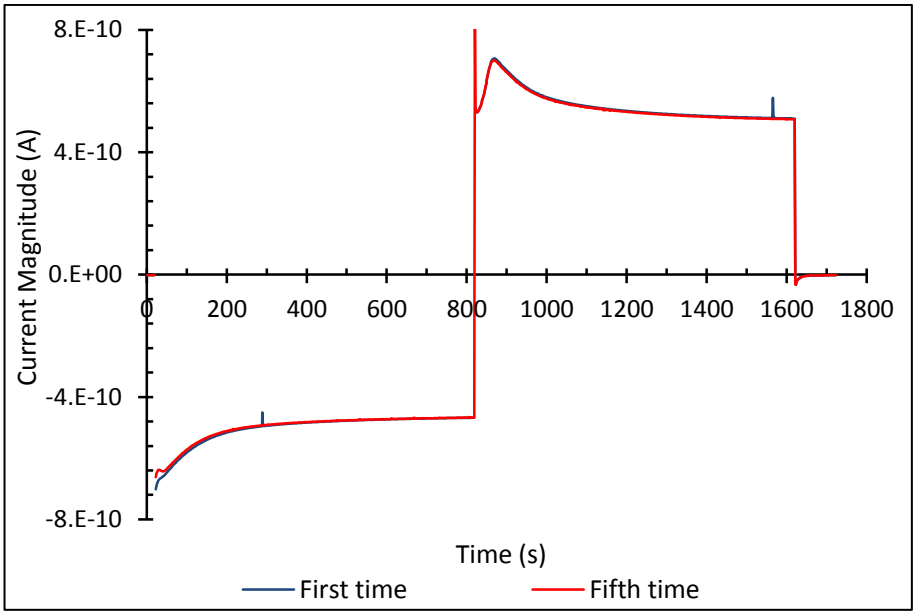

Figure 6-5 Current transients for unaged oil (30V) 1st and 5th measurement in a repeated sequence

The curves obtained from the 5 repeated measurements are consistently close to each other, which indicates that with fresh oil repeated measurements should not have a significant impact on the oil sample in the test cell.

6.7.1.3. Period of polarization

From the literature it was suggested that to achieve consistent results the period of voltage application for polarization should be sufficiently long for the sample to reach an equilibrium state and the current to become stable [**4**] [**54**]. When the time of application of the initial polarizing voltage time was short (polarity reversed before current reached a steady state), the measured value of TOF was strongly dependent on the time of application. If the voltage is applied for a sufficiently long time, charge carriers in the bulk of the liquid will have moved to the electrodes under the influence of the applied field and may have been neutralized. The remaining current is dominated by charge injection and ionization at the cathode. For shorter periods of voltage application although the concentration profiles of the charge carriers will not be uniform significant numbers of charge carriers will be present in the bulk of the liquid. Assuming a single mobility for the movement of charge carriers, when the voltage is reversed the time taken for these carriers to reach the electrodes will be smaller than that for carriers located or produced at an electrode as they have a shorter distance to travel. The presence of these carriers in the bulk and

their non-equilibrium distribution can therefore introduce a peak in the measured current at shorter times or may obscure the peak associated with charge carriers produced at the electrodes. Therefore tests were performed to investigate the influence of the polarization time on the behaviour of the current.

The test cell was filled with a fresh oil sample. A negative 30V DC voltage was applied to the test cell at the beginning. Two types of measurement were made:

Long-period polarization, where a negative voltage of 30V was applied for 1800s before voltage reversal to positive 30V which was applied for 1800s.

Short-period polarization, where the negative 30V was applied for only 800s before the polarity voltage was reversed and applied for 800s.

The current value was recorded every 1.5 second. The experimental results are shown as Figure 6-6. In this graph $t = 0$ is at the point where the polarization voltage was reversed.

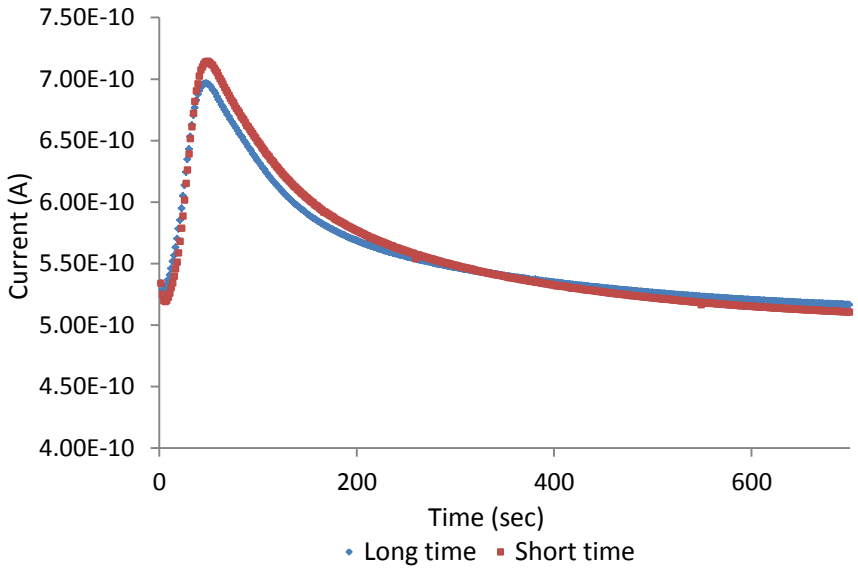

Figure 6-6 Comparison of 1800s polarization with 900s polarization

Comparing the behaviour of the two current transients it can be seen that there are differences: The longer polarization resulted in a peak of 696pA with a TOF of 48s. The peak current for the shorter polarization time is larger and have shifted to a longer time (709pA, TOF value was 49.5s). As the interval between measurements was 1.5s, it is unclear as to whether a shift in peak position has occurred. The peak associated with the shorter time of polarization seems to be broader measurements

appears to be broader. This may be due to the combination of transients due to the non-equilibrium distribution of charge carriers in the bulk and the injection and movement of charge carriers close to the electrode.

The relative change in peak amplitudes is small 10pA in a measured current of ~ 700pA. This indicates that adequate information on the peak behaviour can be obtained for polarization times of the order of 800s.

6.7.1.4. General effect of applied voltage on I_{peak}, I_{dc} TOF

This section reports on early measurements that were made under ambient conditions with the test cell surrounded by a Faraday cage. The sample used was unaged oil and the transient currents were measured using the bipolar negative-positive measurement method under different applied voltages. In each case the voltage magnitude in both the negative and positive sections of the test was the same. The range of applied voltage was from 20V to 70V. The effects of applied voltage on three parameters are considered: peak current (I_{peak}); the current at long times, assumed to approximate the d.c. current (I_{dc}), and Time of flight (TOF). The behaviours of the measured current transients are shown in Figure 6-7. As expected it can be seen that I_{peak} and I_{dc} increase as the applied voltage increases and that the peak in current appears in shorter times as the voltage is increased. The width of the peak current also reduces as the applied voltage is increased. The measured TOF varied from approximate 135s to 19.5s. The observed peak currents were in a range of 56pA to 334pA.

If the movement of charge carriers is dependent by mobility, their drift velocity will depend on the applied electric field: the current reached its maximum value faster due to stronger electric field strength.

The TOF observed in the measurements at 70V was 19s. With an interval between measurements initially limited to 1.5s it was felt that this represented the lower limit of TOF measurements with reasonable resolution. At lower electric fields, when the voltage applied is below 30V the peak becomes so broad that it is difficult to accurately determine the peak position.

This set the general range of voltages, from 30V to 70V that it was practical to apply to the test cell/electrometer combination. If measurements of TOF at higher fields

was needed it would be necessary to design a test cell where the electrode separation was larger or to arrange a higher sampling rate to be able to determine the TOF with reasonable resolution.

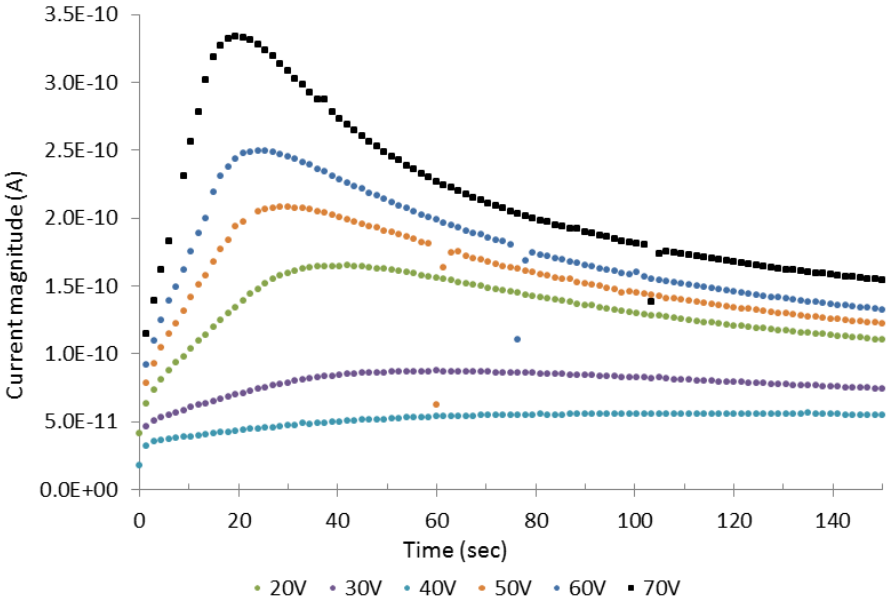

Figure 6-7 Current transient measured under 20V to 70V

.

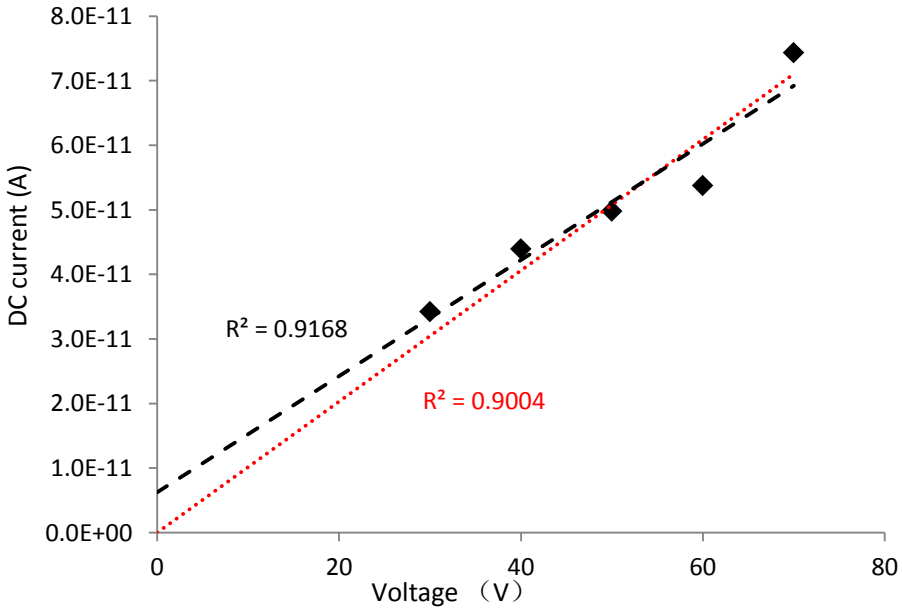

Figure 6-8 Unaged sample d.c. current（Faraday cage）

From the experimental data, it is clear, as expected, that I_{peak} , I_{dc} and TOF are all field dependent parameters. The currents I_{peak} and I_{dc} increase as the applied field is increased while the TOF decreases.

Three separate sets of measurements were made on samples of unaged Shell Diala oil. After each set of measurement, the test cell was cleaned and refilled with an unaged oil sample. The I_{dc}, I_{peak} and TOF obtained from the first time measurement associated with the applied electric field strength are as shown in Figure 6-8, Figure 6-9 and Figure 6-10, respectively

The d.c. current for the unaged sample shows an upward trend with increasing applied voltage. When a polarity voltage of 30V is applied, the associated d.c. current of 38.7pA was measured. When the applied voltage reached 70V, the corresponding d.c. current was 74.3pA. The data can be fitted by an unconstrained straight line as shown but this does not pass through the point (V = 0, I = 0). Constraining the fit to pass through the origin reduces the value of R^2. A linear relationship between current and voltage would be expected if the behaviour of the current is controlled by a mobility dependent drift velocity in the bulk of the liquid.

$$J(t) = qNv_d = qN\mu E = qN\mu\frac{V}{d} \qquad 6\text{-}7$$

Where q is the effective charge on each carrier N is the carrier density and μ is the mobility associated with the carrier motion assumed to be independent of field. A nonlinear behaviour indicates that either the mobility is field dependent, for example due to electrohydrodynamic effects, or that the current is controlled in part by a charge injection processes at the electrodes.

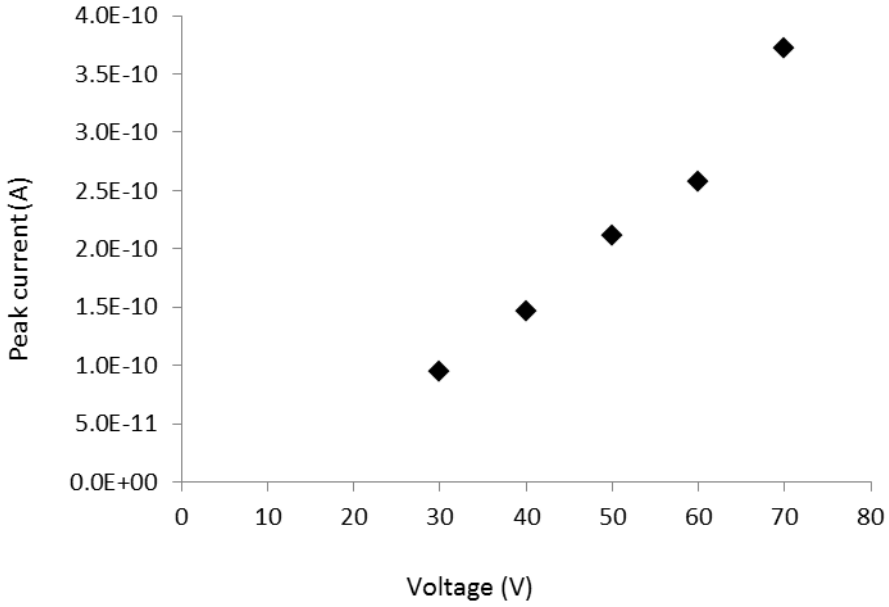

Figure 6-9 Unaged sample Peak current（Faraday cage）

The measured peak current increases with increasing applied voltage. With 70V polarization voltage, the measured peak current was 334pA. When a 30V polarization voltage was applied, the peak current value was only 55.6pA.

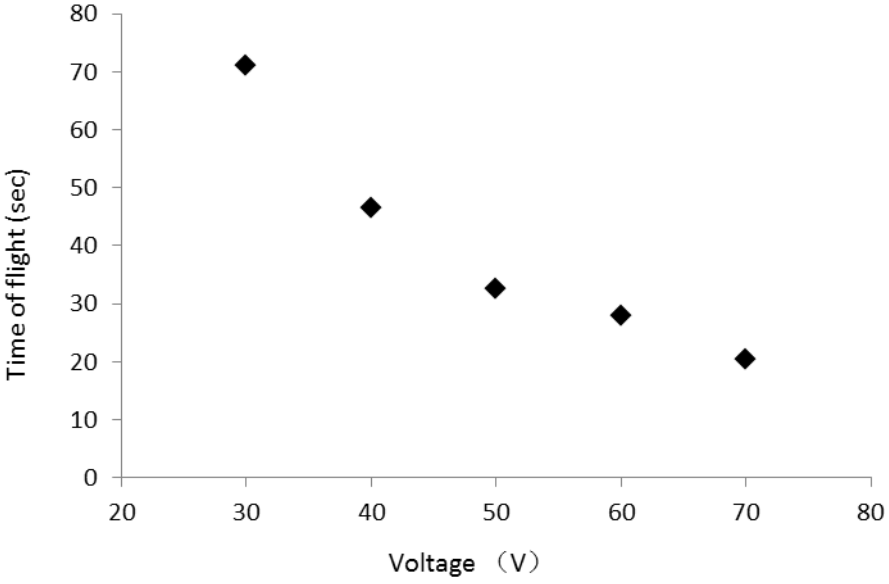

Figure 6-10 Unaged sample Time of Flight（Faraday cage）

If the mobility is constant, it assumed that the expected behaviour of the time of flight would be:

$$T_{TOF} = \frac{d}{v_d} = \frac{d}{\mu E} = \frac{d^2}{\mu V} \qquad 6\text{-}8$$

For the data in Figure 6-10 the relationship to be better fit by a power relationship of the form

$$T_{TOF} = AV^{-B} \qquad 6\text{-}9$$

Where B takes the value of 1.39. This indicates that the mobility of the system must have field dependent.

6.7.1.5. Problems with measurements

Extension of the time of measurement

The initial measurements on unaged oil samples were repeated three times. In the first set of measurements the value of the d.c. current was assumed to be given by the average value of that at the end of the measurement, 800s after polarity reversal, approximately. In section 6.7.1.1 this period of polarization had been shown to be able to produce reproducible values for the peak current and the TOF within a reasonable experimental measurement period. However, when looking at the transient currents for a 50V polarization, Figure 6-11, it is clear that although the rate of change of current is small after 800s the current transient is still decaying. Between t=1600s and t=2200s, the current decreased from 79pA to 70pA. The data at longer time after voltage reversal was fitted to: $I(t) = I_{dc} + I_0 e^{-\frac{t}{\tau}}$. The derived values of the parameters were: $I_{dc} = 66.7\,pA$, $I_0 = 234\,pA$ and $\tau = 543s$. I_{dc} is shown by the red line in Figure 6-11. So increasing the polarization/depolarization periods by 600s, brings the measured d.c. current 13% closer to its actual value. Therefore, for the remaining two tests the polarization periods were increased to 2200s. This would enhance the accuracy of the measurements of I_{dc} and also improve the accuracy of measuring I_{peak} and TOF. In practice due to constraints on practical measuring times a polarization/depolarization period of 1800s was adopted in most cases.

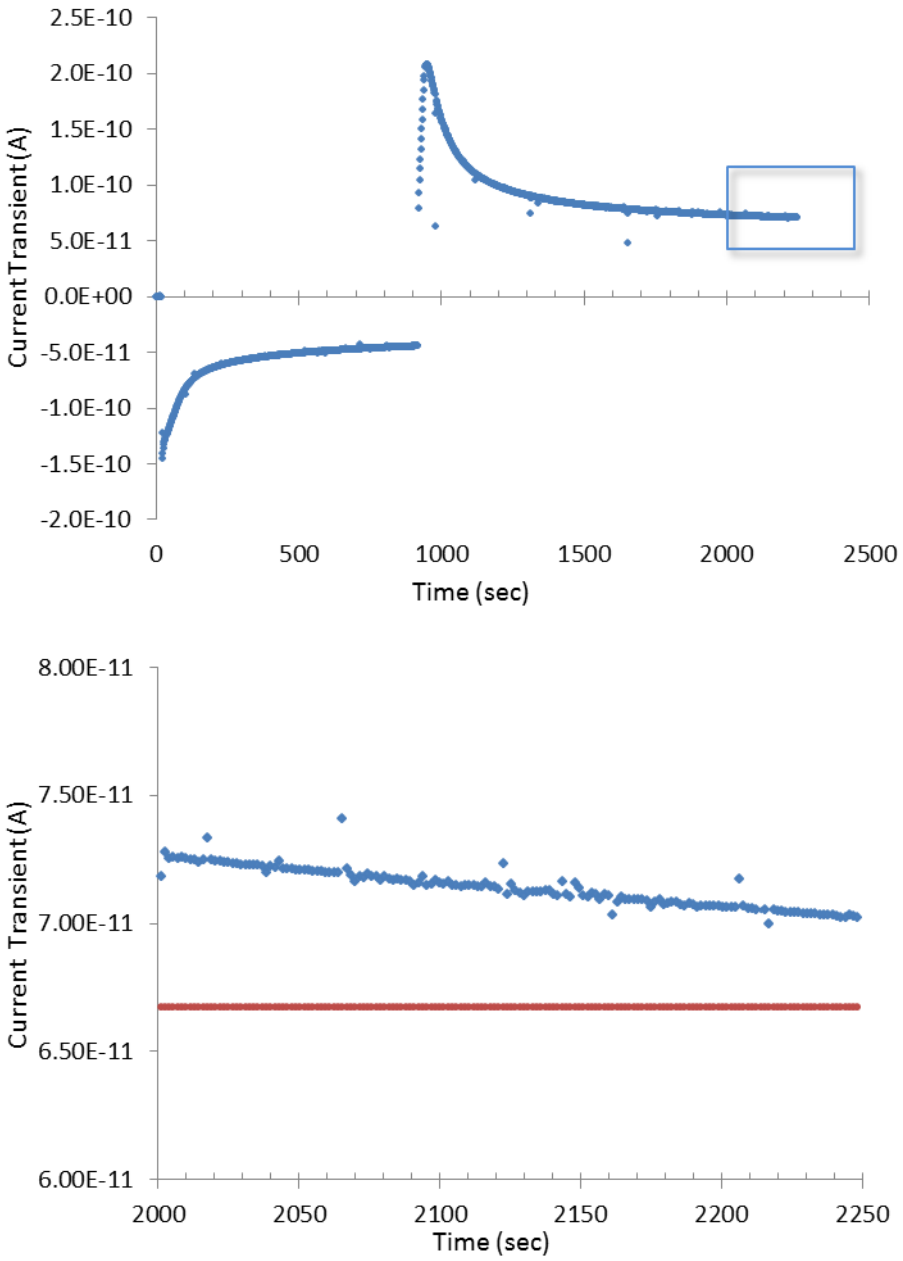

Figure 6-11 Initial measurement at 50V Upper graph for current transient behaviours; lower graph for the magnified area in blue square

Constant initial polarization voltage

In the literature the general approach to bipolar TOF measurements was to use the same voltage magnitude in both the negative and positive sections of the measurement. However, as the voltage in the initial polarization is changed, it would be expected that over a constant polarization time the final distribution of charge carriers close to the electrode would change and this could affect the behaviour of the

current when the voltage was reversed, leading to differences in the measured value for the TOF and peak current independent of the actual value of the mobility. Therefore it was decided to use a constant value of initial polarization voltage, -50V, while varying the voltage after reversal.

6.7.2. MEASUREMENT SYSTEM WITH WATER BATH

The initial measurements on insulating oil samples showed a variation which seems to be a result of the change of the environment temperature. Changes were observed in the values of I_{dc} and I_{peak} for the same applied voltage at different time. A possible explanation was the impact of temperature on the conductivity of the oil [**132**] as the measurements to date had been made under ambient conditions. In addition, [**62**] indicates the temperature dependence of charge carriers mobility. Therefore a new experimental set up was developed to allow control of the sample temperature and to eliminate possible temperature effects on the measurements.

A Grant GP200 Precision stirred thermostatic bath was used in the new experimental system. The internal tank of the water bath is made of stainless steel, with a metal lid at the top. When the lid was closed and appropriate earthing connections made, the whole tank can be considered as an equivalent to a Faraday cage. During the measurement process, the temperature of the water in the tank was relatively stable. Before each measurement, the test cell was first put into a glass beaker to isolate the outer electrode from the water and the earthed surroundings of the tank. The beaker was then filled with insulating oil until most of the test cell was in contact with the oil (The oil level was such that no contact was possible between the sample within the test cell and the external oil). The oil was present to insure good thermal contact between the test cell and the water bath. The outer electrode of the test cell is grounded through the electrometer, current flows between the test cell and the surrounding water bath could be ignored. The beaker with test cell was placed in the middle of the water bath during the measurement process. The water level in the water tank allowed good thermal contact with the beaker. The heating apparatus of the water bath included a circulation system to make the water temperature within the tank homogeneous.

The new measurement system was set up in a screened room that was previously mentioned in section 6.6. The temperature in the water bath was set to 30℃ which was above the highest ambient temperature observed in the laboratory. A RS1319A Digital Thermometer was used to monitor the temperature variations of the test cell during measurement process. The measurement range of this thermometer is from -50℃ to 1300℃. The basic accuracy is 0.3% ±1℃ in the measurement range of 0℃ to 1000℃ [**133**]. The probe of the electronic thermometer was placed inside the central cavity of test cell's inner electrode. After switching on the temperature-control system of the water bath, the temperature of both the water and the central electrode of the test cell were monitored. The temperature of the water came from the built in thermometer in the water bath and the variation of temperature of the sample in the test cell can be obtained through the thermometer. Figure 6-12 shows the variation of temperature of water and temperature of the sample as a function of time in the water bath during the heating process.

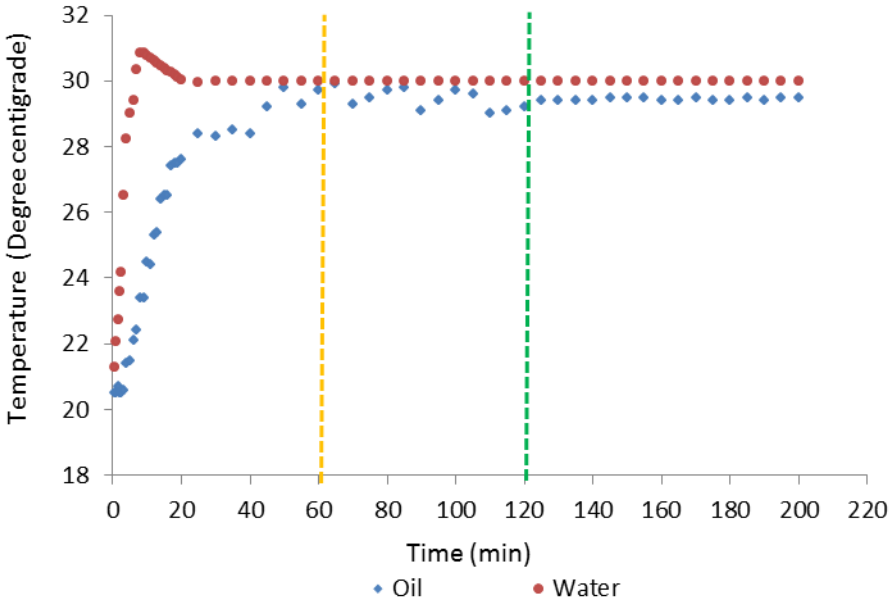

Figure 6-12 Heating with water bath

After switching on the heater of the water bath, the water temperature rose to 30℃ within 30 minutes. After that, there were small variations in the water temperature, with the fluctuation range less than 1℃. The temperature of the test cell lagged behind the water temperature. After 2 hours a relatively stable thermal state inside

the test cell, slightly below the water temperature, was achieved and the temperature of the oil sample was about 29.5℃. Therefore when measurements were taken 2 hours were allowed for the sample to reach the set temperature, this also allowed the electrometer to warm up (section 6.4).

6.7.2.1. Inspection and improvement of the experimental circuit

Initially, the test cell was connected to the measurement circuit without a sample, within the temperature-controlled water bath. The heater of the water tank was not switched on as the purpose was only to check the noise and background performance of the system.

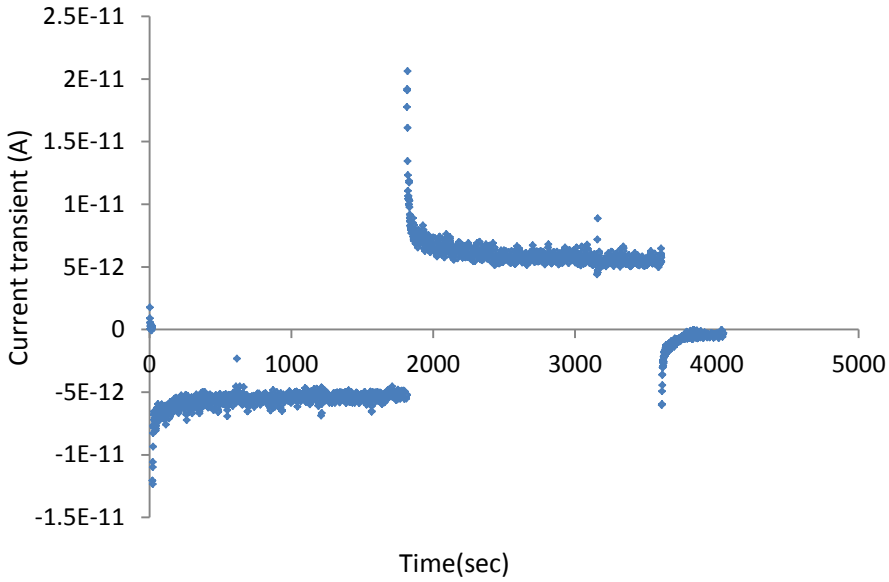

Figure 6-13 Transient Currents in Empty test cell

Figure 6-13 shows the results of a bipolar measurement (-50/+50V) on the empty test cell. Transient currents are observed due to polarization of the system and d.c currents of the order of 5pA are observed. This value is considerably lower than that previously observed in the unaged oil (~50pA). This indicated that the basic system as acceptable.

However, after filling the test cell with a sample that had been aged for 2 days and taking measurement with the lid of the vessel closed and the heater apparatus running, problems were observed in the behaviour of the current transient. Examination of the system showed that small water droplets were forming on the top of the test cell and

at the connections to the voltage supply after heating for half an hour. This was assumed to have affected the measurement by introducing alternate current paths in the system. To avoid the condensation problem measurements were taken with the lid of the water bath open. Under these conditions, no water condensation was observed and the behaviour of the transient was closer to what was expected. However there was a suggestion of a distinct shoulder in the current transients and it was not clear if this was a feature of the aged oils or as a result of incomplete screening of the measurement system leading to problems with electromagnetic interference and capacitive coupling. To avoid this, the lid was kept closed and a small fan was used to circulate the air within the water tank. This prevented the problems with condensation mentioned above. The current transient with this method is shown in the following Figure 6-14.

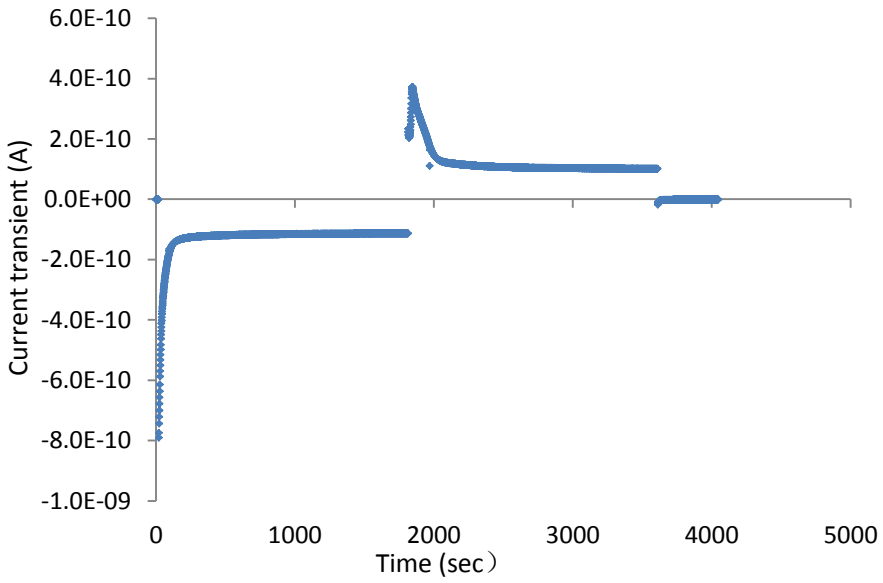

Figure 6-14 Improved measurement setup (Closed lid with fan)

Figure 6-14 above shows that a stable measurement environment had been set up through adding a fan to the measurement apparatus. A relatively stable temperature environment for the oil in the test cell is formed after 120 minutes (less than 1°C variation) during the measurement process.

6.7.2.2. Repeatability of Measurements

During repeated measurements of a single sample using the water bath with aged oil samples, variations in the measured values of I_{peak}, I_{dc} and TOF of the aged oil in the test cell were observed.

Figure 6-15 below shows results for I_{dc} from repeated measurements of a single sample of 2 days aged oil from three sets of measurements. In each set of measurements, 5 successive measurements were performed in a voltage range of 30~70V. The time interval between each set of measurement is 24 hours.

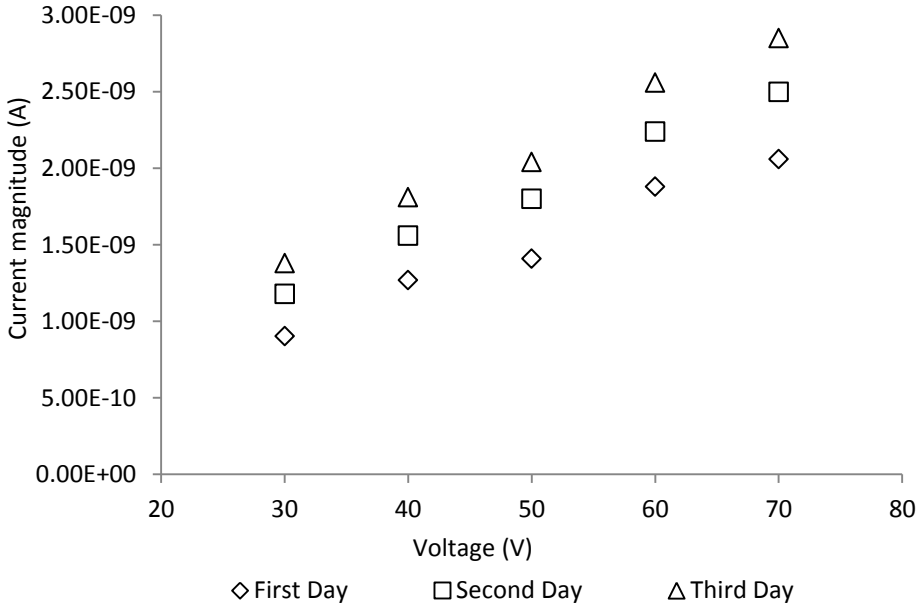

Figure 6-15 DC current values of 2 days aged sample

The measured values of I_{dc} increase with day of measurement for all applied voltages, with changes between 35% and 50% occurring over the three days. Similar behaviour was observed for I_{peak} and TOF values. A possible explanation of these variations is the presence of water vapour in the air space of the water bath which could affect the water content of the oil inside the test cell. The water content of oil has been shown to affect its conductivity [**134**], causing the changes in the I_{peak} and I_{dc} values over the successive measurements.

To test whether the absorption of water was causing the changes in the samples behaviour a sample of 2 days aged oil was kept in the water bath in an open bottle for one week. While a second sample of the aged oil was measured in the test cell. The

water bath temperature was maintained at 30°C during the day with the fan operating. During the night the water bath was switched off. This meant that the open oil sample had been exposed to a similar humidity environment to a sample held in the test cell over the same period of time. If water absorption was the explanation of the observed changes it was expected that the measured values of I_{peak} and I_{dc} in the sample kept in the open bottle would be larger than those found in an initial measurement of the 2 days aged oil.

The measured values for the sample from the open bottle were close to the initial values for the 2 days aged oil and were observed to increase with repeated measurement in a similar manner. Therefore the changes could not be explained simply by water absorption by the samples.

In order to further explore this behaviour a 2 days aged samples were divided into two parts: One of the two parts was filled into the cleaned test cell. The top of the test cell was sealed with wax in order to isolate the sample oil in the test cell from the outer air. With this approach, the ability of the sample oil in the test cell to absorb water from the surrounding environment should be significantly reduced.

The rest of the sample was placed into an open glass bottle which was set in a beaker filled with insulating oil. The beaker was also placed into the water bath alongside the beaker containing the test cell. During the measurement process, the oil sample in the glass bottle was fully in contact with the air and absorbing moisture from the surrounding environment.

In the first week, the time-varying curves of characteristics of the sample in the test cell were measured once a day and the measurement was repeated for five times, so as to obtain the time-variations of the I_{dc}, I_{peak} and TOF of the sample within one week. Then, in the next week, the cleaned test cell was filled with the oil sample which had been in contact with the airspace in the water bath during the period of the first set of measurements and the measurement program was repeated with this sample. The results are shown in Figure 6-16.

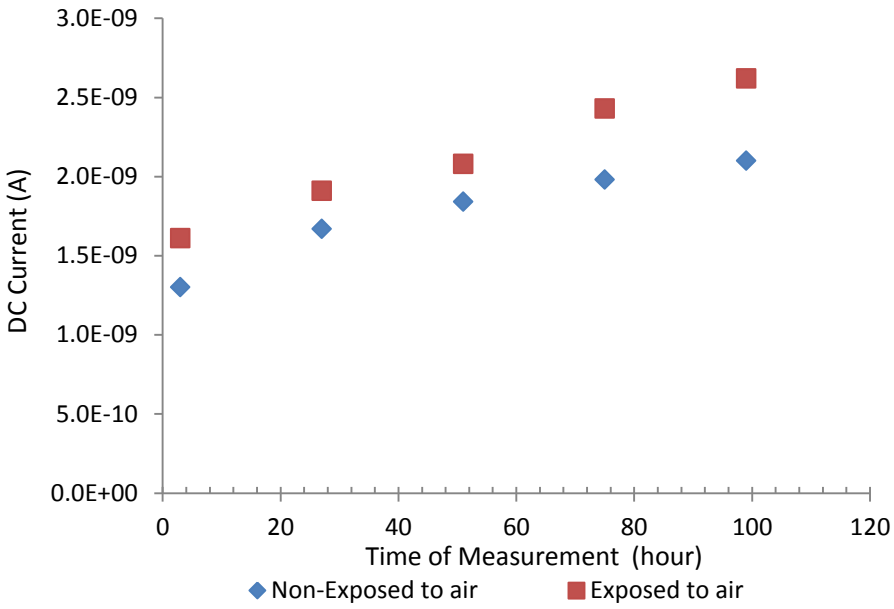

Figure 6-16 Non-Exposed to air VS Exposed to air in d.c. current measurements

The first measurement was taken three hours after the moment when sample was filled into the test cell. The time interval between each measurement was 24 hours so 5 of measurements were performed over the 5 days. The initial d.c. current value of Non-exposed to the air sample measured in the first day was 1.3nA. After 5 days measurements, this d.c. current increased to a value of 2.1nA.. For samples exposed to the humid air, the I_{dc} values changed from 1.61nA to a value of 2.62nA. Both of these two d.c. current curves evidently had an upward trend with time. The sample exposed to the air has slightly larger values of I_{dc} compared with sample sealed in the test cell but the trend is similar. Figure 6-16 suggests that such a change was not likely be caused by any contamination or water absorption due to the exposing to the air. Therefore the changes may be occurring due to some sort of slow chemical reactions taking place under the experimental conditions. Since there were time-variations in the measured values of the I_{peak}, I_{dc} and TOF, the true electrical characteristics are unable to be shown with the data obtained from a single measurement, and it was necessary to fit the behaviour of the changing parameters with curve fitting methods which will be discussed in details in later chapter 7.

Although the direct cause of such an increasing of I_{dc} and I_{peak} is not clear, the modification, i.e. sealing the top of the test cell with wax, was adopted in later

experiments since it was appeared to effectively reduce the risk of being contaminated from the outer environment.

6.8. SUMMARY

A suitable experimental system which can be used for time of flight measurement was successfully developed and has been described in detail in this Chapter. Initially, a series of test results from a measurement system with a Faraday cage have been presented to give an initial idea of the behaviours of bipolar polarization measurements. The problems of the initial measurements when the experimental setup was within a separate Faraday cage were discussed along with the improvements of the measurement system that were required. The final temperature-controlled measurement system with a water bath was then described along with the test results required to establish the suitability of this system. Consistent measurements results can be measured by using the measurement system with the water bath. 2 hours is required to allow the temperature of the water in the water bath to reach the setting temperature before any measurement was taken.

The experimental results discussed in the following chapter were based on this modified measurement system.

7. MEASUREMENTS ON AGED AND UNAGED OIL

7.1. INTRODUCTION

In this chapter, the test liquid was Shell Diala insulating oil (Chapter 5.2). Four samples of 250 ml were subjected to thermal ageing at 120°C for the following times: 0, 48, 96 and 192 hours respectively. The details of thermal ageing treatment have been described in Chapter 5.

Current transients were recorded using the bipolar method described in Chapter 4 at voltages between 30 and 70V. This sequence of measurements was repeated on the sample over 5 successive days. Values have been derived for I_{peak}, I_{dc} and TOF for each group of samples and the effects of ageing on these parameters are discussed in this chapter.

7.2. UNAGED OIL

To establish the baseline behaviour of the insulator measurements were made on a sample of oil that had not undergone any thermal ageing treatment. The initial negative voltage was 50V (Average field 50 kV/m) while the positive voltage was varied between 30 and 70 V in steps of 10 V (Average field 30kV/m to 70kV/m). Once a sample had been placed into the test cell measurements were made over 5 successive days. On each day a period of 3 hours was allowed to ensure that the water tank had reached thermal equilibrium. Measurements were then taken in the next 6 hour period following the pattern shown in Table 7-1. The results obtained from analysis of the transients are shown in AppendixA 1.

Measurement	Negative Voltage (V)	Positive Voltage (V)
1	50	70
2	50	30
3	50	40
4	50	60
5	50	50

Table 7-1 **Measurement Pattern**

7.2.1. PEAK CURRENT AND DC CURRENT

I_{peak} values of unaged samples under different voltages measured for 5 times are shown in Figure 7-1.

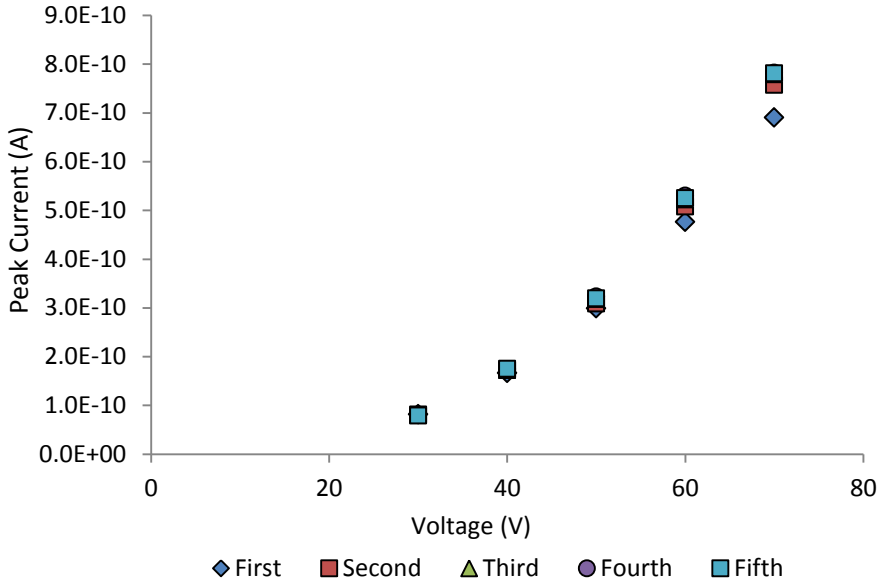

Figure 7-1 Unaged sample peak current

The measured values of peak current are significantly increased due to the increase of applied voltage. At voltages of 50 V and below there is little variation in the values of I_{peak} over the 5 successive measurements. At 60V and above the initial measurement is lower with the remaining measurements close in their value.

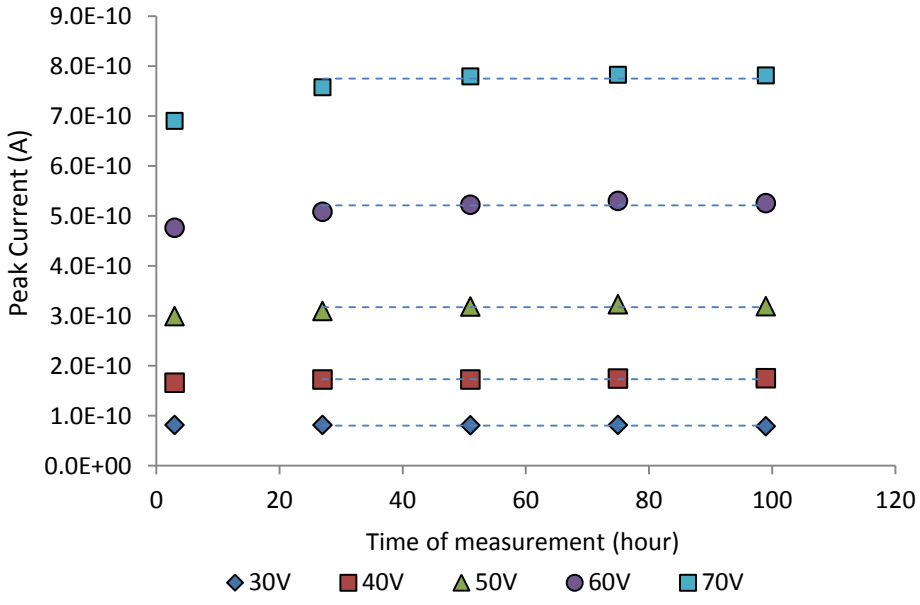

Figure 7-2 Variation of unaged oil peak current with time of measurement

Figure 7-2 indicates that the measured values of I_{peak} in the first set of measurement were smaller than those measured in the rest of the set of measurements at higher voltages. The blue dash lines represent the calculated average values from the last 4 points in each set of measurements. For the results between 2 and 5 days, the peak current does not change significantly with the time of measurement. Therefore, it was decided that the I_{peak} values of unaged oil sample can be best represented by the calculated average value from the last 4 successive measurements.

The fitted values of I_{peak} for unaged oil samples at for different voltages are plotted in Figure 7-3.

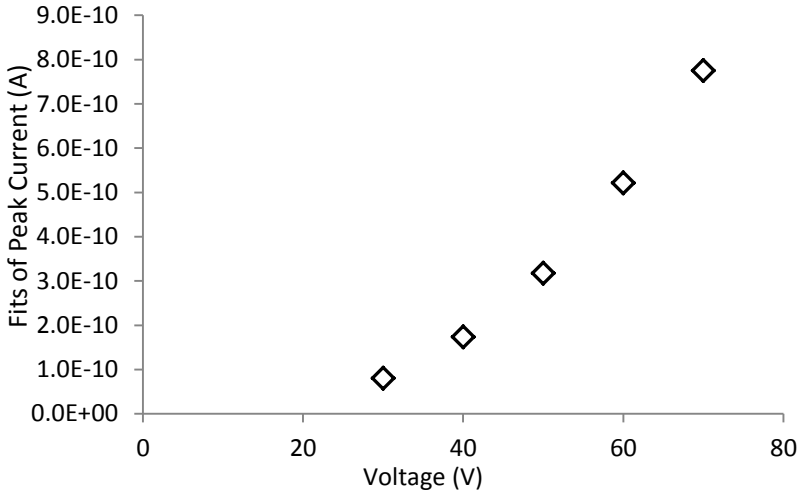

Figure 7-3 Fitted Peak current for unaged sample

The 5 sets of measured d.c. currents are shown in Figure 7-4

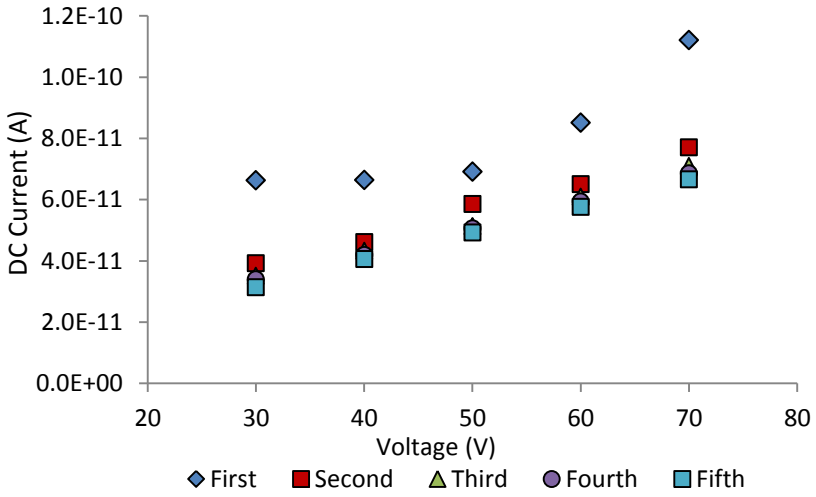

Figure 7-4 DC current of unaged sample measured on 5 successive Days

The d.c. current measured shows a rising trend with the increase of the applied voltage. When measuring unaged oil, I_{dc} values were found to change with time. For the unaged oil samples measured over 5 days, I_{dc} values have a downward trend following the time that the sample has been present in the test cell. This is shown in Figure 7-5.

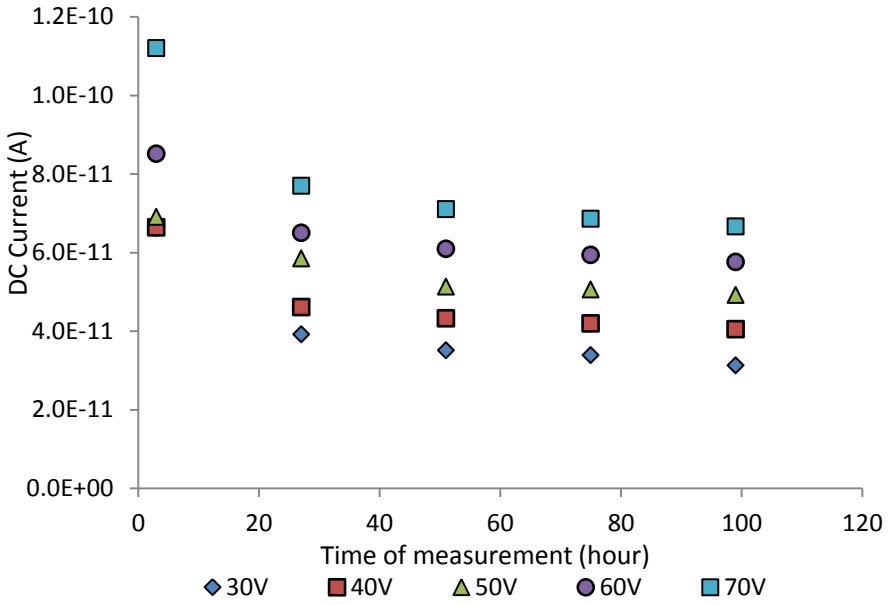

Figure 7-5 Variation of unaged oil with nanoparticles d.c current with time of measurement

From Figure 7-5 the major fall in the value of, I_{dc} occurs in the first 24 hours. The subsequent changes are small and may possibly be as a result of scatter in measurement. As described in section 6.7.2 this behaviour is unlikely to have been caused by water absorption as the current value would be expected to increase with time.

Since there are time-variations in the measured values of the I_{dc} of unaged oil samples, the actual electrical characteristics are unable to be shown neither with the data obtained from just one set of measurement nor by simply calculating the average value from 5 measurements. It is necessary to find parameters which are able to more accurately present the conduction characteristics of the oil samples.

Therefore, it was assumed that the change of I_{dc} with time is due to some sort of simple first order kinetic such as the product generated by some kind of first order

chemical reaction, and I_{dc} values are proportional to the concentration of a reactant. The concentration of reactant would gradually decrease with time until this chemical reaction reaches equilibrium. At this time, the concentration of reactant is constant. If the chemical reaction conforms to a simple first order reaction kinetic, then the change of I_{dc} with time can be expressed by an exponential function $I_{dc}(t)$ of the form:

$$I_{dc} = I_0 e^{(-\frac{t}{\tau})} + I_1 \qquad \textbf{7-1}$$

The data measured from the experiment can be fitted with the above equation to obtain the values of I_0, I_1 and time constant τ in the equation. These values can be then be used in the subsequent comparison and analysis of the behaviour of the system.

When $t = 0$, $I_{t(0)} = I_0 + I_1$ which gives the I_{dc} value that would be expected at the moment that the oil sample was filled into the test cell.

When $t = \infty$, $I_{t(\infty)} = I_1$ the equation shows the I_{dc} values that would be expected when the sample reached a stable equilibrium.

The fitting results of I_{dc} values of unaged sample are shown in Table 7-2.

Voltage (V)	I_1 (pA)	I_0 (pA)	τ (h)	R square value	I_{dc} (A) (t = 0)	I_{dc} (A) (t = ∞)
30	3.27E-11	4.07E-11	15.3	0.990	7.34E-11	3.27E-11
40	4.13E-11	3.05E-11	15.1	0.992	7.19E-11	4.13E-11
50	4.82E-11	2.33E-11	30.4	0.992	7.14E-11	4.82E-11
60	5.84E-11	3.15E-11	18.0	0.997	8.99E-11	5.84E-11
70	6.76E-11	5.34E-11	16.0	0.998	1.21E-10	6.76E-11

Table 7-2 Fitting data of unaged sample d.c. current

With the assumption that the change of I_{dc} values of unaged sample is due to some sort of simple first order kinetic, the expected fitted values of time constant τ for different applied voltage should be a common value as the measurements were made on a single sample. The fitting results shown in Table 7-2 indicate that the value of τ fitted from data measured with 50V applied voltage is significantly different from

those of the other measurements with a value of 30.4 h while the other measurements lie in the range of 15.1 to 18.0. The data at 50V was therefore fitted to equation 7-1 using a value of τ = 17h which gives the minimum value of sum of square residuals (SSR) for the 5 fits combined. The fit line for measurement with 50V applied voltage is shown in Figure 7-6 with a related R^2 value of 0.95.

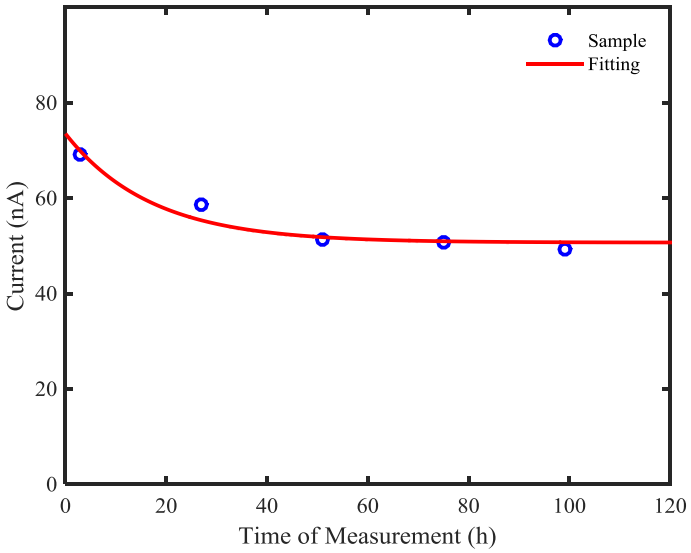

Figure 7-6 Fitting line with τ =17 h for d.c. current of unaged sample at 50V

From Figure 7-6, a reasonable fit to the 50V data can be made with a time constant of 17h. Therefore, with the assumption that the change of I_{dc} was caused by one simple first order kinetic, the measured values of I_{dc} over the 5 days of measurement were fitted using equation 7-1 with a time constant of 17 h. The result parameters of fitting are shown in Table 7-3.

Voltage (V)	I_1	I_0	τ	R square value	I_{dc} (A) (t = 0)	I_{dc} (A) (t = ∞)
30	3.22E-11	4.50E-11	17	0.994	7.72E-11	3.22E-11
40	4.09E-11	3.60E-11	17	0.9951	7.69E-11	4.09E-11
50	5.07E-11	3.12E-11	17	0.952	8.19E-11	5.07E-11
60	5.86E-11	4.03E-11	17	0.996	9.89E-11	5.86E-11
70	6.73E-11	5.63E-11	17	0.997	1.24E-10	6.73E-11

Table 7-3 Fitting data for unaged sample when τ =17 h

Fitting with a time constant value τ of 17 did not have a significant impact on the values of I_0 and I_1.The related R^2 values were larger than 0.99 for all voltages other than 50V. This indicates that fits with the value of time constant of 17 were reasonable and that the changes of I_{dc} in the unaged sample could be explained by the changing of concentration of a reactant due to some sort of first order kinetic during measurement process.

The derived I_{dc} when $t = \infty$ and when $t = 0$, based on the fits were plotted in Figure 7-7 with linear regression lines that pass through the original point.

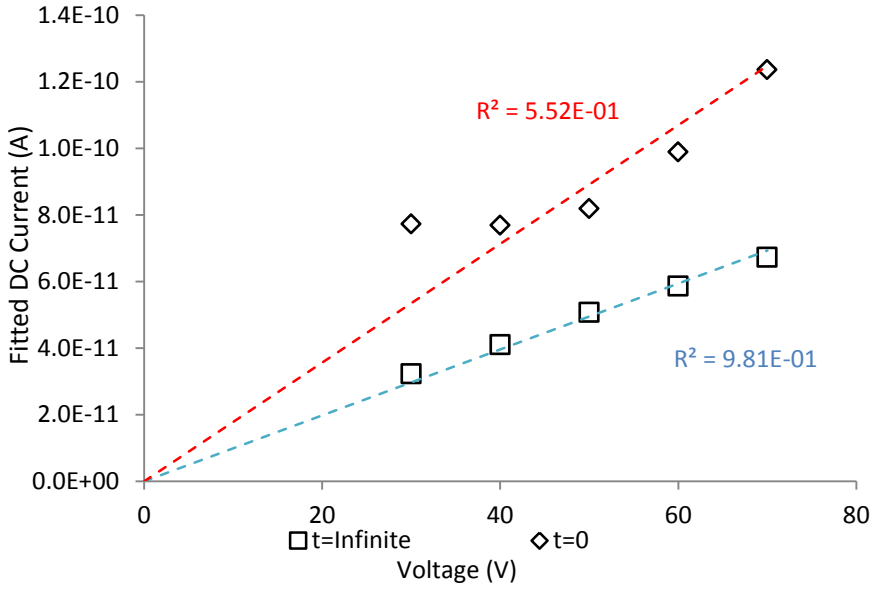

Figure 7-7 Fitted d.c. current for unaged sample (t=∞)

Figure 7-7 indicates that, assuming the oil sample were left in the test cell for a long enough period of time, the measured d.c. current would appear to have a linear behaviour. The conduction characteristic of the oil sample in this case would likely follow Ohm's law. The expected d.c. current at the moment when the unaged sample was filled into the test cell would also be expected to have a linear relationship with the applied voltage passing through the origin since the value of current should be zero when the applied voltage was 0V. However, this was not observed from Figure 7-7. An explanation of this could be because the initial parameter I_0 was sensitive to errors in fitting. Even small amount of error would have a relatively large impact on the fitting results.

7.2.2. TOF AND MOBILITY

The TOF values of unaged insulating oil samples measured for different voltages over five days are shown in Figure 7-8 below.

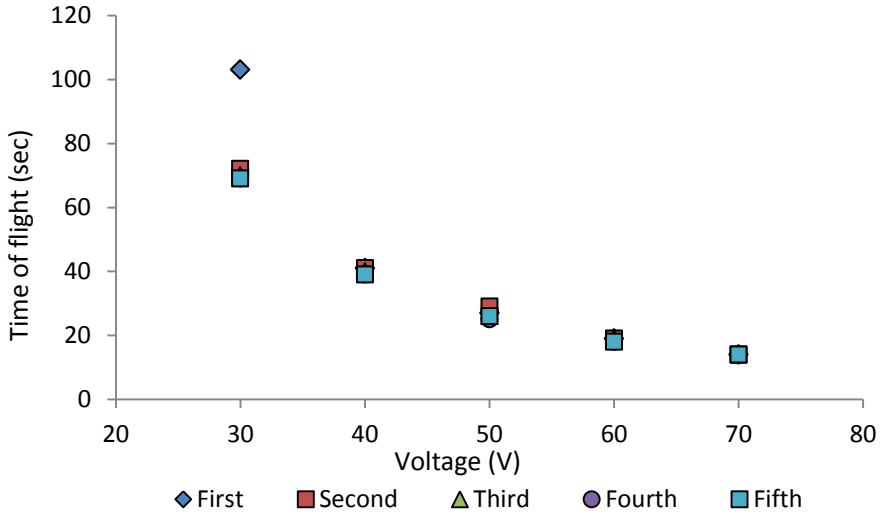

Figure 7-8 TOF of Unaged sample: First, Second, Third, Fourth and Fifth represents measurements taken after 3hours, 27hours, 51hours, 75hours and 99hours, respectively**.**

For voltages above 30V there is little change between the successive measurements. The initial measurement at 30V is significantly larger than subsequent measurements at this voltage whose values are close together. It is not clear why this measurement was so much larger than subsequent measurements.

In the test cell the separation of the two electrodes was 1mm, and the average mobility of charge carriers of samples under corresponding voltage values can be calculated according to the formula $\mu = \frac{d^2}{U \cdot TOF}$. For the 5 sets of successive measurements, the relationship of the calculated mobility and measuring voltage is shown in Figure 7-9.

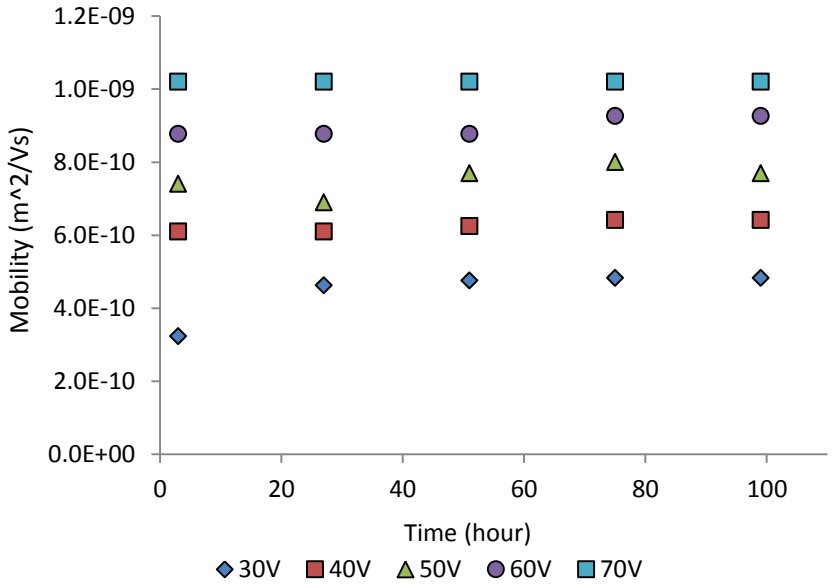

Figure 7-9 Mobility of Unaged sample with different voltage applied

The value of calculated mobility at a given applied voltage appears relatively constant across the set of 5 successive measurements other than the single initial value for 30V where the time of flight was unusually large compared to the other measurements. It is therefore reasonable to take an average value to describe the mobility at each voltage.

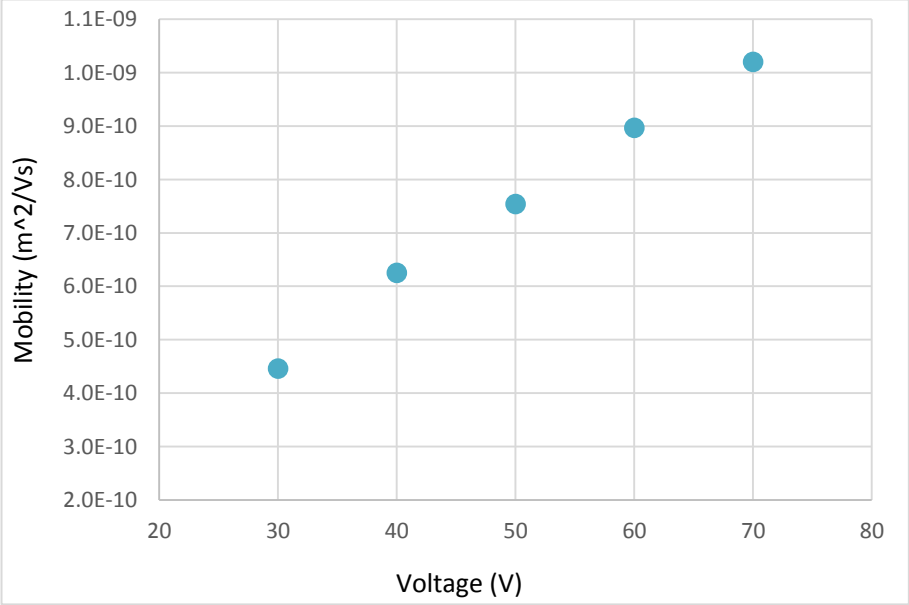

Figure 7-10 Mobility of unaged sample

The behaviour of mobility as a function of voltage is shown in Figure 7-10. It is obvious that the mobility is not constant but increases with voltage. When the applied voltage was 30V, the average value of mobility was 4.01E-7 m^2/Vs.When the voltage rise to 70V, the average value of mobility was 5.00E-6 m^2/Vs. Reasons for this change in mobility behaviour might be due to the EHD effect mentioned in section 3.4.2.

7.3. OIL AGED 2 DAYS

A series of tests following the same approach as used for unaged oil reported in section 7.2 was performed on oil samples that had been thermally aged for 2 days. Again the behaviour of the samples was measured over 5 successive days. The parameters extracted from the current transients are shown in AppendixA 2.

7.3.1. PEAK CURRENT AND DC CURRENT

I_{peak} values of 2 days aged sample under different voltages are shown in Figure 7-11.

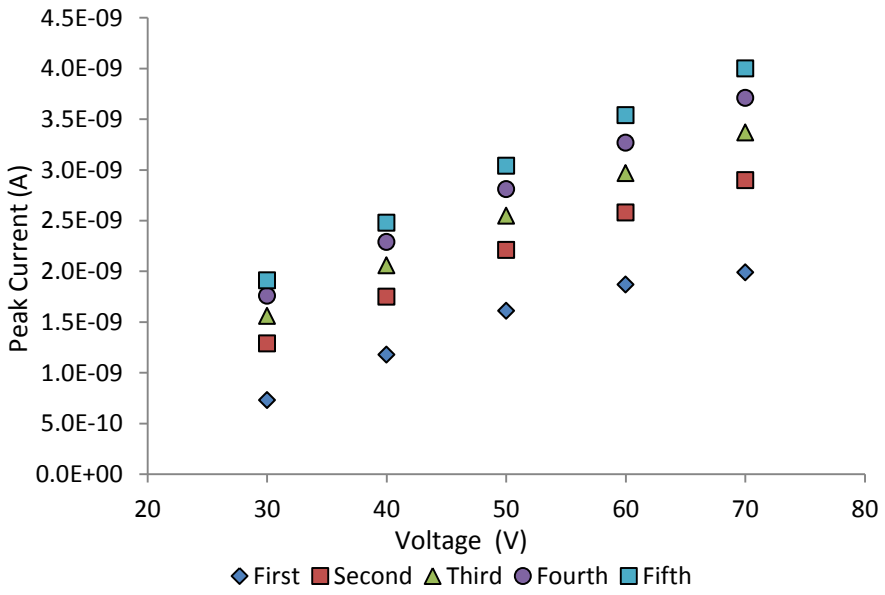

Figure 7-11 Peak current for 2 days aged sample: First, Second, Third, Fourth and Fifth represents measurements taken after 3hours, 27hours, 51hours, 75hours and 99hours, respectively.

From Figure 7-11, it can be seen for each measurement that I_{peak} increases with the applied voltage. There is also a clear change in the measured peak current with the time at which the measurement was taken, with the measured peak current increasing over the 5 successive measurements.

The changes of measured peak current for 2 days aged sample at different voltages are shown in Figure 7-12.

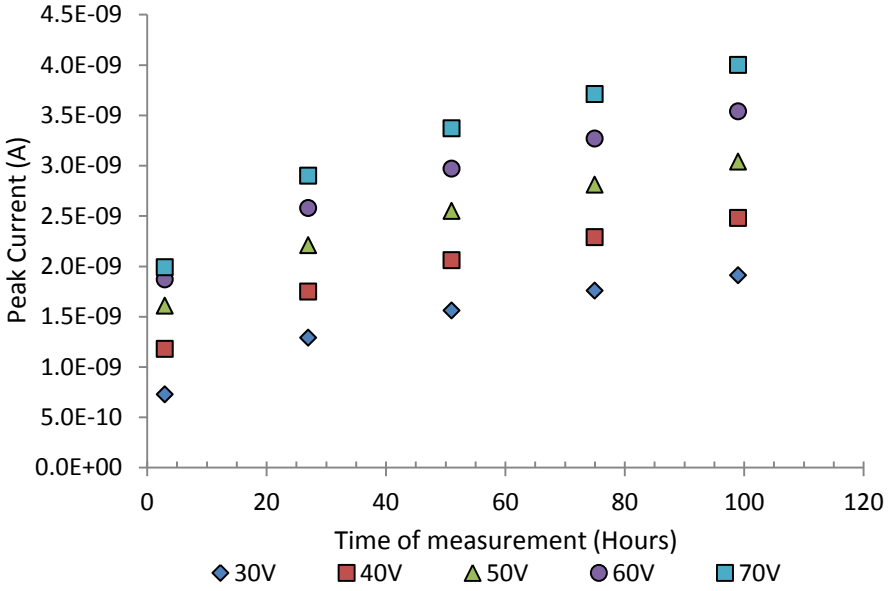

Figure 7-12 Change of peak current with time

It can be seen that the rate of increase in peak current is decreasing with time suggesting that there will be a saturated value at $t = \infty$. Again if the changes were due to simple first order kinetics this suggests a dependence on the concentration of a reactant in the system. The equation below is the simplest that could be used to describe these changes.

$$I_{peak} = I_0\left(1 - e^{(-\frac{t}{\tau})}\right) \qquad \textbf{7-2}$$

However this equation 7-2 leads to a value of $I_{peak} = 0$ for a measurement performed when $\mathrm{t} = 0$ which is unrealistic. Therefore this equation was modified to include a d.c term I_1

$$I_{peak} = I_0\left(1 - e^{(-\frac{t}{\tau})}\right) + I_1 \qquad \textbf{7-3}$$

Unlike the fitting function for I_{dc} of unaged sample in section 7.2.1, the trend of the change of I_{peak} of 2 days aged sample with time was upward. The fitting results of I_{peak} values of 2 days aged sample are shown in Table 7-4.

Voltage (V)	I_1	I_0	τ	R square Value	I_{peak} (A) (t = 0)	I_{peak} (A) (t = ∞)
30	6.51E-10	1.43E-09	48.23	0.998	6.51E-10	2.08E-09
40	1.10E-09	1.66E-09	57.88	0.998	1.10E-09	2.76E-09
50	1.54E-09	1.91E-09	65.61	0.998	1.54E-09	3.44E-09
60	1.78E-09	2.20E-09	64.15	0.998	1.78E-09	3.99E-09
70	1.87E-09	2.50E-09	53.88	0.998	1.87E-09	4.37E-09

Table 7-4 Fitting data of 2 days aged sample peak current

I_{dc} values of 2 days aged sample under different voltages for the 5 successive measurements are shown in Figure 7-13. Similar to the measurements of I_{peak}, it can be seen for each measurement that I_{dc} increases with the applied voltage.

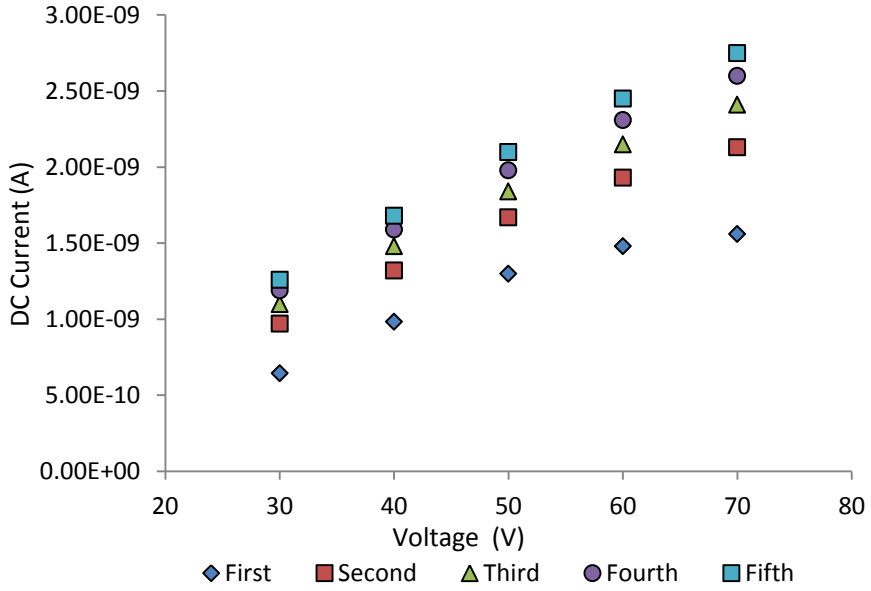

Figure 7-13 DC current for 2 days aged sample: First, Second, Third, Fourth and Fifth represents measurements taken after 3hours, 27hours, 51hours, 75hours and 99hours, respectively.

There is also a clear change in the measured d.c. current with the time at which the measurement was taken, with the measured current increasing over the 5 successive measurements. This trend is shown in Figure 7-14.

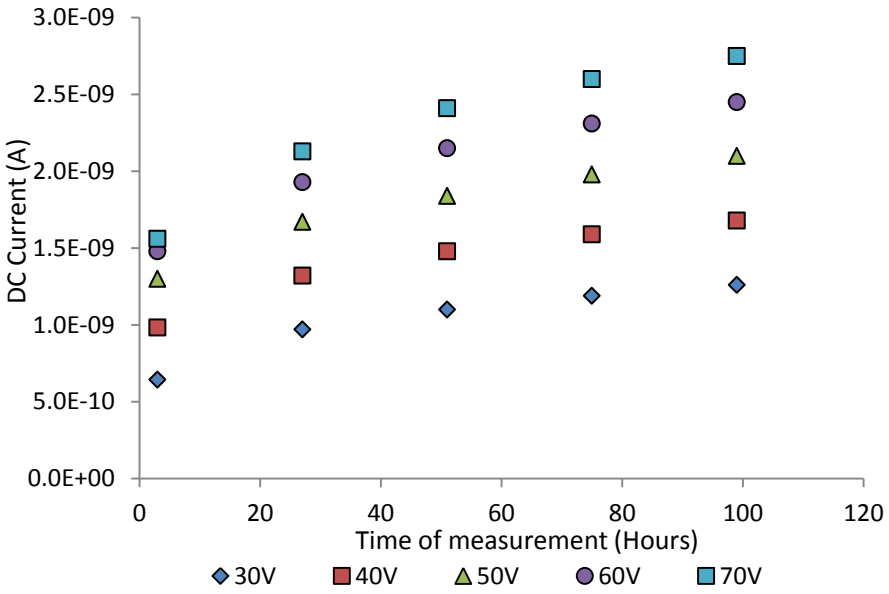

Figure 7-14 Change of d.c. current with time

Again it was decided to fit the data to a curve of the form given in equation 7-3. Fitting results were shown in Table 7-5.

Voltage (V)	I_1	I_0	τ	R^2	I_{dc} (A) (t = 0)	I_{dc} (A) (t = ∞)
30	5.95E-10	7.04E-10	37.929	0.996	5.95E-10	1.30E-09
40	9.36E-10	8.29E-10	46.1134	0.998	9.36E-10	1.76E-09
50	1.25E-09	9.88E-10	53.9863	0.996	1.25E-09	2.24E-09
60	1.42E-09	1.18E-09	51.4664	0.997	1.42E-09	2.61E-09
70	1.48E-09	1.42E-09	46.473	0.998	1.48E-09	2.90E-09

Table 7-5 Fitting data for 2 days aged sample d.c. current

7.3.1.1. Fits to I_{peak} and I_{dc}

Both the I_{dc} and I_{peak} for 2 days aged sample appear to have an upward trend with time during the measurement process suggesting that they are following a first order kinetic. The values of time constant τ in Table 7-4 and Table 7-5 are broadly similar. It was therefore decided to try and fit the data to a common time constant which

would suggest that both I_{peak} and I_{dc} depended on a common property of the system which was changing over time. Such a change would lead to a change of number of charge carriers in the bulk of liquid and have an influence on the current behaviours. Therefore, the change of I_{dc} and I_{peak} were expected to follow a function with same time constant value.

An Excel spreadsheet was used to fit all of the individual data sets to a common value of time constant but with differing values of I_0 and I_1. The value of time constant was adjusted so that the summation of squared residual values across all the fits of the data sets was minimized. The value of time constant τ to optimize the fit across all of the data sets was 54.9 h. The resulting fits to the data for I_{dc} and I_{peak} are shown in Figure 7-15 and Figure 7-16, respectively. The blue lines in Figure 7-15 and Figure 7-16 represent the fitting curves with the common time constant for different measurement voltages.

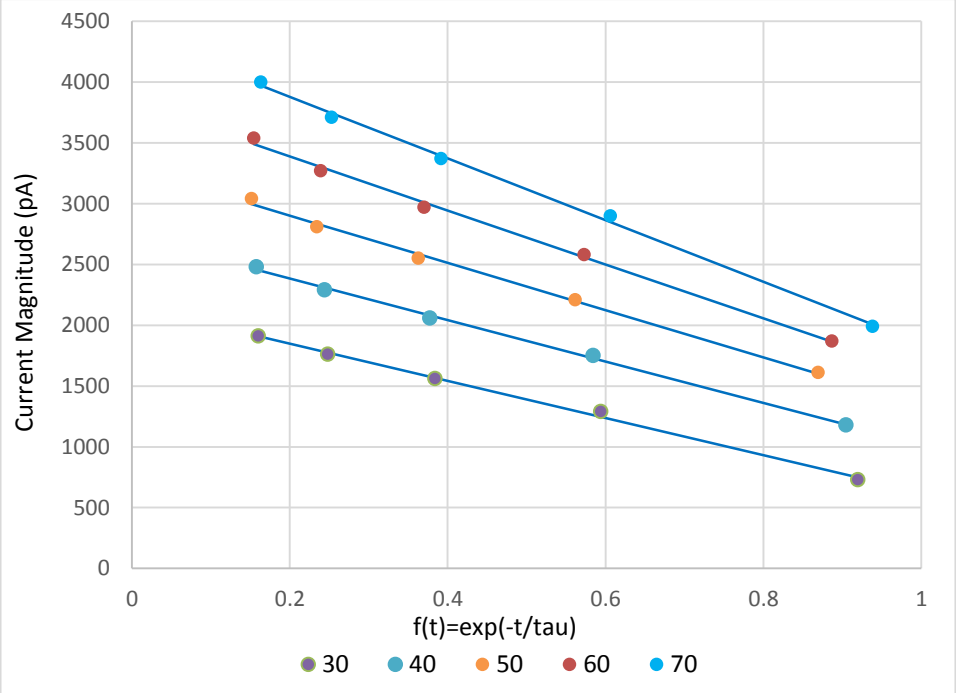

Figure 7-15 Fits of peak current when τ = 54.9 h

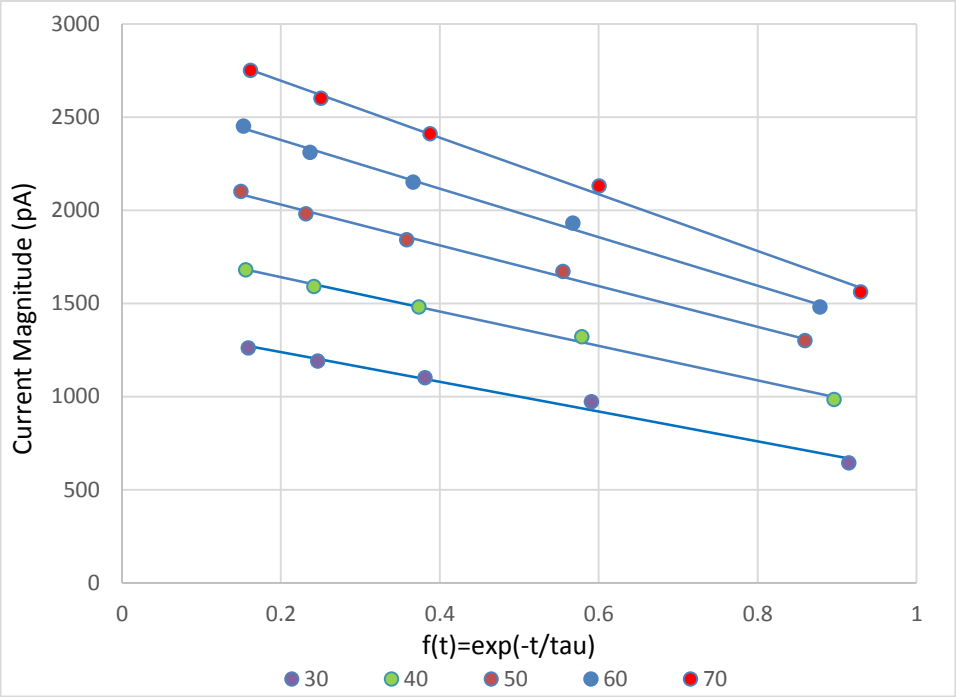

Figure 7-16 Fits of d.c. current when τ = 54.9 h

Figure 7-15 and Figure 7-16 above give evidence that with a common time constant τ of 54.9 h, good fits can be obtained by using equation 7-3. The original measured current values were distributed close to the blue fitting line. The two figures above also indicate that the change of I_{dc} and I_{peak} follows the same function that is in agreement with the first order kinetics.

The values of parameters for the fits with a common time constant τ of 54.9 h to I_{dc} and I_{peak} are shown in Table 7-6 and Table 7-7 with the derived value of R^2 for each individual fit.

Voltage (V)	I_1	I_0	τ	R^2	I_{peak} (pA) (t = 0)	I_{peak} (pA) (t = ∞)
30	626.9	1526.8	54.9	0.997	626.9	2153.7
40	1020.9	1703.8	54.9	0.998	1020.9	2724.7
50	1348.0	1942.1	54.9	0.997	1348.0	3290.2
60	1613.2	2219.2	54.9	0.997	1613.2	3832.5
70	1850.7	2536.1	54.9	0.998	1850.7	4386.8

Table 7-6 Fitting data for 2 days aged sample peak current when time constant τ=54.9 h

Voltage (V)	I_1	I_0	τ	R^2	I_{dc} (pA) (t = 0)	I_{dc} (pA) (t =∞)
30	601.0	797.8	54.9	0.988	601.0	1398.8
40	903.4	921.4	54.9	0.996	903.4	1824.9
50	1155.6	1093.7	54.9	0.996	1155.6	2249.4
60	1334.6	1303.6	54.9	0.997	1334.6	2638.2
70	1476.7	1523.3	54.9	0.997	1476.7	3000.0

Table 7-7 Fitting data for 2 days aged sample d.c. current when time constant τ =54.9 h

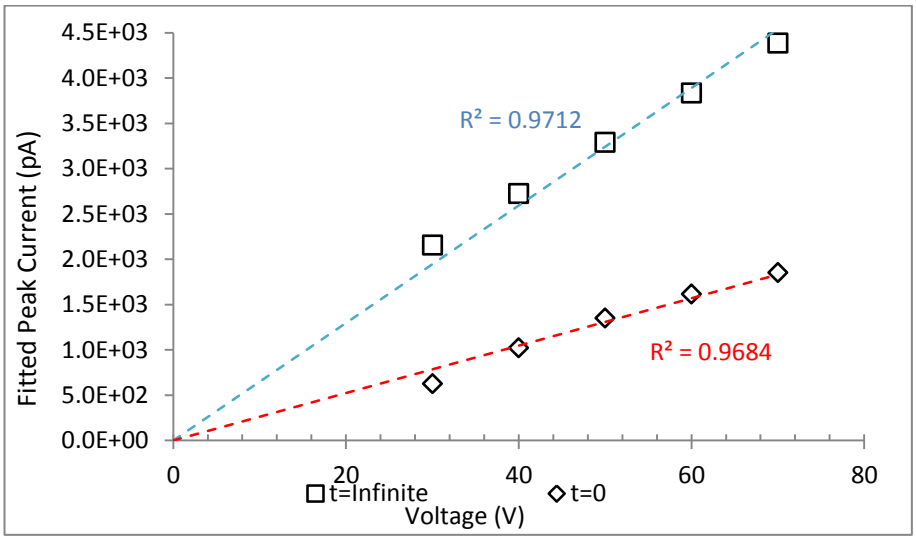

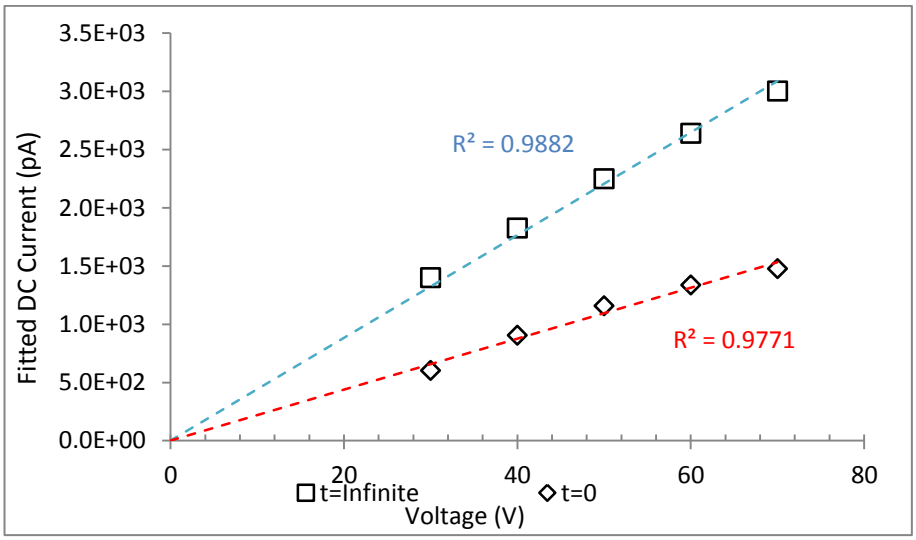

Figure 7-17 Expected results for 2 days aged sample current measurements at initial and equilibrium Upper figure for peak current(a), lower figure for d.c. current(b).

The R^2 values shown in Table 7-6 and Table 7-7 confirm that the fits are appropriate to describe the variation of measured current over the 5 successive measurements. A similar approach was adopted for the analysis of other samples.

Then, derived values of I_{peak} and I_{dc} when $t = 0$ and $t = \infty$ are shown in Figure 7-17.

It is assumed that I_{peak} and I_{dc} would be zero when the applied voltage is equal to zero. The V-I relationship, over the voltage range appears to be linear suggesting an Ohmic behaviour.

7.3.2. TOF AND MOBILITY

The measured TOF values of 2 days aged sample under different voltages for the 5 successive measurements are shown in Figure 7-18.

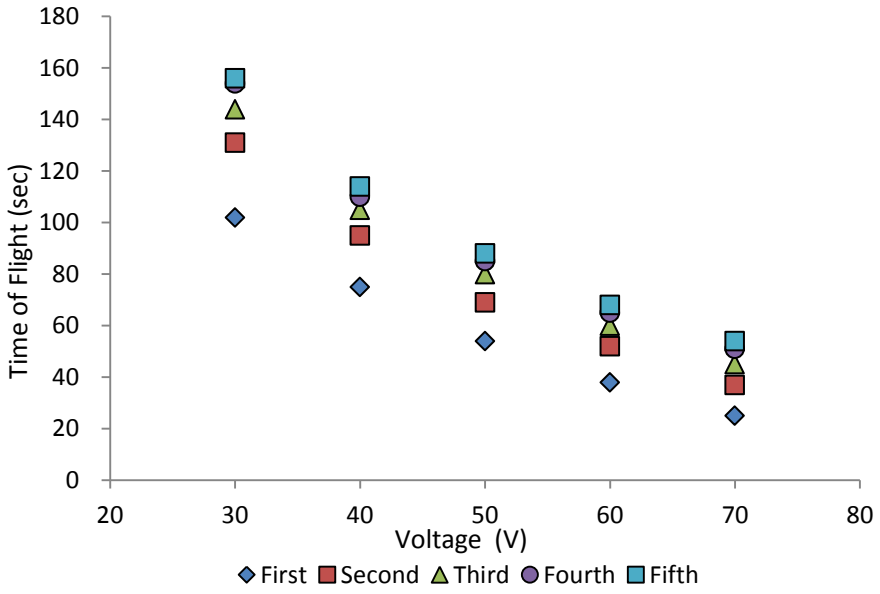

Figure 7-18 Measured TOF of 2 days aged sample

Generally, for oil samples after 2 days ageing treatment, the measured TOF values decrease with the increasing of applied voltage. During the successive measurements over five days, the TOF of aged samples increased with time. This behaviour is different from the measurement of TOF for the samples without ageing where the value appeared to be constant. The time interval of current recording was 1s during the measurement, so the resolution of TOF values was assumed to be ±1s for the experiment results. The rate of change of TOF values decreases with time again suggesting an approach to a constant value at $t = \infty$.

The derived mobility values from the measured TOF are shown in Figure 7-19.

In each set of measurement, the derived mobility increased with the applied voltage. This is similar to the behaviour observed in unaged oil sample. Unlike the unaged oil, the mobility appears to have a downward trend along with the measurement time, with the rate of change decreasing with time.

7.3.2.1. Fitting of Mobility

Looking at the data for 50V the mobility calculated from the first day's measurement is $3.37 \times 10^{-10}\, m^2V^{-1}s^{-1}$, this drops to a value of $2.27 \times 10^{-10}\, m^2V^{-1}s^{-1}$ on the 5th day of measurement. Again this suggests a dependence on a first order kinetic, perhaps occurring due to a chemical reaction.

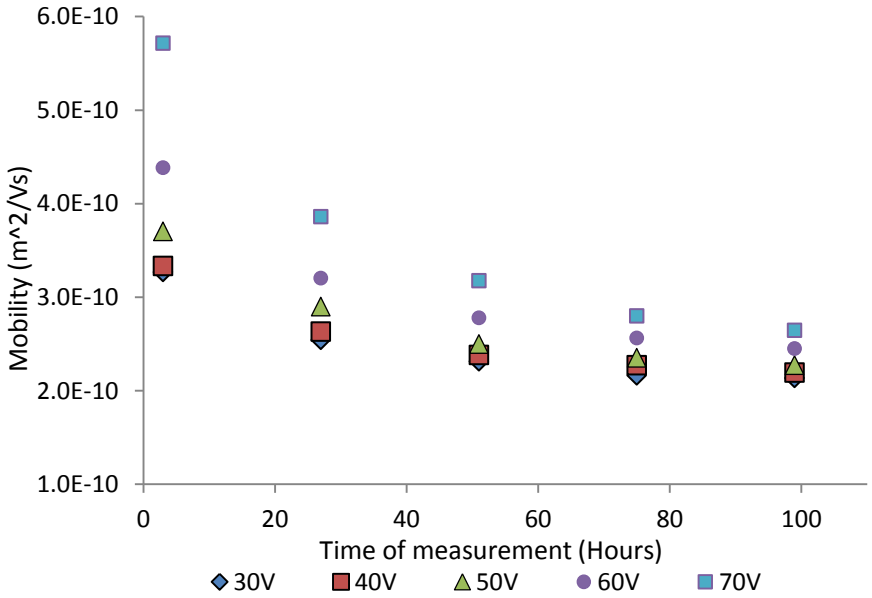

Figure 7-19 Calculated Mobility of 2 days aged sample

The change of mobility could possibly also be explained by a first order kinetics. Therefore, the change of mobility could be expressed by an equation based on a simple reaction kinetic.

$$\mu(t) = \mu_0 e^{(-\frac{t}{\tau})} + \mu_1 \qquad \textbf{7-4}$$

When $t = 0, \mu_{t(0)} = \mu_0 + \mu_1$ which gives the mobility of charge carriers that would be expected at the moment when the oil sample was filled into the test cell.

When $t = \infty$, $\mu_{t(\infty)} = \mu_1$ $\mu_{t(\infty)}$ which gives the mobility of charge carriers that would be expected when sample reached a stable equilibrium.

For mobility measurements, fits were made based on equation 7-4 using a similar process to that used for I_{peak} and I_{dc} where a common value of tau was used for all the fits and the sum of the squares of the residuals were minimized. This process leads to a value of the time constant τ of 29.1 h. The fits with equation 7-4 when τ = 29.1h are shown in Figure 7-20.

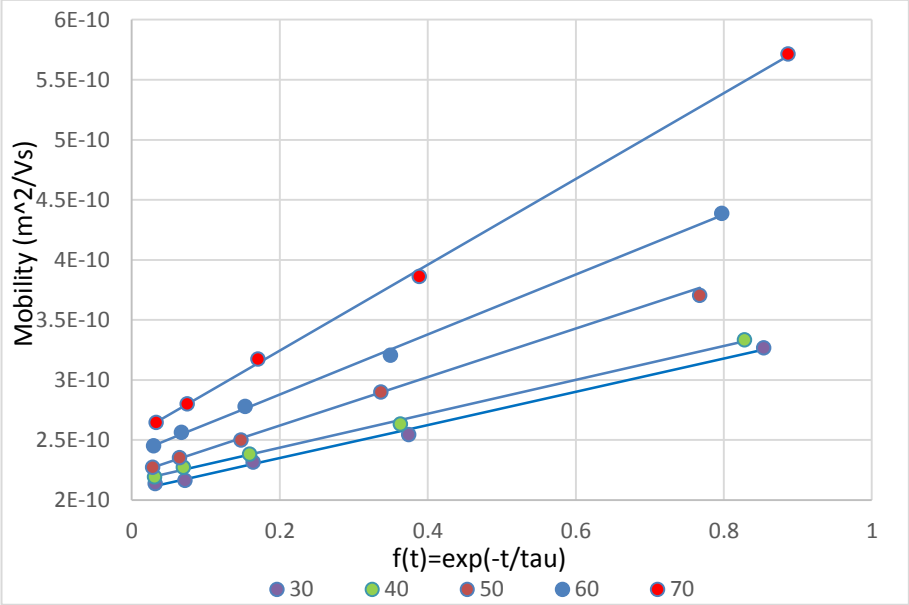

Figure 7-20 Fits of Mobility when τ = 29.1 h

The results of fit parameters are shown in Table 7-8. Figure 7-20 and the values for R^2 in Table 7-8 indicate that a reasonable fit across all the data can be obtained by using a common τ value of 29.1 h.

Voltage (V)	μ_1	μ_0	τ	R^2	Mobility (t = 0)	Mobility (t =∞)
30	2.07E-10	1.38E-10	29.1	0.997	3.45E-10	2.07E-10
40	2.15E-10	1.41E-10	29.1	0.993	3.56E-10	2.15E-10
50	2.21E-10	2.02E-10	29.1	0.979	4.24E-10	2.21E-10
60	2.38E-10	2.50E-10	29.1	0.982	4.88E-10	2.38E-10
70	2.53E-10	3.57E-10	29.1	0.961	6.10E-10	2.53E-10

Table 7-8 Fits of Mobility when τ = 29.1 h

The fitted mobility values were plotted against the applied voltage in Figure 7-21.

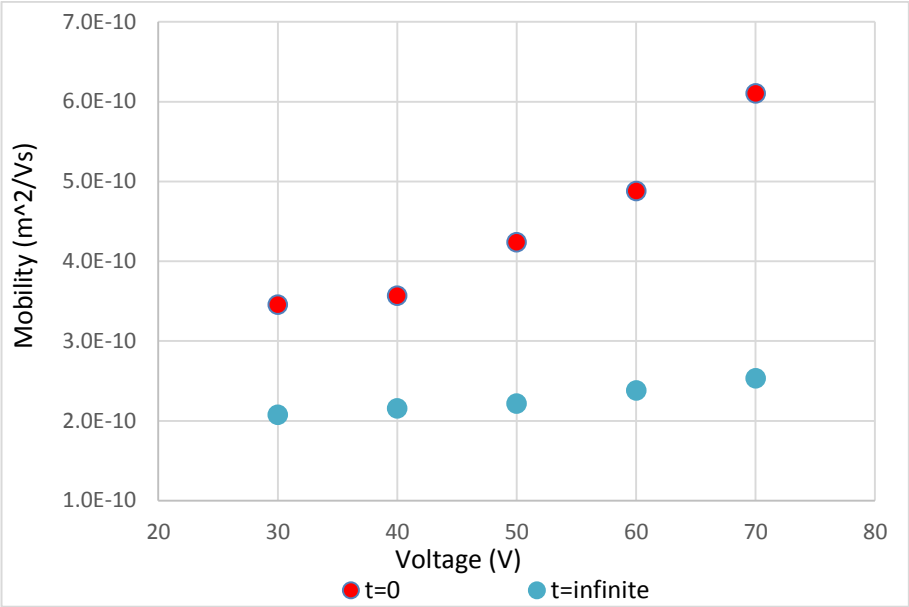

Figure 7-21 Mobility of 2 days aged sample

The measured values of mobility of charge carriers for 2 days aged sample were smaller than that for unaged sample. When $t = 0$, the measured mobility appears to have a clear upward trend with the applied voltage. But this voltage dependence appears to be suppressed when $t = \infty$. Further discussion will be given in section 7.7.

7.4. OIL AGED 4 DAYS

In this section, 250mL Shell Diala insulating oil sample mentioned in section 5.2 were thermally aged for 96 hours. The method of thermal ageing was introduced in pervious section 5.3. Again, 5 successive measurements were done. The parameters derived from the current transients are shown in AppendixA 3.

7.4.1. PEAK CURRENT AND DC CURRENT

Both the I_{peak} and I_{dc} values were significantly increased compared with the measurement results from the 2 days aged sample described in the previous section. Through the 5 successive measurements, the measured I_{peak} and I_{dc} appears to have an upward trend which was similar to that of the 2 days aged sample, therefore the same fitting method was used to characterize the current behaviours for the 4 days

aged sample. The fitting results using equation 7-4 are shown in Table 7-9 and Table 7-10. The R^2 values in Table 7-9 and Table 7-10 confirm that the fits of I_{peak} and I_{dc} are appropriate. However, the optimal value of time constant τ is different from that of 2 days aged sample. In the fits of 2 days sample, the time constant is 52.9 h and the value of time constant in 4 days aged sample is 60.5 h.

The expected values of I_{peak} and I_{dc} values when $t = 0$ and $t = \infty$, derived from the fits, are plotted in Figure 7-22 and Figure 7-23.

Voltage (V)	I_1	I_0	τ	R^2	I_{peak} (A) (t = 0)	I_{peak} (A) (t = ∞)
30	1.16E-09	3.53E-09	60.5	0.999	1.16E-09	4.69E-09
40	1.68E-09	4.25E-09	60.5	0.999	1.68E-09	5.92E-09
50	2.14E-09	4.96E-09	60.5	0.999	2.14E-09	7.10E-09
60	2.48E-09	5.85E-09	60.5	0.999	2.48E-09	8.33E-09
70	2.85E-09	6.82E-09	60.5	0.999	2.85E-09	9.67E-09

Table 7-9 Fitting data for 4 days aged sample peak current when τ= 60.5 h

Voltage (V)	I_1	I_0	τ	R^2	I_{dc} (A) (t = 0)	I_{dc} (A) (t =∞)
30	1.14E-09	1.92E-09	60.5	0.999	1.14E-09	3.05E-09
40	1.59E-09	2.31E-09	60.5	0.999	1.59E-09	3.90E-09
50	2.00E-09	2.74E-09	60.5	0.998	2.00E-09	4.74E-09
60	2.31E-09	3.26E-09	60.5	0.998	2.31E-09	5.57E-09
70	2.58E-09	3.87E-09	60.5	0.998	2.58E-09	6.45E-09

Table 7-10 Fitting data for 4 days aged sample dc current when τ =60.5 h

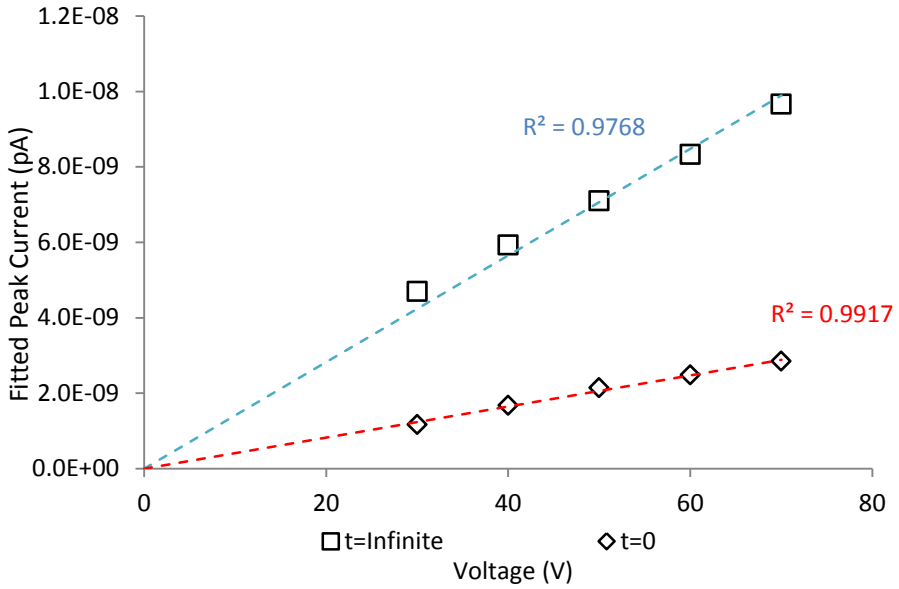

Figure 7-22 Expected peak current of 4 days aged sample

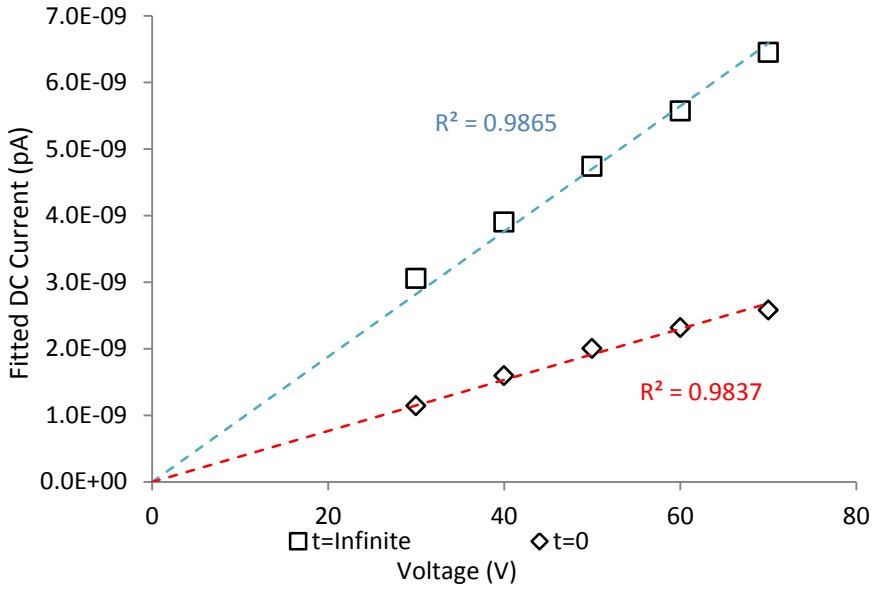

Figure 7-23 Expected d.c current of 4 days aged sample

Again, the expected current values should be zero when the applied voltage was equal to zero. Including this point in the data the derived currents all appear to have linear relationships with the applied voltage as shown in Figure 7-22 and Figure 7-23.

7.4.2. TOF AND MOBILITY

The TOF and mobility behaviours were similar to that in the measurements of the 2 days aged sample. The measured values of TOF for 4 days aged sample appear to have an upward trend with time over the 5 successive measurements process and therefore the derived values of mobility of charge carriers appear to have a downward trend along with the measurement time.

Equation 7-4 was adopted to fit the measured values of mobility. Parameters of fits of mobility are shown in Table 7-11. With a time constant value τ of 14.9 h, a minimum value of SSR can be obtained. The R^2 values in Table 7-11 suggested that the quality of these fits were not as high as were observed for the 2 day aged sample. This was due to the small value of τ causing the majority of the change to occur over the first two data points. The fits to the data for mobility are shown in Figure 7-24. These indicate fits are acceptable since the actual measured values of mobility are located close to the data calculated from the fits.

Voltage (V)	μ_1	μ_0	τ	R^2	Mobility (t = 0)	Mobility (t =∞)
30	3.05E-10	1.91E-10	14.9	0.993	4.97E-10	3.05E-10
40	3.05E-10	1.73E-10	14.9	0.924	4.78E-10	3.05E-10
50	3.05E-10	1.70E-10	14.9	0.949	4.75E-10	3.05E-10
60	3.16E-10	2.52E-10	14.9	0.944	5.68E-10	3.16E-10
70	3.20E-10	4.52E-10	14.9	0.885	7.72E-10	3.20E-10

Table 7-11 Fit data of mobility for 4 days aged sample

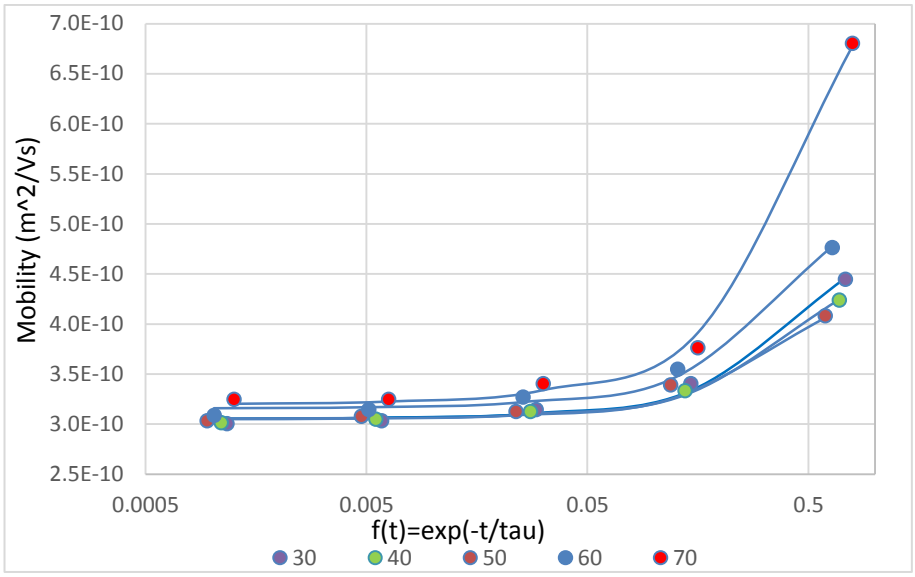

Figure 7-24 Fits of mobility of 4 days aged sample

The mobility parameters for 4 days aged sample when $t = 0$ and $t = \infty$ are plotted in Figure 7-25.

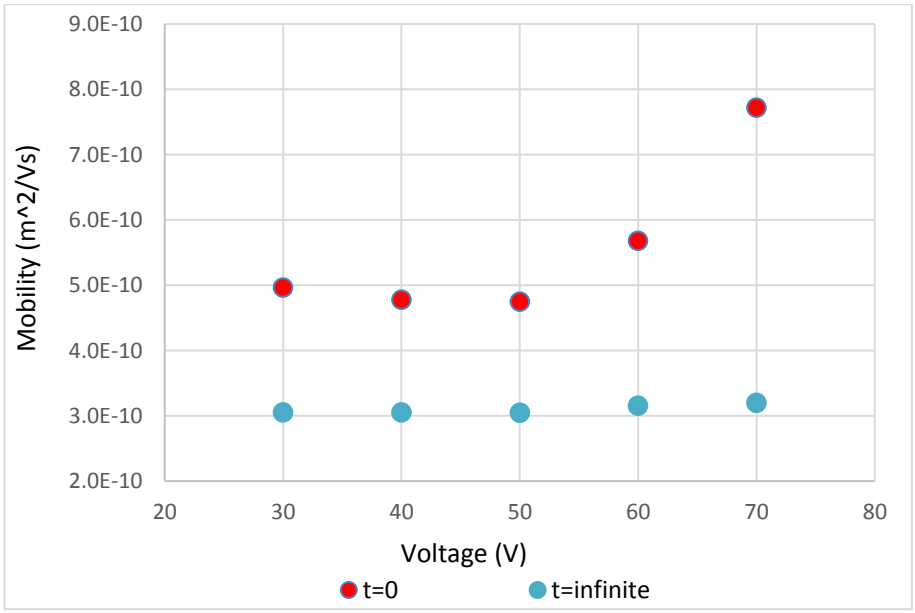

Figure 7-25 Fitted mobility of 4 days aged sample

The measured values of mobility of charge carriers for 4 days aged sample were larger than that for 2 day aged sample. When $t = 0$, the measured mobility appears to have an upward trend with the applied voltage. But this voltage dependence

appears to be suppressed when $t = \infty$. This behaviour is similar to that for 2 day aged sample.

7.5. OIL AGED 8 DAYS

In this section, 250mL Shell Diala oil sample was thermal aged for 192 hours with the same ageing method mentioned previously. Note that for oil sample after 8 days thermal ageing process, a small amount of precipitate was observed in the bulk of the sample which was not seen in the 2 days aged sample and 4 days aged sample. The generated precipitate was expected to be a product of a chemical reaction due to the thermal ageing process. This generation of solid precipitate was also observed and was separated from the oil sample by centrifuging in I. L. Hosier's study [**23**]. In this study however before the sample cell was filled, the aged oil was left for a period of 3 weeks which allowed the precipitate to settle. The cell was then filled with the oil from above the precipitate. The values of $I_{peak,}$ I_{dc} and TOF, were measured using bipolar measurement method over 5 successive measurements. AppendixA 4 presents the recorded data for 8 days sample.

7.5.1. PEAK CURRENT AND DC CURRENT

A similar upward trend in the currents as seen with the 2 day and 4 day aged oils was observed in the measurements of 8 days aged sample. Therefore, the data was fitted to equation 7-3 using an optimized common value of τ. The fitting results are shown in Table 7-12 and Table 7-13 below.

Voltage (V)	I_1 (A)	I_0 (A)	τ	R^2	I_{peak} (A) (t = 0)	I_{peak} (A) (t = ∞)
30	4.22E-09	7.57E-09	49.8	0.996	4.22E-09	1.18E-08
40	6.44E-09	8.71E-09	49.8	0.998	6.44E-09	1.52E-08
50	8.39E-09	1.03E-08	49.8	0.996	8.39E-09	1.87E-08
60	9.80E-09	1.22E-08	49.8	0.998	9.80E-09	2.20E-08
70	1.08E-08	1.46E-08	49.8	0.998	1.08E-08	2.55E-08

Table 7-12 Fitting data for 8 day aged sample peak current when time constant τ =49.8h

Voltage (V)	I_1 (A)	I_0 (A)	τ	R^2	I_{dc} (A) (t = 0)	I_{dc} (A) (t =∞)
30	3.92E-09	4.38E-09	49.8	0.997	3.92E-09	8.29E-09
40	5.65E-09	4.94E-09	49.8	0.999	5.65E-09	1.06E-08
50	7.19E-09	5.76E-09	49.8	0.996	7.19E-09	1.30E-08
60	8.46E-09	6.82E-09	49.8	0.999	8.46E-09	1.53E-08
70	9.46E-09	8.06E-09	49.8	0.997	9.46E-09	1.75E-08

Table 7-13 Fitting data for 8 days aged sample d.c. current when time constant τ=49.8 h

The fitting results of d.c. current and peak current are shown in Figure 7-26 and Figure 7-27.

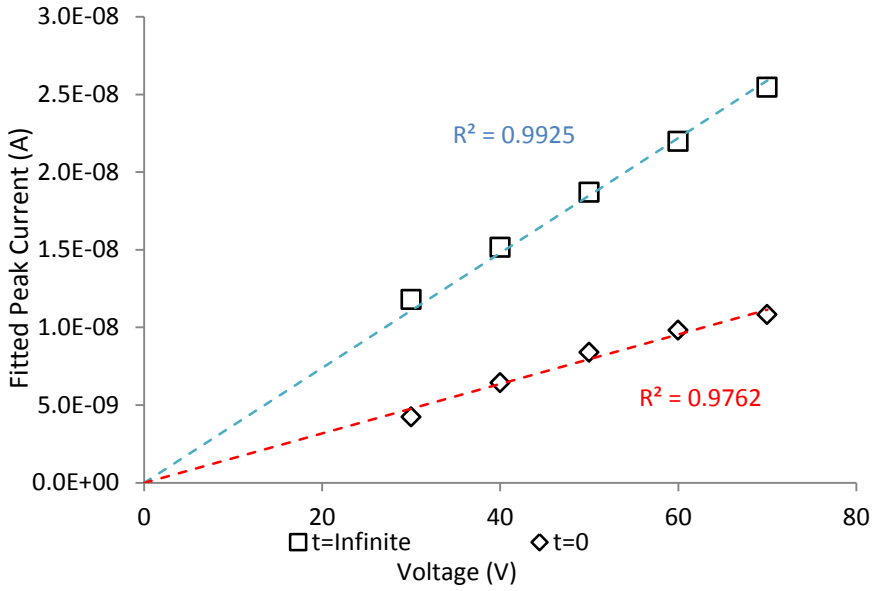

Figure 7-26 Expected peak current of 8 day aged sample

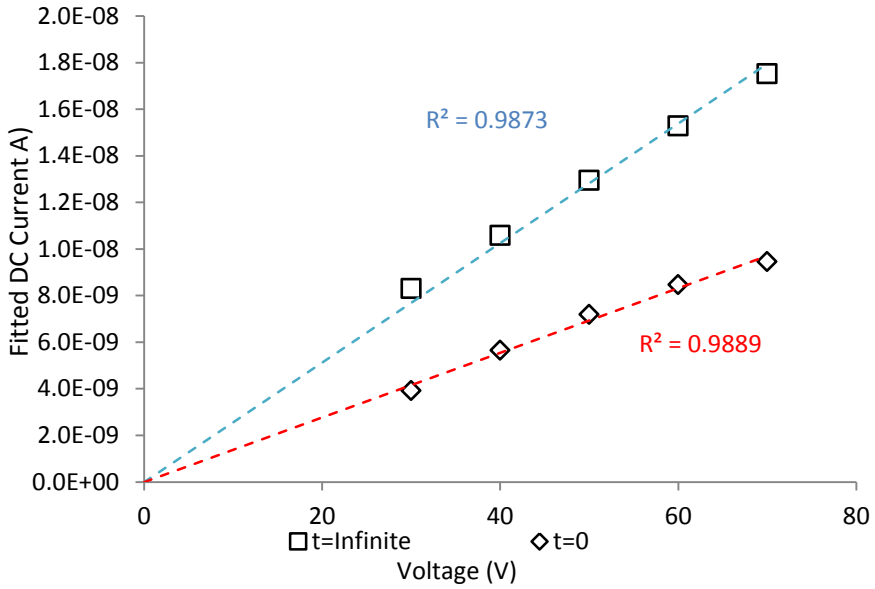

Figure 7-27 Expected d.c. current of 8 day aged sample

Again, with the constraint that the current must be zero when the applied voltage is zero, Ohmic type fits were applied on the data for 8 day aged sample. A linear V-I relationship can be obtained over the voltage range as shown in Figure 7-26 and Figure 7-27.

7.5.2. TOF AND MOBILITY

The calculated mobility of charge carriers in the bulk of 8 days aged sample had a downward trend with measurement time at which the measurement was taken.

Parameters of fits of mobility for 8 days aged oil are shown in Table 7-14.

Voltage (V)	μ_1	μ_0	τ	R^2	Mobility (t = 0)	Mobility (t =∞)
30	4.30E-10	1.48E-10	28.4	0.998	5.78E-10	4.30E-10
40	4.33E-10	1.34E-10	28.4	0.984	5.67E-10	4.33E-10
50	4.39E-10	1.53E-10	28.4	0.984	5.92E-10	4.39E-10
60	4.51E-10	1.57E-10	28.4	0.995	6.08E-10	4.51E-10
70	4.56E-10	2.16E-10	28.4	0.985	6.71E-10	4.56E-10

Table 7-14 Fit data of mobility for 8 days aged sample

The mobility parameters for 8 days aged oil sample when $t = 0$ and $t = \infty$ are plotted in Figure 7-28.

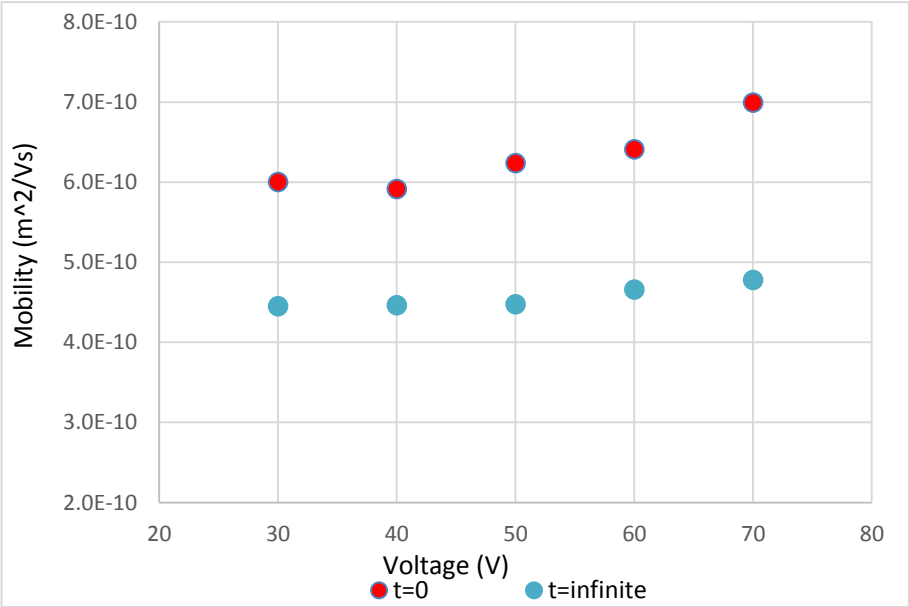

Figure 7-28 Fitted mobility of 8 days aged oil sample

In the derived mobility values when $t = 0$ there might be a slightly upward trend with the applied voltage. But when the system reached equilibrium, this voltage dependence was suppressed. The mobility of charge carriers appears to be a voltage independent parameter in this case.

7.6. CENTRIFUGED AGED OIL

There were concerns that the precipitate which was only seen in the sample aged for 8 days may have an effect on the measurement results despite the oil being left to settle. Therefore part of the 8 day aged oil sample was centrifuged in an attempt to remove the precipitate more completely. Filtering was avoided due to concerns about the oil becoming contaminated with fibers during the filtering process.

50 ml 8 days sample was filled into a plastic tube from the glass bottle (above the precipitate) and centrifuged using a "Heraeus™ Labofuge™ 400R" centrifuge at 2000 revolutions per minute for 30 minutes.

A small amount of precipitate was observed at the bottom of the tube after the sample was centrifuged for 30 min, Figure 7-29. Oil sample above the precipitate

was then used to fill the test cell and a sequence of 5 successive bipolar measurements following the procedure described in section 6.7 was taken.

Figure 7-29 Centrifuging of 8 day aged sample

For the centrifuged 8 day aged oil sample measured over 5 days, I_{peak} and I_{dc} values also have an upward trend following the time that the sample has been present in the test cell. The measured values of I_{peak} and I_{dc} over 5 successive measurements were fitted with equation 7-3. Fitting results are shown in Table 7-15 and Table 7-16.

The range of Pearson correlation coefficient R^2 calculated from fits under different applied voltages is from 0.995 to 0.998 which suggest that the qualities of fits are acceptable. Comparison of the expected values of I_{peak} and I_{dc} measured from centrifuged 8 day aged sample with that measured from 8 day aged sample without centrifuging are plotted in Figure 7-30 and Figure 7-31.

Voltage (V)	I_1	I_0	τ	R^2	I_{peak} (A) (t = 0)	I_{peak} (A) (t = ∞)
30	4.01E-09	1.12E-08	49.9	0.995	4.01E-09	1.52E-08
40	6.22E-09	1.33E-08	49.9	0.997	6.22E-09	1.95E-08
50	8.18E-09	1.56E-08	49.9	0.996	8.18E-09	2.38E-08
60	9.51E-09	1.86E-08	49.9	0.998	9.51E-09	2.81E-08
70	1.05E-08	2.22E-08	49.9	0.997	1.05E-08	3.28E-08

Table 7-15 Fitting data for centrifuged 8 day aged sample peak current when time constant τ = 49.9 h

Voltage (V)	I_1	I_0	τ	R^2	I_{dc} (A) (t = 0)	I_{dc} (A) (t =∞)
30	3.66E-09	6.93E-09	49.9	0.996	3.66E-09	1.06E-08
40	5.44E-09	7.96E-09	49.9	0.997	5.44E-09	1.34E-08
50	7.05E-09	9.32E-09	49.9	0.995	7.05E-09	1.64E-08
60	8.22E-09	1.11E-08	49.9	0.998	8.22E-09	1.93E-08
70	9.12E-09	1.32E-08	49.9	0.997	9.12E-09	2.23E-08

Table 7-16 Fitting data for centrifuged 8 day aged sample d.c. current when time constant τ = 49.9 h

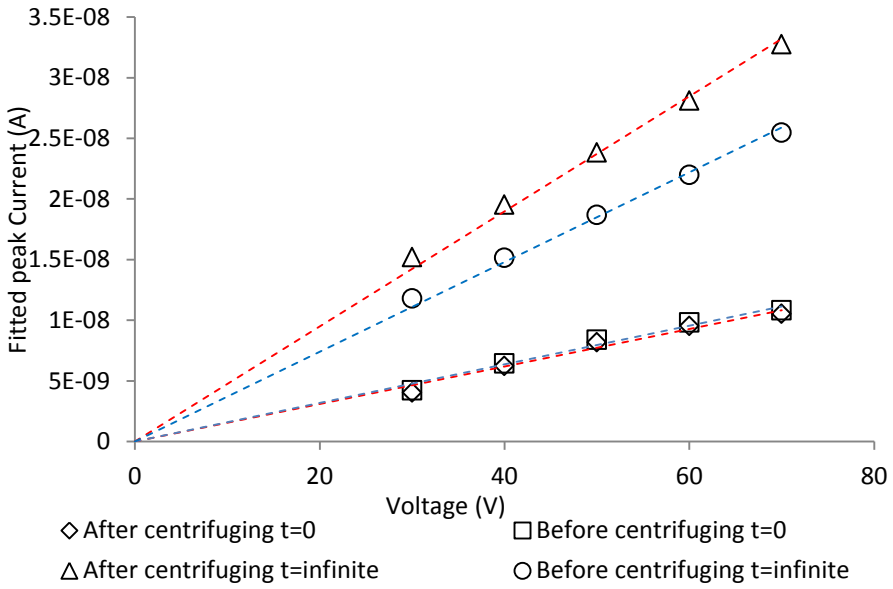

Figure 7-30 Comparison of 8 day aged sample with centrifuged 8 day aged sample Graph for peak current

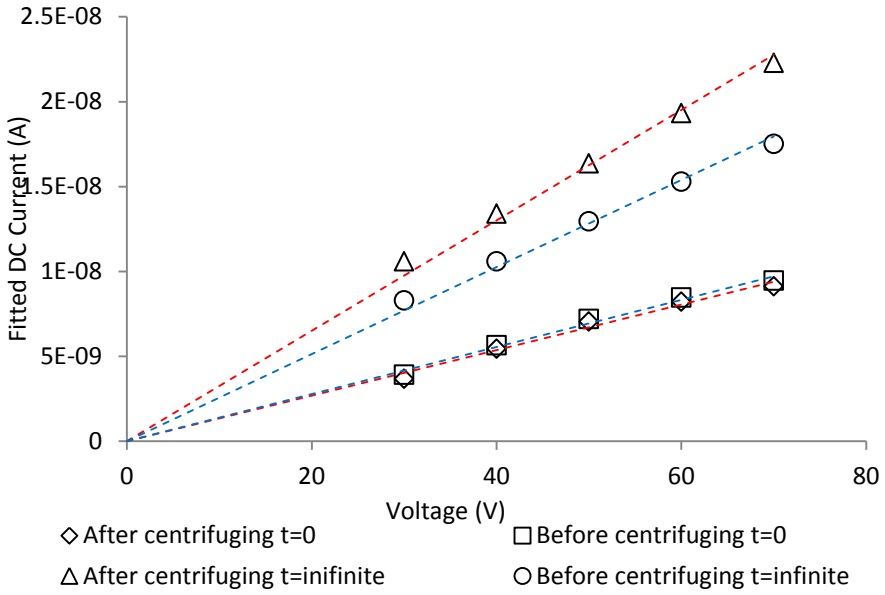

Figure 7-31 Comparison of 8 day aged sample with centrifuged 8 day aged sample Graph for d.c. current

When $t = 0$, the behaviours of I_{peak} and I_{dc} for the centrifuged 8 day aged sample and for original 8 day aged sample are very close in value. It seems that centrifuging did not have a significant effect on the expected peak currents or d.c. current at the moment when oil samples were filled into the test cell. However, when the measurement system reached equilibrium, the expected I_{peak} and I_{dc} magnitude of sample after centrifuging was larger than that of sample without being centrifuged. The derived currents all appear to have linear relationships with the applied voltage as shown in Figure 7-30 and Figure 7-31. These results imply that centrifuging might be a suitable way of removing the precipitate from the samples.

7.7. ANALYSIS AND DISCUSSION

From the experiment results listed previously, I_{peak}. I_{dc} and TOF values varied with time when the tests were done over 5 successive measurements. Therefore, expected values of I_{peak}, I_{dc} and TOF were obtained from the fits of experimental results described in this chapter previously. The parameters derived from these fits will be used for comparison in this section.

7.7.1. PEAK CURRENT AND DC CURRENT

At the moment when the sample was filled into the test cell, the derived peak current values obtained from fits of different samples are plotted together in Figure 7-32(a). The expected values for when the system reached equilibrium are plotted in Figure 7-32(b). For the unaged sample, as no clear trend could be seen in the data over a five day measurement cycle, the average value at each voltage has been used for both $t = 0$ and $t = \infty$.

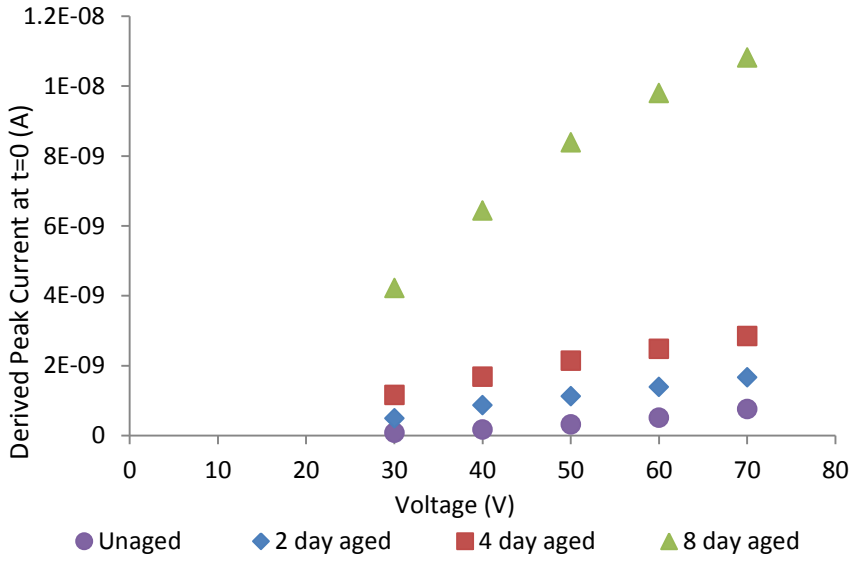

(a)

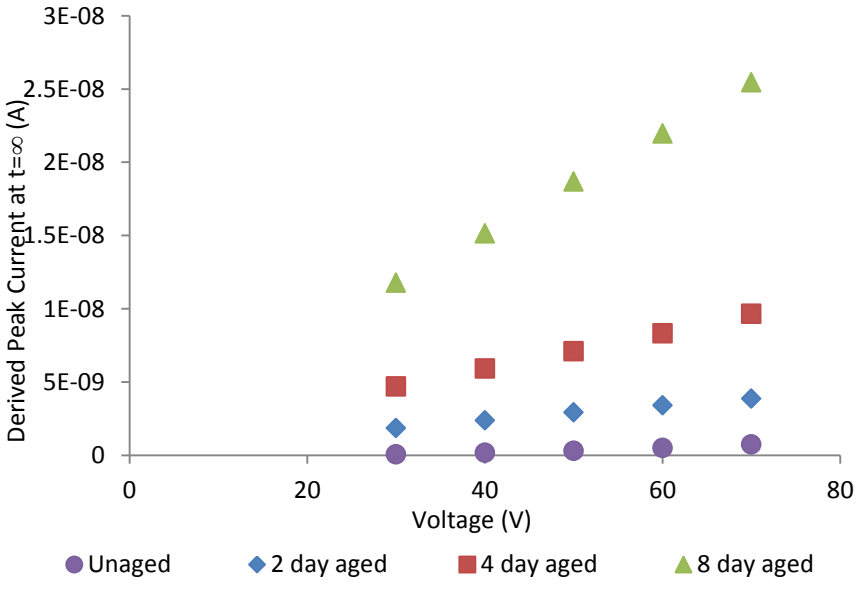

(b)

Figure 7-32 Expected peak currents of unaged sample and aged oil samples Upper graph when t = 0 (a); lower graph when t = ∞(b)

All the derived peak currents can be described by a linear relationship with the applied voltage. The experiment result shows that the peak current of different oil samples increased with the increasing time of thermal ageing treatment which can be seen from the Figure 7-32. The ageing of the sample is having a clear impact on the behaviour of the samples.

The relationship between the expected peak current and the applied voltage at $t = 0$ and $t = \infty$ appears to be linear. It is also expected that the peak current would be zero when the applied voltage is zero. Therefore, linear regression lines that pass through the origin were calculated for each sample. The gradient of these regression lines are shown in Figure 7-33 plotted against ageing time. The unit of the gradient would be conductance, but it should be remembered that it is defined in terms of peak current and d.c. voltage. For convenience the gradient will be defined as the "*peak conductance"*.

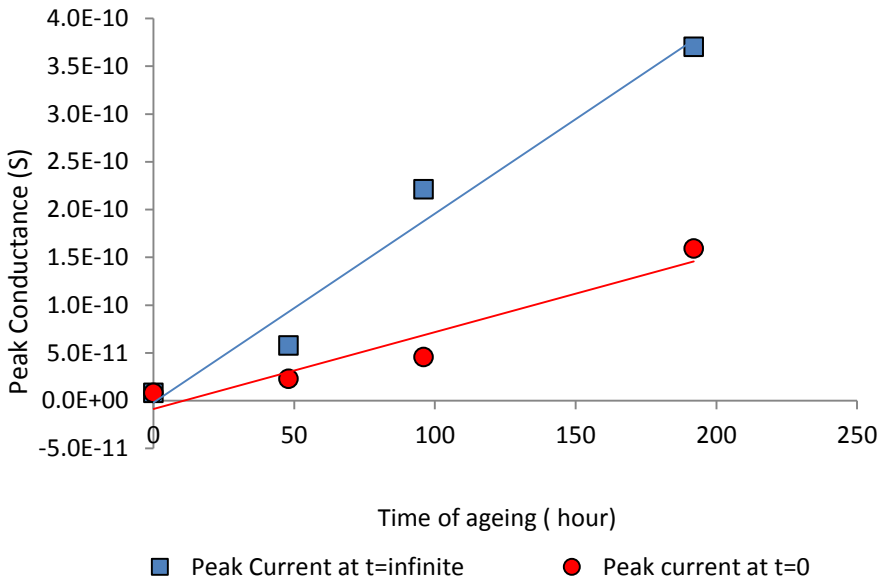

Figure 7-33 Derived peak conductance from peak current

Derived results from the peak current indicate that the peak conductance of the oil sample increased with the increase of thermal ageing time in a broadly linear manner. However, it is not clear if this relationship would hold for longer ageing times.

The derived initial values expected when the test cell was first filled for d.c. current of different samples are plotted in Figure 7-34 (a), while the expected d.c. current

values of samples when the measurement system had reached equilibrium, $t = \infty$ are shown in Figure 7-34 (b). This has been done as for I_{dc} the measured current changed over successive measurements, so values for the expected initial current and equilibrium current from fitting should be plotted rather than the common average values used for the peak current measurements.

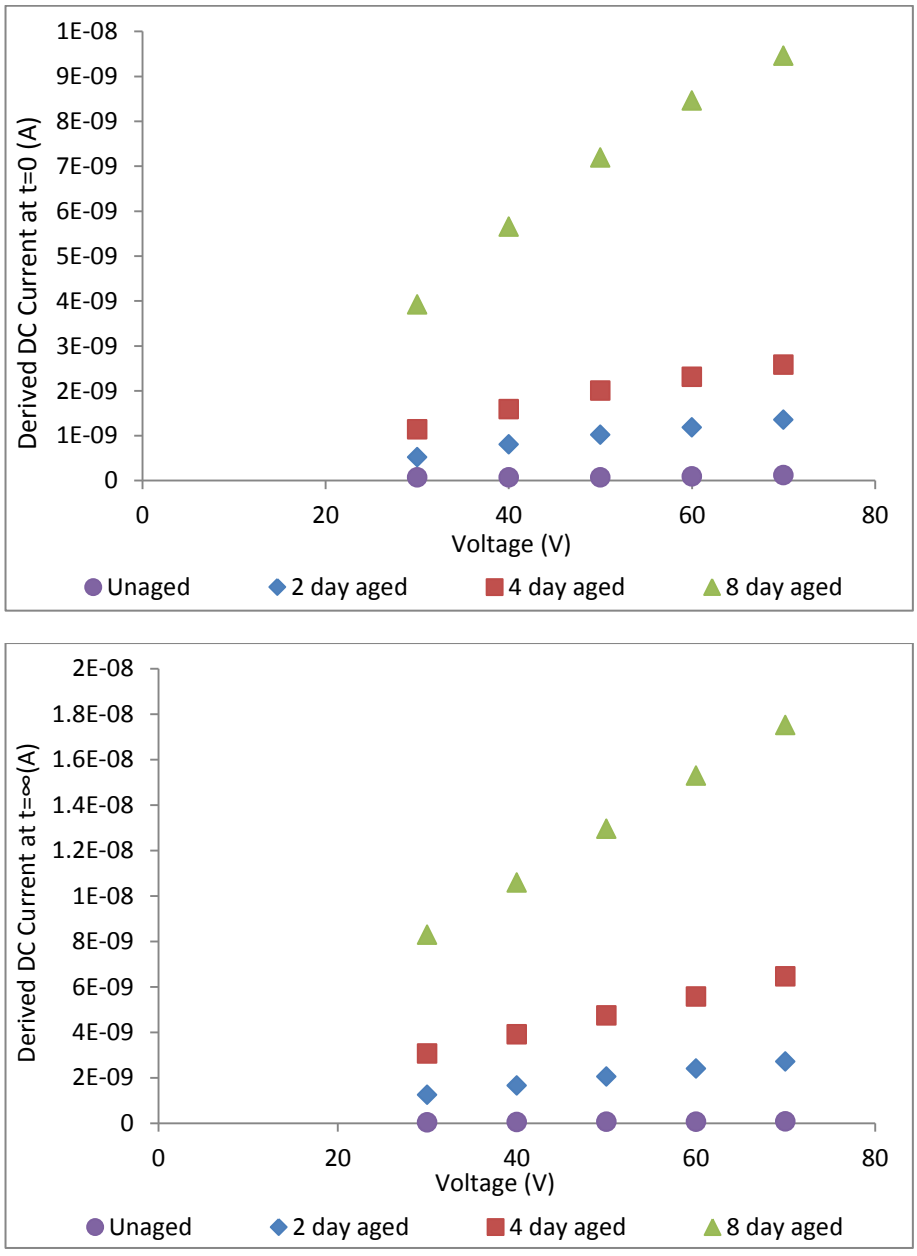

Figure 7-34 Expected d.c. currents of unaged sample and aged oil samples Upper graph when t=0 (a); lower graph when t $= \infty$(b).

Like the peak currents, all the derived d.c. currents can be described by a linear relationship with the applied voltage. Also, the experiment result shows that the d.c.

current measured for the oil samples increased with the increasing time of thermal ageing.

As the relationship between I_{dc} and the applied voltage also appears to be linear, the gradients for linear regression lines for each sample were calculated again assuming that the current was zero when the applied voltage was zero. These gradients which have the units of conductance are plotted in Figure 7-35. Again, for convenient, the derived gradient from the d.c. current when $t = \infty$ is defined as *"d.c. conductance"* as it represents the conductance of the system at an equilibrium steady state.

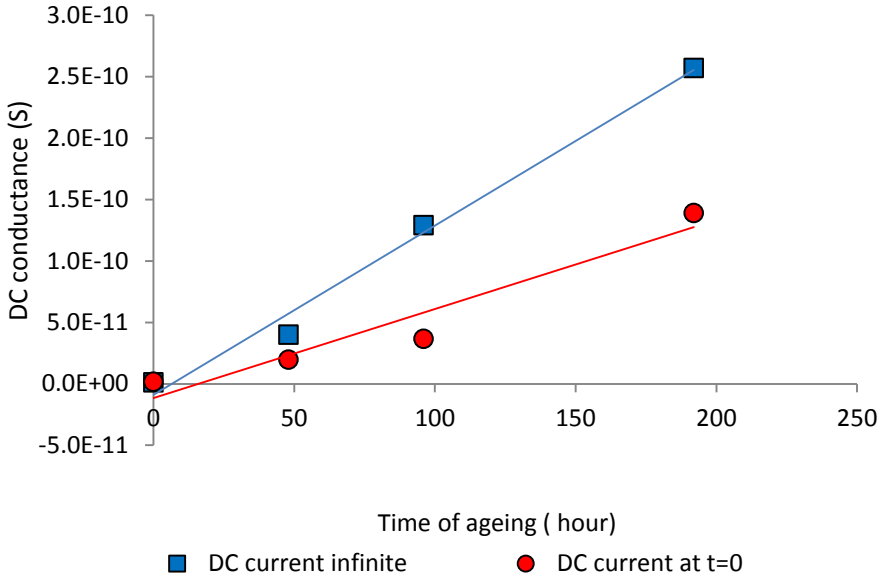

Figure 7-35 Derived conductance from d.c. current

As with I_{peak} the initial and equilibrium values of the d.c. conductance appear to be increasing linearly with time of ageing. This implies that the conductivity of insulating oil measured with a step voltage appears to be increased as a result of thermal ageing. Such a behaviour agrees with previous studies performed by Hosier (with silicone oil) [**135**] and Schober (with mineral oil) [**136**] [**52**]. Both Hosier and Schober suggested that as the electrical conductivity increases with ageing time and it can be used as an indicator of oil ageing.

If the V-I relationship between the applied voltage and the corresponding measured d.c. current at equilibrium ($t = \infty$) follows an Ohmic behaviour then linear fits of d.c. current when ($t = \infty$) must pass through the origin. According to the data analysis

presented in sections 7.2~7.5, it is found that the R^2 values of such fits from unaged and aged samples (Table 7-17) support such an Ohmic behaviour.

	R^2 of Unaged	R^2 of 2 day aged	R^2 of 4 day aged	R^2 of 8 day aged
Pure oil	0.98	0.99	0.98	0.99

Table 7-17 R^2 values for d.c current Ohmic fits (Samples without nanoparticles)

As mentioned in section 3.4.1, for ionic injection in the liquid, with the reasonable assumption that the injected electrons can be adsorbed by the molecules and "lift off" these molecules to provide a low density region for subsequent electron injection (which means the space charge effects can be ignored), it is expected therefore that ionic injection in this project could be explained by a Schottky emission behaviour.

With a certain test cell, the current density J is proportional to the current value, the electric field E is proportional to the applied voltage. As there is a linear relationship between the current density J and the electric field E as shown in Equation 3-23 described in section 3.4.1. There would be also a linear relationship between the Logarithm of current $\ln I$ and the square root of voltage $\sqrt{V}$

$$\mathrm{J} = \frac{4\pi me(k_B T)^2}{h^3} exp\left[\frac{-(\emptyset - e^{1.5}E^{0.5})}{k_B T}\right] \qquad \textbf{3-23}$$

A $\ln I - \sqrt{V}$ plot can be obtained by plotting the Logarithm of current $\ln I$ as a function of the square root of voltage $\sqrt{V}$ based on the fitted values of d.c currents when $\mathrm{t} = \infty$ and the applied voltage which is shown in Figure 7-36.

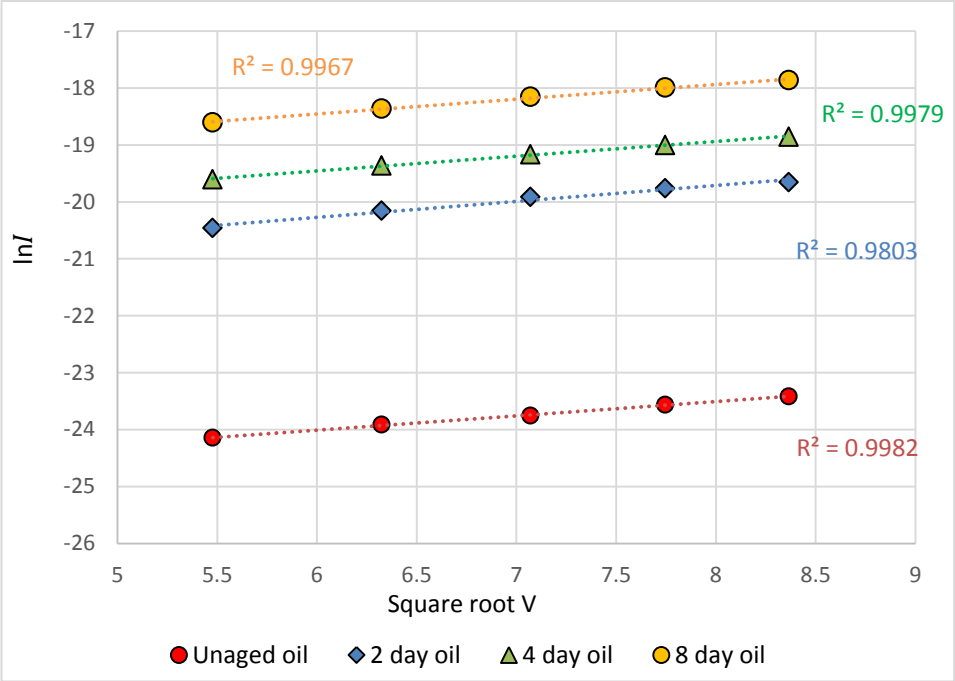

Figure 7-36 Schottky analysis for samples without nanoparticles

The dashed lines in Figure 7-36 are the linear regression lines of the derived data. There seems to be a clear linear relation between $\ln I$ and $\sqrt{V}$ for each sample, which can be seen from Figure 7-36. This implies that the observed voltage current relation could be explained by a Schottky type emission rather than a simple Ohmic behaviour. To be able to differentiate between the two possible processes data at lower voltages would be needed.

Assuming the pre-exponential term in equation 3-23 is independent of voltage equation **7-5** can be obtained by taking the logarithmic function of equation 3-23:

$$\ln I = \ln \alpha + \beta + \gamma\sqrt{V} \qquad \textbf{7-5}$$

The term α corresponds to the pre-exponential term in the equation, β will correspond to the work function for ion injection and the term γ will depend on the charge on the ion and its average thermal energy. The $\ln \alpha + \beta$ term can be obtained from the intercept of the linear regression lines shown in Figure 7-36 and is expected to be a linear function of the work function $\emptyset$. The value of γ can be obtained from the slopes of the linear regression lines.

The derived values of $\ln \alpha + \beta$ term and γ are shown in Table 7-18.

	Unaged		2 day aged		4 day aged		8 day aged	
Pure oil without nanoparticle	$\ln\alpha + \beta$	γ	$\ln\alpha + \beta$	γ	$\ln\alpha + \beta$	γ	$\ln\alpha + \beta$	γ
	-25.5	0.25	-22.0	0.28	-21.0	0.26	-20.0	0.26

Table 7-18 Linear fits results for Schottky analysis

For pure oil without nanoparticles added, the values of $\ln\alpha + \beta$ term increase with the increase of ageing degree, which implies that the work function may be decreasing due to the effect of ageing. There is no significant variation in the value of γ which is consistent with its expected dependence on the charge and thermal energy of the ions. The work function will depend on the permittivity of the liquid that the ions are being injected into. The possible decrease in work function therefore may be a result of an increase in the permittivity of the oil due to the degradation caused by thermal ageing.

According to the above discussion, when a step voltage is applied to the oil samples without nanoparticles, V-I relationship between the applied voltage and the measured d.c. current can be fitted well based on two different mechanisms: Ohmic fit and Schottky emission fit. The fitting results based on the data measured from unaged sample without nanoparticles were shown in Figure 7-37 for instance.

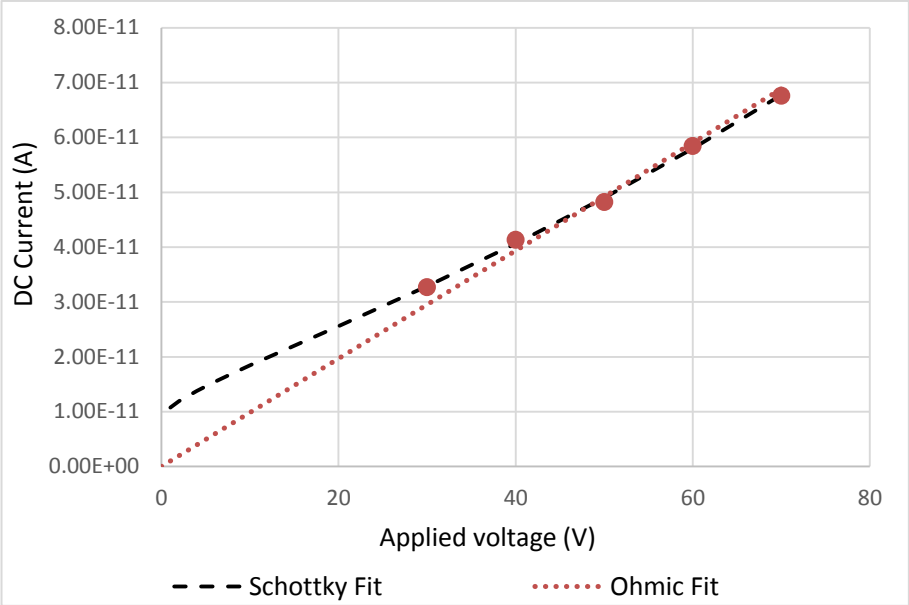

Figure 7-37 Ohmic fit and Schottky fit for unaged sample without nanoparticles

The black dashed line in Figure 7-37 represents the expected d.c. current behaviour based on Schottky emission and the red dashed line represents the results based on the Ohmic behaviour. In the range of applied voltage in this project (30V~70V) the fitting results of these two fit methods are very similar. Fitting results for 2 day aged, 4 day aged and 8 day aged sample can be found in Appendix with similar conclusions to the unaged sample. Therefore it is difficult to decide which type of fitting method is more accurate. Further experiments at a lower applied field might be helpful to investigate the V-I relationship.

7.7.2. TOF AND MOBILITY

Similar to analysis of peak current and d.c. current, the initial expected mobility value when the test cell was filled into the test cell are plotted in Figure 7-38 (a), while the expected mobility values when the measurement system had reached equilibrium $t = \infty$ are plotted in Figure 7-38 (b). For unaged sample, the average values calculated from the 5 measurements have been used at both $t = 0$ and $t = \infty$ since no clear trend could be observed from the experimental data over the 5 days measurements.

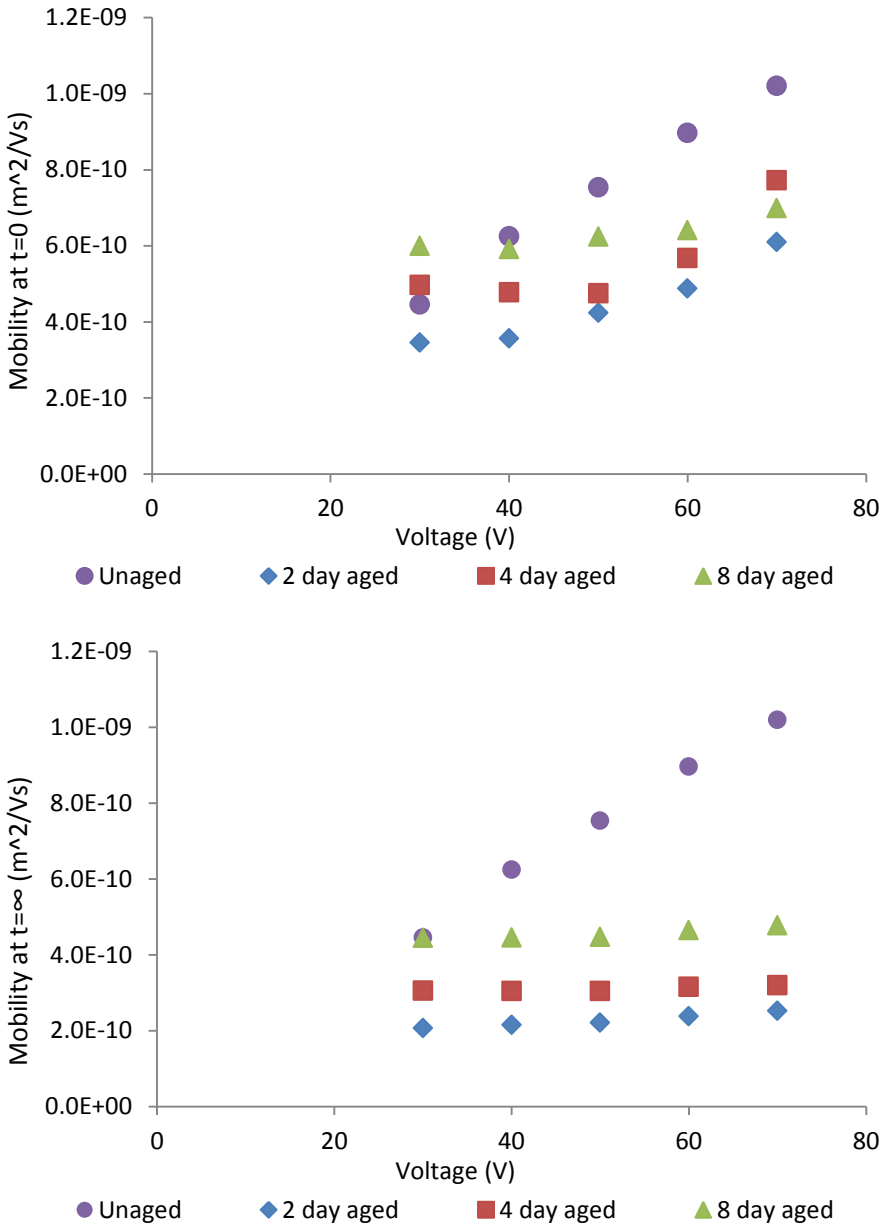

Figure 7-38 Expected Mobility of charge carriers in unaged sample and aged oil samples Upper graph when t=0(a); lower graph when t=∞(b).

With the unaged sample there is a clear dependence of measured mobility with applied field. The field dependence for the derived values of mobility at $t = 0$ in the aged samples seems to be less significant and occurs at higher values of applied field. In general these values of mobility for the aged oils appear to be lower than for the unaged oil. In addition the mobility appears to drop in the initial 2 days of ageing than increases for longer periods of ageing.

The equilibrium values of mobility for the aged samples, $t = \infty$, the change in mobility with applied field is small. Again the equilibrium mobility is lower than that for the unaged sample and a similar behaviour to the initial mobilities is observed with ageing time.

Field dependence of mobility is frequently attributed to EHD effects. In these results it is not clear why ageing of the oil should change the EHD behaviour of the system particularly for the equilibrium mobilities where the field dependent behaviour seems to have been completely suppressed.

7.8. SUMMARY

In this chapter, Shell Diala insulating oil was selected as the test liquid. Four 250mL samples were thermally aged at 120℃ for 0, 48, 96, and 192 hours, respectively. For each sample, 5 sets of measurements were done on successive days using the bipolar method. For each set of measurement, the initial negative polarity voltage was 50V. After 30min, the reversal positive polarity voltage was in a range of 30V to 70V. I_{peak}, I_{dc} and TOF values were obtained for the recorded current traces. The effective mobility values of each sample were calculated from their TOF values.

For unaged oil sample, no clear trend of the measured I_{peak} and TOF over the 5 successive days of measurements was observed. The measured values of I_{peak} and TOF seem to be constant. However, a downward trend was observed for I_{dc} measurement for all of the experimental voltages. An exponential equation assuming a first order kinetic was adopted to express the change of I_{dc} with the time of measurement.

For sample aged 2 days, 4 days and 8 days, I_{peak}, and I_{dc} increased over the 5 successive measurements. The data was shown to fit well to an exponential function with a common time constant. It is therefore assumed that these changes were the results of a first order kinetic. These fits allowed the expected values of I_{peak} and I_{dc} to be derived at $t = 0$ when the sample was filled into the test cell and $t = \infty$ when the measurement system reached equilibrium. The behaviour of the derived current values appears to be linearly dependent on the applied voltage for all the aged samples.

From the experimental results, it can be seen that the thermal ageing has a significant effect on the conduction processes of the insulting oil. The aged samples have much larger I_{peak} and I_{dc} values than those measured from the unaged sample with the current increasing by more than an order of magnitude for I_{peak} and by more than 2 orders of magnitude for I_{dc}. The values I_{peak} and I_{dc} increase with the time of ageing. The relationship between current and ageing time appears to be linear, however there is only data on 4 ageing times so this cannot be stated with total confidence.

The calculated values of mobility could also be fitted well to an exponential function with a common time constant. This time constant had a distinctly different value to that for the current data. This suggests again a first order kinetic, but one that describes a different reaction or process within the oil sample. Unlike the I_{peak} and I_{dc} measurements, there is no simple relationship between the effects of thermal ageing and the measured mobility of charge carriers in the bulk of insulating liquid. There is a significant difference between the unaged and aged samples where the field dependence of mobility is much lower for the aged samples.

8. MEASUREMENTS ON OIL WITH EFH1 NANO PARTICLES

8.1. INTRODUCTION

In this chapter, magnetite nanoparticles were added into an unaged Shell Diala oil sample and aged Shell Diala oil samples. The aged oil samples were the same samples that were used in chapter 7. The samples with the nanoparticle suspension were then measured over 5 successive days using the same protocol as in chapter 7. Again the TOF, I_{peak} and I_{dc} of samples with nanoparticles were measured and a similar fitting method was adopted. This allows direct comparisons to be made on the effects of adding nanoparticles to unaged and aged oil.

8.1.1. NANO PARTICLES USED

The nanoparticles used in this chapter came in the form of a commercially available EFH1 Ferro-Fluid manufactured by Ferrotec (USA) that was supplied in the UK by FIRST 4 MAGNETS. The specific gravity of this ferrofluid was quoted as being in the range of 0.92 to 1.47. Paraffin was used as the carrier liquid. The actual size of nanoparticles is not well defined. According to the study made by Wah-Keat Lee, the mean particle diameter is 11.6nm [**137**]. Cyclodextrins ($C_{42}O_{35}H_{70}$) was used as surfactant to prevent the aggregation of nanoparticles. The range of mass concentration of nanoparticles for this ferrofluid was not precisely defined but was in the range of 0.03 to 0.15 kg/L [**138**] .

8.1.2. METHOD OF ADDING NANOPARTICLES TO OIL

In this section, the method to prepare oil-based nanofluid samples with a constant mass concentration of nanoparticles will be introduced. A fixed volume of the ferrofluid was added into the oil sample. Although the absolute concentration of the nanoparticles in each sample was not known, for certain samples, the concentration should be in the range of 0.003 to 0.015 g/L. As the ferrofluid was drawn from a common source, the concentration in each sample would be identical.

In order to get good dispersion of nanoparticles in the liquid, ultrasonic treatment was used to separate the nanoparticles in the oil samples. Previous experiments [**5**] [**73**] [**139**] [**140**] suggested that ultrasonic treatment is an effective procedure for dispersing nanoparticles into the liquid as it can help the nanoparticles overcome the

effect of Van der Waal's forces which can cause the aggregation of nanoparticles (Section 4.9). Ultrasonic treatment relies on the formation of low density cavitation regions in the liquid which become unstable and implode [**141**]. A shock wave can be generated by such an implosion which can provide sufficient energy to separate the aggregated nanoparticles. Therefore, a relatively homogenous distribution of nanoparticles in the liquid can be achieved through the application of ultrasonic treatment.

In this project, a volume of 0.02ml EFH1 ferrofluid was added into 200ml oil sample. Therefore, the range of concentration of nanoparticles is from 0.003 g/L to 0.015 g/L. After the nanoparticles were added to the oil samples, the samples were treated in an ultrasonic bath for 30 minutes so that a homogeneous dispersion of nanoparticles can be obtained in the liquid. The ultrasonic bath used in this project is a U100 1.5 litre Ultrasonic Bath manufactured by Ultrawave Ltd. The Ultrasonic power per litre is 23.3W/litre and the operating frequency is 44 kHz. The stability of these suspensions was good with no precipitation phenomenon being observed after these samples were left undisturbed over a period of four weeks.

8.2. UNAGED OIL WITH NANOPARTICLES

Part of the unaged Shell Diala insulating oil sample whose measurements were reported in chapter 7 had nanoparticles added. Five successive measurements were taken using the same approach adopted for the pure unaged and aged samples without nanoparticles measurements presented in chapter 7. The results obtained from analysis of the current transients are shown in AppendixA 5.

8.2.1. PEAK CURRENT AND DC CURRENT

I_{peak} values of unaged samples with nanoparticles for different voltages are shown for the five successive daily measurements in Figure 8-1.

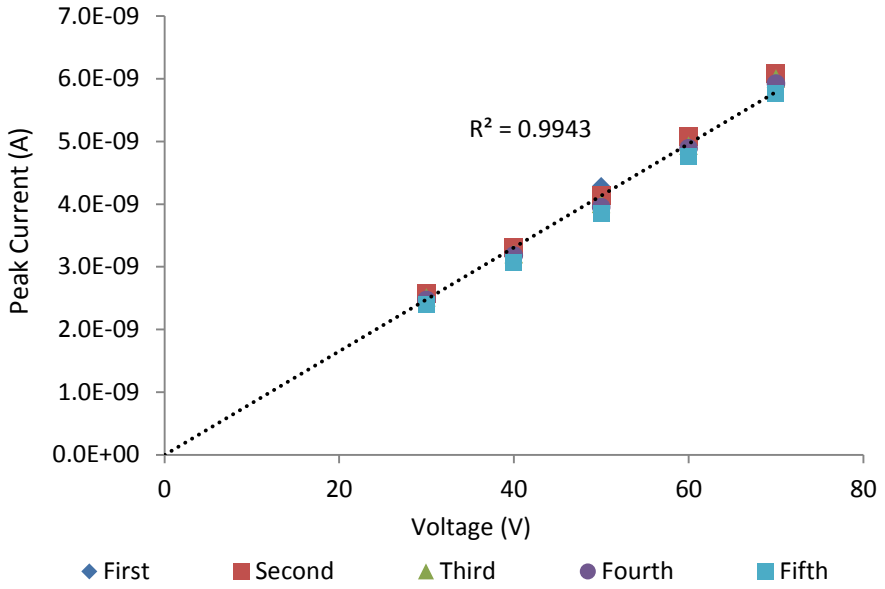

Figure 8-1 Peak current for unaged sample with Nanoparticles First, Second, Third, Fourth and Fifth represents measurements taken after 3hours, 27hours, 51hours, 75hours and 99hours, respectively.

Figure 8-1 indicates that the measured peak current increased with the increase of applied voltage. The measured current results varied over the 5 successive measurements, therefore the peak currents are plotted along with the time at which the measurement was taken in Figure 8-2.

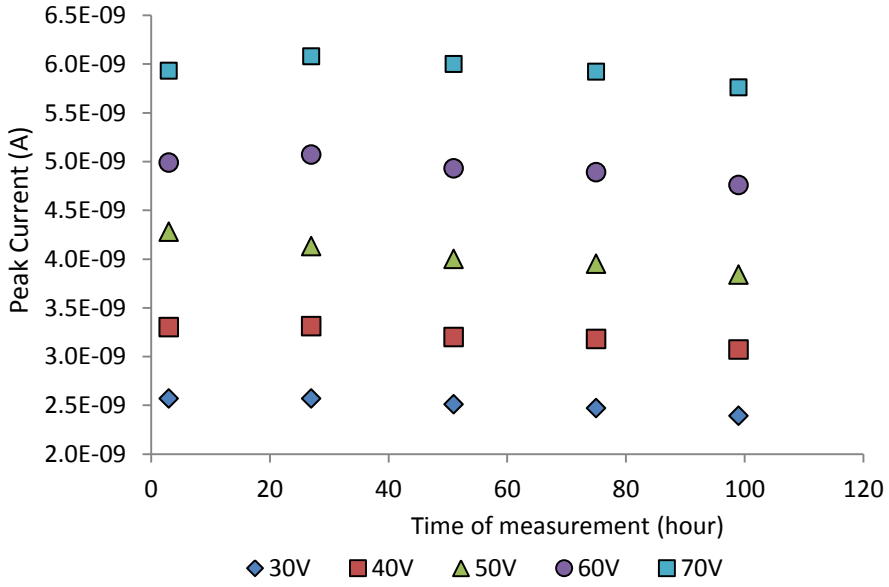

Figure 8-2 Variation of peak current with time of measurement

The magnitudes of the currents in the unaged sample with nanoparticles are much greater than that for the unaged oil without nanoparticles. There is a slight downward trend of peak current over the 5 successive measurements. This is different from the behaviour observed in the unaged oil without nanoparticles. The variation however is very small, less than 10%. As the data is trending downwards and as it would be expected that I_{peak} would have a finite value after infinite time a linear fit is unreasonable. Using more appropriate fits, for example the exponential fit associated with a first order kinetic is difficult with such a small variation in the data. For this reason, it has been assumed that the I_{peak} value of the unaged oil sample with nanoparticles can best be represented by the calculated average value from the 5 measurements.

The measured d.c. current values for unaged sample with nanoparticles present are shown in Figure 8-3 below.

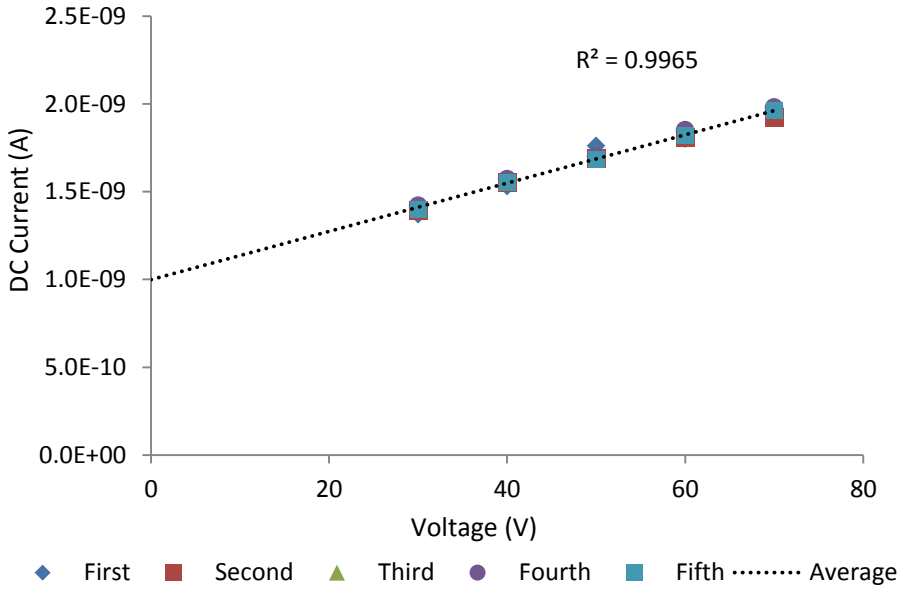

Figure 8-3 D.c current for unaged sample with nanoparticles

Similar to the results for I_{peak}, it can be seen for each measurement that I_{dc} increases with the applied voltage. The I_{dc} behaviour over 5 day's measurements are shown in Figure 8-4.

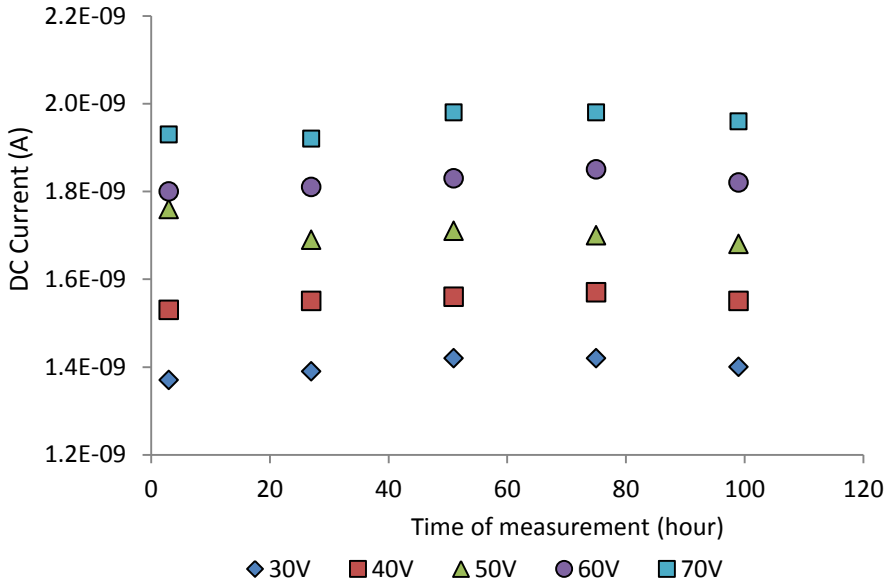

Figure 8-4 Variation of d.c. current with time of measurement

It can be seen from Figure 8-4 that there was a variation of d.c. current values with the time at which the measurement was taken for each different applied voltage. Again, when looking at the variation of d.c. current from the measurements with 50V applied voltage, the variation amplitude in 5 successive measurements is approximately 4.6% of the average value. As with the I_{peak} measurements it was decided to use the average value calculated from the 5 successive measurements to represent the d.c. current behaviour.

It can be seen in Figure 8-1 and Figure 8-3 that there appears to be a linear dependence on voltage for both currents.

8.2.2. TOF AND MOBILITY

The measured values of TOF decreases as the applied field increases indicating an increased drift velocity. This behaviour was similar to that in the measurements of pure aged oil samples without adding nanoparticles (section 7.3-7.5). The calculated mobility values of unaged sample with nanoparticles measured under different voltages over five successive measurements are shown in Figure 8-5.

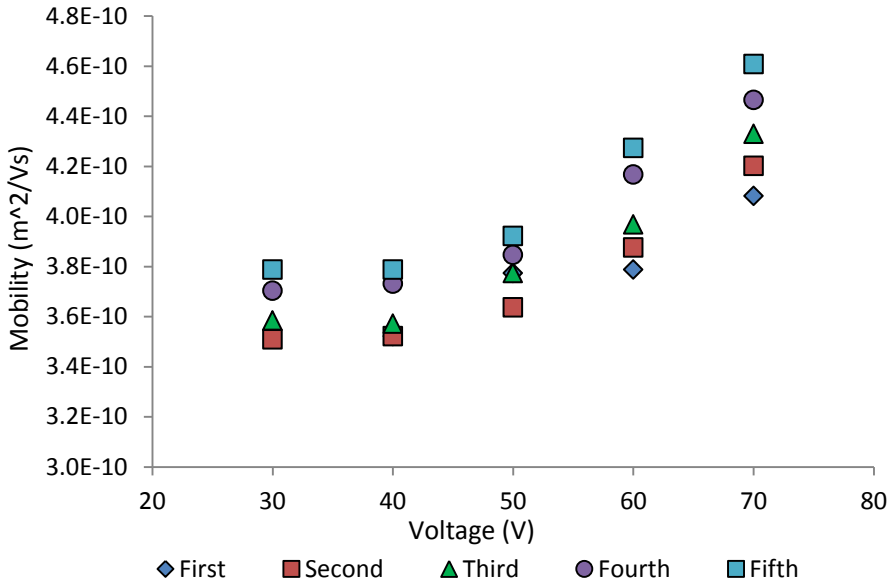

Figure 8-5 Calculated mobility for unaged sample with Nanoparticles First, Second, Third, Fourth and Fifth represents measurements taken after 3hours, 27hours, 51hours, 75hours and 99hours, respectively.

From Figure 8-5, for the set of measurements taken on any individual day little change in the mobility value is observed below 40V. Above this value the mobility seems to increase with applied voltage. This is unlike the results for unaged oil without nanoparticles where the mobility appeared to be constant over successive measurement days, here the value of calculated mobility at a given applied voltage increases across the set of 5 successive measurements. A plot of the mobility values with the time at which the measurements were taken is shown in Figure 8-6.

This relatively small change makes it difficult to fit data to either of the first order behaviours in equation 7-1 and equation 7-3. Therefore the average values of mobilities measured from the 5 successive measurements were used to represent the mobility behaviours of unaged sample with EFH1 nanoparticles as a function of the applied voltage shown in Figure 8-7. The relatively small change in mobility at low voltages with a more significant change in mobility at higher voltages can be clearly observed in this figure.

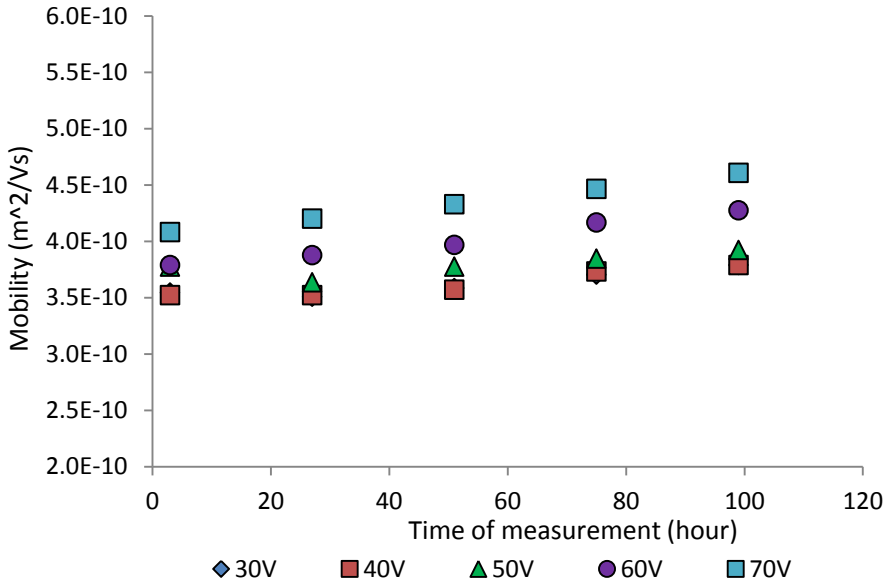

Figure 8-6 Mobility of Unaged sample with Nanoparticles at different applied voltage

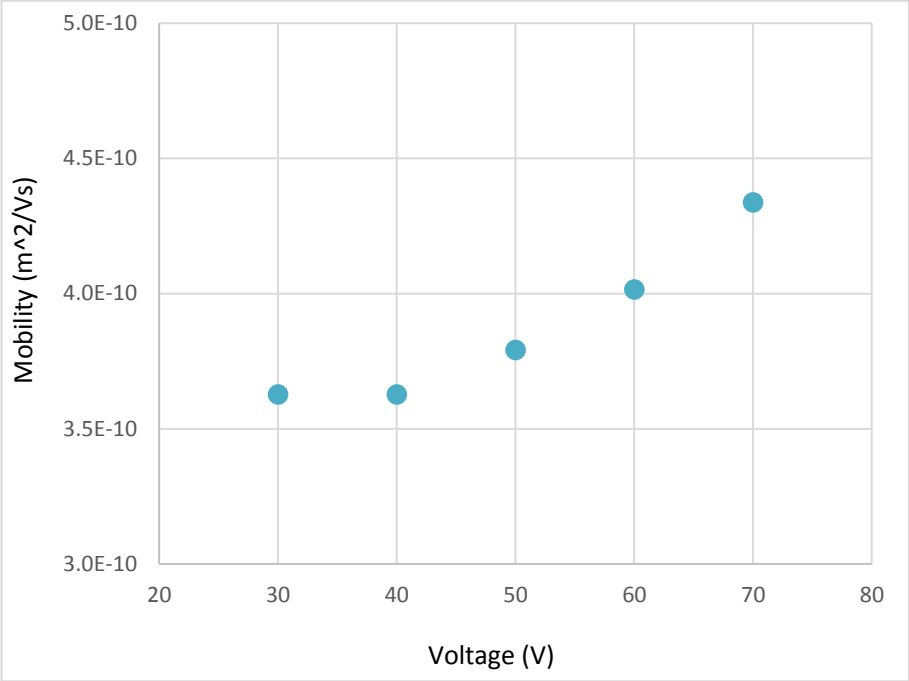

Figure 8-7 Mobility of unaged sample with EFH1 nanoparticles

8.3. OIL AGED 2 DAYS WITH NANOPARTICLES ADDED POST AGEING

A test sample was prepared by adding the nanoparticles into a new sample taken from the oil that had been aged for 2 days (section 7.3). The same procedure as in

section 8.2 was followed to mix the nanoparticles with the oil. The results obtained from the recorded current transient are shown in AppendixA 6.

8.3.1. PEAK CURRENT AND DC CURRENT

Similar to the V-I relationship in the measurement of unaged sample with nanoparticles present, the measured I_{peak} and I_{dc} of 2 days aged sample with nanoparticles increased with the applied voltage. After nanoparticles were added into the 2 days aged oil sample, the measured I_{peak} and I_{dc} magnitude were significantly increased compared with the measurement results from 2 days aged sample presented in section 7.3. However, a downward trend of variation of measured results over 5 day measurements was observed which is opposite to the trend in the 2 days aged sample without nanoparticles present. It is interesting that this trend is similar to the current behaviours in the measurements of d.c. currents of unaged sample (section 7.2.2). Therefore the approach described in section 7.3.1.1 was used to fit equation 7-1 with a common time constant to both the I_{peak} and I_{dc} was for the data of 2 days aged sample with nanoparticles. The fitting results are shown in Table 8-1 and Table 8-2.

The R^2 values shown in Table 8-1 and Table 8-2 confirm that the fits are appropriate to describe the variation of measured current over the 5 successive measurements.

Voltage (V)	I_1	I_0	τ	R^2	I_{peak} (A) (t = 0)	I_{peak} (A) (t = ∞)
30	3.73E-09	1.41E-09	30.2	0.996	5.14E-09	3.73E-09
40	4.94E-09	1.53E-09	30.2	0.998	6.47E-09	4.94E-09
50	6.18E-09	1.81E-09	30.2	0.997	7.99E-09	6.18E-09
60	7.57E-09	2.37E-09	30.2	0.998	9.94E-09	7.57E-09
70	9.04E-09	3.21E-09	30.2	0.999	1.22E-08	9.04E-09

Table 8-1 Fitting data for 2 days aged sample with nanoparticles peak current when time constant τ= 30.2 h

Voltage (V)	I_1	I_0	τ	R^2	I_{dc} (A) (t = 0)	I_{dc} (A) (t =∞)
30	2.76E-09	1.35E-09	30.2	0.992	4.11E-09	2.76E-09
40	3.36E-09	1.32E-09	30.2	0.998	4.68E-09	3.36E-09
50	3.90E-09	1.36E-09	30.2	0.998	5.26E-09	3.90E-09
60	4.44E-09	1.67E-09	30.2	0.998	6.11E-09	4.44E-09
70	4.94E-09	2.10E-09	30.2	0.998	7.04E-09	4.94E-09

Table 8-2 Fitting data for 2 days aged sample with nanoparticles d.c. current when time constant τ =30.2 h

The derived values of I_{peak} and I_{dc} when t = 0 and t = ∞ are shown in Figure 8-8 and Figure 8-9. Again, it is assumed that I_{peak} and I_{dc} would be zero when the applied voltage is equal to zero. For I_{peak} at $t = 0$ and $t = \infty$ the behaviour appears to be linear and passes through the origin suggesting an Ohmic behaviour. Attempts to make an Ohmic fit to the data for I_{dc} are not reasonable. This is different from the behaviours of I_{dc} in the measurements of 2 day aged sample without nanoparticles that have a relatively clear Ohmic behaviour. A better fit of the data to a linear trend is possible if the fit was not constrained to pass through the origin. This behaviour will be discussed in more detail in section 8.7.

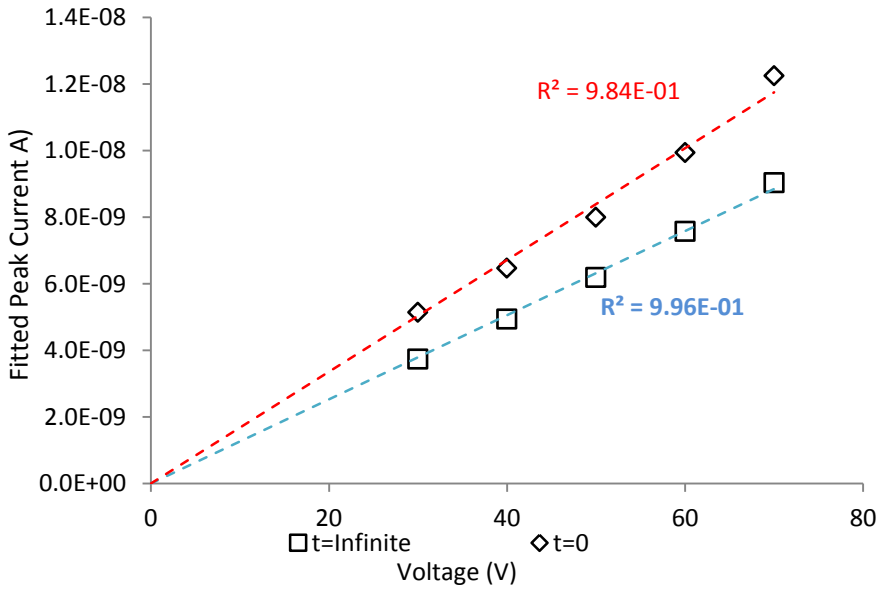

Figure 8-8 Expected peak current of 2 day aged sample with EFH1 nanoparticles

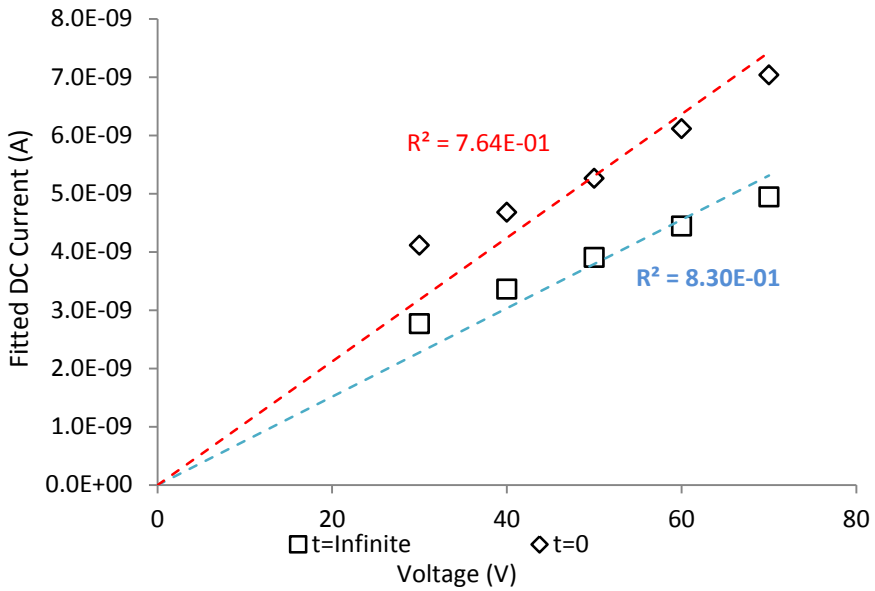

Figure 8-9 Expected d.c. current of 2 day aged sample with EFH1 nanoparticles

8.3.2. TOF AND MOBILITY

Comparing with the 2 day aged sample without nanoparticles added, the mobility was significantly increased by adding EFH1 nanoparticles. However, the trends for TOF and therefore mobilities with the time of measurement were similar to that for the measurements of the 2 days aged sample without nanoparticles. The derived values of mobility of charge carriers have a downward trend with the time of measurement. Equation 7-4 was adopted to fit the measured values of mobility. Parameters of fits of mobility are shown in Table 8-3.

Voltage (V)	μ_1	μ_0	τ	R^2	Mobility (t = 0)	Mobility (t $= \infty$)
30	1.11E-09	6.72E-10	25.2	0.999	1.78E-09	1.11E-09
40	1.18E-09	6.18E-10	25.2	0.996	1.79E-09	1.18E-09
50	1.24E-09	7.92E-10	25.2	0.995	2.03E-09	1.24E-09
60	1.30E-09	1.37E-09	25.2	0.984	2.67E-09	1.30E-09
70	2.40E-09	6.20E-10	25.2	0.698	3.02E-09	2.40E-09

Table 8-3 Fit data of mobility for 2 days aged sample with nanoparticles

A minimum value of SSR can be obtained when the time constant value was equal to 25.2 h. The R^2 values for measurements below 60V are close to 1 which suggests that these fits are reasonable to represent the behaviours of mobilities. For measurement with 70V applied, the values of TOF over 5 days were relatively small and only varied from 5 second to 6 second. This explains the low value associated with the R^2 value.

The mobility parameters for 2 days aged sample with nanoparticles when $t = 0$ and $t = \infty$ are plotted in Figure 8-10.

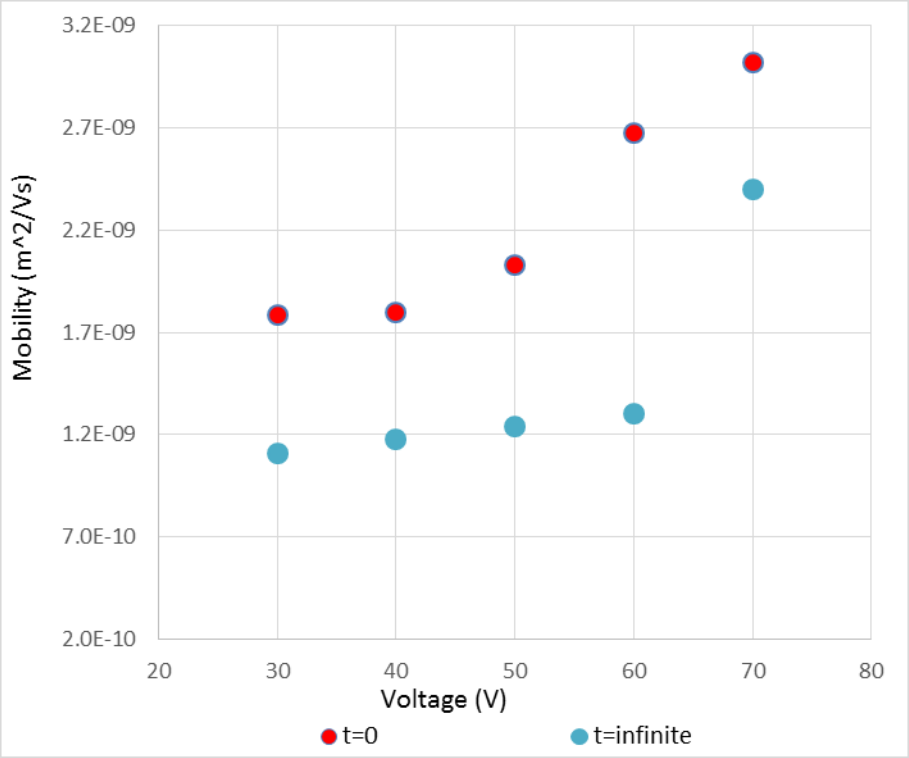

Figure 8-10 Fitted mobility of 2 days aged sample with nanoparticles

The values at 70 V should be treated with some caution due to the lower quality of fit. The value of mobility obtained in equilibrium state with 70V applied voltage seems significantly higher than the expected value. This might be a result of the measured small TOF values. Over the 5 successive measurements, the measured TOF values varied from 5s to 6s. Fitting with an exponential would lead to a poor quality fit at 70V.

A similar voltage dependence of the mobility in unaged sample with EFH1 nanoparticles was also observed, especially for the results when $t = 0$. Little change

in the mobility value was observed when the applied voltage was below 50 V. Above this value, the mobility seems to increase with applied voltage. When $t = \infty$, apart from the value at 70V, only a slightly upward trend of the mobility can be observed along with the applied voltage. Further discussion will be given in section 8.6.

8.4. OIL AGED 4 DAYS WITH NANOPARTICLES ADDED POST AGEING

A test sample was prepared by adding the nanoparticles into a new sample taken from the oil that had been aged for 4 days (section 7.4). Again, Ultrasonic treatment was used for 30min in order to get a uniform dispersion of nanoparticles in the oil. Five successive measurements were done following the common approach adopted across all measurements. Measurement results from the recorded data are presented in AppendixA 7.

8.4.1. PEAK CURRENT AND DC CURRENT

The I_{peak} and I_{dc} values were significantly increased compared with the measurement results from 4 days aged sample without nanoparticles (section 7.4). The measured I_{peak} and I_{dc} appears to have a downward trend which was similar to that of the 2 days aged sample with nanoparticles (section 8.3), therefore the same fitting method was adopted to characterize the current behaviours for 4 days aged sample with nanoparticles. A common time constant τ = 44.7 h gives the minimum value of SSR. The fitting results are shown in Table 8-4 and Table 8-5 below.

Voltage (V)	I_1	I_0	τ	R^2	I_{peak} (A) (t = 0)	I_{peak} (A) (t = ∞)
30	1.20E-08	1.48E-09	44.7	0.992	1.35E-08	1.20E-08
40	1.53E-08	2.43E-09	44.7	0.808	1.77E-08	1.53E-08
50	1.95E-08	2.41E-09	44.7	0.999	2.19E-08	1.95E-08
60	2.36E-08	2.89E-09	44.7	0.999	2.65E-08	2.36E-08
70	2.78E-08	3.89E-09	44.7	0.999	3.17E-08	2.78E-08

Table 8-4 Fitting data for 4 days aged sample with nanoparticles peak current when time constant τ = 44.7 h

Voltage (V)	I_1	I_0	τ	R^2	I_{dc} (A) (t = 0)	I_{dc} (A) (t =∞)
30	8.69E-09	2.18E-09	44.7	0.992	1.09E-08	8.69E-09
40	1.06E-08	2.44E-09	44.7	0.999	1.30E-08	1.06E-08
50	1.22E-08	2.70E-09	44.7	0.999	1.49E-08	1.22E-08
60	1.39E-08	3.18E-09	44.7	0.999	1.70E-08	1.39E-08
70	1.54E-08	3.86E-09	44.7	0.992	1.92E-08	1.54E-08

Table 8-5 Fitting data for 4 days aged sample with nanoparticles d.c. current when time constant τ = 44.7 h

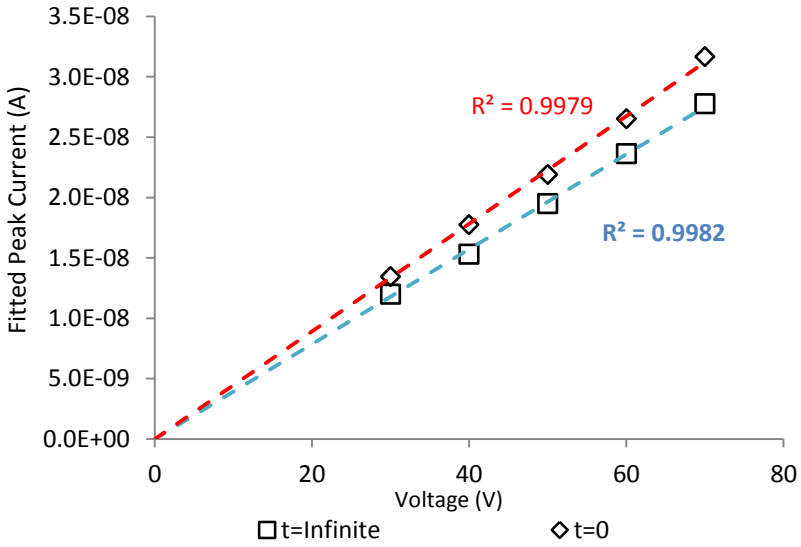

Figure 8-11 Expected peak current of 4 day aged sample with EFH1 nanoparticles

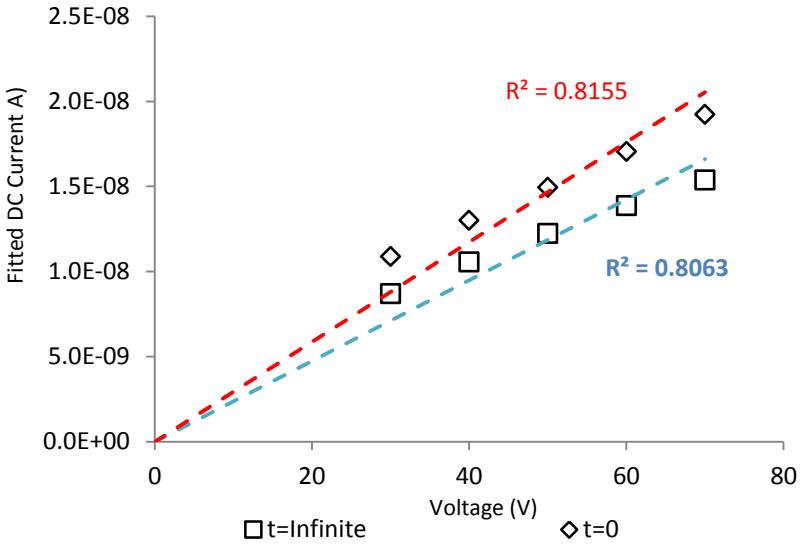

Figure 8-12 Expected d.c. current of 4 day aged sample with EFH1 nanoparticles

The expected values of I_{peak} and I_{dc} values when $t = 0$ and $t = \infty$, derived from the fits, are plotted in Figure 8-11 and Figure 8-12.

Fits of the peak current of 4 day aged sample with nanoparticles shows a clear Ohmic relation between the expected current and the applied voltage at $t = 0$ and $t = \infty$. For the d.c currents as with the 2 day aged sample with nanoparticles a linear fit passing through the origin appears to be unrealistic. A better linear fit to the data can be obtained if the constraint of passing through the origin is removed. More detailed discussion will be given in section 8.6.

8.4.2. TOF AND MOBILITY

There is an upward trend for the measured TOF values over the 5 successive measurements. Therefore, the calculated mobilities have a downward trend. This is similar to that in the measurements of 2 day aged sample with nanoparticles. The same fitting method to equation 7-4 as adopted and the results are shown in Table 8-6.

Voltage (V)	μ_1	μ_0	τ	R^2	Mobility (t = 0)	Mobility (t =∞)
30	1.15E-09	1.27E-09	25.1	0.995	2.42E-09	1.15E-09
40	1.15E-09	1.14E-09	25.1	0.995	2.30E-09	1.15E-09
50	1.20E-09	1.09E-09	25.1	0.986	2.30E-09	1.20E-09
60	1.21E-09	1.13E-09	25.1	0.989	2.34E-09	1.21E-09
70	1.24E-09	1.36E-09	25.1	0.983	2.60E-09	1.24E-09

Table 8-6 Fit data of mobility for 4 days aged sample with nanoparticles

With a time constant value equal to 25.1 h, a minimum value of SSR across all the data was obtained. Reasonable fits were obtained in this way which is suggested by the R^2 values in Table 8-6 above. The mobility parameters for 4 days aged sample with nanoparticles when $t = 0$ and $t = \infty$ are plotted in Figure 8-13.

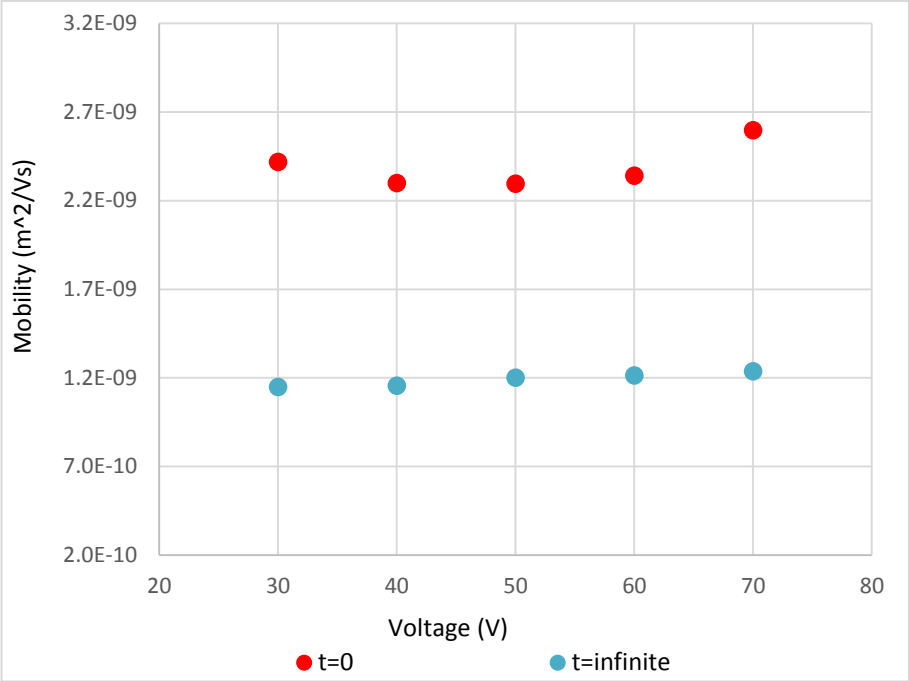

Figure 8-13 Fitted mobility of 4 days aged sample with nanoparticles

For the values derived for equilibrium conditions any increase in the mobility with applied voltage is reduced compared to the 2 day aged sample with EFH1 nanoparticles. At t = 0 the behaviour of mobility as the applied field is changed. Further comparison and analysis will be given in section 8.6.

8.5. OIL AGED 8 DAYS WITH NANOPARTICLES ADDED POST AGEING

In this section, a test sample was prepared by adding the nanoparticles into a new sample taken from the oil that had been aged for 8 days (section 7.5). Note that for the 8 day aged sample, as mentioned in section 7.5, precipitate was observed to have settled in the bottom of the bottle after ageing. Therefore 100ml of the aged sample was carefully poured into a fresh container avoiding disturbance to the precipitate. Note that centrifuging was not adopted in this section to minimum the parameters possible to affect the experimental results. The nanoparticles were then added into the container of precipitate free oil with the same concentration range of 0.003 to 0.015 g/L.

Ultrasonic treatment was applied to the 8 day sample with nanoparticles for 30min before measurements. Five successive measurements were taken with the same approach used in last section. Measurement results are presented in AppendixA 8.

8.5.1. PEAK CURRENT AND DC CURRENT

A slight downward trend in the currents measurements was observed in the measurements of 8 day aged sample with nanoparticles over 5 daily measurements. This can be seen from Figure 8-14.

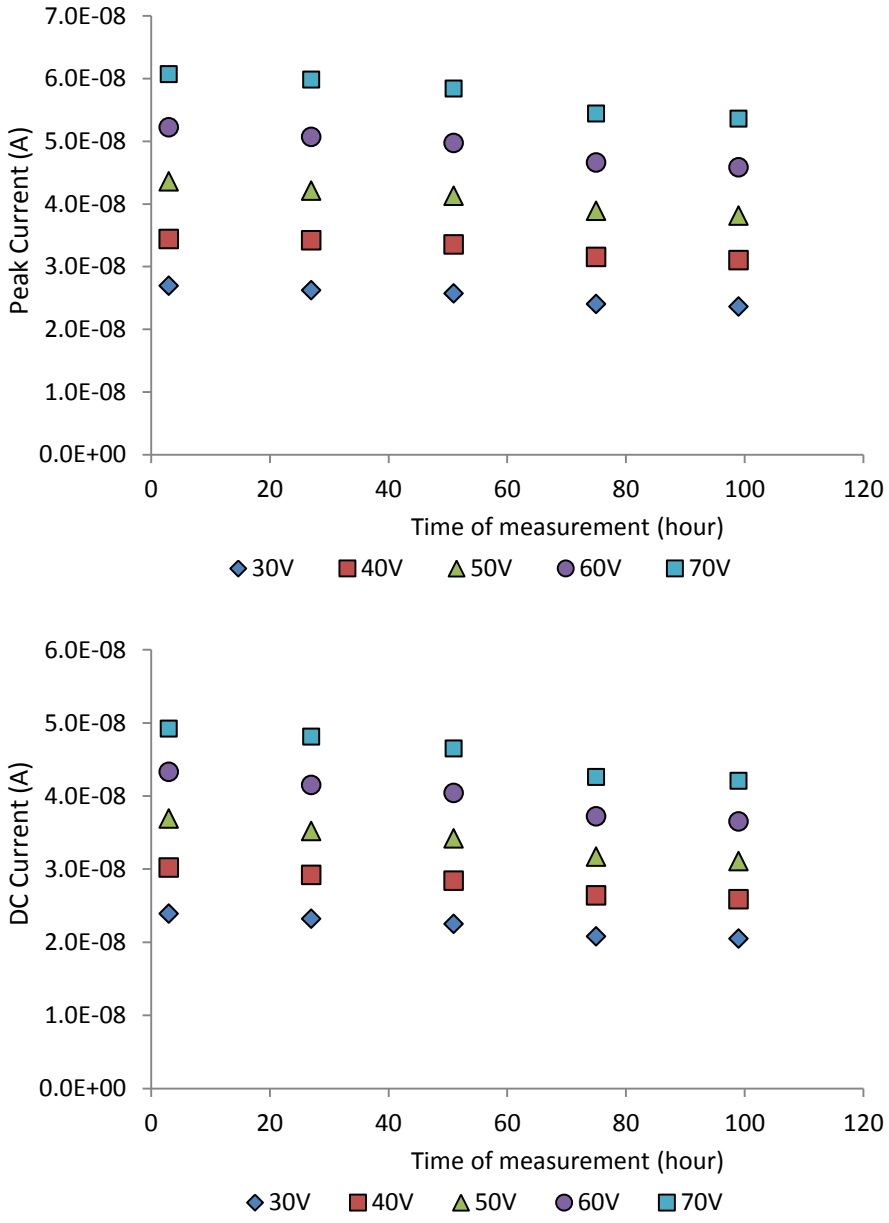

Figure 8-14 Measured peak current and d.c. current for 8 day aged sample with nanoparticles Upper graph for peak current(a) and Lower graph for d.c. current (b)

The magnitude of the change of I_{peak} is of the order of ~1nA. However, when these measured peak current values were initially fitted to equation 7-1, it was found that in this case a relatively small value of SSR could only be obtained with a large value of time constant τ (over 1000 h). In addition, changing the value of τ did not change the shape of the fitting curve significantly in this case. This indicates that the behaviour of I_{peak} mainly depends on the value of I_1 in equation 7-1 rather than the exponential term. A linear fit to the data would not be reasonable as it implies that given sufficient time the peak and d.c. currents would be zero when the voltage was applied. Looking at the percentage changes in current for both I_{peak} and I_{dc} over all the measurement voltages it appears that the major part of the change occurs after the first 4 days with a much smaller changer of the order of 1.5% occurring between the 4^{th} and 5^{th} days. One approach would be to assume that the value for the currents at $t = 0$ can be approximated by the value measured on the first day and that the values of the current at $t = \infty$ can be reasonably approximated by the values measured on day 5. A second approach is to assume that I_{peak} and I_{dc} for the 8 day aged oil sample with nanoparticles can be represented by the calculated average value from the 5 successive measurements.

The calculated average values of I_{peak} and I_{dc} using these two approaches for 8 day aged sample with nanoparticles are shown in Figure 8-15.

Figure 8-15 shows that there is no significant difference between the fit results of these two approaches. For the measurements with 30V applied voltage, the expected current values calculated from these two methods are close to each other. The shift of the current values increased slightly with the associated applied voltages. In terms of broad comparisons of behaviour either way of fitting is not likely to have a big influence on the conclusions of the comparisons.

Fits of peak current of 8 day aged sample with EFH1 nanoparticles shows a clear Ohmic relation between the average current and the applied voltage. For the d.c currents an Ohmic fit is possible but as with the 2 and 4 day aged sample with EFH1 nanoparticles, the quality of fits are poor and a better linear fit to the data can be

obtained if the constraint of passing through the origin is removed. For 8 day aged sample with EFH1 nanoparticles, current values from Ohmic fit will be used for further comparison in section 8.6.

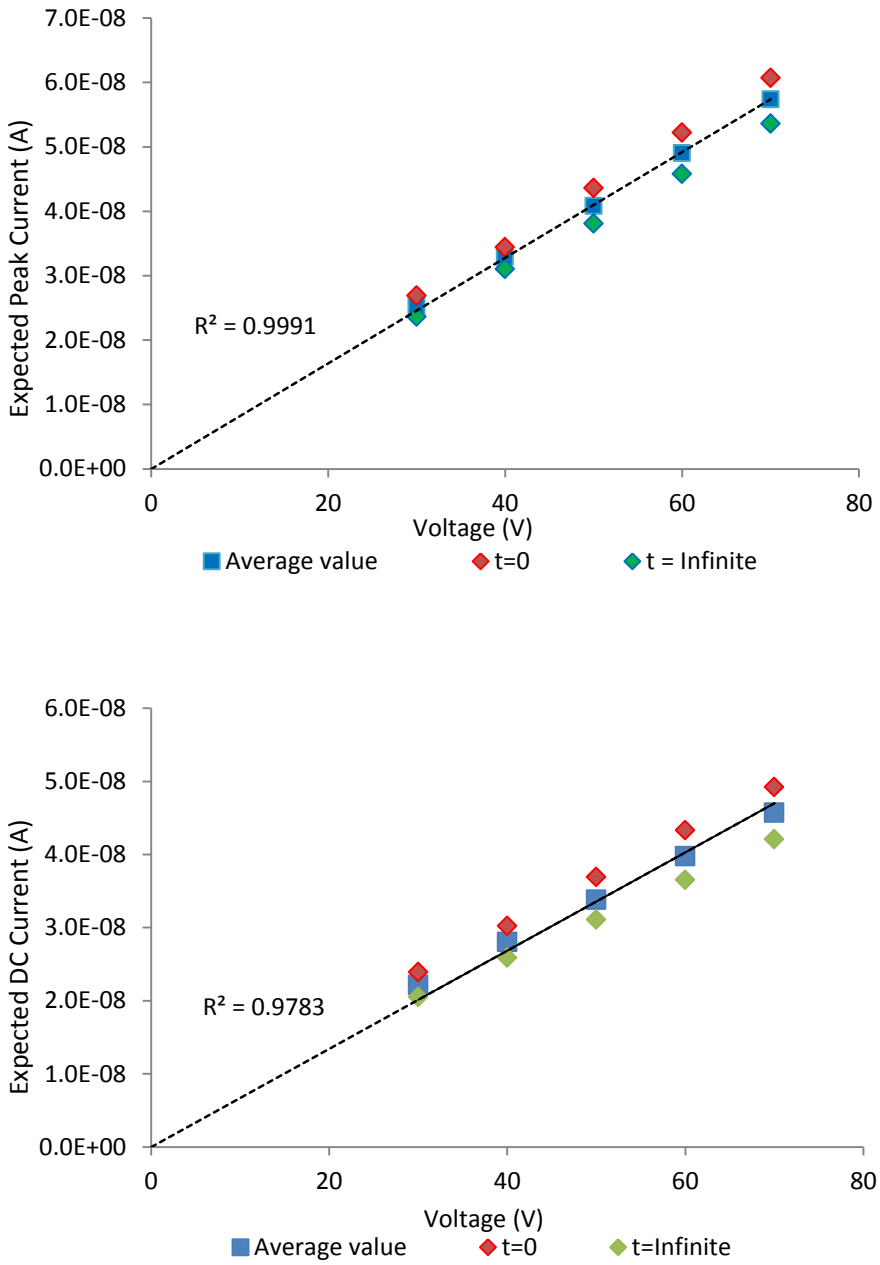

Figure 8-15 Calculated average values of peak current and d.c. current for 8 day aged sample with nanoparticles Upper graph for peak current(a) and lower graph for d.c. current(b)

The magnitudes of the currents in the 8 day aged sample with EFH1 nanoparticles are much greater than that for the 8 day aged sample without nanoparticles, which is

consistent with the other comparisons between samples with nanoparticles and samples without nanoparticles.

8.5.2. TOF AND MOBILITY

The magnitude of the values of mobility measured in 8 day aged sample with EFH1 nanoparticles were significantly larger than that in 8 day aged sample without nanoparticles added (section 7.5). The derived values of mobility of charge carriers appear to have a downward trend along with the time of measurement which is similar to the behaviours observed in the measurements of the 2 day aged and 4 day aged samples with EFH1 nanoparticles. The data was fitted to a common time constant following equation 7-4. Parameters of fits are shown in Table 8-7.

Voltage (V)	μ_1	μ_0	τ	R^2	Mobility (t = 0)	Mobility (t =∞)
30	9.84E-10	1.22E-09	44.7	0.980	2.20E-09	9.84E-10
40	1.13E-09	1.08E-09	44.7	0.965	2.21E-09	1.13E-09
50	1.25E-09	1.15E-09	44.7	0.953	2.40E-09	1.25E-09
60	1.34E-09	1.16E-09	44.7	0.978	2.50E-09	1.34E-09
70	1.45E-09	1.02E-09	44.7	0.989	2.47E-09	1.45E-09

Table 8-7 Fit data of mobility for 8 day aged sample with nanoparticles

The minimum value of SSR was obtained with a time constant value τ of 44.7 h, the minimum value of SSR was obtained. The mobility parameters for 8 days aged sample with nanoparticles when $t = 0$ and $t = \infty$ are plotted in Figure 8-16. Note that when $t = \infty$, the values of mobility show an upward trend with the increase of applied voltage. More detailed discussion will be given in section 8.6.

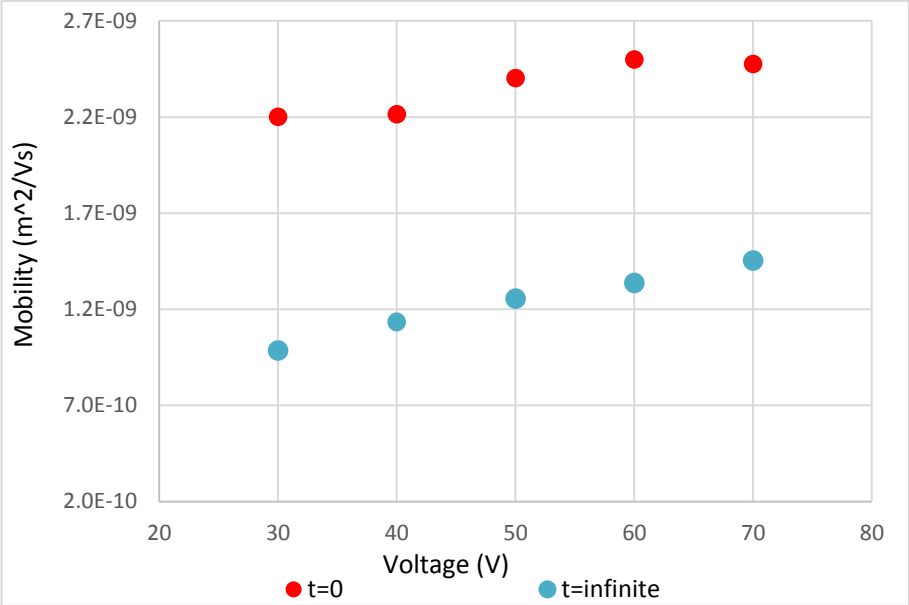

Figure 8-16 Fitted mobility of 8 days aged sample with nanoparticles

8.6. ANALYSIS AND DISCUSSION

Experiment results of unaged and aged oil samples with nanoparticles were presented in the previous sections. Similar to the measurements of samples without nanoparticles, variation of the values of I_{peak}, I_{dc} and TOF with the measurement time over 5 successive measurements were observed. The expected values of I_{peak}, I_{dc} and TOF were then obtained from either the exponential fits or the average values of experimental results which had been described in previous sections (8.2 - 8.5). Comparison between samples without nanoparticles and samples with nanoparticles added are given in this section based on these fits.

8.6.1. PEAK CURRENT AND DC CURRENT

For 2 day aged sample with nanoparticles and 4 day aged sample with nanoparticles, the changes of currents with time are significant. The measured values of I_{peak} and I_{dc} decreased over the 5 successive measurements. The behaviour of I_{peak} and I_{dc} with time can be fitted to an exponential function with the assumption that this change follows a first order kinetic. Therefore, current behaviours for 2 day aged sample with nanoparticles and 4 day aged sample with nanoparticles are presented based on the expected fit results. For the unaged sample with nanoparticles and 8 day aged sample with nanoparticles, the percentage variation of measured currents over 5

successive measurements were relatively small. Although the measured currents might have slight trends with the time of measurement, fitting with an exponential function is difficult and the quality of fit was low. For this reason, the current behaviours for the unaged and 8 day aged samples with nanoparticles at different applied voltage were presented by the average value calculated from the 5 measurements.

The current values plotted are those for $t = \infty$ as they represent a steady state behaviour in the system. These values at $t = \infty$ come from the exponential fits when these were appropriate and from the average value when such fits could not be performed.

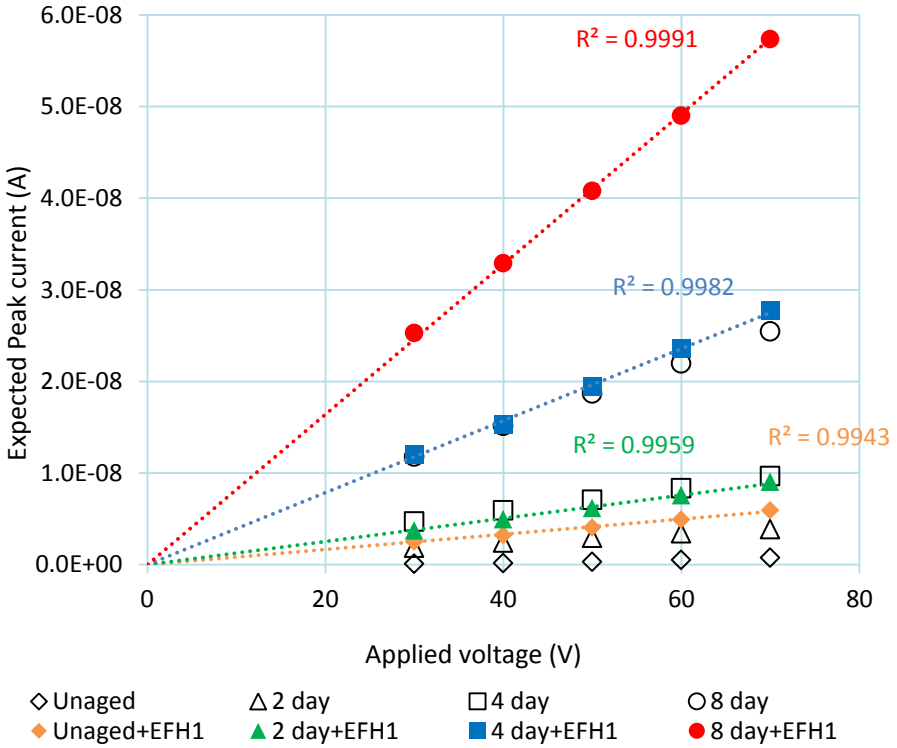

Figure 8-17 Expected peak currents for samples without nanoparticles and samples with EFH1 nanoparticles (Unaged, 2 day, 4 day and 8 day represent the samples aged 0h, 48h, 96h and 192h without nanoparticles; Unaged + EFH1, 2 day + EFH1, 4 day + EFH1 and 8 day + EFH1 represent the samples with nanoparticles added after ageing 0h, 48h, 96h and 192h, respectively.)

The magnitudes of the peak currents increase with ageing time for both types of sample. The values of the currents for samples with nanoparticles are consistently higher than for the corresponding samples without nanoparticles. The values of

expected peak current of 4 day aged sample with nanoparticles appear to be close to that of 8 day aged sample without nanoparticles. The expected peak currents of each sample increase linearly with the increase of applied voltage for both samples without nanoparticles and samples with nanoparticles added post ageing. The gradient of the V-I relationship at each ageing time is larger for samples with nanoparticles. The V-I relation of I_{peak} for all of the samples follows an Ohmic behaviour. Therefore the gradient of a linear regression line passing through the origin can be calculated and expected values of peak conductance (mentioned in section 7.8) could be obtained. These are plotted in Figure 8-18.

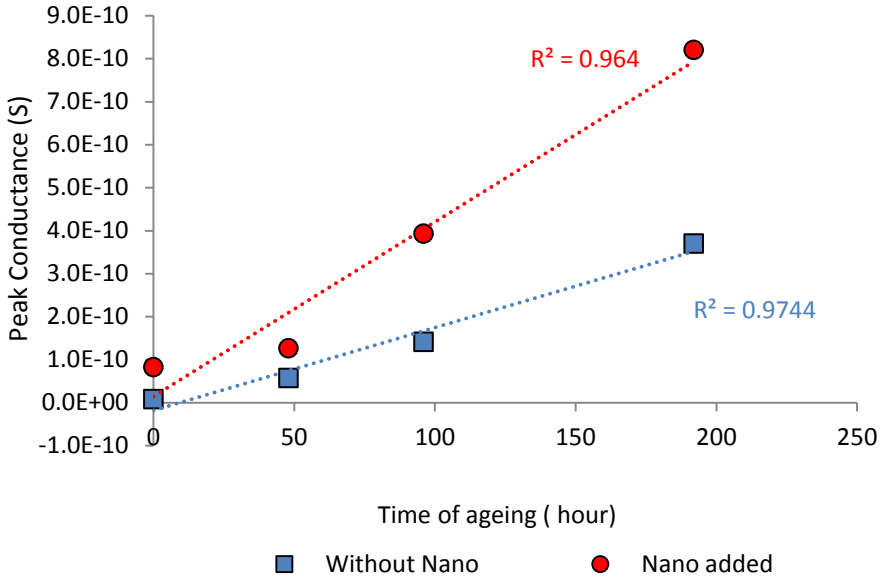

Figure 8-18 Derived peak conductance for samples without nanoparticles and samples with nanoparticles

It can be seen from Figure 8-18 that the derived peak conductance increases with the increasing time of ageing treatment. For the data for samples without nanoparticles and with nanoparticles added, their relationships appear broadly linear. Possibly the rate of change in the conductance is greater at ageing times larger than 48 hours for both types of samples. This implies that the products generated due to thermal ageing might also have an effect on the rate of accelerated ageing leading to a more rapidly degradation of the insulting oil. The peak conductance value is always higher for the sample with nanoparticles added and increases more rapidly with the increased ageing time.

The expected d.c. currents of samples without nanoparticles and samples with nanoparticles are shown in Figure 8-19. Again the current values plotted are those for $t = \infty$ as they represent a steady state behaviour in the system. These values at $t = \infty$ come from the exponential fits when these were appropriate and from the average value when such fits could not be performed.

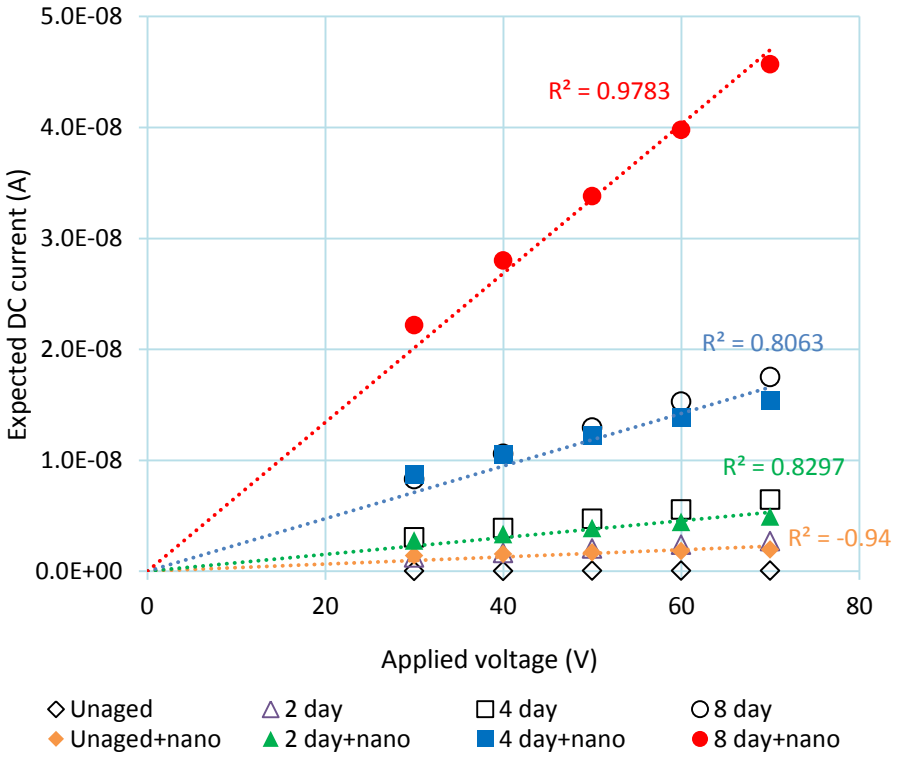

Figure 8-19 Expected d.c currents for samples without nanoparticles and samples with nanoparticles

Like the peak currents, for both types of sample, the expected d.c. currents increase with the ageing time. The d.c. currents for samples with nanoparticles are consistently higher than that for the corresponding samples without nanoparticles. Again, the expected d.c. currents of 4 day aged sample with nanoparticles are close to that of 8 day aged sample without nanoparticles. The data is broadly linear and if the assumption is made that the behaviour is Ohmic then the gradient of the best linear fit passing through the origin would be the "d.c. conductance". This approach has been used to fit the data. The assumption that the V-I relationship follows an Ohmic behaviour implies that the mobility of charge carriers in the bulk of liquid

must be field independent if the number of charge carriers in the liquid per volume is constant. The equation 4-2 described in Chapter 4 gives a common expression of the current density associated with the applied electric field.

$$J = q \cdot N \cdot \mu \cdot E \qquad \textbf{4-2}$$

Where J is the current density, q is unit charge, N is the total number of charge carriers per unit volume, μ is the average mobility of charge carriers and E is the applied electric field. This is valid under the d.c. conduction situation. If the linear relationship between the applied voltage and the expected d.c. current is real, the product of the total number of charge carriers and the mobility of charge carriers should be a constant.

Similar to the results of "peak conductance", the calculated "d.c. conductance" of samples also increases with the increase of time of ageing (solid points in Figure 8-20). After being thermally aged over the same amount of time, samples with nanoparticles added appear to have a larger d.c. conductance compared with samples without nanoparticles.

The R^2 values of fits of d.c. conductance from samples with EFH1 nanoparticles were shown in Table 8-8 below with the constraint that the linear fit line must pass the origin.

	R^2 of Unaged	R^2 of 2 day aged	R^2 of 4 day aged	R^2 of 8 day aged
EFH1 Nanofluid	0.94	0.83	0.82	0.97

Table 8-8 R^2 values for d.c. current Ohmic fits (Samples with EFH1 nanoparticles)

Unlike the Ohmic fits in pure oil samples without nanoparticles (section 7.7.1), it is clear that the qualities of fit based on an Ohmic relationship are poor, except for the fit for 8 day aged sample with EFH1 nanoparticles. The Ohmic behaviour therefore seems not valid to explain the conduction behaviour of the oil samples after adding EFH1 nanoparticles. As mentioned in sections 8.3 to 8.5, a better linear fit could be obtained if the constraint of passing through the origin was removed. This would

require: either a non-Ohmic conduction mechanism or some change in conduction mechanism to have occurred at voltages below 30V so that the physical requirement of the current being zero when the applied voltage was zero was met.

Linear fits without the constraint of passing through the origin were therefore made. The gradients for these fits can be described as a "dynamic conductance". The derived values of the d.c. and "dynamic conductance" for each sample are plotted in Figure 8-20.

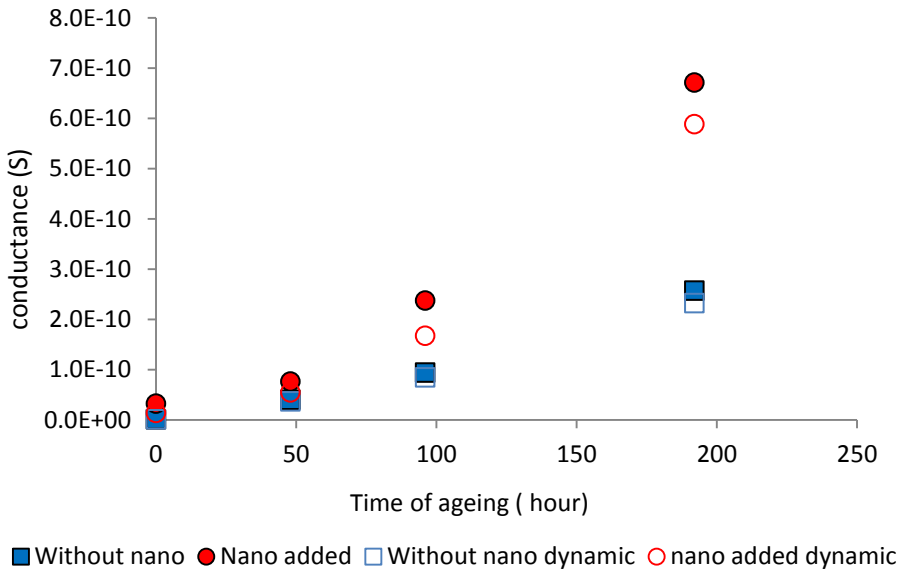

Figure 8-20 Derived conductance for samples without nanoparticles and samples with nanoparticles

It can be seen from Figure 8-20 that the derived d.c. conductance and "dynamic conductance" both increase with increasing time of ageing treatment. The values of "dynamic conductance" are consistently smaller than the values of "d.c. conductance" for each sample. Like the peak conductance, the values of d.c. conductance and dynamic conductance are higher for the samples with nanoparticles added and increase more rapidly with increased ageing. The rate of change of dynamic conductance appears to be more marked for ageing time greater than 48 hours. These indicate that for unaged and aged samples, the conductivity of Shell Diala insulating oil is increased due to the presence of EFH1 nanoparticles. This enhancement of conductivity appears to be more significant for samples with higher ageing degree.

The possibility of nanoparticles themselves contributing to charge transfer was a concern. When an external electric field is applied to the nanofluid, the nanoparticles in the liquid will be polarized. Electrons will be deposited at the potential well close to the surface of the nanoparticle. Therefore, nanoparticles in the liquid with a d.c. applied electric field are charged and can also be regarded as charge carriers as described in section 4.7. Assuming the nanoparticles are spheres, equation 3-29 based on Stokes' law can be used to estimate the velocity of motion of nanoparticles in the liquid.

According to equation 3-29 introduced in section 3.4.2, when the electrostatic force is equal to the friction damping force related to the viscosity of insulating oil the nanoparticle will move with a constant velocity v_{nano}.

$$\frac{\mathrm{Q}_{nano} \cdot \mathrm{V}}{d} = 6\pi\eta R v_{nano} \qquad \textbf{8-1}$$

The nanoparticles carrying trapped electrons can be effectively regarded as a slow negative ion. As $\eta = 0.02\ \mathrm{Pa \cdot s}$ is a representative value for the viscosity of insulating oil [**94**] [**142**], this viscosity value will be used for the following estimation. The mobility of the negatively charged nanoparticles in the liquid can be derived by:

$$\mu_{nano} = \frac{\mathrm{Q}_{nano}}{6\pi\eta R} \qquad \textbf{8-2}$$

The maximum total electron saturation charge for a nanoparticle can be expressed by:

$$Q_s = -12\pi\epsilon_1 R^2 E \qquad \textbf{8-3}$$

Where: $\mathrm{Q_s}$ is the saturation value of charge; ϵ_1 is the permittivity of nanoparticle, R is the radius of the nanoparticle and E is the applied electric field. Equation 8-3 was derived based on the theory introduced in section 4.7 [**94**] [**100**]**.**

In [**94**], a calculation based on magnetite nanoparticles with a radius of $R = 5 \times 10^{-9} m$ was performed. The permittivity value of representative magnetite (Fe_3O_4) is $\epsilon_1 = 80\epsilon_0$.When the applied electric field is $\mathrm{E'} = 10^8 V/m$, the suggested value of the saturation charge Q_s is equal to $-1.836 \times 10^{-18} C$. This illustrates that each nanoparticle can trap a maximum of about 11 electrons and the corresponding

mobility of nanoparticle in this situation is $9.7 \times 10^{-10} m^2 V^{-1} s^{-1}$. In this project, the radius of nanoparticles used in this project was also approximately equal to 5 nm but the electric field strength is in the order of magnitude of $10^4 V/m$ which is much lower than the electric field used in [**94**]. From equation 8-3, the calculated saturation charge for each nanoparticle suggests that a maximum of only one electron can be captured per single nanoparticle. In the case of a single electron the mobility of the particle will be reduced by a factor of 11 from the value above leading to an expected mobility of $\mu_{nano} = 0.85 \times 10^{-10} m^2 V^{-1} s^{-1}$

The total number of nanoparticles per unit volume can be estimated based on the mass concentration of nanoparticles in the nanofluid and the density of the magnetite material (5.17g/cm^3). With the previous assumption that the nanoparticles are spheres, the average mass of each nanoparticle should be equal to $2.7 \times 10^{-18} g$. Assuming a uniform distribution of nanoparticles in the insulating oil, this gives a total number of 10^6 suspended nanoparticles per cubic millimetre. To calculate the expected current density based on equation 4-2, the following parameter values are used: electron charge $e = 1.6 \times 10^{-19} C$, electric field $E = 5 \times 10^4 V/m$, mobility of nanoparticle $\mu_{nano} = 0.85 \times 10^{-10} m^2 V^{-1} s^{-1}$ and number density of nanoparticle $N = 10^6\ mm^{-3}$ .The current density calculated by these parameters is $6.8 \times 10^{-21} A/mm^2$. From the geometry of the test cell introduced in section 6.3.4, the total effective surface area of the inner electrode is approximately equal to $8.17 \times 10^3 mm^2$ hence the estimated total current relating to the motion of charged nanoparticles is $5.6 \times 10^{-15} A$.

This estimation indicates that the total current caused by the motion of charged nanoparticles in this project is below the expected resolution of the electrometer. As the change of current magnitude observed due to adding the EFH1 nanoparticles to the system is of the order on nano amps, a total error of 5 orders of magnitude in the estimate would be required if the change in current was due solely to charge transport associated with nanoparticle motion. Therefore it is believed that any current measured is due to the motion of ions and electron hopping processes in the liquid.

The dynamic conductance approach assumes that the low field conductivity is described by a different mechanism. An alternative using a single mechanism is to describe the current behaviour in terms of ions overcoming an image force barrier similar to the Schottky type emission analysis for unaged and aged samples without nanoparticles described in section 7.7.1. For unaged and aged samples with EFH1 nanoparticles, the $\ln I$ vs $\sqrt{V}$ plot based on the fitted d.c current values when $t = \infty$ and the applied voltages were also plotted as shown in Figure 8-21.

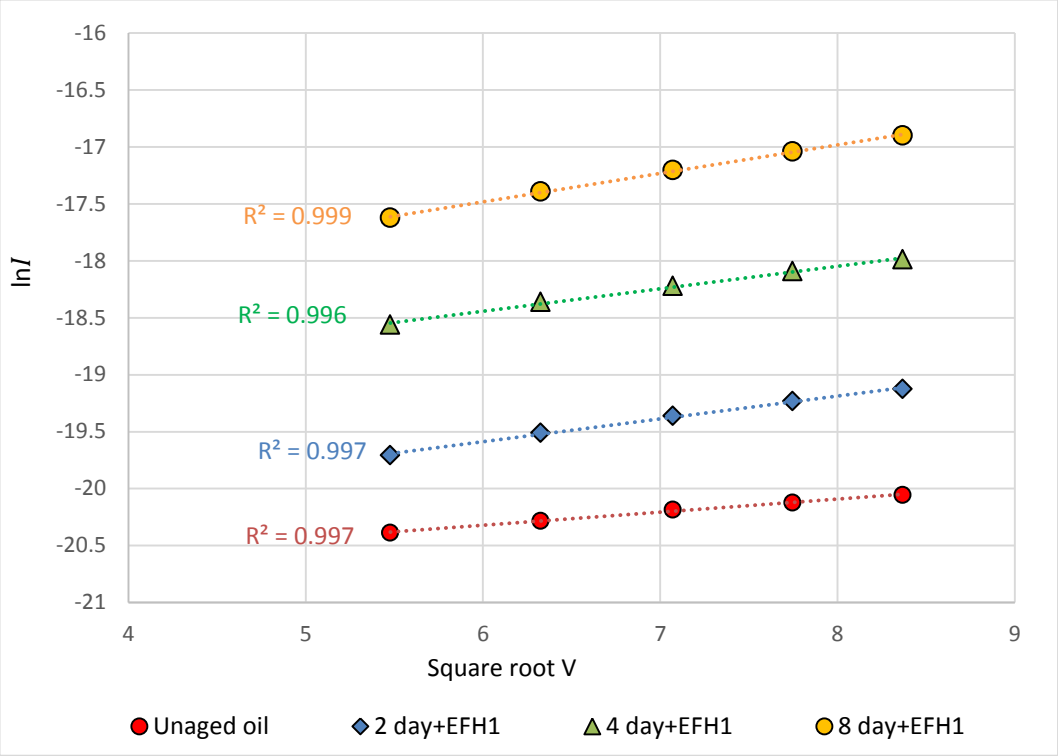

Figure 8-21 Schottky analysis for samples with EFH1 nanoparticles

A linear relationship between $\ln I$ and $\sqrt{V}$ can be observed which implies that the V-I relation for unaged and aged samples with EFH1 nanoparticles might follow a Schottky emission mechanism. Therefore similar analysis to that used for samples without nanoparticles (section 7.7.1) can be performed. The derived values of the $\ln \alpha + \beta$ term and γ are shown in Table 8-9.

	Unaged		2 day aged		4 day aged		8 day aged	
EFH1 Nanofluid	$\ln\alpha + \beta$	γ	$\ln\alpha + \beta$	γ	$\ln\alpha + \beta$	γ	$\ln\alpha + \beta$	γ
	-21.0	0.12	-20.8	0.20	-19.68	0.19	-18.96	0.25

Table 8-9 Linear fits results for Schottky analysis (Samples with EFH1 nanoparticles)

It would be expected that the calculated values of γ for the samples with nanoparticles would be similar in value to those derived in section 7.7.1. However the values shown in Table 8-9 are in general smaller. There also seems to be a greater variability between the calculated values. Similar to the results obtained from samples without nanoparticles, values of $\ln\alpha + \beta$ term also increase with the increase of ageing degree. Again, this might imply a decrease in the work function of charge injection related to an increase of permittivity of the oil samples.

As proposed earlier, to attempt to clarify the behaviour of the system, a series of measurements at lower voltages were undertaken using an unaged sample with nanoparticles. It was believed that the larger currents that were observed in this type of sample would allow measurement of a reasonable magnitude of current at these lower voltages. For this purpose, part of the unaged Shell Diala insulating oil sample with EFH1 nanoparticles whose measurements were reported in section 8.2 was filled into the cleaned test cell again. Bipolar measurements were taken with the same approach mentioned in this chapter. The negative initial polarity voltages were 50V while the positive voltage was varied between 1 and 70 Volts. The measured values of I_{dc} for unaged sample with nanoparticles associated with the applied field are plotted in Figure 8-22.

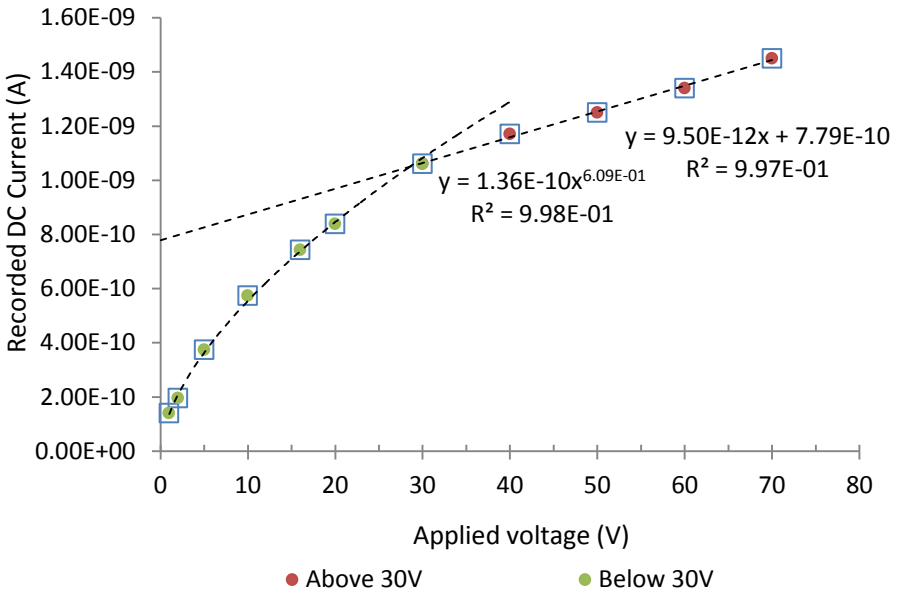

Figure 8-22 D.c current for unaged oil sample with EFH1 nanoparticles at low field region

When the applied voltage was higher than 30 Volts, the measured values of I_{dc} follow a good linear relation with the applied field as shown in Figure 8-22. Again, the linear regression line of the measured I_{dc} does not pass through the origin which is consistent with the earlier measurements of the unaged sample with nanoparticles. When the applied voltage was lower than 30V, a clearly different behaviour of the d.c. current is observed. The values of I_{dc} at voltages below 10V were derived from the transient after a period of 120 minutes. The transient may still have been occurring at this time so the values shown in Figure 8-22 may be slightly higher than the actual values. Empirically there appear to be a power law relationship between the measured d.c. current and the applied voltage at low field region. This supports that the previous fits of d.c. current with the assumption that the constraint of passing through the origin was removed are reasonable. The values of current obtained in this set of measurements in the range of 30 to 70 volts are comparable to those obtained in the earlier measurements.

The power law relationship at low voltage does not follow the typical space charge limited current behaviour which can be expressed by [**66**] [**143**]:

$$\mathrm{J} = \frac{9\varepsilon\mu V^2}{8d^3} \qquad \textbf{8-4}$$

As the exponent for voltage dependence is~0.6. As, Schottky emission type fitting had been shown to be applicable at higher voltages it was extended into the low field region. The relationship between $\ln I$ and $\sqrt{V}$ was plotted in Figure 8-23.

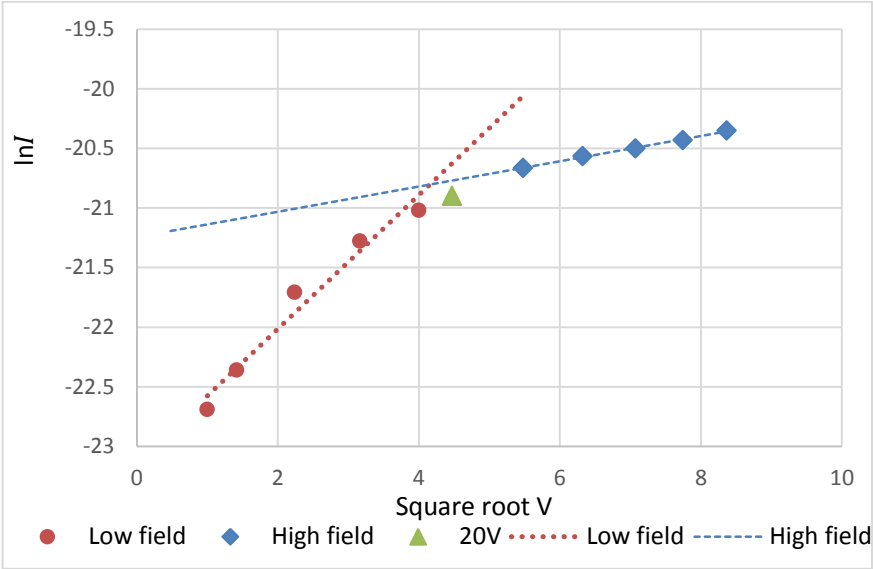

Figure 8-23 Schottky emission analysis for lower filed

It can be seen from Figure 8-23 that there is not a single straight line behaviour in the data. A change in gradient appears to be occurring at voltages around 20V. The predicted d.c. current based on a Schottky fit to the voltages above 20 V is plotted in Figure 8-24 together with the actual measured d.c. currents.

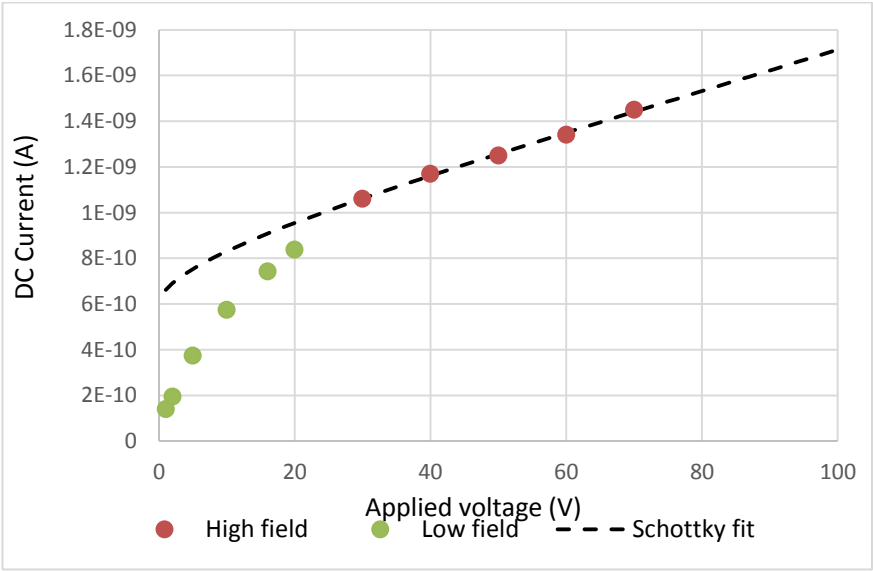

Figure 8-24 Predicted Schottky fit result

As can be seen from Figure 8-24, at each particular applied voltage, the actual measured d.c. current values within low applied field region were smaller than the expected current values obtained from a simple Schottky emission fitting based on high field data. This would be expected from the change in gradient observed in Figure 8-23. Therefore, the measured d.c. current at low field region seems to follow a different behaviour from the Schottky emission when the applied voltage is in a range of 30V to 70V. Note that the Schottky emission is based on the assumption that the injected ions from the electrode can be immediately swept away from the vicinity of the electrode. No significant effect caused by the presence of space charge is considered in this approach. However, this may not be true especially in the low field region where injected ions may remain close to the electrode due to their relatively low velocities. Therefore a region of space charge would be likely to be formed which would modify the potential barrier considerably and reduce further injection of charges. For this reason, the measured current would be smaller than the predicted values derived based on the high field Schottky fitting results.

8.6.2. TOF AND MOBILITY

For 2, 4 and 8 day aged sample with EFH1 nanoparticles, the changes of apparent mobility with time are significant. The measured values of TOF for each sample increased over the 5 successive measurements. Therefore, the derived values of mobility decreased over the 5 measurements. Similar to the approach for I_{peak} and I_{dc} analysis, the behaviour of expected mobility with time can be fitted to an exponential function using a common time constant, with the assumption that this change follows a first order kinetic. The value of this time constant was in general different from the values found for the fitting of the peak and d.c. currents. Therefore, for aged sample with nanoparticles, the mobility behaviours is presented based on the results from these fits. For the unaged sample with nanoparticles, the magnitudes of the derived mobility are small, and the percentage variations of mobility over 5 successive measurements were also relatively small. Fitting with an exponential function was difficult and the quality of fit was low. Therefore, the mobility behaviours for the

unaged sample with nanoparticles at different applied voltage were presented as the average value calculated from the 5 measurements.

Comparison between the expected mobility of samples with nanoparticles and that of samples without nanoparticles are shown in Figure 8-25. The current values plotted are those for $t = \infty$ as they represent a steady state behaviour in the system. These values at $t = \infty$ come from the exponential fits when these were appropriate and from the average value when such fits could not be performed.

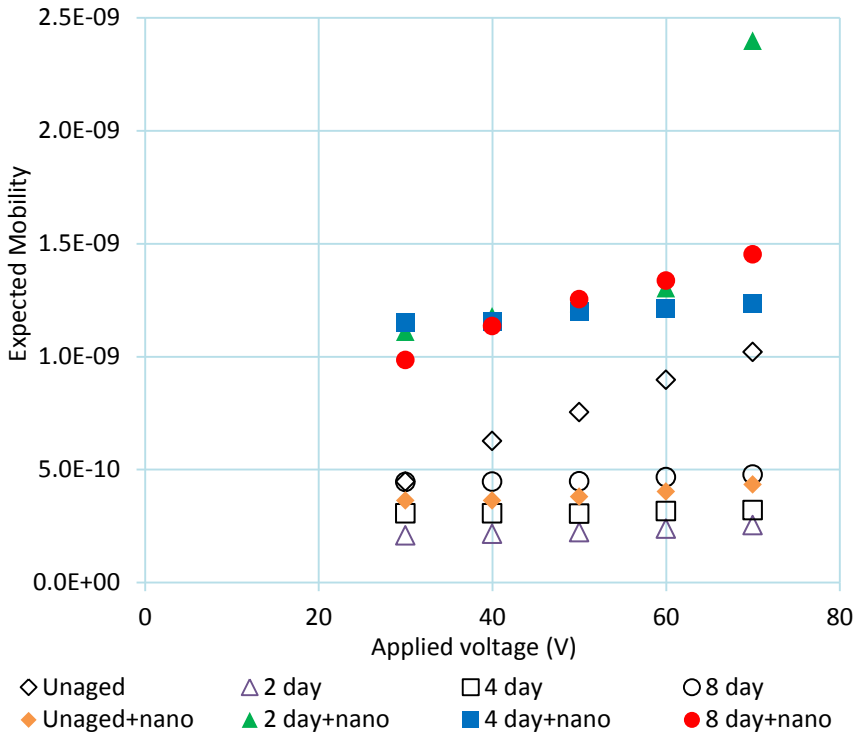

Figure 8-25 Expected mobilities for samples without nanoparticles and samples with nanoparticles (Unaged, 2 day, 4 day and 8 day represent the samples aged 0h, 48h, 96h and 192h without nanoparticles; Unaged + nano, 2 day + nano, 4 day + nano and 8 day + nano represent the samples with nanoparticles added after ageing 0h, 48h, 96h and 192h, respectively.)

For the sample aged 2 days with nanoparticles added, the derived mobility at 70V is atypical since its magnitude is significantly larger than that of the rest of the values for aged oil with nanoparticles added measurements. Based on the results for mobility measurements, it is assumed that the expected mobility for each sample follows an approximately linear behaviour with the applied voltage. Therefore, a modified value for the expected mobility of 2 day aged sample with nanoparticles at

70V can be obtained from the linear regression expression. The modified results are then shown in Figure 8-26.

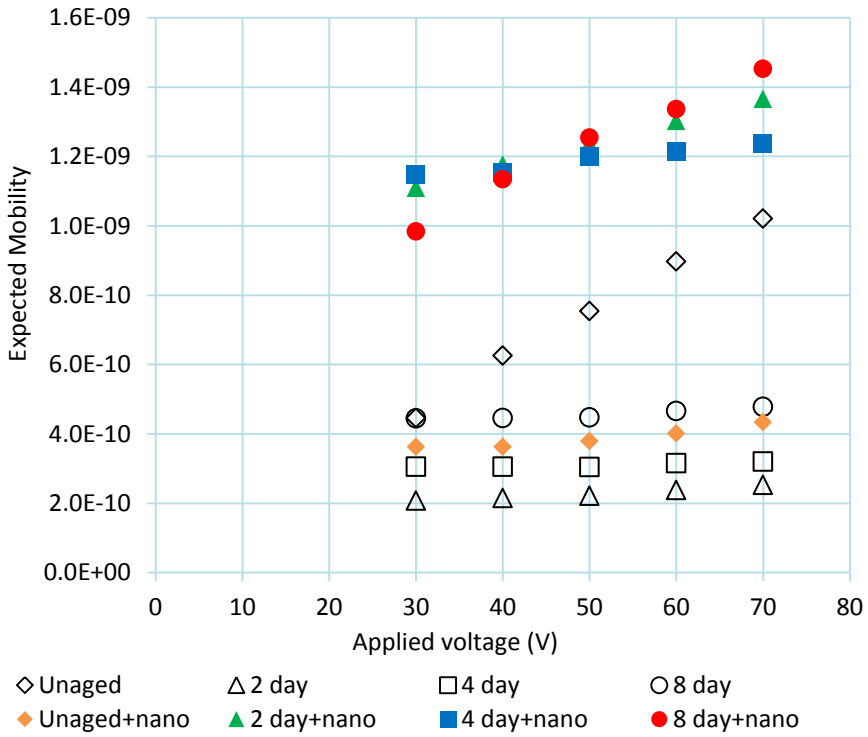

Figure 8-26 Modified mobilities for samples without nanoparticles and samples with nanoparticles

It seems that the effect of the presence of EFH1 nanoparticles on unaged oil sample is quite different from that on aged oil samples. From Figure 8-26, by adding EFH1 nanoparticles into the unaged oil sample the measured mobility of the charge carriers has been decreased and the voltage dependence is much reduced. This is different from the expectation that adding nanoparticles could increase the number of traps of charges. As increase in the total number of traps would lead to an increase in the "seats" of charge carriers, the diffusion of charge carriers would be increased which could also lead to an enhancement of the mobility of charge carriers. The reason for this is not clear. This may be due to the formation of deep traps in the system reducing the effective mobility of the charge carriers. However, adding nanoparticles into the aged oil samples leads to a significant increase in the calculated mobility values and slightly increases the field dependence. The measured mobility values of samples aged for different times appear broadly similar with no clear trend on ageing

time. This enhancement of mobility values caused by adding EFH1 nanoparticles into the aged oil samples is in agreement with the recent study of Du in 2015 with TiO_2 nanoparticles [**144**], who suggested that a fraction of ageing by-product molecules can be bonded to the interface between the nanoparticles and oil, changing the interface structure which could lead to an increase of the trap density of charge carriers. As the charge hopping process in the liquid is related to the total number of traps, higher trap density will lead to a larger mobility of charge carriers in the liquid, consequently leading to an increase of the conductivity.

It is interesting to note that, after adding EFH1 nanoparticles, the differences in the measured mobility values for 2 day aged sample, 4 day aged sample and 8 day aged sample are small. However, the changes in conductivity between these three samples are much larger as shown in section 8.6.1. Therefore the differences in conductivity must be explained by changes in the total number of charge carriers. The reason for this could be due to the difference in the degree of ageing and therefore concentration of ageing by-products or due to the difference in the effects caused by the combination of EFH1 nanoparticles and the ageing by-product molecules.

From the previous analysis of current behaviours, adding EFH1 nanoparticles into unaged and aged oil samples leads to significant changes in the behaviour of the conductivity and the mobility of charge carriers. In order to further understand the differences between them, the difference of mobility values and d.c. current between samples without nanoparticles and samples with EFH1 nanoparticles added were calculated and then, this value was normalized to the values observed for the data of the sample without nanoparticles. The results were shown in Table 8-10 below.

Aging time (Hours)	Change in Mobility	Change in Current
0	-44.7%	3398.2%
48	443.0%	96.4%
96	282.8%	160.3%
192	165.9%	162.6%

Table 8-10 Changes due to the presence of EFH1 nanoparticles

It seems that by adding EFH1 nanoparticles into the unaged insulating sample, the apparent mobility was reduced while the measured d.c. current was significantly increased. This suggests an increase in the total number of charge carriers in the unaged insulating oil sample.

For samples aged less than 96 hours, the samples with EFH1 nanoparticles added exhibit a significantly larger mobility of charge carriers compared with the corresponding samples without nanoparticles added. The normalized increase in the mobility of charge carriers is more significant than that in the d.c. current. This indicates that the difference in d.c. current values between aged samples without nanoparticles and aged samples with EFH1 nanoparticles added is mainly due to the increase of the mobility. For samples aged for 192 hours, the difference in the mobility of charge carriers is very close to the difference in the d.c. current, the larger current measured in the samples with EFH1 nanoparticles appears to be a result of the increase of the mobility of charge carriers.

Assuming that the apparent mobility measured through TOF measurements does describe the mobility under d.c. conditions, from the data on the d.c. conductivity and the mobility, an estimate of the number of charge carriers present in the system can be derived, equation 4-2, the estimates of the number of charge carriers present for the aged oil with EFH1 nanoparticles and the aged oil in their absence are shown in Figure 8-27.

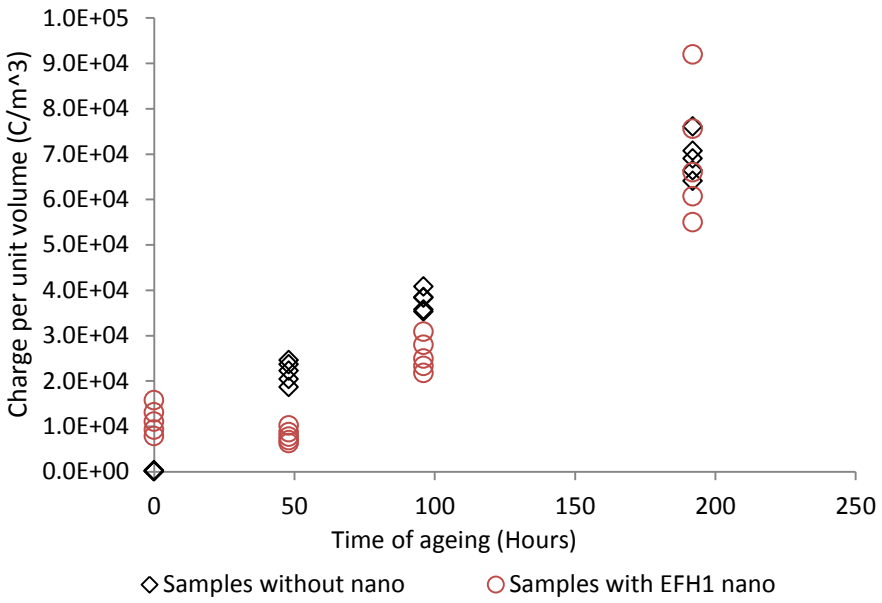

Figure 8-27 Charge density in the EFH1 nanoparticles modified samples

The calculated number of charge carriers increases in both the pure aged insulating oil samples and the samples where nanoparticles were added post ageing increases as ageing time increases. However the differences in the number of charge carriers for both types of sample are broadly similar for longer ageing times Again, this supports the hypothesis that the change in the observed current after adding of EFH1 nanoparticles is mainly due to the change in the mobility of charge carriers rather than the change in the number of charge carriers present in the oil samples.

8.7. SUMMARY

In this chapter, a series of Shell Diala oil samples with magnetite nanoparticles were prepared by adding a fixed volume of EFH1 ferrofluid into the unaged and aged oil samples described in chapter 7. The concentration of the nanoparticles in each sample is in the range of 0.003 to 0.015 g/L. Ultrasonic treatment was used to disperse the nanoparticles in the oil samples. After applying the Ultrasonic treatment for 30 minutes, a homogeneous dispersion of nanoparticles can be obtained in the liquid. The stability of these suspensions was good since no precipitation phenomenon was observed after these samples were left undisturbed over a period of four weeks.

For each sample, 5 sets of measurements were done on successive days following the same approach introduced in chapter 6 and adopted in chapter 7. I_{peak}, I_{dc} and TOF values were obtained for the recorded current traces. Appropriate fits were performed on each sample based on the trend over the 5 successive measurements. I_{peak}, I_{dc} and values of mobility obtained from the fit results were used to be able to express the characteristics of samples well.

In general, changes can be observed in the I_{peak}, I_{dc} and mobility due to the addition of EFH1 nanoparticles. For both unaged and aged samples, adding of nanoparticles leads to larger I_{peak} and I_{dc} values, which indicates that the addition of EFH1 nanoparticles can enhance the d.c. conduction process of unaged and aged Shell Diala insulating oil.

The effect of adding nanoparticles on the apparent mobility after the ageing process is still elusive. Adding EFH1 nanoparticles into unaged Shell Diala insulating oil appears to decrease the apparent mobility and suppress the voltage dependence. However, adding EFH1 nanoparticles into the aged oil samples increased the apparent mobility significantly.

When the applied voltage was in a range of 30 to 70 volts, the measured d.c. currents for each sample seem to follow the Schottky emission type behaviour well. However, the measured d.c. conduction behaviours at lower fields seem to be quite different. Possible reason for this difference might be related to the different effects of space charge close to the electrode region.

9. MEASUREMENTS ON OIL WITH SIGMA NANO PARTICLES

9.1. INTRODUCTION

In this chapter, the effects of subjecting a magnetite nano-suspension in Shell Diala insulating oil to thermal ageing are reported. The suspensions were thermally aged at 120℃ for 0, 48, 96 and 192 hours respectively, using the method described in Chapter 5. TOF, I_{peak} and I_{dc} of samples were measured as described in Chapter 3 and similar fitting methods were adopted for analyzing the characteristics of the aged insulating oil with nanoparticles present. The influence of the presence of nanoparticles on the ageing of insulating oil samples were investigated by comparing the experimental results and the results presented in Chapter 7.

9.1.1. NANO PARTICLES USED

Initially, the EFH1 Ferrofluid manufactured by Ferrotec (section 8.1.1) was added to the Shell Diala insulating oil as described in Chapter 8 to obtain the nanofluid samples for ageing. Although these nanoparticles had remained stable and well distributed in unaged and aged Shell Diala insulating oil for more than one month, exposure to the thermal ageing process appeared to cause the nanoparticles settling out from the insulating oil and a precipitate formed after 24 hours of ageing at 120°C. Figure 9-1 shows the change of nanofluid sample due to the 24 hours thermal ageing process. Therefore, tests were performed with an alternative source of nanoparticles: Sigma-Aldrich 07318 - magnetic iron oxide nanoparticles [**145**]. The concentration of magnetic iron oxide nanoparticles of this ferrofluid was in a range of 0.5 to 0.7%. The carrier liquid of this ferrofluid was heptane and the density was 0.69 g/mL at 20℃. The surfactant used in this ferrofluid was Oleic Acid. The type of nanoparticles in this ferrofluid was Fe_3O_4 magnetite and the particle's diameter was in a range of 6.5 nm±3.0 nm.

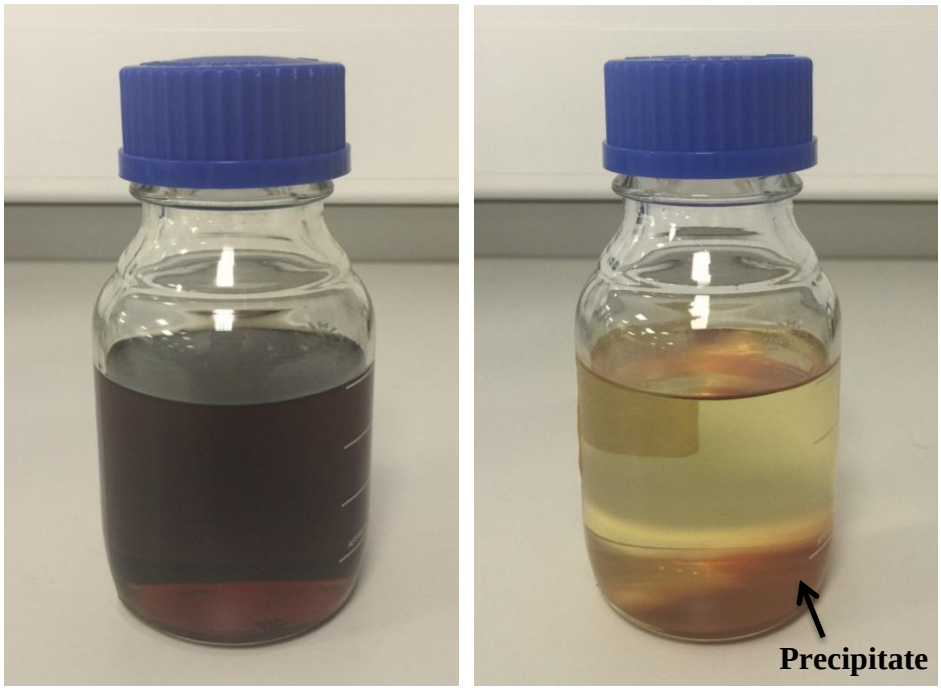

Figure 9-1 Effect of thermal ageing on EFH1 nanofluid: Left image for nanofluid before ageing (a); right image for nanofluid after 24h ageing process (b).

A similar method to that used with EFH1 ferrofluid was adopted to prepare the oil-based nanofluid samples with a constant mass concentration using the Sigma nanoparticles. A fixed volume of 0.1ml ferrofluid was added into 200ml oil sample followed by 30 minutes ultrasonic treatment which was described in section 8.1.2. For nanofluid samples prepared with the Sigma-Aldrich nanoparticles, the range of concentration of nanoparticles is from 0.00175 g/L to 0.00245 g/L. The stability of these suspensions was good with no precipitation observed after these samples were left undisturbed at ambient over a period of one month. In addition, this new nanofluid exhibits a good thermal stability with no precipitate observed after thermal ageing for 96 hours at 120°C. As the materials of these two types of nanoparticles are the same (Fe_3O_4), the difference in thermal stability might be due to the different surfactant used for coating the nanoparticles. In addition, the liquid carrier used in the EFH1 nanofluid was a paraffin rather than heptane. Paraffin will contain hydrocarbons with between 6 to 16 carbon atoms per molecule which may affect the behaviour of the system. Also it is not clear how pure the paraffin used in the EFH1 nanofluid was. The possible presence of impurities in the EFH1 ferrofluid could be another cause of the difference between these two types of nanofluid.

Therefore, this alternative nanofluid was used to investigate the effect of the presence of nanoparticles on the ageing of insulating oil samples.

Figure 9-2 shows samples of unaged oil and samples that have been aged for 2 days, 4 days and 8 days with and without Sigma nanoparticles presence.

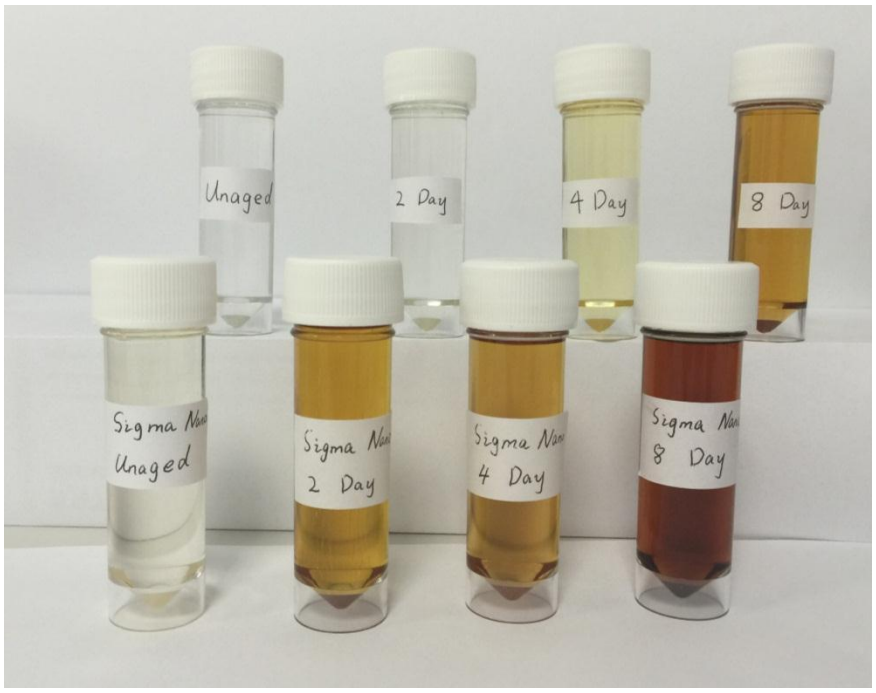

Figure 9-2 Samples aged without nanoparticles and samples aged with Sigma nanoparticles added

For each ageing time there are two samples one without nanoparticles added and one containing nanoparticles. The presence of the nanoparticles has not had a significant effect on the colour of the unaged sample, however at each specific ageing time, the sample which was aged with nanoparticles present seems to be significantly darker.

9.2. UNAGED OIL WITH NANOPARTICLES

An unaged Shell Diala insulating oil sample containing the Sigma-Aldrich nanoparticles was investigated to allow comparison with the results in chapter 7 and chapter 8. Five successive measurements were taken using the approach adopted for the other measurements. The results obtained from analysis of the current transients are shown in AppendixA 9.

9.2.1. PEAK CURRENT AND DC CURRENT

I_{peak} values of unaged samples with Sigma-Aldrich nanoparticles for different voltages are shown for the 5 successive daily measurements in Figure 9-3 below.

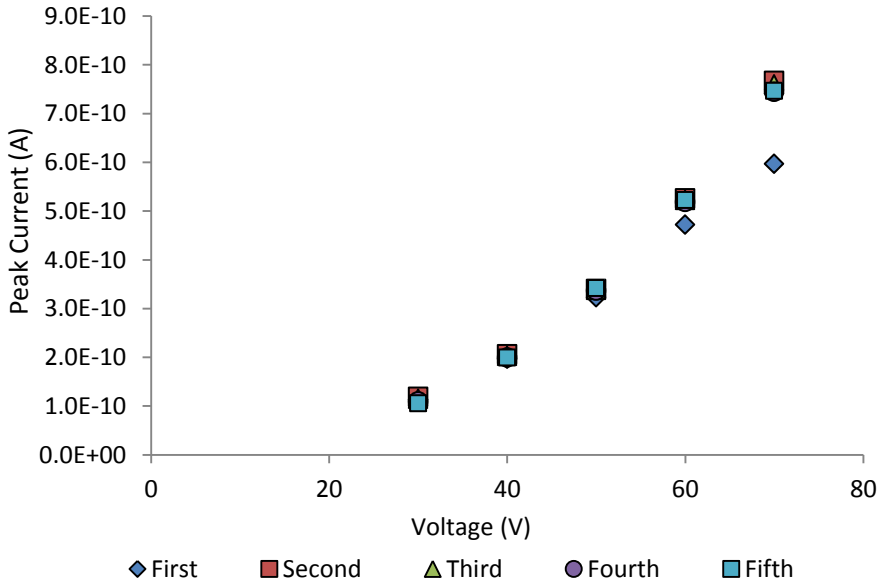

Figure 9-3 Peak current for unaged sample with Sigma nanoparticles First, Second, Third, Fourth and Fifth represents measurements taken after 3hours, 27hours, 51hours, 75hours and 99hours, respectively.

The behaviour of peak current of the unaged sample with nanoparticles was very similar to that of the unaged sample without nanoparticles as shown in Figure 7-1.

The measured peak current increased with the increase of applied voltage. The magnitudes of the currents in the unaged sample with Sigma-Aldrich nanoparticles are close to those for the unaged oil without nanoparticles and are considerably smaller compared with the results for unaged oil with Ferrotec ferrofluid described in chapter 8.2. This may be due to the difference of nanoparticles' concentrations between samples discussed in chapter 8 and the samples in this chapter. For nanofluid prepared with EFH1 ferrofluid, the concentration of nanoparticles is in a range from 0.003 to 0.015 g/L, while for nanofluid prepared with the Sigma-Aldrich nanoparticles, the range of concentration of nanoparticles is from 0.00175 to 0.00245 g/L. The measured current results varied slightly over the 5 successive measurements as shown in Figure 9-4.

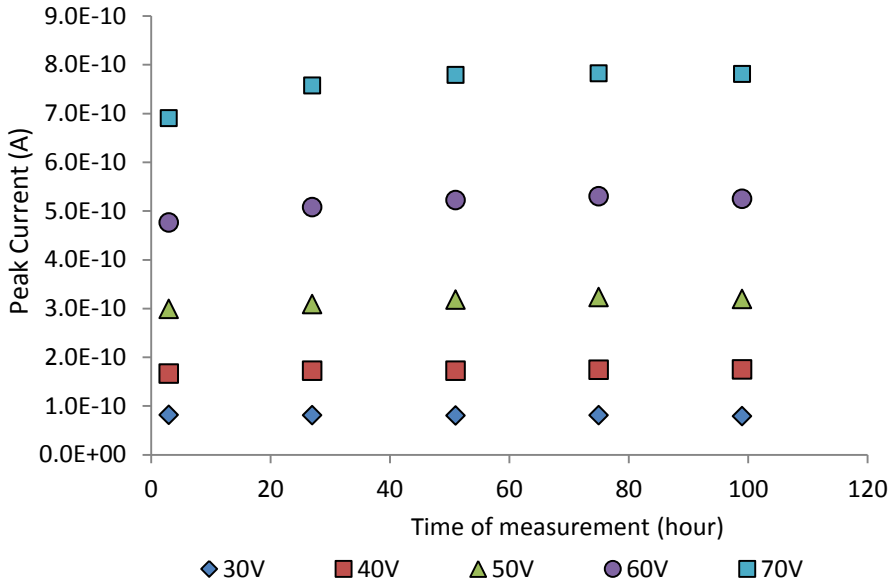

Figure 9-4 Variation of peak current for unaged Sigma nanofluid over 5 successive measurements

At higher voltages, the measured values of I_{peak} in the first set of measurement were smaller than those measured in the rest of the set of measurements. For the results between 2 and 5 days, the peak current does not change significantly with the time of measurement. It was therefore decided that the I_{peak} values of unaged oil sample with Sigma nanoparticles can be best represented by the calculated average value from the final 4 successive measurements. This is assumed to be equivalent to the values calculated at $t = \infty$ for the exponential fits used on some of the other data sets.

The measured d.c. current values for unaged sample with nanoparticles present are shown in Figure 9-5. The values of measured d.c. current at different applied voltage are close to that of the pure unaged oil sample. Comparing with the EFH1 nanofluid sample shown in Figure 8-2, the magnitudes of d.c. current for Sigma nanofluid are much smaller, approximately equal to only 3% of that for EFH1 nanofluid.

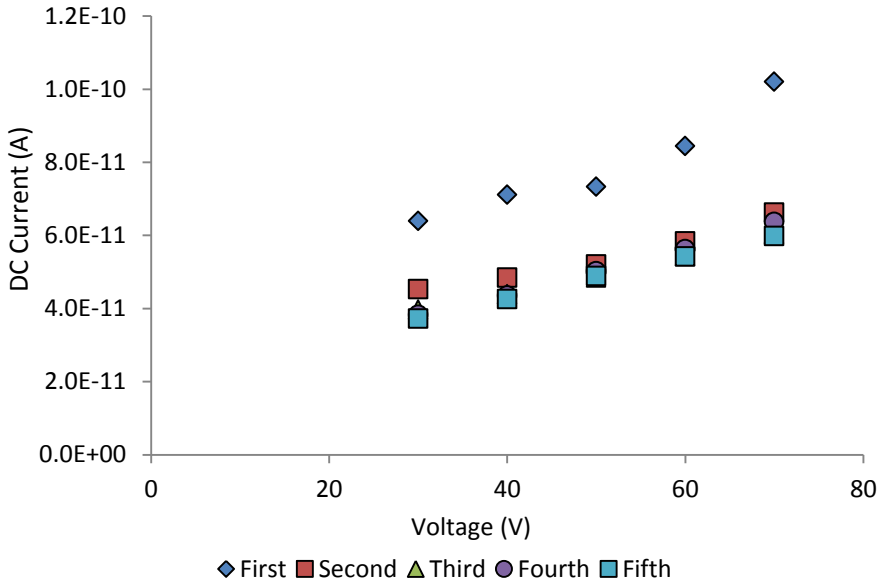

Figure 9-5 D.c current for unaged sample with Sigma nanoparticles

Similar to the measurements of I_{peak}, it can be seen for each measurement that I_{dc} increases with the applied voltage. The behaviour of I_{dc} over 5 days measurements are shown in Figure 9-6 below.

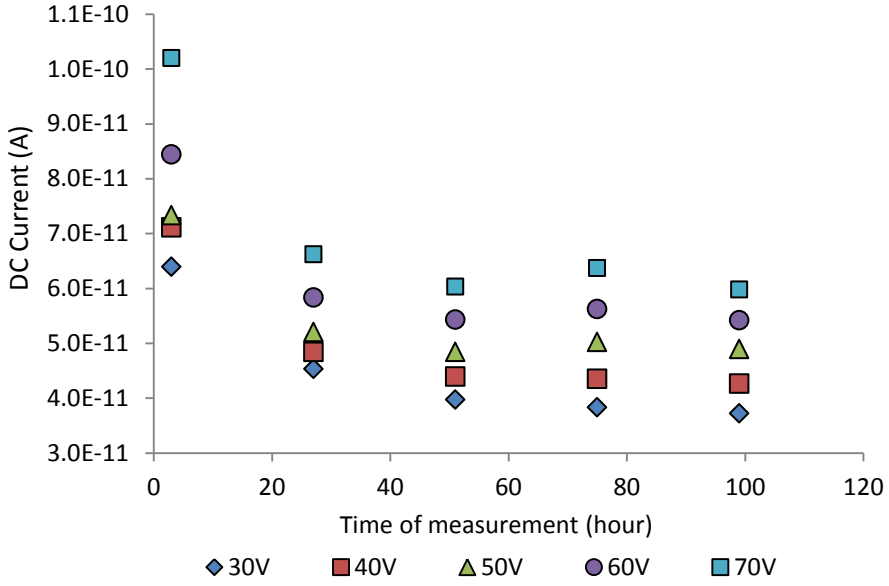

Figure 9-6 Variation of d.c. current for unaged Sigma nanofluid over 5 successive measurements

It can be seen from Figure 9-6 that there was a variation of d.c. current values with the time at which the measurement was taken for each different applied voltage with

the values decreasing with time. This is again similar to the behaviour seen in the unaged oil and the exponential equation 7-1 was used again to fit the measured data with the assumption that this change is a result of a first order kinetic. The minimum sum of residual of the 5 fits can be obtained with a value of time constant τ of 12.8h. The parameters of fitting are shown in Table 9-1.

Voltage (V)	I_1	I_0	τ	R square value	I_{dc} (A) (t = 0)	I_{dc} (A) (t = ∞)
30	3.89E-11	3.73E-11	12.8	0.980	7.61E-11	3.89E-11
40	4.33E-11	4.46E-11	12.8	0.9979	8.79E-11	4.33E-11
50	4.88E-11	4.67E-11	12.8	0.993	9.55E-11	4.88E-11
60	5.44E-11	5.20E-11	12.8	0.994	1.06E-10	5.44E-11
70	6.07E-11	5.63E-11	12.8	0.991	1.17E-10	6.07E-11

Table 9-1 Fitting data for unaged sample with Sigma nanoparticles

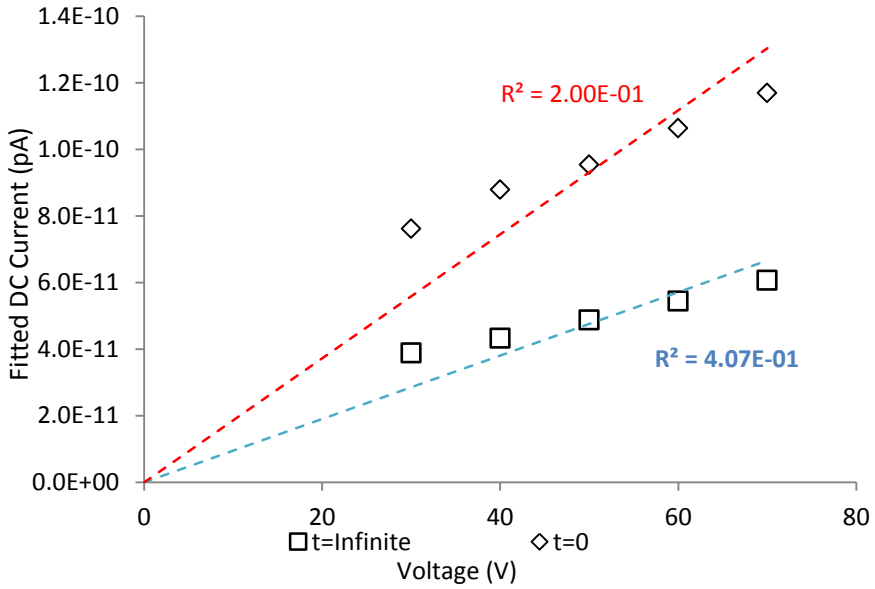

Figure 9-7 Fitted d.c. current for unaged sample with Sigma nanoparticles

The R^2 values in Table 9-1 indicate that the qualities of fits are acceptable. Therefore, it is reasonable to use the fitting results to represent the behaviour of I_{dc} of unaged oil with nanoparticles present. The derived I_{dc} when $t = \infty$ and $t = 0$, based on the fits were plotted in Figure 9-7 with a linear regression line that pass through the origin.

9.2.2. TOF AND MOBILITY

The measured values of TOF decrease as the applied field increases. The measured TOFs for the Sigma based nanofluid are close to those observed in the pure oil and smaller than those observed in the EFH1 based nanofluid (section 8.2). The calculated mobility values of unaged sample with nanoparticles measured under different voltages over five successive measurements are shown in Figure 9-8.

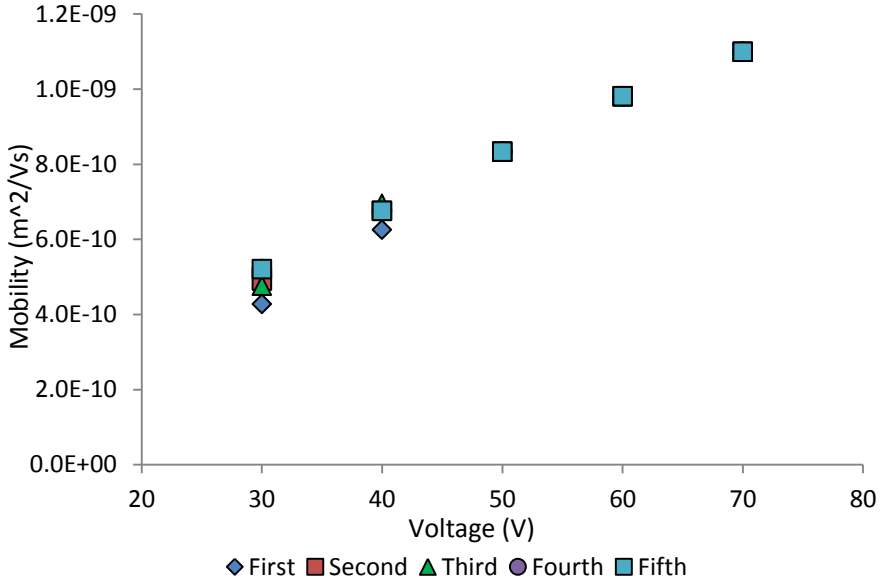

Figure 9-8 Calculated mobility for unaged sample with Sigma nanoparticles

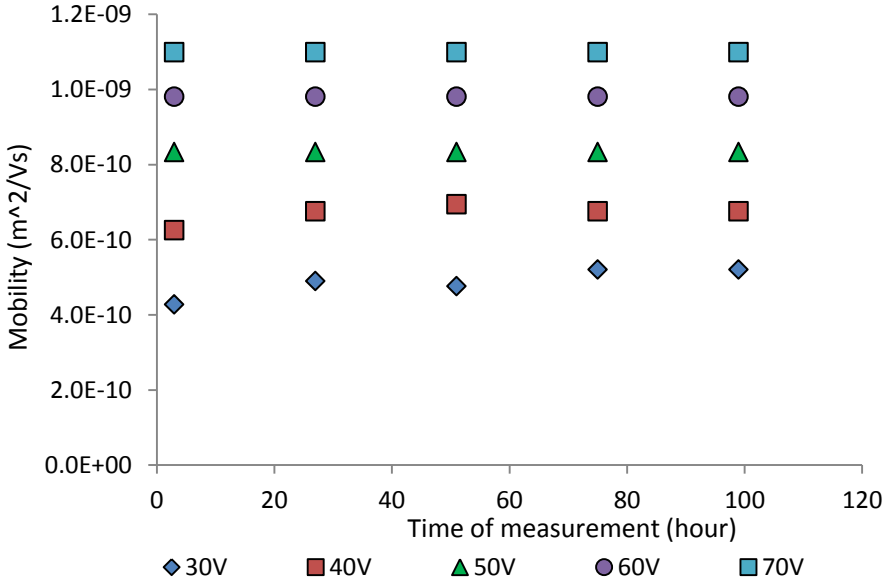

Figure 9-9 Mobility of Unaged sample with Sigma nanoparticles at different applied voltage

It can be seen from Figure 9-8 that the calculated mobility increases with the associated applied voltage. This increase of mobility is similar to that for an unaged oil sample without nanoparticles (section 7.2). A plot of the mobility values with the time at which the measurements were taken is shown in Figure 9-9.

Over the set of 5 successive measurements, the value of calculated mobility at a given applied voltage appears to be broadly constant which was also in accord with the behaviour of pure unaged oil. This is slightly different from the behaviour of unaged oil with EFH1 nanoparticles which appeared to have a small upward trend with the time at which the measurement was taken. The average value calculated from the 5 successive measurements was therefore used to describe the mobility at each voltage.

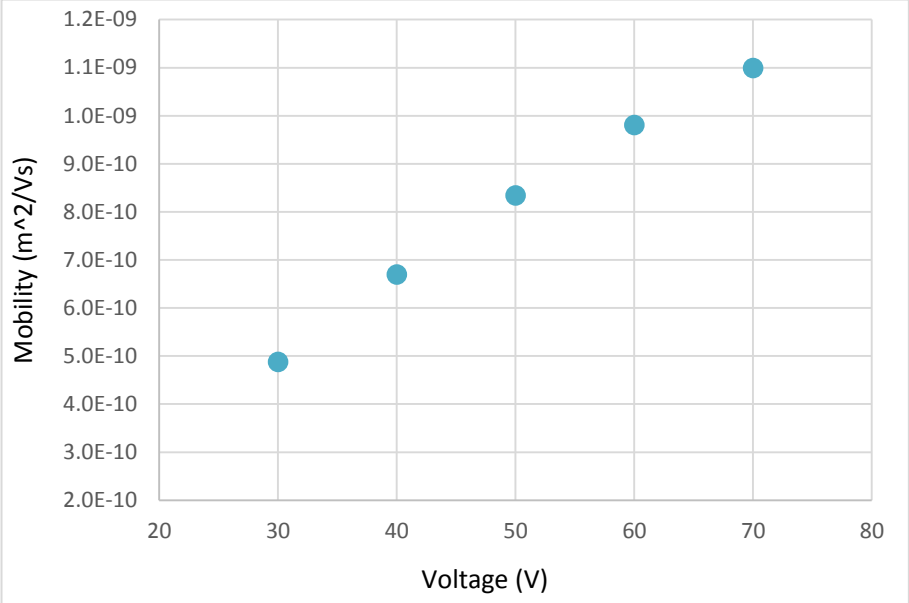

Figure 9-10 Average value of mobility of unaged sample with Sigma nanoparticles

Plotting the calculated average mobility as a function of applied voltage gives Figure 9-10 which suggests that there might be a linear relationship between the mobility and the applied voltage over the range of values considered.

9.3. OIL AGED 2 DAYS WITH NANOPARTICLES

200ml test nanofluid sample was prepared by adding the Sigma nanoparticles into unaged Shell Diala insulating oil. Ultrasonic treatment was used for 30 minutes to obtain a uniform separation of nanoparticles in the oil. The nanofluid was then thermally aged for 48 hours at 120℃. Again, five successive measurements were done following the common approach adopted across all measurements. The results obtained from analysis of the current transients are shown in AppendixA 10.

9.3.1. PEAK CURRENT AND DC CURRENT

Similar to the V-I relationship in the measurement of the unaged sample with nanoparticles present, the measured I_{peak} and I_{dc} of the 2 days aged sample with Sigma nanoparticles present increases with the applied voltage. The measured I_{peak} and I_{dc} magnitudes of the 2 day aged nano-added oil sample were larger than the results from a sample without nanoparticles aged for 2 days (section 7.3). For both I_{peak} and I_{dc} measurements, an upward trend of variation of measured results over 5 day measurements was observed which is consistent with the trend in the 2 days aged sample without nanoparticles. Following the same fitting approach used in section 7.3, equation 7-3 was used for fitting the recorded data of 2 days aged sample with nanoparticles present. The fitting results are shown in Table 9-2 and Table 9-3.

Voltage (V)	I_1	I_0	τ	R^2	I_{peak} (A) (t = 0)	I_{peak} (A) (t = ∞)
30	1.09E-09	4.40E-09	61.7	0.993	1.09E-09	5.49E-09
40	1.66E-09	5.34E-09	61.7	0.996	1.66E-09	6.99E-09
50	2.24E-09	6.15E-09	61.7	0.994	2.24E-09	8.38E-09
60	2.51E-09	7.27E-09	61.7	0.995	2.51E-09	9.78E-09
70	2.74E-09	8.41E-09	61.7	0.994	2.74E-09	1.11E-08

Table 9-2 Fitting data for 2 days aged sample with Sigma nanoparticles present peak current when time constant τ = 61.7h

Voltage (V)	I_1	I_0	τ	R^2	I_{dc} (pA) (t = 0)	I_{dc} (pA) (t =∞)
30	9.45E-10	2.68E-09	61.7	0.988	9.45E-10	3.63E-09
40	1.44E-09	3.21E-09	61.7	0.993	1.44E-09	4.65E-09
50	1.91E-09	3.69E-09	61.7	0.993	1.91E-09	5.60E-09
60	2.15E-09	4.44E-09	61.7	0.993	2.15E-09	6.59E-09
70	2.28E-09	5.27E-09	61.7	0.991	2.28E-09	7.55E-09

Table 9-3 Fitting data for 2 days aged sample with Sigma nanoparticles present d.c current when time constant τ =67.1h

The quality of fits are good from the R^2 values shown in Table 9-2 and Table 9-3, therefore, the variation of measured currents over the 5 successive measurements can be described using the same method as shown in section 7.3. Plotting the derived values of I_{peak} and I_{dc} when $t = 0$ and $t = \infty$ associated with the applied voltage gives Figure 9-11 and Figure 9-12.

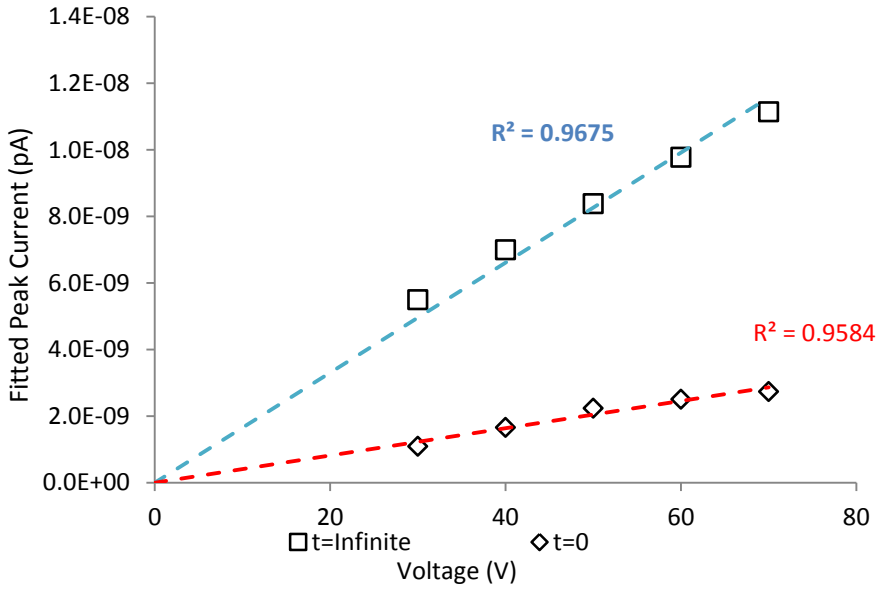

Figure 9-11 Expected peak current of 2 day aged sample with Sigma nanoparticles

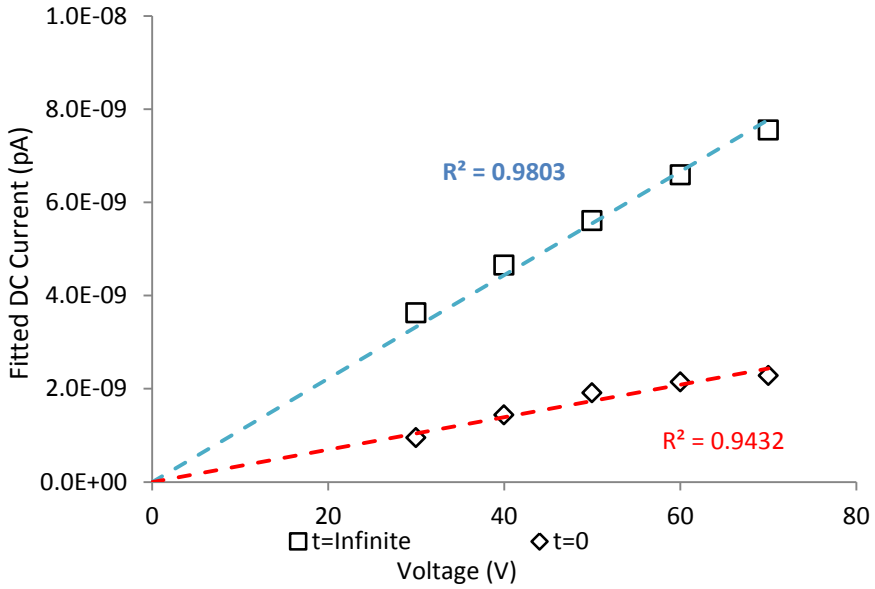

Figure 9-12 Expected d.c. current of 2 day aged sample with Sigma nanoparticles

Assuming that I_{peak} and I_{dc} would be zero when the applied voltage is equal to zero. For the peak current at $t = 0$ and $t = \infty$ the behaviour appears to be roughly linear suggesting an Ohmic behaviour. This linear fit is also possible for d.c. current, but the data suggests that better linear fits would be possible if the constraint of passing through the origin was removed.

9.3.2. TOF AND MOBILITY

The behaviours of TOF and mobility were similar to that in the measurements of the 2 days aged sample without nanoparticles described in section 7.3. The measured values of TOF for 2 days aged sample with Sigma nanoparticles have an upward trend with time over the 5 successive measurements and therefore the derived values of mobility of charge carriers have a downward trend along with the measurement time. Equation 7-4 was adopted to fit the measured values of mobility. Parameters of fits of mobility are shown in Table 9-4.

A minimum value of SSR can be obtained when the time constant value was equal to 28.7h. The R^2 values for measurements are all larger than 0.97 which indicates that the fit results can be reasonably used to represent the behaviours of mobilities.

Voltage (V)	μ_1	μ_0	τ	R^2	Mobility (t = 0)	Mobility (t = ∞)
30	2.73E-10	1.29E-10	28.7	0.975	4.03E-10	2.73E-10
40	2.63E-10	1.28E-10	28.7	0.997	3.91E-10	2.63E-10
50	2.59E-10	1.27E-10	28.7	0.996	3.87E-10	2.59E-10
60	2.65E-10	1.57E-10	28.7	0.993	4.23E-10	2.65E-10
70	2.61E-10	2.38E-10	28.7	0.992	4.98E-10	2.61E-10

Table 9-4 Fit data of mobility for 2 day aged sample with Sigma nanoparticles

The mobility parameters for 2 days aged sample with nanoparticles added before ageing when t = 0 and t = ∞ are plotted in Figure 9-13.

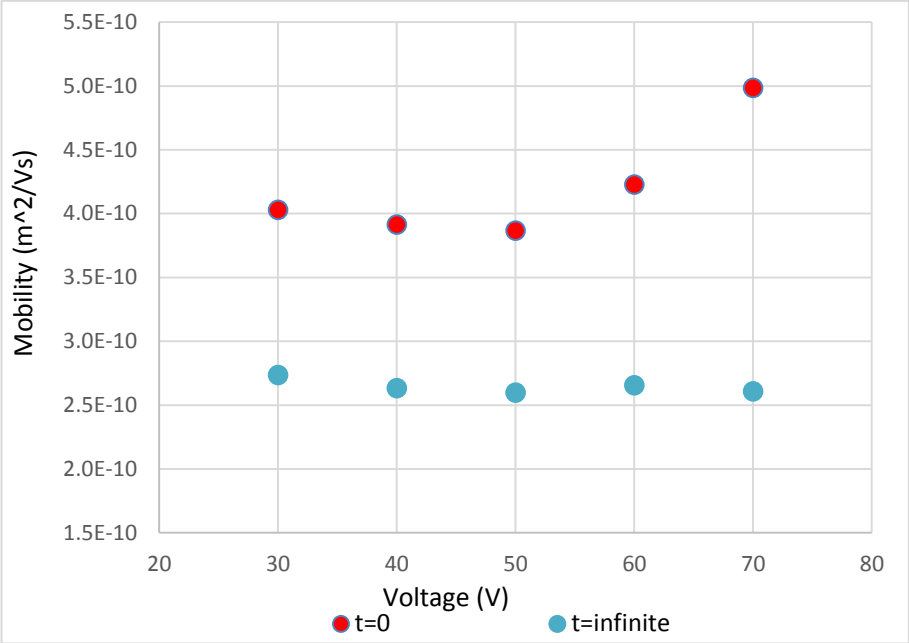

Figure 9-13 Fitted mobility of 2 days aged sample with Sigma nanoparticles

When the measurement system reached equilibrium at $t = \infty$, the mobilities under different applied voltage appears to be constant. Further analysis and comparisons will be given in section 9.8.

9.4. OIL AGED 4 DAYS WITH NANOPARTICLES

A series of tests following the same approach as used for 2 day aged sample with Sigma nanoparticles reported in section 9.3 was performed on oil samples that had been thermally aged for 4 days with nanoparticles present. The method of thermal

ageing has been described in chapter 5. Again the behaviour of the samples was measured over 5 successive days. Measurement results from the recorded data are presented in AppendixA 11.

9.4.1. PEAK CURRENT AND DC CURRENT

The upward trend of peak current and d.c. current over 5 successive measurements for 4 day aged sample with Sigma nanoparticles present appears to be similar to the 4 day aged oil sample without nanoparticles added. The measured peak current and d.c. current are shown in Figure 9-14 associated with the time of measurement.

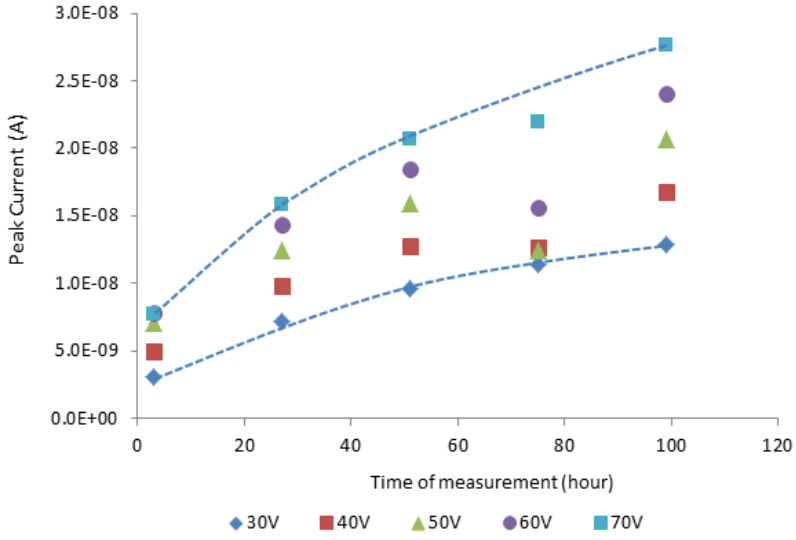

(a)

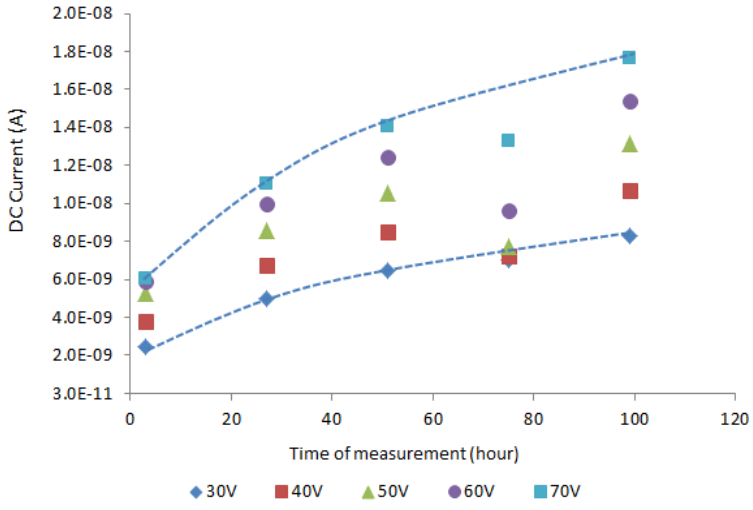

(b)

Figure 9-14 Variation of 4 day aged oil with nanoparticles peak current and d.c current associated with time of measurement

Generally, the measured I_{peak} and I_{dc} magnitudes of the 4 day aged nano-added oil sample were about three times larger than the measurement results from a sample without nanoparticles aged for 4 days (section 7.4). Both the measured peak currents and d.c. currents are increased with the time over the 5 successive measurements. However, the results taken from the fourth set of measurement appears to be quite different from the behaviour of the other results. The reason for this difference is not clear. Ignoring the results obtained from the fourth set of measurement, a similar exponential fit approach used in section 7.4 can also be adopted based on the 4 remaining sets of measurements. The fitting results are shown in Table 9-5 and Table 9-6 below.

Voltage (V)	I_1	I_0	τ	R^2	I_{peak} (A) (t = 0)	I_{peak} (A) (t = ∞)
30	2.21E-09	1.36E-08	65.3	0.999	2.21E-09	1.58E-08
40	3.62E-09	1.66E-08	65.3	0.999	3.62E-09	2.03E-08
50	4.74E-09	1.99E-08	65.3	0.999	4.74E-09	2.46E-08
60	5.57E-09	2.33E-08	65.3	0.999	5.57E-09	2.88E-08
70	6.28E-09	2.71E-08	65.3	0.999	6.28E-09	3.33E-08

Table 9-5 Fitting data for 4 days aged sample with Sigma nanoparticles present peak current when time constant τ= 65.3h

Voltage (V)	I_1	I_0	τ	R^2	I_{dc} (A) (t = 0)	I_{dc} (A) (t =∞)
30	1.97E-09	8.18E-09	65.3	0.999	1.97E-09	1.01E-08
40	3.06E-09	9.76E-09	65.3	0.999	3.06E-09	1.28E-08
50	3.96E-09	1.16E-08	65.3	0.999	3.96E-09	1.56E-08
60	4.65E-09	1.37E-08	65.3	0.999	4.65E-09	1.83E-08
70	5.26E-09	1.60E-08	65.3	0.999	5.26E-09	2.13E-08

Table 9-6 Fitting data for 4 days aged sample with Sigma nanoparticles present d.c. current when time constant τ= 65.3h

R^2 values in Table 9-5 and Table 9-6 indicate that for the fits from the remaining four sets of measurements, the fits quality of I_{peak} and I_{dc} are good since the R^2 values are close to 1. The expected values of I_{peak} and I_{dc} values when $t = 0$ and $t = \infty$, derived from the fits, are plotted in Figure 9-15 and Figure 9-16.

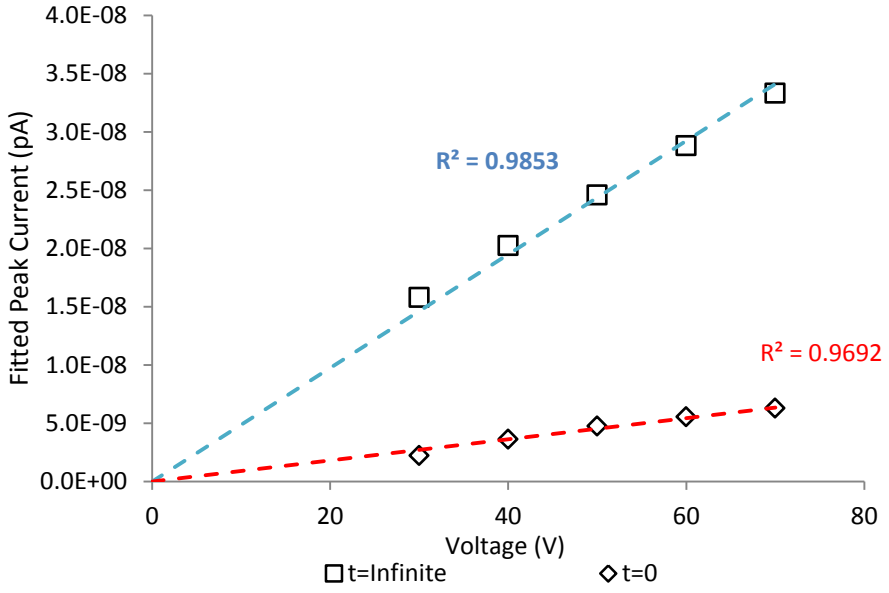

Figure 9-15 Expected peak current of 4 day aged sample with Sigma nanoparticles

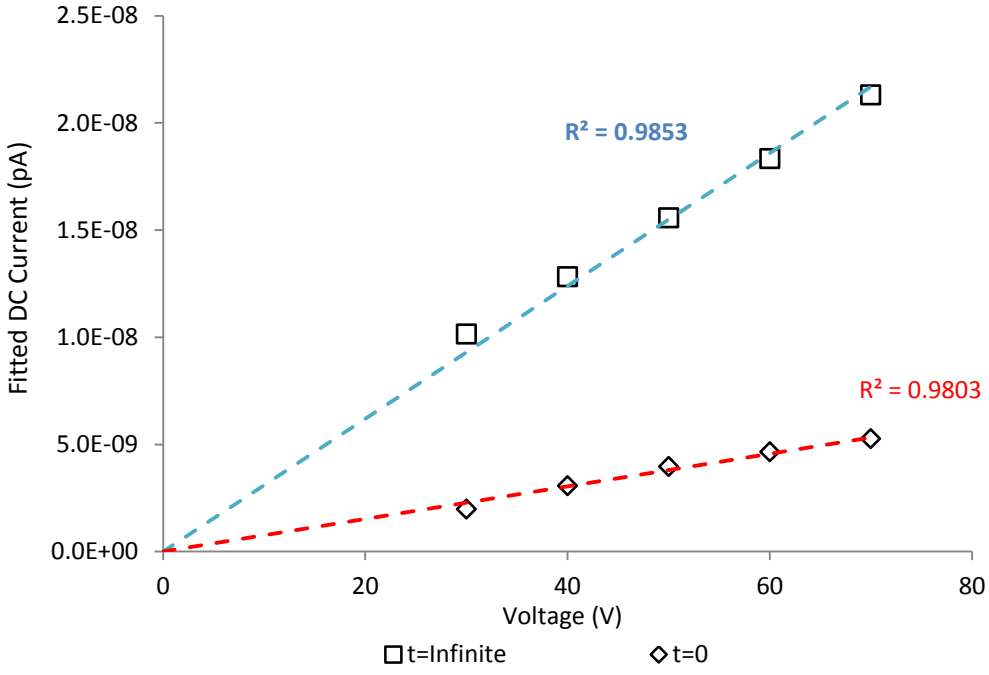

Figure 9-16 Expected d.c current of 4 day aged sample with Sigma nanoparticles

Again, the expected current values should be zero when the applied voltage was equal to zero. Including this point in the data the derived currents all appear to have linear relationships with the applied voltage as shown in Figure 9-15 and Figure 9-16. This indicates that their behaviour is Ohmic or close to Ohmic. However, in particular with the results expected for I_{dc} at equilibrium the data suggests that the behaviour is deviating from that expected from Ohmic conduction but can be fit well by the Schottky type fitting.

9.4.2. TOF AND MOBILITY

The behaviours of TOF and mobility were similar to that in the measurements of the 4 days aged sample without nanoparticle added. The measured values of TOF have an upward trend with time over the 5 successive measurements and therefore the derived values of mobility of charge carriers have a downward trend along with the measurement time.

Similar to the fitting approach used in section 7.4, Equation 7-4 was adopted again to fit the measured values of mobility. To be consistent with the approach taken for the current fitting the measurements taken after 4 days was excluded. Parameters of fits of mobility are shown in Table 9-7.

Voltage (V)	μ_1	μ_0	τ	R^2	Mobility (t = 0)	Mobility (t = ∞)
30	2.73E-10	1.29E-10	28.7	0.975	4.03E-10	2.73E-10
40	2.63E-10	1.28E-10	28.7	0.997	3.91E-10	2.63E-10
50	2.59E-10	1.27E-10	28.7	0.996	3.87E-10	2.59E-10
60	2.65E-10	1.57E-10	28.7	0.993	4.23E-10	2.65E-10
70	2.61E-10	2.38E-10	28.7	0.992	4.98E-10	2.61E-10

Table 9-7 Fit data of mobility for 4 day aged sample with Sigma nanoparticles

A minimum value of SSR can be obtained when the time constant value was equal to 28.7h. The R^2 values for indicate the qualities of fits are good. The mobility parameters for 4 days aged sample with Sigma nanoparticles added when $t = 0$ and $t = \infty$ are plotted in Figure 9-17. When the measurement system reached

equilibrium at $t = \infty$, the mobilities under different applied voltage appears to be constant. Again further analysis and comparisons will be given in section 9.8.

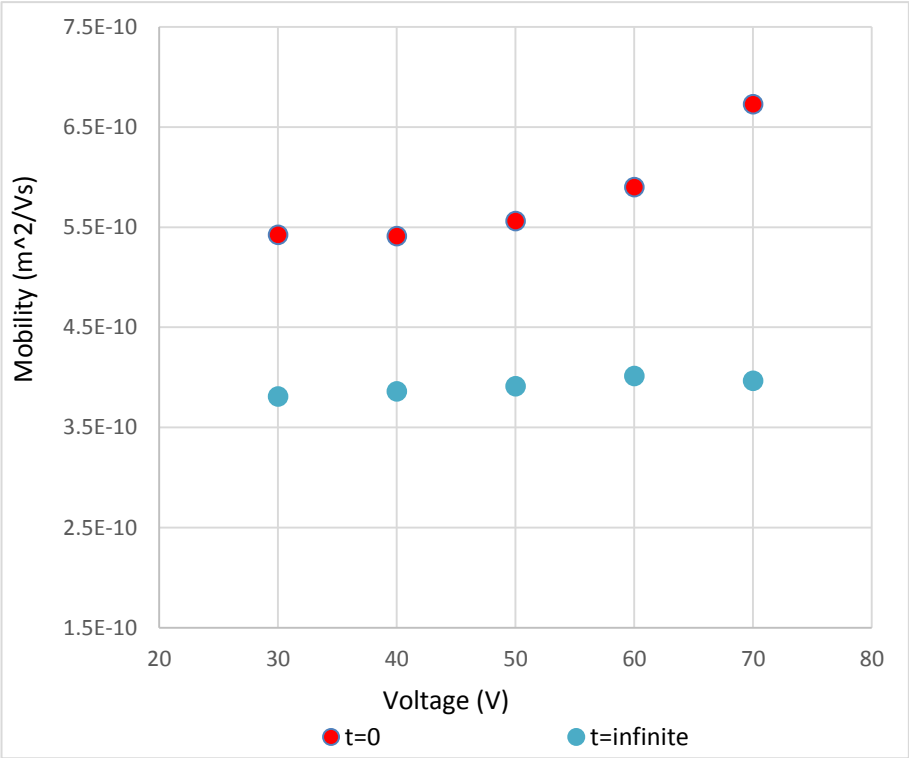

Figure 9-17 Fitted mobility of 4 days aged sample with Sigma nanoparticles

9.5. OIL AGED 8 DAYS WITH NANOPARTICLES

In this section, 200mL Shell Diala oil sample with Sigma nanoparticles present was thermally aged for 192 hours using the same ageing method mentioned previously. Note that, as mentioned in section 7.5, for an oil sample without nanoparticles after 8 days thermal ageing process, a small amount of precipitate was observed in the bulk of the sample. This time, it was difficult to tell if this precipitate was generated as the nanofluid sample is dark after 192 hours ageing. Before the sample cell was filled, the sample was left over 3 weeks which allowed the possible precipitate to settle and the cell was then filled with the oil from the top part of the bottle. The values of I_{peak}, I_{dc} and TOF were measured using the standard protocol and the results from the recorded data are presented in AppendixA 12.

9.5.1. PEAK CURRENT AND DC CURRENT

The measured V-I relationship is similar to that in the measurement of 8 day aged sample without nanoparticles present (section 7.5) with the measured values of I_{peak}

and I_{dc} of 8 days aged sample with Sigma nanoparticles increasing with the applied voltage. Compared with the oil samples aged without any nanoparticles added, the current values for both I_{peak} and I_{dc} at different voltages are approximately two times larger. An upward trend of variation of measured results over 5 success measurements was observed which is corresponding to the trends observed in oil samples aged for 2 days and 4 days with Sigma nanoparticles presence. Equation 7-2 was used for fitting the measurement I_{peak} and I_{dc} values of 8 days aged sample with Sigma nanoparticles. The fitting results are shown in Table 9-8 and Table 9-9.

Voltage (V)	I_1	I_0	τ	R^2	I_{peak} (A) (t = 0)	I_{peak} (A) (t = ∞)
30	7.70E-09	1.24E-08	80.5	0.996	7.70E-09	2.01E-08
40	1.09E-08	1.53E-08	80.5	0.998	1.09E-08	2.62E-08
50	1.39E-08	1.84E-08	80.5	0.998	1.39E-08	3.23E-08
60	1.65E-08	2.18E-08	80.5	0.998	1.65E-08	3.83E-08
70	1.89E-08	2.58E-08	80.5	0.998	1.89E-08	4.47E-08

Table 9-8 Fitting data for 8 days aged sample with Sigma nanoparticles present peak current when time constant τ= 80.5 h

Voltage (V)	I_1	I_0	τ	R^2	I_{dc} (pA) (t = 0)	I_{dc} (pA) (t =∞)
30	6.91E-09	7.96E-09	80.5	0.997	6.91E-09	1.49E-08
40	9.51E-09	9.71E-09	80.5	0.998	9.51E-09	1.92E-08
50	1.19E-08	1.16E-08	80.5	0.998	1.19E-08	2.35E-08
60	1.42E-08	1.35E-08	80.5	0.998	1.42E-08	2.76E-08
70	1.62E-08	1.57E-08	80.5	0.998	1.62E-08	3.18E-08

Table 9-9 Fitting data for 8 days aged sample with Sigma nanoparticles present d.c. current when time constant τ =80.5 h

The fitting results of peak current and d.c. current are shown in Figure 9-18 and Figure 9-19.

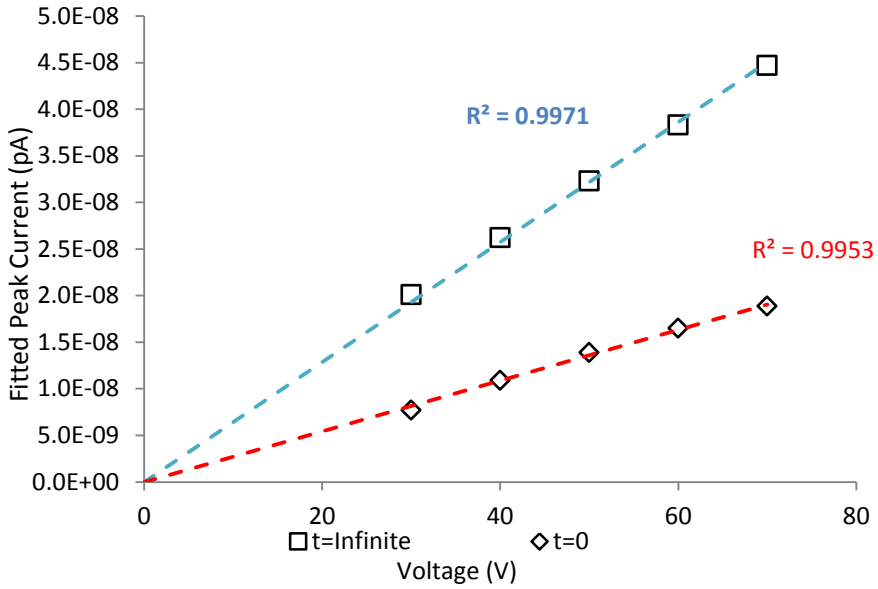

Figure 9-18 Expected peak current of 8 day aged sample with Sigma nanoparticles presence

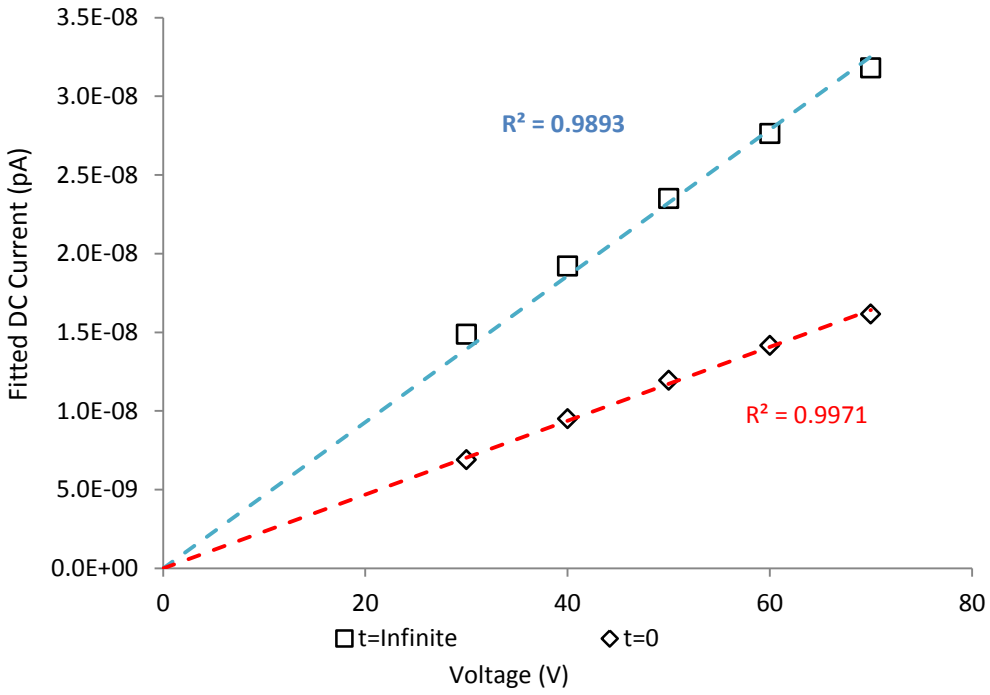

Figure 9-19 Expected d.c current of 8 day aged sample with Sigma nanoparticles presence

Linear fits passing through the origin can be made again indicating that the behaviour for both I_{peak} and I_{dc} is Ohmic or close to Ohmic. However, again with the results expected for I_{dc} at equilibrium the data suggests that the behaviour is deviating from that expected from Ohmic conduction.

9.5.2. TOF AND MOBILITY

The behaviours of TOF and related mobility were also similar to that in the measurements of the 8 day aged samples without nanoparticles. Again, a downward trend with time over the 5 successive measurements process was observed in the calculated values of mobility for 8 day aged sample. Similar fitting method was used with the assumption that change of the mobility follows a first order kinetic. Parameters of fits are shown in Table 9-10.

Voltage (V)	μ_1	μ_0	τ	R^2	Mobility (t = 0)	Mobility (t =∞)
30	6.70E-10	4.98E-11	18.1	0.872	7.20E-10	6.70E-10
40	6.90E-10	6.41E-11	18.1	0.766	7.54E-10	6.90E-10
50	7.19E-10	1.23E-10	18.1	0.935	8.42E-10	7.19E-10
60	7.55E-10	1.77E-10	18.1	0.993	9.32E-10	7.55E-10
70	7.98E-10	2.67E-10	18.1	0.969	1.06E-09	7.98E-10

Table 9-10 Fit data of mobility for 8 day aged sample with Sigma nanoparticles

With a time constant value τ of 18.1h, a minimum value of SSR can be obtained. The R^2 values in Table 9-10 suggested that the quality of the fits below 50V were relatively not very good. These relatively low values of R^2 were caused by the small variation over the 5 successive measurements, since the related TOF values measured with 30V voltage were only in a range of 47s to 50s. For measurement with 40V applied voltage, the measured TOF values were in a range of 34s to 37s. To investigate the validity of this fitting approach, the average mobility values were calculated and the results were plotted in Figure 9-20, together with the mobility values derived from the fitting results when $t = 0$ and $t = \infty$.

There is not a significant difference between the average values and the fit results when $t = \infty$. For the measurements with relatively low voltage (below 50V), the expected values obtained from these two methods are close to each other. The difference between these two approaches increased slightly with the applied voltage. The calculated mobility values from exponential fitting method when $t = \infty$ can

therefore be used to represent the behaviour of mobility of charge carriers in 8 day aged samples with Sigma nanoparticles. Further analysis and comparisons will be given in section 9.8.

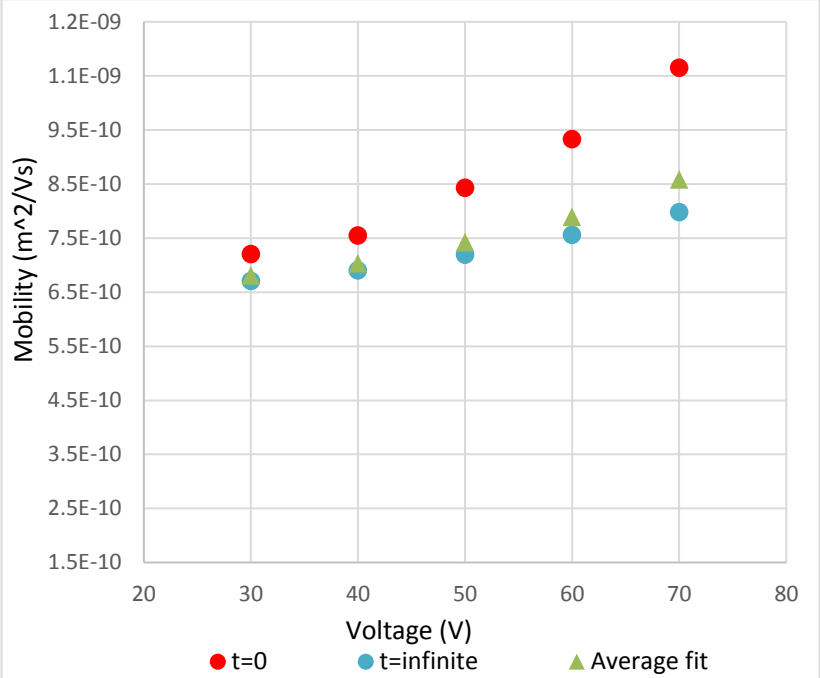

Figure 9-20 Fitted mobility of 8 days aged sample with Sigma nanoparticles

9.6. UNAGED OIL WITH HIGH CONCENTRATION OF NANOPARTICLES

From the experimental results presented in section 9.2-9.5, the observed current magnitudes were lower in the samples aged with Sigma nanoparticles present compared to samples with EFH1 nanoparticles added after ageing. The reasons for this are not clear. Possible reasons might be: differences in the nanoparticles, size and coating; a change in the ageing mechanism due to the presence of the nanoparticles; differences between the liquid carriers for the ferrofluid or differences in the concentration of nanoparticles. Therefore, an additional experiment was performed to test if a change in the concentration of nanoparticles is responsible for the change in observed current values. A new test sample was prepared by adding 0.5ml Sigma nanofluid into 200ml unaged Shell Diala insulating oil using the same methods as in section 9.1.1. This resulted in the range of concentration of Sigma nanoparticles increasing to between 0.00875 g/L to 0.01225 g/L which was close to the maximum possible concentration of samples prepared with EFH1 based

nanofluid sample (0.003 g/L to 0.015 g/L). Five successive measurements were performed using the same approach adopted in this project. Measurement results from the recorded data are presented in AppendixA 13.

9.6.1. PEAK CURRENT AND DC CURRENT

The behaviours of the measured I_{peak} and I_{dc} both increase with the applied voltage. The magnitudes of the currents in the high-concentration Sigma nanofluid sample are larger than that measured in the Sigma based sample with the lower concentration described in section 9.2. The variation of I_{peak} over the 5 successive measurements can be seen in Figure 9-21.

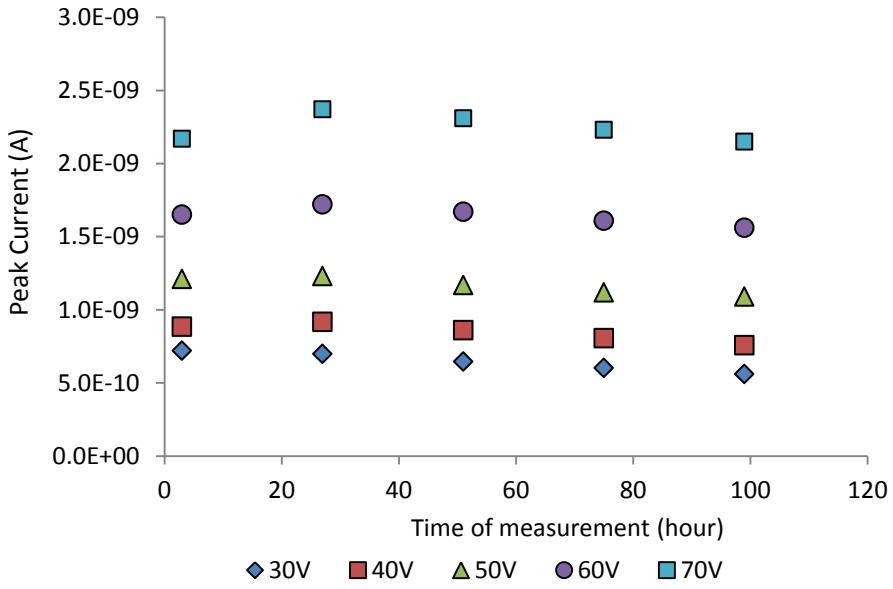

Figure 9-21 Variation of d.c current for unaged high-concentration Sigma nanofluid over 5 successive measurements

At higher voltages, the measured values of I_{peak} in the first set of measurement were smaller than those measured in the rest of the set of measurements. For the results between 2 and 5 days, the peak current measured at higher voltage appears to decrease slightly. However, the calculated standard derivations from the results are less than 8.2% of their average value. Therefore it is assumed that the measured I_{peak} values do not change significantly with the time of measurement after 24 hours. In this case, the same analysis method used in section 9.2 can be adopted with the I_{peak} values represented by the calculated average value from the final 4 successive measurements. The measured d.c. current values for unaged sample with high-

concentration Sigma nanoparticles present are shown in Figure 9-22 below associated with the time of measurement. Similar to the peak current, larger d.c. current values were observed compared with the measured data in the Sigma based sample with the lower concentration

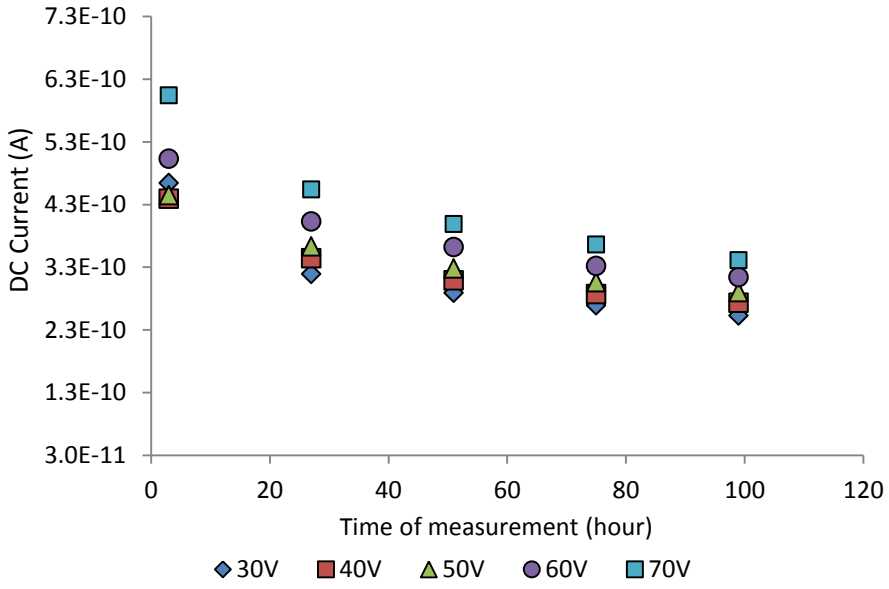

Figure 9-22 Variation of d.c. current for unaged sample with high-concentration Sigma nanoparticles over 5 successive measurements

From Figure 9-22, it appears that the d.c. currents variation in high-concentration Sigma sample follows a downward trend with time. Therefore, equation 7-1 was used to fit the measured data. The result parameters of fitting are shown in Table 9-11.

Voltage (V)	I_1	I_0	τ	R square value	I_{dc} (A) (t = 0)	I_{dc} (A) (t = ∞)
30	3.89E-11	3.73E-11	12.8	0.980	7.61E-11	3.89E-11
40	4.33E-11	4.46E-11	12.8	0.998	8.79E-11	4.33E-11
50	4.88E-11	4.67E-11	12.8	0.993	9.55E-11	4.88E-11
60	5.44E-11	5.20E-11	12.8	0.994	1.06E-10	5.44E-11
70	6.07E-11	5.63E-11	12.8	0.991	1.17E-10	6.07E-11

Table 9-11 Fitting data for high-concentration Sigma nanofluid

The R^2 values in Table 9-11 indicate that the qualities of fits are acceptable so these fitting parameters can be used to represent the behaviour of I_{dc} of unaged oil with nanoparticles present.

Again, the derived I_{dc} and I_{peak} when $\mathbf{t} = \infty$, based on the fits were plotted in Figure 9-23 with a linear regression line that pass through the origin. These results clearly show that the behaviour of the high concentration system is not Ohmic.

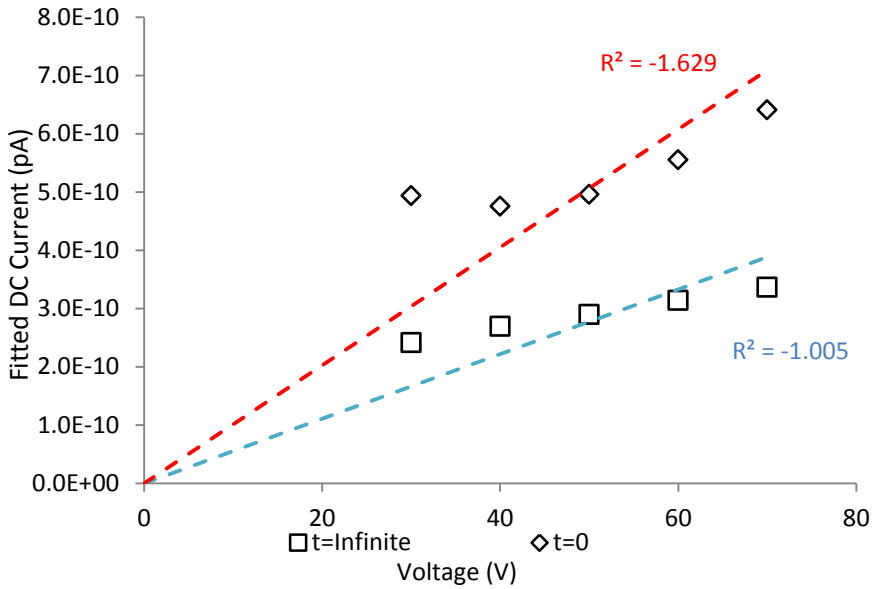

Figure 9-23 Fitted d.c. current for unaged sample with high-concentration Sigma nanoparticles

9.6.2. TOF AND MOBILITY

The calculated mobility values of high-concentration Sigma sample over 5 successive measurements are plotted in Figure 9-24.

Similar to the peak currents behaviours, the calculated mobility at given applied voltage also appears to have a similar behaviours to that in the lower concentration Sigma nanofluid. Although the data in the first set of measurement appears to be larger than that in the rest 4 sets of measurement, the variation amplitude in 5 successive measurements is less than 15% of the average value. Therefore, the average value calculated from the 5 successive measurements was used to describe the mobility at each voltage. Plotting the calculated average mobility as a function of

applied voltage gives Figure 9-25. Results for unaged sample without nanoparticles added were also plotted as reference.

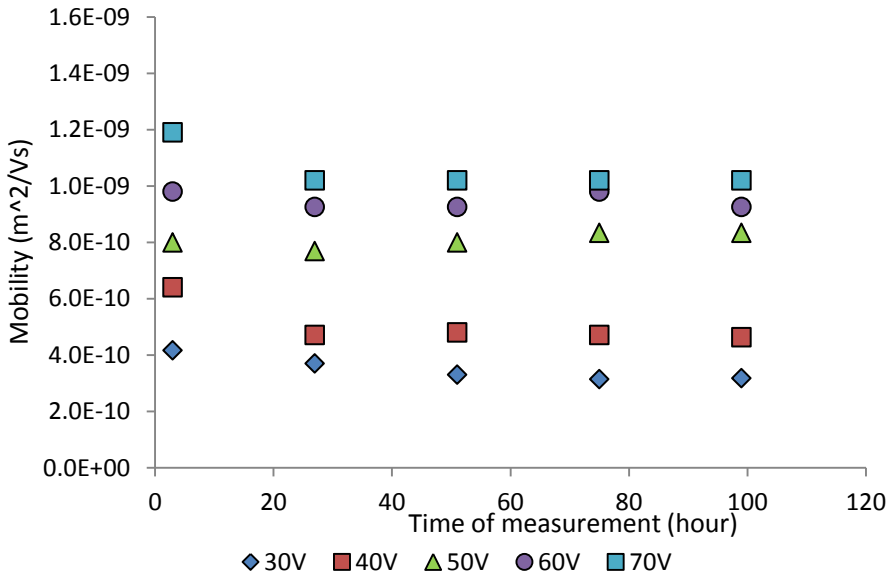

Figure 9-24 Mobility of high-concentration Sigma based sample

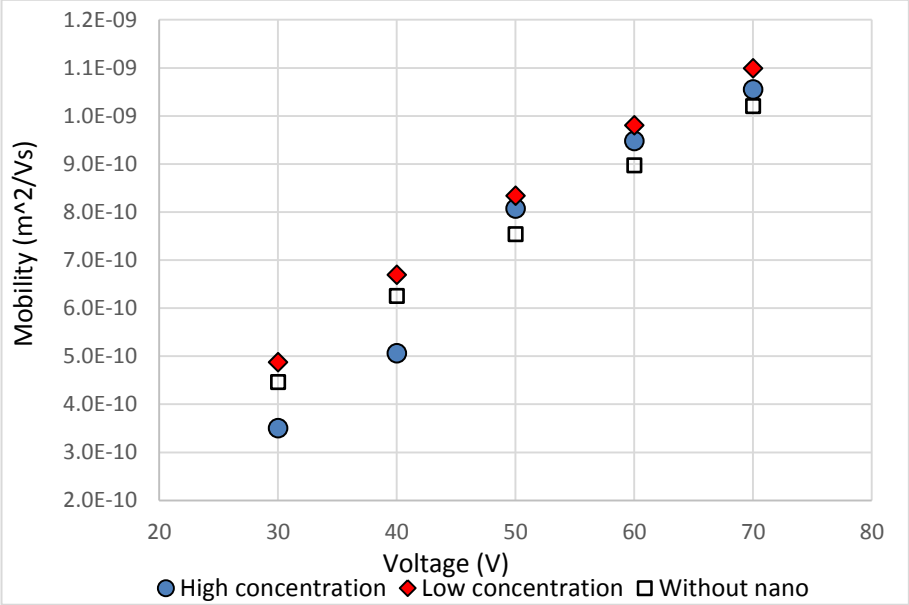

Figure 9-25 Fitted mobility of 8 days aged sample with sigma nanoparticles

Based on the analysis above, it is interesting to note, especially for when the applied voltage is above 50V, that: for the high-concentration Sigma sample in this section, the behaviours of the I_{peak}, I_{dc} and measured mobility over the 5 successive measurements are quite similar to the behaviours in the lower concentration Sigma

sample (section 9.2) and the behaviour of a sample without nanoparticles added. This implies that the concentration of Sigma nanoparticles does not change the apparent mobility of charge carriers in Shell Diala insulating oil significantly in this voltage range. For these three sample types, the measured mobility values show an obviously upward trend along with the applied voltage. However the mobility for the sample with the higher concentration of Sigma nanoparticles seems to be lower than the other two samples at voltages below 50V.

9.6.3. COMPARISON WITH EFH1 BASED NANOFLUID SAMPLE

Comparisons between the results for the unaged high-concentration Sigma based sample (section 9.6) and the unaged EFH1 based sample were performed.

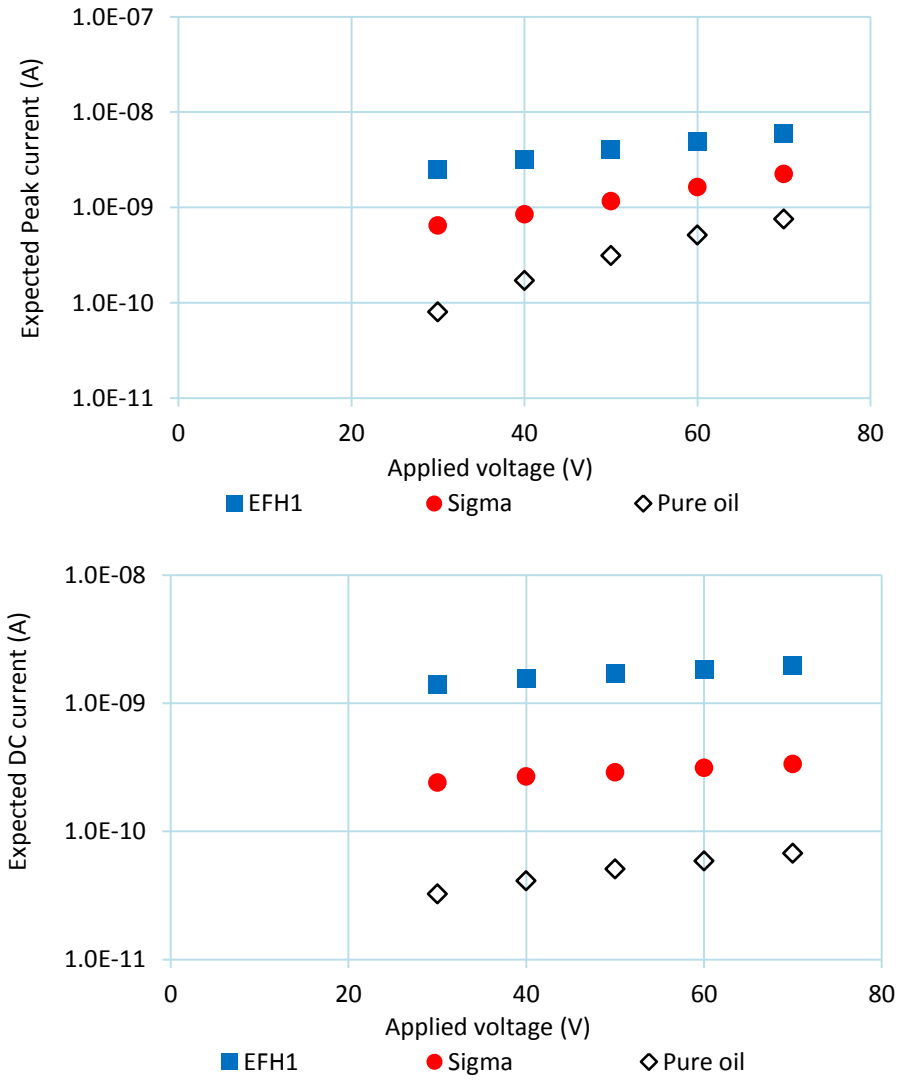

Figure 9-26 Comparison between EFH1 and high-concentration Sigma: Upper graph for peak current (a) and lower graph for d.c current (b)

The expected I_{peak} and I_{dc} values based on earlier analysis are plotted in Figure 9-26 as a function of the applied voltage. Expected I_{peak} and I_{dc} of unaged pure oil sample described in section 7.2 were also plotted in Figure 9-26 as a reference.

Figure 9-26 indicates that the presence of nanoparticles in the Shell Diala leads to an increase of both the peak current and the d.c. current. Changes related to the addition of EFH1 ferrofluid are more significant compared with the change caused by the addition of Sigma ferrofluid with a broadly similar concentration of nanoparticles. The relatively larger d.c. current measured in samples with nanoparticles implies that the d.c. conductivity of insulating oil was increased by adding nanoparticles. This is likely to be a result of the increased traps of electrons generated by the presence of nanoparticles as the possible role of nanoparticles as charge carriers was eliminated in an earlier analysis (Section 8.6.1). Electron traps can be formed close to the surface of nanoparticles relating to the high chemical activity of the surface atoms. Equation 4-2 presented in section 4.8 indicates that the measured d.c. current should be proportional to the total number of charge carriers and the velocity of these charge carriers. Addition of nanoparticles increases the number of electron traps in the bulk of liquid which could enhance the injection of electrons from the electrode. Therefore, the total number of charge carriers in the liquid can be increased which could lead to an increase of the measured d.c. current.

Expected values of mobility for high-concentration Sigma sample, EFH1 sample and unaged pure oil sample were plotted in Figure 9-27.

From Figure 9-27, it seems that the mobility measured with Shell Diala insulating oil containing the EFH1 nanoparticle behaves differently from that measured with oil containing the Sigma nanoparticle. The mobility values are generally lower in the sample containing EFH1 and do not change as significantly with the applied field. There seems to be little difference in the mobility behaviour of the pure oil and the oil containing the Sigma nanoparticles. This is not what would be predicted if adding nanoparticles resulted in an enhanced diffusion of charge carriers due to there being more “seats” for electrons to jump between.

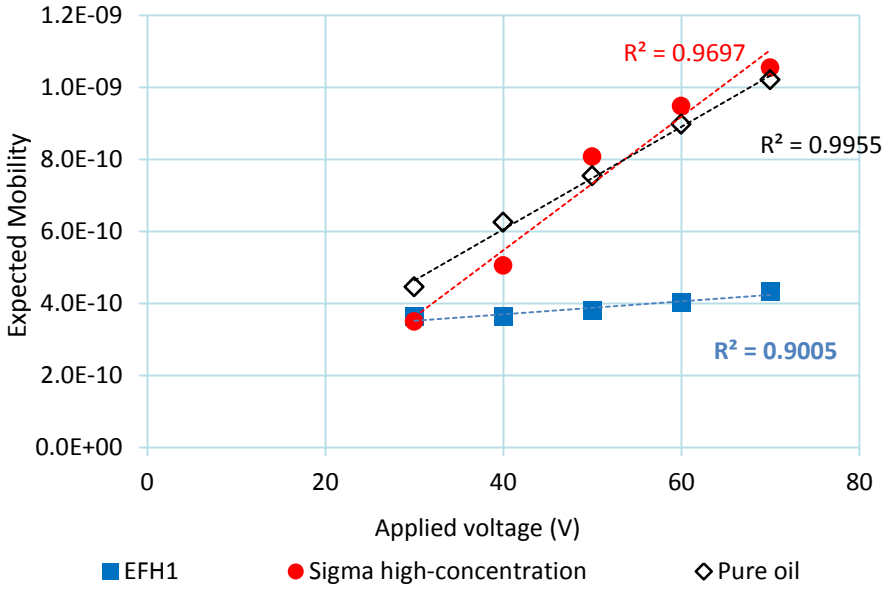

Figure 9-27 Comparison between EFH1 and Sigma: Mobility of charge carriers

Assuming that the apparent mobility measured from TOF reflects the actual mobility of the charge carriers under steady state conditions, it is interesting to note that when the applied voltage is 30V, the measured mobility values from these three samples are close, while the measured d.c. current values at this voltage are different. This indicates that the reason for the increase of conductivity is more likely to be due to an increase of the total number of charge carriers, controlled by injection rather than due to an increase in the velocity of the motion of charge carriers through the liquid. With higher applied voltages, a much stronger field dependence of mobility in the pure oil sample and the sample containing Sigma nanoparticles can be observed compared with EFH1 sample. This field dependence of mobility might be a result of the EHD effect as mentioned in section 3.4.2. If this is true, the EHD convection appears to be less significant in the EFH1 sample. This might be due to the different in the size of nanoparticles. As the size of EFH1 nanoparticles is larger than that of the Sigma nanoparticles, when the collision between the charge carriers and the nanoparticles occurring, assuming the kinetic energy obtained by nanoparticles were constant. The increased velocity of the EFH1 nanoparticles was expected to be lower than that of the Sigma nanoparticles.

As previously mentioned, the I_{peak} and I_{dc} values measured in the higher concentration Sigma sample are higher than those measured in lower concentration Sigma sample. This is consistent with the hypothesis in section 4.8 that the diffusion of charge carriers is related to the concentration of nanoparticles. Larger concentration of nanoparticles means more traps can be generated in the liquid which could have a positive effect on both the mobility of charge carriers and the injection process. As the same kind of magnetite material (Fe_3O_4) was used in EFH1 and Sigma, the density of these two nanoparticles is expected to be similar. However, the volume of EFH1 nanoparticles (particle diameter = 11.6nm) was approximately 6 times larger than that of Sigma nanoparticles (particle diameter = 6.5nm), hence with an approximately similar mass concentration, the total number of nanoparticles in the Sigma sample should also be roughly 6 times larger than that in EFH1 sample. If the number of "seats" is proportional to the number of nanoparticles the d.c. current measured from the high-concentration Sigma sample should be higher than that measured from EFH1 sample due to the increase in trapping sites. The experimental results are contrary to this hypothesis. The higher conductivity associated with the smaller number concentration of nanoparticles in the EFH1 sample might result from the following reasons:

- **Depth of trap**: The surface energy should increase with decreasing particle size as described in section 4.4. The specific surface area (ratio of surface area to mass) of Sigma nanoparticles would be about 2 times larger than that of the EFH1 nanoparticles, which means the Sigma nanoparticles will have a higher chemical activity than the EFH1 nanoparticles. It is more difficult for trapped electrons to escape away from the Sigma nanoparticles due to the relatively stronger attraction between Sigma nanoparticles and electrons. The depth of electron traps around Sigma nanoparticles are therefore deeper than the traps generated by EFH1 nanoparticles
- **Number of traps per nanoparticle:** As mentioned above, traps that capture electric charges can be generated around the nanoparticles in the liquid. According to [**95**], the total charge of a perfectly conducting nanoparticles in insulating liquid under a d.c. electric field is proportional to the surface area of the nanoparticles. This means that the total number of traps of each

nanoparticle should also be proportional to the surface area of each nanoparticle. As the surface area of EFH1 nanoparticles is expected to be about 4 times larger than that of Sigma nanoparticles, more traps are likely be generated around each EFH1 nanoparticle compared with that around each Sigma nanoparticle.

- **Different Surfactant**: Both of these types of nanoparticle were modified by surfactants in order to prevent aggregation. Previous studies suggest that electron trapping occurs not only at the surface of the nanoparticles but also in the surrounding region which can be affected by the properties of surfactant molecules [**146**]. Therefore differences in the surfactant used might lead to differences in the trapping behaviour and therefore to differences in conduction.
- **Liquid carriers**: As mentioned previously, the liquid carrier used in the EFH1 ferrofluid was paraffin rather than heptane used in Sigma ferrofluid. Although the chemical structure of a paraffin and heptane are similar, the number of carbon atoms per molecule of paraffin is not precisely defined (6-12). This may affect the behaviour of the system. Also the possible presence of impurities in the EFH1 ferrofluid as a result of manufacture cannot be eliminated and could be another cause of the difference in behaviours between these two types of nanofluid

9.7. SIGMA NANOPARTICLES ADDED POST AGEING

In the earlier sections, clear difference in conductivity and mobility of charge carriers can be observed between the pure aged oil samples and samples aged with Sigma nanoparticles present. It was not clear from the data whether the changes were due to the nanoparticles affecting the ageing mechanism or due to the interactions between the nanoparticles and the products of the ageing process. In an attempt to address this question a sample of the Shell Diala insulating oil was aged for 2 days at 120 ℃. After the ageing process, the conductivity and the mobility of charge carriers were measured in one part of the sample. Then, Sigma nanoparticles was added to the remainder of the sample with a concentration of 0.00175 g/L to 0.00245 g/L, which

is the same as that for the samples used in sections 9.3~9.5. To allow a comparison to be made within a reasonable time period only a single set of measurements were made in each case rather than repeating the measurements over 5 successive days. Measurements were however performed over the same voltage range of 30~70V.

Figure 9-28 shows data on the behaviour of the d.c. current obtained at 50 V. The lines show the fits obtained in sections 7.3 and 9.3 for a 2 day aged sample and a sample aged for 2 days in the presence of Sigma nanoparticles giving the expected behaviour of the d.c. current over 5 successive days of measurement. The points represent the measured values of d.c. current obtained from the new aged sample and the current when this sample had sigma nanoparticles added.

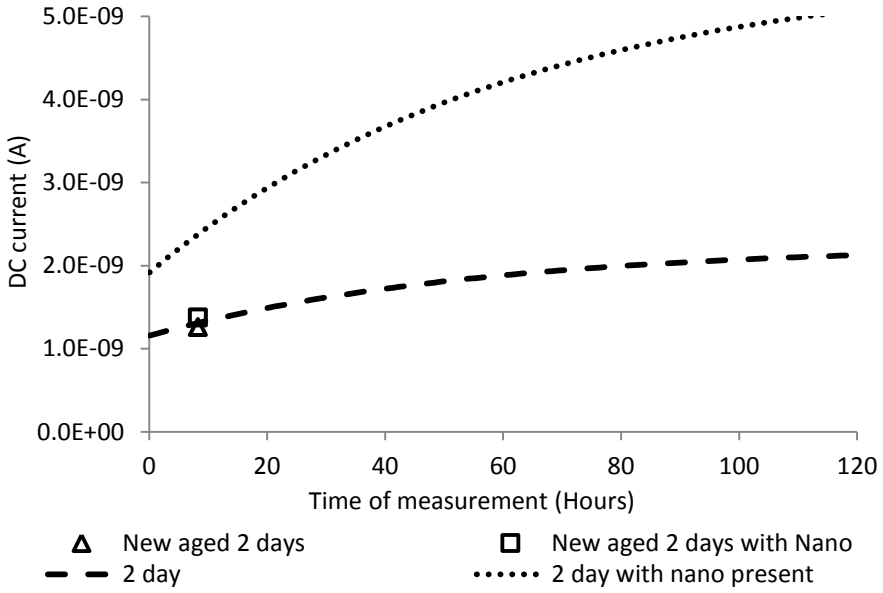

Figure 9-28 D.c. current for samples with Sigma nanoparticles added post ageing at 50V: New aged 2 day for pure oil aged for 2 days; New aged 2 day with Nano for 2 day aged samples with Sigma nanoparticles added post ageing.

It can be seen that there is little difference between the measured current for the newly aged sample and the earlier work with oil aged under similar conditions. There is also little difference for the sample with nanoparticles added post ageing. The points fall considerably below the fit line obtained for the samples aged with Sigma nanoparticles present. Similar behaviour as observed in the measurements performed at other voltages. This is different from the measured data for aged samples with EFH1 nanoparticles added post ageing (sections 8.3~8.5) where a significant

increase of the d.c. current can be observed as a results of adding nanoparticles. This data supports the idea that the presence of the Sigma nanoparticles has a direct effect on the ageing of the liquid.

The influence of the presence of Sigma nanoparticles added post ageing on the mobility value for a 2 Day aged samples at 50V is shown in Figure 9-29.

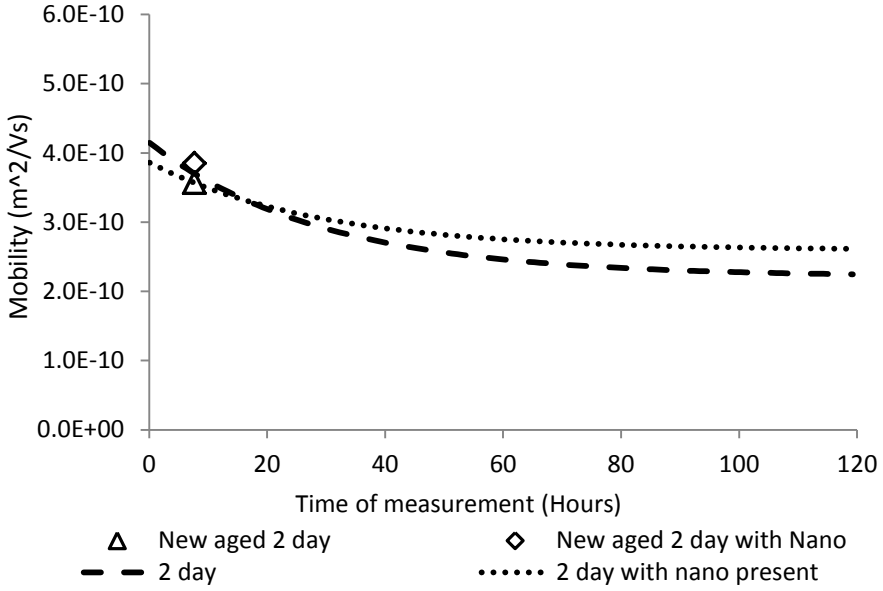

Figure 9-29 Mobility for samples with Sigma nanoparticles added post ageing at 50V

Figure 9-29 shows that there is little change in the measured mobility as a result of adding the Sigma nanoparticles post ageing. The derived mobility values are similar to those obtained from the original sample of aged oil and from the sample aged with nanoparticles present. Again, measurements at other applied voltages exhibit similar results as shown in Figure 9-29.

The analysis above provides evidence that adding Sigma nanoparticles at a relatively low concentration does not change the behaviour of aged oil samples' conductivity and mobility of charge carriers significantly. Therefore, the different behaviours between pure aged samples and samples aged with Sigma nanoparticles present is expected to be more likely due to the difference of thermal ageing mechanism rather than simply due to the interaction between nanoparticles and the molecules of the aged oil samples. More measurements are required to confirm that similar behaviours

would be observed after longer times in the measurement cell. It was not possible to perform such measurements within this project due to time constraints.

9.8. ANALYSIS AND DISCUSSION

In previous sections (9.2 - 9.5), experiment results of unaged and aged oil samples with Sigma nanoparticles presence were presented. Variations of the values of I_{peak}, I_{dc} and TOF with the measurement time over 5 successive measurements were observed. The expected values of I_{peak}, I_{dc} and TOF were then obtained from either the exponential fits or the calculated average values.

Comparison between samples aged without adding nanoparticles and samples aged with Sigma nanoparticles present will be given in this section based on these fits. It is interesting to note that, under each ageing condition, the fitting methods used for samples with Sigma nanoparticles are same as these for samples without nanoparticles added, which implies that the behaviours of I_{peak}, I_{dc} and TOF with time in these two types of samples follow a similar function. This is different from the situation in EFH1 based samples.

For unaged oil samples and unaged sample with Sigma nanoparticles:

- Peak currents over 5 successive measurements appear to be constant and are represented by the calculated average value.
- DC currents show a downward trend and are represented by the exponential fit results based on equation 7-1.
- Calculated mobility values appear to be constant over 5 successive measurements and are represented by the calculated average value.

For 2 day, 4 day, 8 day aged oil samples and the samples with Sigma nanoparticles presence that was ageing for 2 days, 4 days, 8 days:

- Peak current and d.c. current over 5 successive measurements increase with the time of measurement and are represented by the exponential fit when $t = \infty$.

- Calculated mobility values also appear to have an upward trend over 5 successive measurements and are represented by the exponential fit when $t = \infty$.

9.8.1. PEAK CURRENT AND DC CURRENT

Expected peak currents of oil samples without nanoparticles (sections 7.2-7.5) and samples with Sigma nanoparticles present (sections 9.2-9.5) are plotted in Figure 9-30.

The thermal ageing process leads to an increase of the magnitude of the peak currents for both types of sample. Addition of a relatively low concentration of Sigma nanoparticles to the unaged Shell Diala insulating oil does not change the behaviour of the peak current significantly. However, after thermal ageing for periods longer than 48 hours, samples with Sigma nanoparticles present show consistently larger peak current values compared with samples without nanoparticles added. For the unaged samples with and without Sigma nanoparticles, the relationship between the applied voltage and the peak current is nonlinear. This is different from the results measured from unaged samples with EFH1 nanoparticles (section 8.2). For aged samples without nanoparticles and with Sigma nanoparticles, a good linear fit line passing through the origin can be obtained which is similar to the behaviours observed in aged samples with EFH1 nanoparticles.

The experimental data and analysis in Chapter 8 shows that adding the EFH1 nanoparticles to unaged Shell Diala insulating oil and to aged oil samples led to a significant increase in peak current in every case. With Sigma particles added to unaged oil little difference was observed in the behaviour of the peak current.

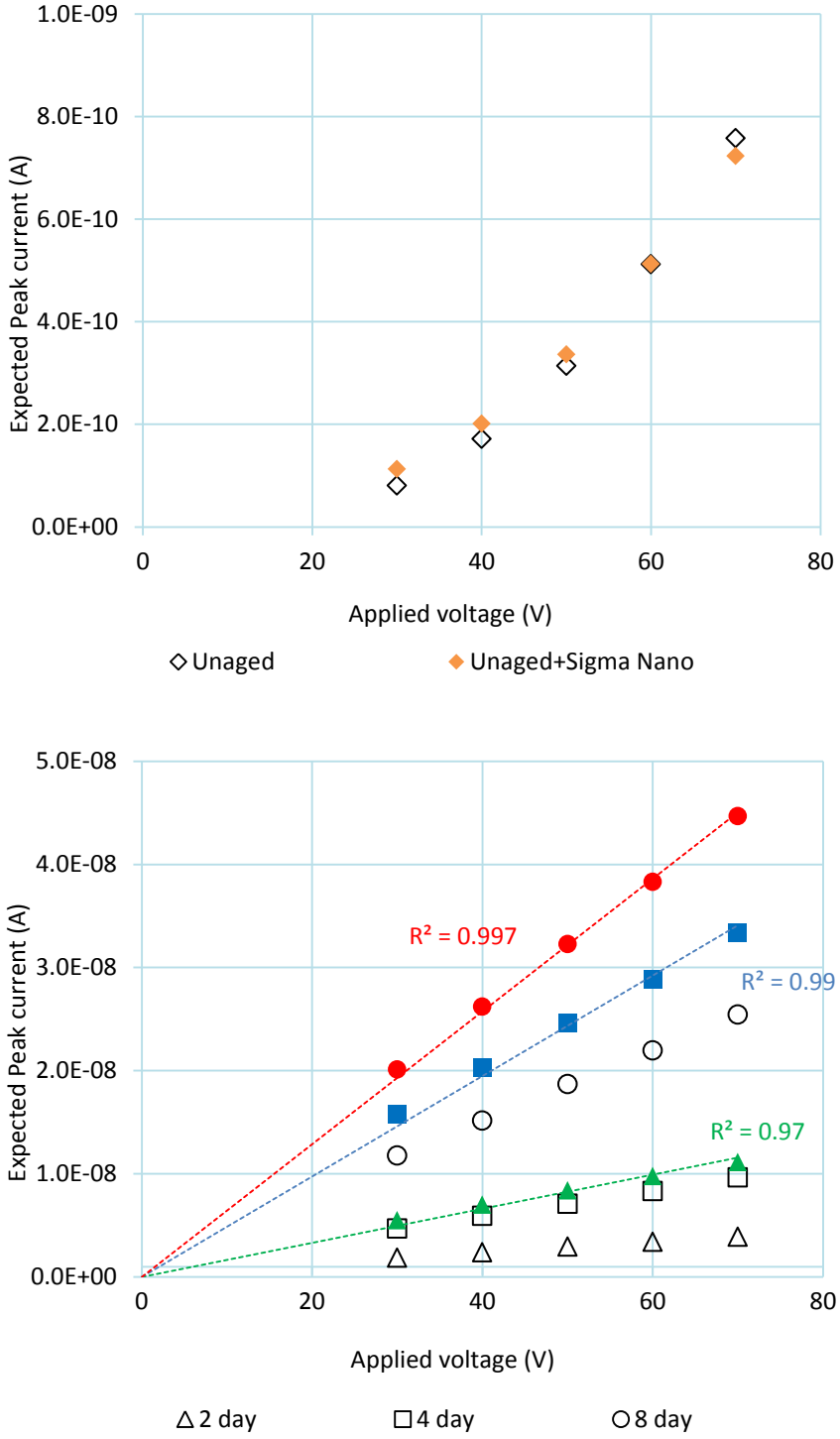

Figure 9-30 Expected peak currents for samples without nanoparticles and samples with Sigma nanoparticles: Upper graph for unaged samples (a) and lower graph for aged samples (b)

However samples aged with Sigma nanoparticles present showed a significant increase in peak current compared to samples aged without nanoparticles. Therefore, the considerable increase of peak current observed due to the ageing in the presence

of nanoparticles is likely to be related to some enhancement of degradation caused by the presence of the Sigma nanoparticles. It was not possible to determine whether the presence of EFH1 nanoparticles would enhance ageing due to their thermal instability (section 9.1.1). The EFH1 nanoparticles were not suggested to be used at high temperature due to their relatively low thermal stability.

A linear increase of the expected peak current can be observed as a result of the increase of applied field in samples aged with and without nanoparticles. As can be seen from Figure 9-30 (a) and Figure 9-30 (b), in every case of ageing, the gradients of the V-I relationship in samples without nanoparticles are smaller than that in samples with Sigma nanoparticles presence. The values of "peak conductance" which have been defined in section 7.8 were calculated and plotted in Figure 9-31 as a function of ageing time.

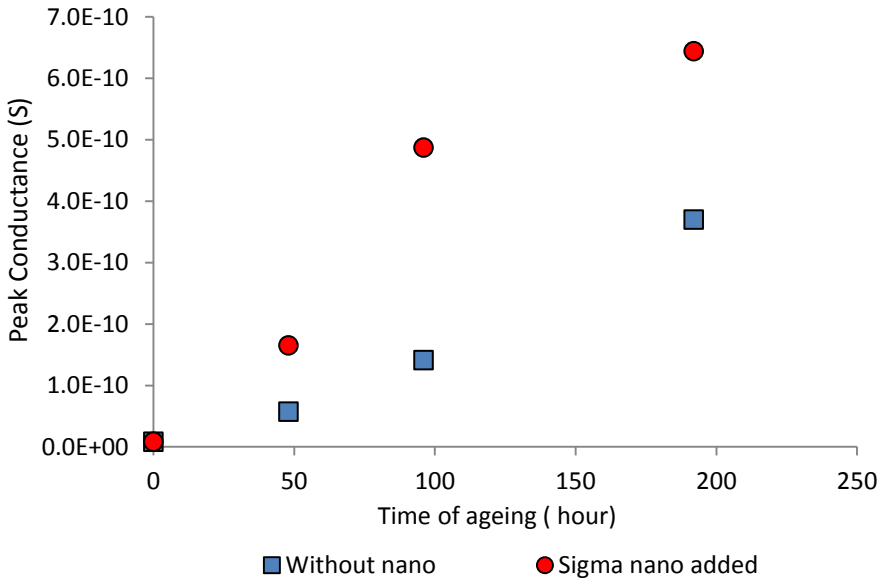

Figure 9-31 Derived peak conductance (pure oil and Sigma nanofluid)

For samples with Sigma nanoparticles added, the derived peak conductance value increases with the ageing time which corresponds to the behaviours of samples without nanoparticles added. For thermal ageing time up to 192h, samples with Sigma nanoparticles added always shown a larger peak conductance in any case of ageing.

The expected d.c. currents of samples without nanoparticles and samples with Sigma nanoparticles are shown in Figure 9-32.

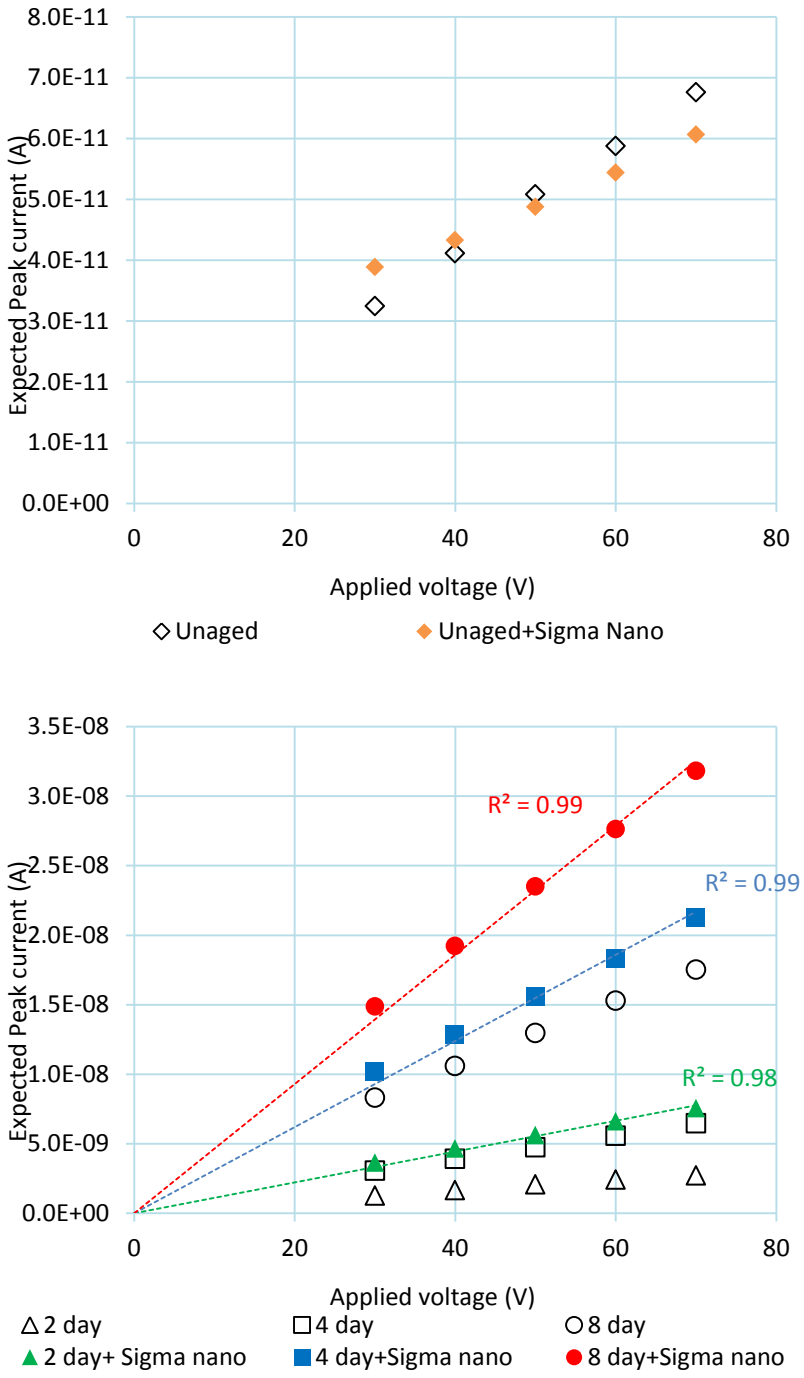

Figure 9-32 Expected d.c. currents for samples without nanoparticles and samples with Sigma nanoparticles

The thermal ageing process also leads to an increase of the magnitude of the d.c. currents for both samples without nanoparticles and samples with Sigma

nanoparticles added. For unaged samples, no significant change can be observed as a result of adding a relatively low concentration of Sigma nanoparticles. For an unaged sample without nanoparticles the V-I characteristic appears to be Ohmic. This is not the case when the Sigma nanoparticles are added where a linear relationship is seen but this does not pass through the origin. This is similar to the behaviour of unaged sample with EFH1 nanoparticles. For aged samples with Sigma nanoparticles, the measured current magnitude at each specific ageing condition is larger than that for samples aged without nanoparticles present. An Ohmic type linear fit line passing through the origin can be obtained, however the experimental data suggests that better fits could be obtained if the constraint of passing through the origin was removed This is similar to the behaviours observed in aged samples without nanoparticles (section 7.3~7.5) and aged samples with EFH1 nanoparticles (sections 8.3~8.5).

For d.c. conductance, R^2 values of fits from samples with Sigma nanoparticles are shown in Table 9-12 below with the constraint that the linear fit line must pass the origin.

	R^2 of Unaged	R^2 of 2 day aged	R^2 of 4 day aged	R^2 of 8 day aged
Sigma Nanofluid	0.41	0.98	0.99	0.99

Table 9-12 R^2 values for d.c current Ohmic fits (Samples with Sigma nanoparticles)

With the physical limitation that the V-I linear regression line passed through the origin, quality of fits for aged samples are good with R^2 values closed to 0.99. However, for unaged sample with Sigma nanoparticles, quality of fit is poor with the constraint of passing through the origin. Therefore, for samples with Sigma nanoparticles, both the "d.c. conductance" and the "dynamic conductance" mentioned in section 7.8 were calculated and plotted in Figure 9-33.

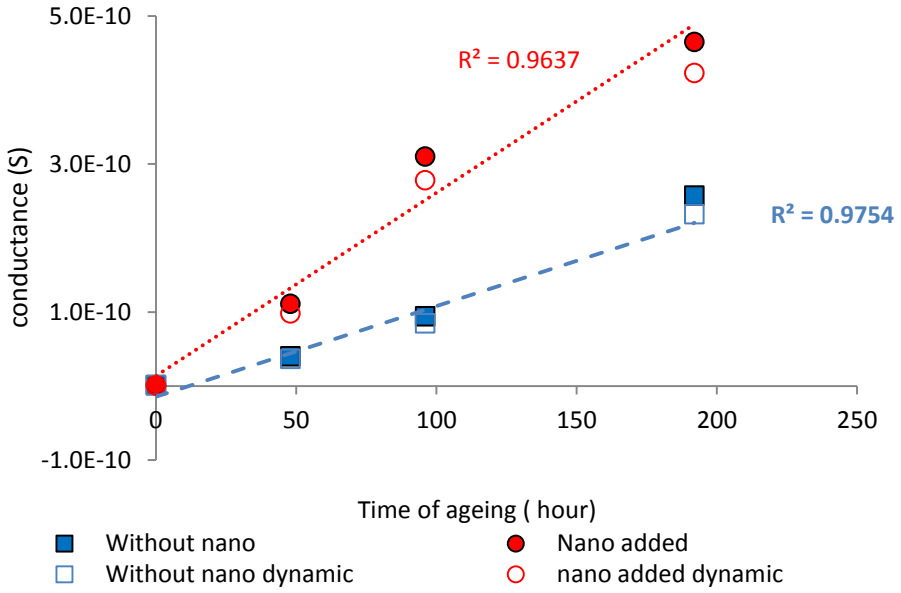

Figure 9-33 Derived d.c conductance: pure oil and Sigma nanofluid

It can be seen from Figure 9-33 that the derived d.c. conductance and the dynamic conductance both increase with increasing time of ageing treatment. Like the peak conductance, the values of d.c. conductance and dynamic conductance are higher for the samples with nanoparticles added and increase more rapidly with increased ageing time. The differences between the values of the dynamic and d.c. conductance are small, but may be more significant for longer ageing times.

The experimental results presented in chapter 8 indicate that addition of nanoparticles into oil samples after ageing where the ageing mechanism could not be influenced by the presence of nanoparticles can lead to an increase of d.c. conductivity. However a significant change in conductivity was also observed when EFH1 nanoparticles were added to unaged oil. For the samples aged with the Sigma nanoparticles present the Author believes that the changes in conductance are coming from a change in ageing mechanism as a result of the nanoparticles being present. The reasons for this belief are as follows: The oil aged with nanoparticles present was significantly darker than the corresponding samples of oil aged without nanoparticles (section 9.1.1); Adding Sigma nanoparticles had little effect on the conduction properties of unaged oil (section 9.2.1) and finally no significant effect was observed when Sigma nanoparticles were added to a sample of oil after it was

aged (section 9.7). Therefore, the increase of d.c. conductance observed in the samples aged with nanoparticles should be a result of an change in the ageing mechanism.

Schottky analysis was also performed with the same fitting methods as used in section 7.7.1. The $\ln I - \sqrt{V}$ plot based on the fitted d.c. current values and the applied voltages are shown in Figure 9-34.

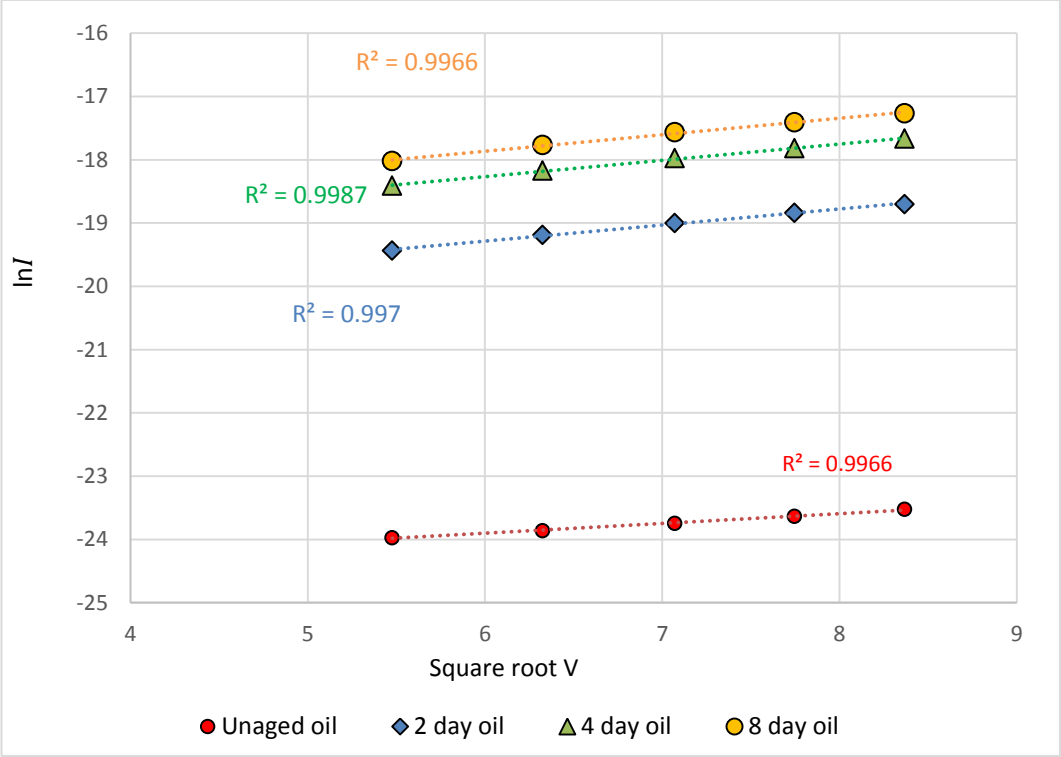

Figure 9-34 Schottky analysis for samples with Sigma nanoparticles

For both unaged and aged sample with Sigma nanoparticles, the $\ln I - \sqrt{V}$ relationship also appears to be linear. Again, this implies a possible Schottky emission relation between the d.c. current and the applied voltage. Note that the Schottky analysis on samples with high-concentration Sigma nanoparticles also shows a good linear $\ln I - \sqrt{V}$ relationship. The derived values of $\ln \alpha + \beta$ term and γ are shown in Table 9-13.

	Unaged		2 day aged		4 day aged		8 day aged	
Sigma Nanofluid	$\ln\alpha + \beta$	γ	$\ln\alpha + \beta$	γ	$\ln\alpha + \beta$	γ	$\ln\alpha + \beta$	γ
	-25.8	0.16	-20.8	0.25	-19.8	0.26	-19.4	0.26

Table 9-13 Linear fits results for Schottky analysis (Samples with Sigma nanoparticles)

Similar to the oil samples without nanoparticles and samples with EFH1 nanoparticles, an increase of the values of the $\ln\alpha + \beta$ term was observed with the increase of ageing degree, which again, implies a possible decrease in the work function due to an increase of the permittivity of the oil samples due to the thermal ageing process. The change in the value of $\ln\alpha + \beta$ after 8 days of ageing is slightly larger in the presence of Sigma nanoparticles than in the pure oil. The change of the value of this $\ln\alpha + \beta$ term in samples without nanoparticles is about 5.5 which are smaller than that in samples with Sigma nanoparticles (change of value of $\ln\alpha + \beta$ term is 6.4). If the Schottky emission related hypothesis is true in this project, the change of the values of $\ln\alpha + \beta$ term would be able to reasonably represent the change of the work function. Therefore, this relatively larger value of $\ln\alpha + \beta$ term implies that the change of permittivity in oil samples with Sigma nanoparticles is more significant than that in pure oil samples without nanoparticles.

However, the trend and reason of the variation of γ values associated with ageing time is not clear. The γ values for aged samples are close to each other, larger than that for unaged samples. In the Schottky equation this term reflects the change in potential of a unit electronic charge as it moves caused by the external applied field. This change in potential should not be affected by changes in the bulk permittivity of the liquid as the change in potential across the electrodes is fixed. One possible explanation is that rather than dealing with singly ionized ions we are dealing with a distribution of singly and multiple charged ions. Differences in the relative concentrations of these species may lead to changes in the derived value of the parameter γ. A second reason for changes in γ is that the Schottky emission process

ignores the presence of space charge in the dielectric liquid. This was suggested as a reason for the deviation from the Schottky behaviour observed at very low voltages in section 8.6. The presence of the nanoparticles and their influence on ageing may result in changes in the space charge distribution.

The accurate expression of the relation between the ageing time and the increase of the d.c. conductivity is difficult to estimate based on the limited data. More samples with different ageing time would be needed in order to provide further understanding about the effects of ageing on the conductivity of insulating oil (for example to see if a maximum conductance can be achieved after a longer period time of ageing)

9.8.2. TOF AND MOBILITY

For 2, 4 and 8 day aged sample with Sigma nanoparticles, the changes of expected mobility with time are significant. The measured values of TOF for each sample increased over the 5 successive measurements. Therefore, the derived values of mobility decreased over the 5 measurements. Again, the behaviour of expected mobility with time were fitted to an exponential function using a common time constant, with the assumption that this change follows a first order kinetic. For aged sample with Sigma nanoparticles, the mobility behaviours is presented based on the results from these fits. For the unaged sample with nanoparticles, the magnitudes of the derived mobility are small, and the percentage variations of mobility over 5 successive measurements were also relatively small. Fitting with an exponential function is difficult and the quality of fits was low. Therefore, the mobility behaviours for the unaged sample with nanoparticles at different applied voltage were presented by the average value calculated from the 5 measurements.

Comparison between the expected mobility of samples with Sigma nanoparticles and that of samples without nanoparticles are shown in Figure 9-35. Again the current values plotted are those for $t = \infty$ as they represent a steady state behaviour in the system. These values at $t = \infty$ come from the exponential fits when these were appropriate and from the average value when such fits could not be performed.

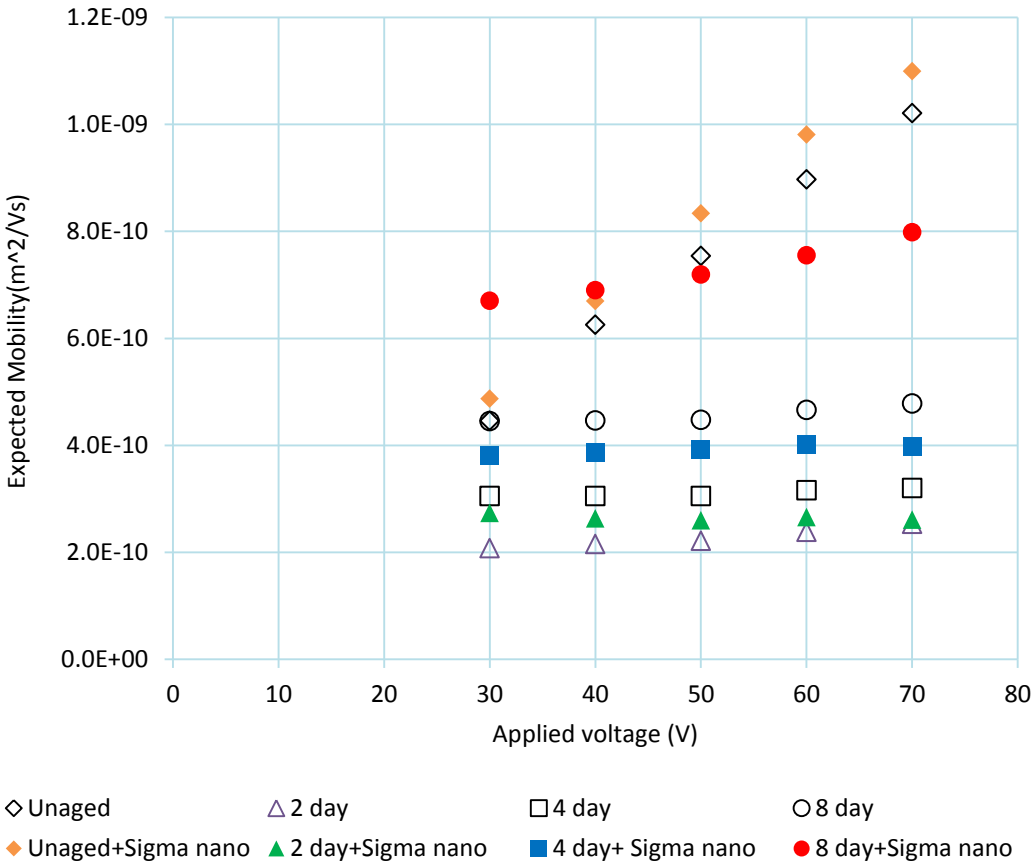

Figure 9-35 Expected mobilities for samples without nanoparticles and samples with Sigma nanoparticles (Unaged, 2 day, 4 day and 8 day represent the samples aged 0h, 48h, 96h and 192h without nanoparticles; Unaged + Sigma nano, 2 day + Sigma nano, 4 day + Sigma nano and 8 day + Sigma nano represent the samples with Sigma nanoparticles added after ageing 0h, 48h, 96h and 192h, respectively.)

In general, the mobility for aged samples appears to vary slightly with the applied field. For the unaged sample with and without the sigma nanoparticles the field dependence of mobility seems to be much stronger. This implies that for samples with and without Sigma nanoparticles added, the thermal ageing process reduces the voltage dependence of the mobility. For all the aged samples, those with Sigma nanoparticles always exhibit a higher mobility value compared to the samples without nanoparticles present.

For both the pure oil sample and the oil sample with Sigma nanoparticles, a clear decrease in the mobility of charge carriers can be seen between unaged and aged for 48 hours. The difference in mobility between the pure aged sample and the sample aged with Sigma nanoparticles is relatively small. For longer ageing times the

mobility for both types of sample increase and the difference in the mobility between pure and samples aged with nanoparticles becomes more significant. The presence of Sigma nanoparticles has an influence on the variation in the mobility due to the thermal ageing process. In the samples aged without nanoparticles present there is an increase in the mobility with ageing time for times greater than 48 hours. This behaviour is also observed in the samples aged with Sigma nanoparticles but the changes in mobility at longer ageing times are larger than in the pure samples.

As with the peak and d.c. conductivity results this suggests an increase in the ageing rate of the samples due to the presence of nanoparticles. The nanoparticles may be acting as a catalyst for an existing ageing reaction or they may introduce a new reaction pathway in the system. An alternative process is that additional traps are introduced into the system due to bonding between the nanoparticles and the ageing by-product molecules as previously mentioned in section 8.6.2. Unlike the current measurements, where significant differences in the behaviours of current were observed between samples aged with Sigma nanoparticles present and samples with these nanoparticles added post ageing, there is little difference in the measured mobility behaviours so the mobility measurements cannot be used to determine which of these two processes may be occurring.

From the previous analysis of current behaviours, it is certain that for samples without nanoparticles and samples with Sigma nanoparticles that adding Sigma nanoparticles lead to significant changes in the current behaviour which has been attributed to a change of the ageing mechanism. However, the changes of the mobility of charge carriers caused by the thermal ageing process are complex. Therefore, in order to have a better understanding of the differences in the behaviour of the d.c. conductivity and mobility as a result of having nanoparticles present during ageing, the difference of mobility values μ and d.c. current I_{dc} between samples aged with Sigma nanoparticles and samples without nanoparticles were calculated. This value was then normalized to the values observed for the data of the sample aged without nanoparticles. This allows the relative effect of the presence of nano particles during ageing to be assessed. Note that, data shown in Table 9-14 was calculated based on the average value of the normalized differences calculated at the different applied voltages used in the measurements.

Aging time (Hours)	Increase in Mobility	Increase in Current
0	9.5%	1.1%
48	16.7%	179.2%
96	26.6%	231.5%
192	57.2%	81.4%

Table 9-14 Changes due to the presence of Sigma nanoparticles during ageing process

As previously discussed, and can be seen in Table 9-14, the presence of Sigma nanoparticles did not change the behaviours of unaged insulating oil significantly. There appears to be an increase in mobility but the average d.c. currents are not affected.

For samples aged less than 96 hours, the samples aged with Sigma nanoparticles show a significantly larger mobility of charges carriers than those for the corresponding samples aged without nanoparticles. The trend in both mobility and current is increasing with ageing time. However, the normalized increase in d.c. current is much more significant than the increase in mobility. (The d.c. current was approximately two times larger when Sigma nanoparticles were present during ageing compared with samples without nanoparticles added). This indicates that the different current behaviours between samples aged without nanoparticles and samples aged with nanoparticles present are mainly due to changes in the total number of charge carriers rather than due to the change of velocity of the charge carriers' motion in the liquid. The number of charge carriers is likely to be controlled by injection mechanisms or dissociation mechanisms. For samples aged for 192 hours the differences in mobility is larger than observed in the samples aged for shorter times. The d.c. current under these conditions is still larger than the d.c. current observed in the sample aged without nanoparticles. But the relative difference between the two samples is much smaller than that observed at shorter ageing times. This behaviour could occur if there is a limit in the change of current as a result of the effects of the ageing mechanism. The acceleration of the ageing due to

the presence of nanoparticles would cause this limit to be reached more quickly leading to a decrease in the difference of the currents at longer ageing times.

Again, with the data on the d.c. conductivity and the mobility it is possible to derive an estimate of the number of charge carriers present in the system, assuming that the apparent mobility measured through TOF measurements does describe the mobility under d.c. conditions using. Equation 4-2 results for estimates on the number of charge carriers present for the oil aged with Sigma nanoparticles and the oil aged in their absence are shown in Figure 9-36.

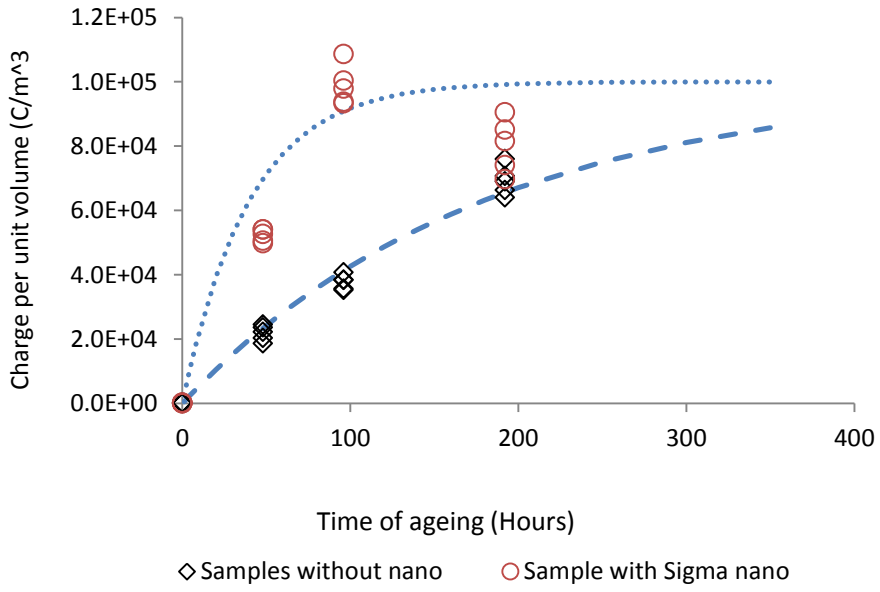

Figure 9-36 Charge density in the Sigma nanoparticles modified samples

It can be seen that the number of charge carriers present in the system appears to saturate with ageing time for the samples aged with sigma nanoparticles present. A similar saturation seems to be occurring for the samples aged without nanoparticles. These behaviours are illustrated in the figure through the dotted lines assuming a simple exponential saturation. This supports the suggestion that the change in observed currents is chiefly due to a change in the number of charge carriers present and that the presence of the Sigma nanoparticles increases the rate of ageing and the behaviour related to charge injection at the electrodes or dissociation in the bulk of the liquid.

9.9. SUMMARY

The ageing behaviour of a nanofluid has been reported in this chapter. A magnetite nanoparticles suspension in heptane (Sigma-Aldrich 07318) was added into Shell Diala insulating oil samples using the same mixing method in Chapter 8. Four 200ml samples were then thermally aged for 2 day, 4 day and 8 day at 120°C, respectively. Time of flight measurements were performed on unaged and aged sample containing the Sigma nanoparticles following the standard experimental approach used in this project. For both unaged and aged Sigma nanofluid sample, similar time dependent variations as were observed in pure Shell Diala oil samples occurred. The average or exponential fitting methods used in Chapters 7 and 8 were applied in order to derive the behaviours of I_{peak}, I_{dc} and mobility of charge carriers. The fitting approaches for each sample have been described in this chapter.

For unaged samples, the addition of the Sigma nanoparticles had little effect on I_{peak} , I_{dc} and mobility of charge carriers unlike the measured results in EFH1 based nanofluid sample, where significant increases I_{peak} and I_{dc} and a decrease in mobility was observed. Additional tests were performed on samples with a higher concentration of Sigma nanoparticles which should have been similar to the concentration in the EFH1 samples to allow a more direct comparison to be made. This showed that increasing the concentration of Sigma nanoparticles in unaged oil had no effect on the apparent mobility. The measured values of I_{peak} and I_{dc} did increase but cannot be explained simply in terms of the concentration of nanoparticles or the expected increase in the number of traps. The reasons for the differences between the two unaged nanofluids are not clear at this point but possible explanations have been discussed.

For Sigma based nanofluid samples aged for periods greater than 48 hours, there is always a clear difference in the I_{peak} and I_{dc} values compared with insulating oil samples without nanoparticles that have been aged for the same time. Sample aged with Sigma nanoparticles always exhibit a higher conductivity than that in samples aged without nanoparticles added. Differences were also observed in the measure

mobility for oil aged with Sigma nanoparticles present compared to the oil samples without nanoparticles where the measured mobility was consistently higher. However the changes in the mobility as a result of the thermal ageing process is complex with an initial decrease in both types of sample occurring in the first 48 hours of ageing followed by an increase with further ageing.

To test whether the changes observed in the behaviour of the aged samples were due to the presence of the nanoparticles during the thermal ageing process, tests were performed with an identical concentration of nanoparticles being added to oil that had been aged without nanoparticles after ageing had been completed. No significant change of the conductivity and the mobility of charge carriers were observed due to the presence of Sigma nanoparticles added to the oil post ageing.

Experimental data presented in this section therefore suggests that the presence of nanoparticles at a relatively low concentration in an insulating liquid could result an enhancement of the thermal ageing mechanism which consequently leads to an increase in the conductivity of the oil and enhances the mobility of charge carriers.

10.CONCLUSIONS AND FUTURE WORK

10.1. GENERAL CONCLUSIONS

The primary objective of this work is to investigate the influence of nanoparticles on the characteristics of insulating oil that has been thermally aged. It had previously been shown that adding nanoparticles to insulating liquids can improve the breakdown strength of oils [**29**] [**6**] [**86**] and [**144**]. Emphases were placed upon the change of the conductivity of the insulating oil and the mobility of charge carriers in the liquid due to the ageing process. The conductivity of insulating oil and the mobility of charge carriers was studied using time-of-flight measurements based on bipolar d.c. electric field activation which has been suggested in earlier studies to be an effective approach of the mobility investigation [**4**]. A temperature controlled bipolar polarization measurement system was developed and it was demonstrated that repeatable measurements can be performed on different types of insulating oil samples. Values of the peak current and the d.c. current can be measured from the recorded current values at particular applied electric field to allow the conductivity of the insulating liquid to be calculated.

A simple model for the behaviour of charge carrier motion during the time-of-flight measurement process, based on Fick's Laws was developed. The modeling results raise concerns as to the relationship between the apparent mobility measured from the time of flight and the actual mobility of the charge carriers in the insulating liquid. This problem relates to the influence of diffusion during the motion of charge carriers across the system under the influence of the relatively low electric fields used in the experimental work. A criterion has been suggested that allows an estimate of acceptable voltage levels which can be used in such measurements to be assessed.

A set of experiments were carried out to study the combined effects on Shell Diala S3 ZX-I insulating oil caused by thermal ageing performed at 120 ℃ and magnetite nanoparticles. Three sets of liquid insulating samples were investigated: samples that were thermally aged as received; samples that were thermally aged as received with the post-ageing addition of a magnetite nanoparticle (EFH1 ferrofluid); and samples that were thermally aged with magnetite nanoparticles added prior to ageing (Sigma-Aldrich 07318). For each set of samples, four period of ageing was selected: unaged, 2 day aged, 4 day aged and 8 day aged. Estimates were made on the degree of acceleration of the ageing process as compared to service conditions but these have a large range of possible values (acceleration of between 13 to 100 times the ageing expected at a temperature of 80°C. Conclusions drawn from the current analysis, the mobility analysis and the estimations of charge carrier number are presented below.

10.1.1. CONDUCTIVITY

Based on the data for the peak current and d.c. current, the following conclusions can be made:

- The addition of the EFH1 nanofluid to the insulating oil (both unaged and aged) leads to a significant increase in both the d.c. and peak conductivities. This was not observed when the Sigma nanofluid was added to samples. The difference in the behaviour of the EFH1 and Sigma samples does not come from the difference in nanoparticle concentration and it is believed that the differences cannot be explained by the difference in nanoparticle dimension. This leaves the differences in surfactant or the carrier liquid as possible explanations of the observed changes.
- Thermal ageing leads to an increase of the d.c. conductivity of the insulating oil without nanoparticles, which is consistent with results reported in the literature [**52**]. The addition of the EFH1 nanofluid post ageing leads to a further increase in the current. For an unaged sample the d.c. current at 50 V was 50pA, after ageing for 8 days the current increased to 12 nA, when the

EFH1 nanofluid was added to the 8 day aged sample the current increased to 34 nA

- The changes of conductivity in samples aged with nanoparticle present were more significant than that in samples aged without nanoparticles. For an unaged sample with Sigma nanoparticles added, the d.c. current measured at 50V was 49pA. After ageing for 8 days, the current was increased to 24nA. This coupled with the relatively small influence on the conductivity of adding the Sigma nanoparticles post ageing, indicates that the presence of these nanoparticles in the insulating liquid have an influence on the thermal ageing mechanism. The insulating oil with Sigma nanoparticles present appears to degrade more rapidly than that without any nanoparticles added.
- From the analysis of the relationship between the measured d.c. current and the applied voltage a linear relationship is observed over the voltage range considered. This relationship is frequently not Ohmic but can be fitted to a Schottky emission process. These fits suggest that the work function for the injection of charge carriers is reduced by the thermal ageing process. This could be due to an increase of the permittivity of the insulating oil as a result of ageing.
- The significant increase in conductivity caused by the addition of the EFH1 nanofluid allowed measurements of the current transients to be performed at extremely low fields (140 pA measured with an applied voltage of 1V corresponding to a field of 0.01kV/cm). The d.c. current behaviour was observed to deviate from the Schottky emission process at fields below 0.1kV/cm.

10.1.2. MOBILITY

From the measured values of TOF, which is related to the apparent mobility of the charge carriers, the following conclusions can be made:

- For the pure insulating oil the behaviour of mobility with ageing time is complex. The mobility initially decreases in the first 48 hours of ageing and

then increases with further ageing time. However within the 196 hours of ageing the mobility does not increase above the values measured in the unaged oils.

- For unaged oil the apparent mobility has a strong field dependence, perhaps due to EHD effects. After ageing this field dependence is suppressed.
- The addition of the EFH1 nanofluid to unaged samples leads to a reduction in the apparent mobility and suppression of the field dependence. If the EFH1 nanofluid is added to aged samples the apparent mobility is significantly increased to values above that observed in an unaged sample without nanoparticles. The difference in mobility for samples with EFH1 nanoparticles for different ageing times is small and seems independent of ageing time.
- When samples are aged with Sigma nanoparticles present the mobility behaves in a similar manner to the oil aged without nanoparticles, i.e. decreases in the first 48 hours before increasing at longer ageing times. The field dependence was also suppressed. The mobility values however are larger for the Sigma modified oil for all ageing times. The values of mobility are significantly lower than those observed in the sample with EFH1 nanofluid added post ageing.

10.1.3. NUMBER OF CHARGES

From the apparent mobility and the measured d.c. currents and calculations of assuming that the carriers carry a single charge, the number of charge carriers present in the system have been performed

- In aged samples without nanoparticles the number of charge carriers was observed to increase with ageing time in a broadly linear manner.
- In the samples where EFH1 was added post ageing the calculated number of charges carriers seems to be similar or smaller than the corresponding sample without nanoparticles. This suggests that the considerable increase in current is as a result of the observed change in mobility in the system.

- For the samples aged in the presence of Sigma nanoparticles the behaviour is different, the calculated number of charge carriers increases with ageing time and then appears to saturate. Over the ageing time considered it is not clear if the samples aged without nanoparticles present would also reach saturation with further ageing.

10.1.4. General Observations

Some additional conclusions and comments can be made.

- Measurement of the apparent mobility is challenging and the field dependence and its variation with ageing conditions makes it difficult to perform simple comparisons. Based on data measured at 30V one behaviour may be observed while at 70V a different conclusion may be drawn. For example at 30V there was little difference between the mobility values derived for unaged oil and that for oil that had been aged for 8 days. If the data obtained at 70 V was compared, the mobility in the aged oil was considerably lower. Therefore care is needed when examining published data on the mobility behaviour.
- Despite the efforts made to develop a consistent measurement system the behaviour of the samples was observed to change over the 5 days of repeated measurement. This was addressed by curve fitting to allow initial and steady state values to be calculated. Again it is not clear whether similar effects may have occurred in the reported literature.
- Nanoparticle suspensions, for example EFH1, may not be stable when exposed to higher temperatures.
- Although adding nanoparticles into insulating oil provides a mechanism to alter the dielectric properties of the liquid insulating material there may be draw backs to this approach. From the nanofluids considered in this project, addition of the EFH1 nanoparticles lead to very significant increase in the conductivity and therefore losses within the insulation system. The Sigma nanoparticles were shown to increase the ageing of the oil (as defined by

changes in conductivity). Further investigation of the mechanisms by which nanoparticles improve breakdown strength, contribute to conductivity and effect ageing of insulating liquids is clearly required.

10.2. FUTURE WORK

Based on the work performed to date there are several areas where further investigation would be useful.

- In this project, Shell Diala insulating oil was adopted as the liquid insulating material. Its insulating properties were used as a reference in the analysis of the effects of ageing. Tests using different kinds of liquid insulating material such as vegetable oil would be useful as these could provide evidence to show whether the behaviours found in this project are common to most insulating liquids or relate specifically to the mineral oil.
- For accelerated thermal ageing, the longest ageing time is 192 hours in this project. Further ageing would probably lead to significant precipitate generation in the bulk liquid. However, from the work performed it seems that the precipitate can be removed from the aged samples using a centrifuge without changing the parameters of interest significantly. This suggests that there might be a way to investigate the behaviours of conductivity and mobility in samples that have been aged more heavily. This could be useful to allow confirmation of the possible saturation of charge carrier number in the system as a result of ageing.
- There could also be advantages in ageing the samples for longer times at lower temperature, firstly to establish the Arrhenius relationship for ageing and secondly to allow a more detailed examination of the changes in the system with degree of ageing.
- It has been assumed that the small influence on the system properties of adding Sigma nanoparticles post ageing found in the 2 day aged sample was also valid for other ageing times. This assumption needs to be confirmed or disproved.
- It is clear that the EFH1 nanoparticles were affected by thermal treatment with possible oxidation of the Fe_3O_4 into Fe_2O_3 or FeO. Although the Sigma

material did not come out of suspension it is possible that similar oxidation reactions were occurring. It is therefore important that the long term thermal stability of nanoparticles intended for use in liquid insulation is assessed. This will apply to all types of nanoparticles not just magnetite nanoparticles.

REFERENCES

[1] Masanori Kohtoh, Shuhei Kaneko, and Shigemitsu Okabe, "Ageing Effect on Electrical Characteristics of Insulating Oil in Field Transformer," *IEEE Transactions on Dielectrics and Electrical Insulation*, vol. 16, no. 6, pp. 1698-1705, December 2009.

[2] Mohammad R. Meshkatoddini and Shahid Abbaspour, "Aging Study and Lifetime Estimation of Transformer Mineral Oil," *American J. of Engineering and Applied Sciences*, vol. 4, pp. 384-388, 2008.

[3] Shigemitsu Okabe, Shuhei Kaneko, Masanori Kohtoh, and Tsuyoshi Amimoto, "Analysis results for insulating oil components in field transformers," *IEEE Transactions on Dielectrics and Electrical Insulation*, vol. 17, no. 1, pp. 302-311, February 2010.

[4] Lijun Yang et al., "Measurement of ion mobility in transformer oils for HVDC applications," in *2012 International Conference on High Voltage Engineering and Application*, Shanghai, 2012, pp. 17-20.

[5] Yue-fan Du, Yu-zhen Lv, Jian-Quan Zhou, Xiao-xin Li, and Cheng-rong Li, "Breakdown properties of transformer oil-based TiO2 nanofluid," *Electrical Insulation and Dielectric Phenomena (CEIDP), 2010 Annual Report* , pp. 1-4, Oct. 2010.

[6] Y. Z. Lv et al., "Nanoparticle Effect on Electrical Properties of Aged Mineral Oil Based Nanofluids," in *Cigré Canada Conference on Technology and Innovation* , Montreal, Canada, 2012, pp. 1-6.

[7] Santosh K. Upadhyay, *Chemical Kinetics and Reaction Dynamics*. India: Springer Science & Business Media, 2007.

[8] Richard E. Sonntag, Claus Borgnakke, and Gordon J. Van Wylen, *Fundamentals of Thermodynamics*, sixth edition ed., April 2002.

[9] A. M. Emsley, X. Xiao, R. J. Heywood, and M. Ali, "Degradation of cellulosic insulation in power transformers. Part 2: formation of furan products in insulating oil," *IEE Proceedings - Science, Measurement and Technology*, vol.

147, no. 3, pp. 110-114, May 2000.

[10] H. William and P. E. Bartley, "Analysis of Transformer Failures," in *International Association of Engineering Insurers 36th Annual Conference*, Stockholm, 2003.

[11] K.J. Laidler, *Chemical Kinetics*, Third Edition ed., 1987.

[12] P. Cygan and J. R. Laghari, "Models for insulation aging under electrical and thermal multistress," *IEEE Transactions on Electrical Insulation*, vol. 25, no. 5, pp. 923-934, Oct. 1990.

[13] Thomas W. Dakin, "Electrical Insulation Deterioration Treated as a Chemical Rate Phenomenon," *Transactions of the American Institute of Electrical Engineers*, vol. 67, no. 1, pp. 113-122, Jan. 1948.

[14] A. Ciuriuc, P. V. Notingher, R. Setnescu, L. M. Dumitran, and T. Setnescu, "Lifetime estimation of vegetable oil for transformers," *High Voltage Engineering and Application (ICHVE), 2014 International Conference*, pp. 1-4, 8-11 Sept. 2014.

[15] (2016, December) Partical Discharge Testing: What it is and What it means. [Online]. http://www.ti.com/lit/an/sboa045/sboa045.pdf

[16] Mohammad Saleh Moonesan and Edward Cherney, "Effect of Temperature and Humidity on Surface Discharge Activities under High Voltage Unipolar Pulses," *Proc.ESA Annual Meeting on Electrostatics*, pp. 1-7, 2015.

[17] The API White Oil Workgroup, "API Mineral Oil Review," Health and Environmental Sciences Department, 1992.

[18] "C57.91-2011 - IEEE Guide for Loading Mineral-Oil-Immersed Transformers and Step-Voltage Regulators," pp. 1-123, March 7 2012.

[19] I. L. Hosier, A. S. Vaughan, and S. G. Swingler, "Studies on the ageing behavior of various synthetic and natural insulation oils," *2008 IEEE International Conference on Dielectric Liquids*, pp. 1-4, June 2008.

[20] T. K. Saha, "Review of modern diagnostic techniques for assessing insulation

condition in aged transformers," *IEEE Transactions on Dielectrics and Electrical Insulation* , vol. 10, no. 5, pp. 903-917, Oct. 2003.

[21] M. Wang, A. J. Vandermaar, and K. D. Srivastava, "Review of condition assessment of power transformers in service," *IEEE Electrical Insulation Magazine*, vol. 18, no. 6, pp. 12-25, Nov.-Dec. 2002.

[22] D. H. Shroff and A. W. Stannett, "A review of paper aging in power transformers," *IEE Proceedings C - Generation, Transmission and Distribution*, vol. 132, no. 6, pp. 312-319, November 1985.

[23] I. L. Hosier, A. S. Vanghan, S. J. Sutton, and F. J. Davis, "Chemical, Physical and Electrical Properties of Aged Dodecylbenzene: Thermal Ageing of Mixed Isomers in Air," *IEEE Transactions on Dielectrics and Electrical Insulation*, vol. 14, no. 5, pp. 1113-1124, October 2007.

[24] I. L. Hosier, A. S. Vaughan, S. J. Sutton, and F. J. Davis, "Chemical, Physical and Electrical Properties of Aged Dodecylbenzene 2: Thermal Ageing of Single Isomers in Air," *IEEE Transactions on Dielectrics and Electrical Insulation*, vol. 15, no. 5, pp. 1393-1405, October 2008.

[25] I. L. Hosier, A. S. Vaughan, S. J. Sutton, J. Cooper, and F. J. Davis, "Chemical, physical and electrical properties of aged dodecylbenzene 3: thermal ageing of mixed isomers in nitrogen and under sealed conditions," *IEEE Transactions on Dielectrics and Electrical Insulation*, vol. 15, no. 4, pp. 1056-1064, August 2008.

[26] Alexandra Ciuriuc, Mirela Stefanic Vihacencu, Laurentiu Marius Dumitran, and Petru V. Notingher, "Comparative study on power transformers vegetable and mineral oil ageing," *Applied and Theoretical Electricity (ICATE), 2012 International Conference*, pp. 1-6, Oct. 2012.

[27] Jong-Wook Jung and Jin-soo Jung, "The effect of thermal ageing on the electrical characteristics of insulating oil for pole transformers," *Condition Monitoring and Diagnosis, 2008. CMD 2008. International Conference* , pp. 303-306, 21-24 April 2008.

[28] Martin Marci and Iraida Kolcunová, "Electric breakdown strength measurement in liquid dielectrics," *Environment and Electrical Engineering (EEEIC), 2010 9th International Conference*, pp. 427 - 430, May 2010.

[29] Mu-tian Chen et al., "Effect of nanoparticles on the dielectric strength of aged transformer oil," *Electrical Insulation and Dielectric Phenomena (CEIDP), 2011 Annual Report*, pp. 664-667, 16-19 Oct. 2011.

[30] R. T. Arun Ram Prasath, P. Thomas, Ann Pamla Cruze, S. N. Mahato, and N. K. Roy, "Ageing analysis of mineral insulating oils using CCTO Nanofluids," *2015 International Conference on Energy, Power and Environment: Towards Sustainable Growth (ICEPE)*, pp. 1-7, 12-13 June 2015.

[31] P. Pahlavanpour, Eklund, and M. A. Martins, "Insulating paper ageing and furfural formation," pp. 283-288, 23-25 Sept. 2003.

[32] B. Pahlavanpour, M. A. Martins, and A. De Pablo, "Experimental investigation into the thermal-ageing of Kraft paper and mineral insulating oil," *Electrical Insulation, 2002. Conference Record of the 2002 IEEE International Symposium*, pp. 341-345, Apr. 2002.

[33] A. de Pablo, "Furfural and ageing: how are they related," *Insulating Liquids*, pp. 5/1-5/4, 1999.

[34] A. M. Emsley, X. Xiao, R. J. Heywood, and M. Ali, "Degradation of cellulosic insulation in power transformers. Part 2: formation of furan products in insulating oil," *IEE Proceedings - Science, Measurement and Technology* , vol. 147, no. 3, pp. 110-114, May 2000.

[35] R. Blue, D. Uttamchandani, and O. Farish, "Infrared detection of transformer insulation degradation due to accelerated thermal aging," *IEEE Transactions on Dielectrics and Electrical Insulation*, vol. 5, no. 2, pp. 165-168, Apr. 1998.

[36] Joseph J. Kelly, "Transformer Fault Diagnosis by Dissolved-Gas Analysis," *IEEE Transactions on Industry Applications* , vol. IA-16, no. 6, pp. 777-782, Nov. 1980.

[37] Revision of IEEE Std C57.104-1991, "IEEE Guide for the Interpretation of Gases Generated in Oil-Immersed Transformers," pp. 1-45, Feb. 2 2009.

[38] Zhenjiang Wang, Jian Li, Lijun Yang, and Ruijin Liao, "Characteristics of acid value in vegetable insulating oil during thermal aging," *High Voltage Engineering and Application (ICHVE), 2014 International Conference on*, pp. 1-4, 8-11 Sept. 2014.

[39] M. Hilaire, C. Marteau, and R. Tobazeron, "Apparatus developed for measurement of the resistivity of highly insulating liquids," *IEEE Transactions on Electrical Insulation*, vol. 23, no. 4, pp. 779-789, Aug 1988.

[40] Thoma Judendorfer, Alexander Pirker, and Michael Muhr, "Conductivity measurements of electrical insulating oils," *2011 IEEE International Conference on Dielectric Liquids*, pp. 1-4, 26-30 June 2011.

[41] Uno Gafvert, Olof Hjortstam, Yuriy Serdyuk, Christer Tornkvist, and Lars Walfridsson, "Modeling and Measurements of Electric Fields in Composite Oil/Cellulose Insulation," *2006 IEEE Conference on Electrical Insulation and Dielectric Phenomena*, pp. 154-157, 15-18 Oct. 2006.

[42] A. DENAT, B. GOSSE, and J. P. GOSSE, "Ion Injections in Hydrocarbons," *Journal of Electrostatics*, pp. 205-225, July 1979.

[43] T. Mechlia, B. Gosse, A. Denat, and J. P. Gosse, "Electrophoretic Determination of the Charge at the Liquid-Solid Interface : Relation with Conduction Phenomena," *IEEE Transactions on Electrical Insulation*, vol. EI-20, no. 2, pp. 365-370, April 1985.

[44] T. J. Lewis, "Nanometric Dielectrics," *IEEE Transactions on Dielectrics and Electrical Insulation*, vol. 1, no. 5, pp. 812-825, October 1994.

[45] Adam Marcus Namisnyk, "A survey of electrochemical supercapacitor technology," Thesis for the Degree of Bachelor of Engineering 2003 June 23.

[46] (2016,01/07)Wikipedia.https://en.wikipedia.org/wiki/Boltzmann_distribution#opennewwindow[Online]

[47] John Shrimpton, *Charge Injection Systems-Physical Principles,Experimental and Theoretical Work*. United Kingdom: Springer, 2009.

[48] T. J. Lewis, "Interfaces: nanometric dielectrics," *Journal of Physics D: Applied Physics,* vol. 38, no. 2, pp. 202-212, January 2005.

[49] Guozhong Cao and Ying Wang, *Nanostructures and Nanomaterials:Synthesis,Properties, and Applications*, 2nd ed.: World Scientific, 2011.

[50] A. J. Morin, M. Zahn, and J. R. Melcher, "Fluid electrification measurements of transformer pressboard/oil insulation in a Couette charger," *IEEE Transactions on Electrical Insulation*, vol. 25, no. 5, pp. 870-901, Oct 1991.

[51] J. Kedzia and B. Willner, "Electrification current in the spinning disk system," *IEEE Transactions on Dielectrics and Electrical Insulation*, vol. 1, no. 1, pp. 58-62, Feb 1994.

[52] F. Schober, A. Kuchler, and C. Krause, "Oil Conductivity - An Important Quantity for the Design and the Condition Assessment of HVDC Insulation Systems," *FHWS Sci. J.*, vol. 1, no. 2, pp. 59-79, 2013.

[53] CENELEC, *Insulating liquids-Measurement of relative permittivity,dielectric dissipation factor (tan δ) and d.c. resistivity (IEC 60247:2004)*. United Kingdom, 2004.

[54] R. Tobazeon, J. C. Filippini, and C. Marteau, "On the measurement of the conductivity of highly insulating liquids," *IEEE Transactions on Dielectrics and Electrical Insulation*, vol. 1, no. 6, pp. 1000-1004, August 2002.

[55] G. A. Khrapak and W. F. Schmidt. (2016, 03 Feb.) Mobility of Simple Ions in NonpolarDielectric.http://citeseerx.ist.psu.edu/viewdoc/download?doi=10.1.1.490.4433&rep=rep1&type=pdf.[Online].

[56] Werner F. Schmidt and A. O. Allen, "Mobility of Electrons in Dielectric Liquids," *The Journal of Chemical Physics 52, 4788 (1970)*, vol. 52, no. 9, pp. 4788-4794, May 1970.

[57] Peter S. Winokur, Marvin L. Roush, and Joseph Silverman, "Ion mobility measurements in dielectric liquids," *The Journal of Chemical Physics 63, 3478 (1975)*, vol. 63, no. 8, pp. 3478-3489, October 1975.

[58] Werner F. Schmidt, "Electron mobility in nonpolar liquids: the effect of molecular structure, temperautre, and electric field," *Canadian Journal of Chemistry*, vol. 55, pp. 2197-2210, 1977.

[59] Augustine O. Allen, Matthijs P.de Haas, and Andries Hummel, "Measurement of ionic mobilities in dielectric liquids by means of concentric cylindrical electrodes," *The Journal of Chemical Physics 64, 2587*, vol. 64, no. 6, pp. 2587-2592, March 1976.

[60] U. Gafvert, A. Jaksts, C. Tornkvist, and L. Walfridsson, "Electrical field distribution in transformer oil," *IEEE Transactions on Electrical Insulation*, vol. 27, no. 3, pp. 647-660, June 1992.

[61] Farzaneh Vahidi et al., "Electrical conductivity measurement and determination of ion mobility in insulating oil," *Electrical Insulation Conference (EIC),IEEE*, pp. 313-317, June 2013.

[62] M. Watanabe, K. Sanui, and N. Ogata, "ionic conductivity and mobility in network polymers from poly (propyleneoxide) containing lithium perchlorate," *Journal of Applied Physics*, vol. 57, no. 1, pp. 123-128, 24 July 1984.

[63] E. O. Forster, "The Metal/Liquid Interface: the Charge Injection Process," *IEEE Transactions on Electrical Insulation*, vol. EI-19, no. 6, pp. 524-528, Dec. 1984.

[64] A. Alj, A. Denat, B. Gosse, J. P. Gosse, and I. Nakamura, "Creation of charge carriers in non-polar liquids," *Conduction and Breakdown in Dielectric Liquids*, pp. 101-105, 24-27, July 1984.

[65] M. Nemamcha, J. P. Gosse, A. Denat, and B. Gosse, "Temperature Dependence of Ion Injection by Metallic Electrodes into Non-Polar Dielectric Liquids," *IEEE Transactions on Electrical Insulation* , vol. 22, no. 4, pp. 459-465, Aug. 1987.

[66] Bart Van Zeghbroeck. (2016) Principles of Semiconductor Devices. [Online]. http://ecee.colorado.edu/~bart/book/book/chapter3/ch3_9.htm

[67] S-C Jeng, W M Fairbank, and M Miyajima, "Measurements of the mobility of alkaline earth ions in liquid xenon," *Journal of Physics D: Applied Physics*, vol. 42, no. 3, pp. 1-9, December 2008.

[68] N. J. Felici, "Electrostatics and hydrodynamics," *Journal of Electrostatics*, vol. 4, no. 2, pp. 119-129, January 1978.

[69] P. Atten, "Electrohydrodynamic instability and motion induced by injected space charge in insulating liquids," *Conduction and Breakdown in Dielectric Liquids,1993., ICDL '93., IEEE 11th International Conference*, pp. 20-29, July 1993.

[70] Stuart Lindsay, *Introduction to Nanoscience*. Published in the United States: Oxford Universtiy.

[71] M. Hilaire, C. Marteau, and R. Tobazeon, "Apparatus developed for measurement of the resistivity of highly insulating liquids," *IEEE Transactions on Electrical Insulation* , vol. 23, no. 4, pp. 779-789, Aug. 1988.

[72] (2016,01,Augest)http://www.resnet.wm.edu/~jxshix/math490/lecturechap3.pdf [Online].

[73] C. Green and A. Vaughan, "Nanodielectrics- How much do we really understand," *IEEE Insulation Magazine*, vol. 24, pp. 6-16, 2008.

[74] Zhidong Lin, *Nano-material properties and applications (Chinese edition)*, University of Beijing, Ed. Beijing, China, August 2010.

[75] N.Taniguchi, "On the Basic Conept of "Nano Technology"," *Proc. Intil.Conf.Prod. Eng.Tokyo,Part II, Japan Society of Precision Engineering*, pp. 18-23, 1974.

[76] Stephen U.-S. Choi, "Nanofluid technology: Current status and future research," *Korea-U.S. Techinical Conf. on Strategic Technonlogies, Vienna, V.A.*, pp. 22-24, Oct. 1999.

[77] Y. Kojima et al., "One-pot synthesis of nylon 6-clay hybrid," *Journal of Polymer Science Part A: Polymer Chemistry*, vol. 31, no. 7, pp. 1755-1758, June 1993.

[78] T. J. Lewis, "Interfaces and nanodielectrics are synonymous," *Solid Dielectrics, 2004. ICSD 2004. Proceedings of the 2004 IEEE International Conference* , vol. 2, pp. 792-795, July 2004.

[79] T. J. Lewis, "Interfaces are the dominant feature of dielectrics at the nanometric level," *IEEE Transactions on Dielectrics and Electrical Insulation* , vol. 11, no. 5, pp. 739-753, Oct. 2004.

[80] M. F. Frechette, M. L. Trudeau, H. D. Alamdar, and S. Boily, "Introductory remarks on nanodielectrics," *IEEE Transactions on Dielectrics and Electrical Insulation* , vol. 11, no. 5, pp. 808-818, Oct. 2004.

[81] T. Imai, Y. Hirano, H. Hirai, S. Kojima, and T. Shimizu, "Preparation and properties of epoxy-organically modified layered silicate nanocomposites," *Electrical Insulation, 2002. Conference Record of the 2002 IEEE International Symposium* , pp. 379-383, Apr 2002.

[82] J. K. Nelson, J. C. Fothergill, L. A. Dissado, and W. Peasgood, "Towards an understanding of nanometric dielectrics," *Electrical Insulation and Dielectric Phenomena, 2002 Annual Report Conference* , pp. 295-298, 2002.

[83] Tatsuo Takada, Yuji Hayase, Yasuhiro Tanaka, and Tatsuki Okamoto, "Space charge trapping in electrical potential well caused by permanent and induced dipoles for LDPE/MgO nanocomposite," *IEEE Transactions on Dielectrics and Electrical Insulation*, vol. 15, no. 1, pp. 152-160, February 2008.

[84] L.D. Zhang and J.M. Mou, *Nanomaterials and Nanostructures*, 1st ed. Beijing, China: Science Press, 2001(in Chinese).

[85] Zhijun Xu and Ruiqing Chu, *Nanomaterials and Nanotechnology*, 1st ed. Beijing, China: Chemical Industry Press, 2010.

[86] V. Segal, A. Hjortsberg, A. Rabinovich, D. Nattrass, and K. Raj, "AC (60 Hz) and impulse breakdown strength of a colloidal fluid based on transformer oil

and magnetite nanoparticles," *Proceeding of IEEE International Symposium on Electrical Insualtion*, vol. 2, pp. 619-622, June 1998.

[87] Baimei Wang, Jian Li, Bin Du, and Zhaotao Zhang, "Study on the stability and viscosity of Fe3O4 nano-particles vegetable insulating oils," *High Voltage Engineering and Application (ICHVE), 2012 International Conference*, pp. 307-310, Sept. 2012.

[88] TsungHan Tsai, Shengkou Long, Pinghei Chen, Dasheng Lee, and ChinTing Yang, "Applications of Ferro-Nanofluid on a Micro-Transformer," *Sensors*, vol. 10, no. 9, pp. 8161-8172, September 2010.

[89] Peter Kopcansky et al., "The DC dielectric breakdown strength of magnetic fluids based on transformer oil," *Proceedings of the 10th International Conference on Magnetic Fluids*, vol. 289, pp. 415-418, March 2005.

[90] T.J.Lewis, "A new model for the primary process of electrical breakdown in liquids," *IEEE Trans.Dielectr. Electr.Insul.*, vol. 5, no. 3, pp. 306-315, 1998.

[91] Yuefan Du et al., "Effect of electron shallow trap on breakdown performance of transformer oil-based nanofluids," *Journal of Applied Physics*, pp. 1-4, Nov. 2011.

[92] Wenxia Sima, Jian Shi, Qing Yang, Sisi Huang, and Xuefei Cao, "Effects of conductivity and permittivity of nanoparticle on transformer oil insulation performance: experiment and theory," *IEEE Transactions on Dielectrics and Electrical Insulation* , vol. 22, no. 1, pp. 380-390, Feb 2015.

[93] Yilong Chen et al., "Influence of nanoparticles on the surface discharge marks in oil-pressboard insulation," *Electrical Insulation and Dielectric Phenomena (CEIDP), 2012 Annual Report Conference*, pp. 517-520, 14-17 Oct. 2012.

[94] J. George Hwang et al., "Effects of nanoparticle charging on streamer development in transformer oil-based nanofluids," *Journal of Applied Physics*, vol. 107, no. 1, January 2010.

[95] J. George Hwang et al., "Modeling of Streamer Propagation in Transformer Oil-Based Nanofluids," *IEEE Conference on Electrical Insulation and*

Dielectric Phenomena, pp. 361-366, October 2008.

[96] Tatsuo Takada, Yuji Hayase, Yasuhiro Tanaka, and Tatsuki Okamota, "Space charge trapping in electrical potential well caused by permanent and induced dipoles for LDPE/MgO nanocomposite," *IEEE Transactions on Dielectrics and Electrical Insulation*, vol. 15, no. 1, pp. 152-160, February 2008.

[97] Y. Du, Y. Lv, Chengrong Li, and Y. Liu, "Insulating property and mechanism of semiconducting nanoparticles modified transformer oils," *Hongguo Dianji Gongcheng Xuebao/Proceedings of the Chinese Society of Electrical Engineering 32(10)*, pp. 177-182, April 2012.

[98] Yuefan Du et al., "Effect of semiconductive nanoparticles on insulating performances of transformer oil," *IEEE Transactions on Dielectrics and Electrical Insulation* , vol. 19, no. 3, pp. 770-776, June 2012.

[99] Yuanxiang Zhou et al., "Breakdown Characteristics in Transformer Oil Modified by Nanoparticles," *Gaodianya Jishu/High Voltage Engineering*, vol. 36, no. 5, pp. 1155-1159, May 2010.

[100] F.M. O'Sullivan, "A model for the initiation and propagation of electrical streamers in transformer oil and transformer oil based nanofluids," Massachusetts Institute of Technology, Doctroal dissertation 2007.

[101] M. Chiesa and Sarit K. Das, "Experimental investigation of the dielectric and cooling performance of colloidal suspensions in insulating media," *Colloids and Surfaces A: Physicochemical and Engineering Aspects*, vol. 335, no. 1-3, pp. 88-97, March 2009.

[102] Jin Miao, Ming Dong, and Liang-Ping Shen, "A modified electrical conductivity model for insulating oil-based nanofluids," *Condition Monitoring and Diagnosis (CMD), 2012 International Conference on*, pp. 1126-1129, Sept. 2012.

[103] Yuzhen Lv et al., "TiO_2 nanoparticle induced space charge decay in thermal aged transformer oil," *Applied Physics Letters 102, 132902 (2013)*, vol. 102, no. 13, April 2013.

[104] A. A. Abrikosov, L. P. Gorkov, and I. E. Dzyaloshinsky, *Methods of Quantum Field Theory in Statistical Physics.*, 1963-1975, ch. 6 Electromagnetic Radiation in an Absorbing Medium.

[105] Masahiro Hanai, Satohiko Hosomi, Hiroki Kojima, Naoki Hayakawa, and Hitoshi Okubo, "Dependence of TiO2 and ZnO nanoparticle concentration on electrical insulation characteristics of insulating oil," *2013 Annual Report Conference on Electrical Insulation and Dielectric Phenomena*, pp. 780-783, Oct. 2013.

[106] Muhammad Rafiq, Danish Khan, and Muhammad Ali, "Dielectric properties of transformer oil based silica nanofluids," *Power Generation System and Renewable Energy Technologies (PGSRET), 2015*, pp. 1-3, 10-11 June 2015.

[107] B. X. Du, X. L. Li, J. Li, and X. Y. Tao, "Effects of BN nanoparticles on thermal conductivity and breakdown strength of vegetable oil," *2015 IEEE 11th International Conference on the Properties and Applications of Dielectric Materials (ICPADM)*, 19-22 July 2015.

[108] Jian Li, Zhaotao Zhang, Ping Zou, Stanislaw Grzybowski, and Markus Zahn, "Preparation of a vegetable oil-based nanofluid and investigation of its breakdown and dielectric properties," *IEEE Electrical Insulation Magazine*, vol. 28, no. 5, pp. 43-50, 16 August 2012.

[109] Irwanto, C. G. Azcarraga, Suwarno, A. Cavallini, and F. Negri, "Ferrofluid effect in mineral oil: PDIV, streamer, and breakdown voltage," *High Voltage Engineering and Application (ICHVE), 2014 International Conference*, pp. 1-4, 8-11 Sept. 2014.

[110] Bin Du, Jian Li, Baimei Wang, Junru Xiang, and Zhaotao Zhang, "Influence of water content on the electrical properties of insulating vegetable oil-based nanofluids," *2013 IEEE Electrical Insulation Conference (EIC)*, pp. 49-51, June 2013.

[111] M. J. Given et al., "The influence of magnetite nano particles on the behaviour of insulating oils for pulse power applications," *Electrical Insulation and*

Dielectric Phenomena (CEIDP), 2011 Annual Report , pp. 40-43, 16-19 Oct. 2011.

[112] Bin Du, Jian Li, Bai-Mei Wang, and Zhao-Tao Zhang, "Preparation and breakdown strength of Fe3O4 nanofluid based on transformer oil," *High Voltage Engineering and Application (ICHVE), 2012 International Conference*, pp. 311-313, 17-20 Sept. 2012.

[113] Diaa-Eldin A. Mansour, Eman G. Atiya, Reham M. Khattab, and Ahmed M. Azmy, "Effect of titania nanoparticles on the dielectric properties of transformer oil-based nanofluids," *Electrical Insulation and Dielectric Phenomena (CEIDP), 2012 Annual Report* , pp. 295-298, 14-17 Oct. 2012.

[114] M. Bakrutheen, R. Karthik, and R. Madavan, "Investigation of critical parameters of insulating mineral oil using semiconductive nanoparticles," *Circuits, Power and Computing Technologies (ICCPCT), 2013 International Conference* , pp. 294-299, March 2013.

[115] Muhammad Rafiq et al., "Insulating and aging properties of transformer oil-based TiO2 nanofluids," *2014 IEEE Conference on Electrical Insulation and Dielectric Phenomena (CEIDP)*, pp. 457-461, Oct. 2014.

[116] Yue-fan Du, Yu-zhen Lv, Xinli Xiao, Fo-chi Wang, and Cheng-rong Li, "Preparation and breakdown strength of TiO2 fluids based on transformer oil," *Electrical Insulation and Dielectric Phenomena (CEIDP), 2010 Annual Report*, pp. 1-3, Oct. 2010.

[117] Muhammad Rafiq et al., "Preparation and breakdown properties of mineral oil based alumina nanofluids," *Emerging Technologies (ICET), 2015 International Conference on*, pp. 1-3, 19-20 Dec. 2015.

[118] Dong-Jin Kweon, Kyo-Sun Koo, Jung-Wook Woo, and Joo-Sik Kwak, "A Study on the Hot Spot Temperature in 154kV Power Transformers," *Journal of Electrical Engineering & Technology*, vol. 7, no. 3, pp. 312-319, 2012.

[119] I. V. Timoshkin, M. J. Given, R. A. Fouracre, and S. J. MacGregor, "Charge Injection Energy Barriers and Charge Mobilities in Insulating Liquids,"

Electrical Insulation and Dielectric Phenomena, 2009. CEIDP '09. IEEE Conference, pp. 613 - 616, October 2009.

[120] Shell Lubricants. (2016, 1st, May) Shell Diala S3 ZX-IG Dried-Premium Inhibited Electrical Insulating Oil. [Online]. http://s02.static-shell.com/content/dam/shell/static/ind/downloads/lubes-b2b/diala/shell-diala-s3-zxigdried.pdf

[121] Abdul Rajab, Aminuddin Sulaeman, Sudaryatno Sudirham, and Suwarno, "A Comparison of Dielectric Properties of Palm Oil with Mineral and Synthetic Types Insulating Liquid under Temperature Variation," *ITB Journal Eng. Sci.*, vol. 43, no. 3, pp. 191-208, 2011.

[122] Y. Bertrand and L. C. Hoang, "Vegetable oils as substitute for mineral insulating oils in medium-voltage equipments," *CIGRE Session,Paris*, 2004.

[123] P. Semančík, R. Cimbala, and K. Záliš, "Thermal – Oxidation Stability of Insulating Fluids," *Acta Polytechnica*, vol. 48, no. 4, 2008.

[124] I. L. Hosier, C. Rogers, A. S. Vaughan, and S. G. Swingler, "Ageing behavior of vegetable oil blends," *Electrical Insulation and Dielectric Phenomena (CEIDP), 2010 Annual Report Conference on*, no. 0084-9162, pp. 1-4, Oct 2010.

[125] T. V. Oommen, "Vegetable oils for liquid-filled transformers," *IEEE Electrical Insulation Magazine*, vol. 18, no. 1, pp. 6-11, Jan.-Feb. 2002.

[126] Václav Mentlík, Radek Polanský, Pavel Prosr, and Josef Pihera, "Activation Energy of Transformer Oils ," *Zeszyty Problemowe – Maszyny Elektryczne*, pp. 45-49, Aug 2008.

[127] Zhifeng Hu et al., "Thermal aging properties of transformer oil-based TiO2 nanofluids," *Dielectric Liquids (ICDL), 2014 IEEE 18th International Conference*, pp. 1-4, June 30-July 3 2014.

[128] Toshihiro Tsuboi, Jun Takami, Shigemitsu Okabe, Kiyoshi Inami, and Kazuaki Aono, "Aging effect on insulation reliability evaluation with weibull distribution for oil-immersed transformers," *IEEE Transactions on Dielectrics*

and Electrical Insulation , vol. 17, no. 6, pp. 1870-1876, Dec. 2010.

[129] Masanori Kohtoh, Genyo Ueta, Shigemitsu Okabe, and Tsuyoshi Amimoto, "Transformer insulating oil characteristic changes observed using accelerated degradation in consideration of field transformer conditions," *IEEE Transactions on Dielectrics and Electrical Insulation* , vol. 17, no. 3, pp. 808-818, June 2010.

[130] Keithley Instruments Inc. (1984) Model 617 Programmable Electrometer Instruction Manual.

[131] Keithley Instruments Inc. (2016, May) Tesla Systems Research. [Online]. http://www.teslasystems.com/ebay/batch/datasheets/1/617-keithley

[132] Behrouz Abedian and Kenneth N. Baker, "Temperature effects on the electrical conductivity of dielectric liquids," *IEEE Transactions on Dielectrics and Electrical Insulation* , vol. 15, no. 3, pp. 888-892, June 2008.

[133] (2015, May 2nd) RS Digital Thermometer 1319A Instruction Manual. http://docs-europe.electrocomponents.com/webdocs/0e37/0900766b80e370eb.pdf[Online]

[134] A. Ebe, M. Sone, H. Mitsui, and K. Takaoka, "Effect of dissolved water on electrical conduction in dielectric liquid," *Conduction and Breakdown in Dielectric Liquids, 1990. ICDL 1990. Conference Record*, pp. 201-205, September 1990.

[135] I. L. Hosier, H. Ma, and A. S. Vaughan, "Effect of electrical and thermal ageing on the breakdown strength of silicone oil," *Dielectric Liquids (ICDL), 2014 IEEE 18th International Conference*, pp. 1-4, September 2014.

[136] F. Schober, M. H. Zink, A. Kuchler, M. Liebschner, and Ch. Krause, "Diagnosis of HVDC insulation systems by use of oil-conductivity measuring methods," *Condition Monitoring and Diagnosis (CMD), 2012 International Conference*, pp. 250-253, Sept. 2012.

[137] Wah-Keat Lee and Jan LLavsky, "Particle size distribution in ferrofluid macro-clusters," *Journal of Magnetism and Magnetic Materials*, vol. 330, pp. 31-36,

March 2013.

[138] (2016,16th,June)First4Magnetswebsite. http://www.first4magnets.com/other-c89/efh1-ferrofluid-20ml-with-90mm-petri-dish-pipette-science-art-p6440[Online].

[139] Seonae Hwangba, Mincheol Chu, Jungsoon Kim, and Moojoon Kim, "Nanoparticle dispersion by focused ultrasound from cylindrical transducer," *2013 IEEE International Ultrasonics Symposium (IUS)*, no. 978-1-4673-5684-8, pp. 2126-2129, July 2013.

[140] Diaa-Eldin A. Mansour, Eman G. Atiya, Reham M. Khattab, and Ahmed M. Azmy, "Effect of titania nanoparticles on the dielectric properties of transformer oil-based nanofluids," *Electrical Insulation and Dielectric Phenomena (CEIDP), 2012 Annual Report*, pp. 295-298, Oct. 2012.

[141] L. D. Rozenberg, *Physical Principles of Ultrasonic Technology*.: Springer Science & Business Media, 11 Dec 2013.

[142] J. George Hwang, Markus Zahn, and A.A. Pettersson Leif, "Mechanisms behind positive streamers and their distinct propagation modes in transformer oil," *IEEE Transactions on Dielectrics and Electrical Insulation*, vol. 19, no. 1, pp. 162-174, February 2012.

[143] K. Asano and A. W. Bright, "Space-charge-influenced current in a dielectric liquid," *Journal of Physics D: Applied Physics*, vol. 4, no. 9, pp. 1306-1314, Jan. 1971.

[144] Yuefan Du, "Effect of Ageing By-produts at Nanoparticle-oil Interface on Charge Transport in Aged Transforer Oil-based Nanofluid," *International Journal of Advances in Engineering & Technology*, vol. 8, no. 6, pp. 1040-1049, Dec. 2015.

[145] Sigma-Aldrich LTD. (2016, 15th May) Sigma-Aldrich Ltd. Website. [Online]. http://www.sigmaaldrich.com/catalog/product/sial/07318?lang=en&region=GB

[146] Jian Li, Bin Du, Feipeng Wang, Wei Yao, and Shuhua Yao, "The effect of nanoparticle surfactant polarization on trapping depth of vegetable insulating oil-based nanofluids," *Physics Letters A*, vol. 380, no. 4, pp. 604-608, February 2016.

[147] IEEE STANDARDS ASSOCIATION, *"IEEE Guide for Loading Mineral-Oil-Immersed Transformers"*. USA, 7 December 2011.

[148] L. H. Lee, *Fundamentals of Adhesion.*.: Springer Science & Business Media, 1991.

[149] Mengjun Wang, "Investigation of the degradaation products of solid insulation ageing in the transformer (Chinese edition)," Huazhong University of Science and Technology, Msc Thesis 2011.

[150] Wayne Nelson, "Analysis of Accelerated Life Test Data - Part I: The Arrhenius Model and Graphical Methods," *IEEE Transactions on Electrical Insulation*, vol. EI-6, no. 4, pp. 165-181, Dec. 2007.

[151] Brian T. Murphy, Robert E. Hebner, and Edward F. Kelley, "Simulating mode transitions during breakdown in liquids," *IEEE Transactions on Dielectrics and Electrical Insulation*, vol. 18, no. 3, pp. 682-691, June 2011.

[152] Yue-fan Du et al., "Effect of nanoparticles on the dielectric strength of aged transformer oil," *Electrical Insulation and Dielectric Phenomena (CEIDP), 2011 Annual Report* , pp. 664-667, 16-19 Oct. 2011.

APPENDIX A: MEASURED RESULTS

	First Measurement			Second Measurement			Third Measurement			Fourth Measurement			Fifth Measurement		
Time after filled in test cell (h)	3 to 10			27 to 34			51 to 58			75 to 82			99 to 106		
Voltage (V)	Peak Current (pA)	TOF (sec)	DC Current (pA)	Peak Current (pA)	TOF (sec)	DC Current (pA)	Peak Current (pA)	TOF (sec)	DC Current (pA)	Peak Current (pA)	TOF (sec)	DC Current (pA)	Peak Current (pA)	TOF (sec)	DC Current (pA)
30	82	103	66	81	72	39	80	70	35	81	69	34	79	69	31
40	166	41	66	172	41	46	172	40	43	174	39	42	175	39	41
50	299	27	69	309	29	59	318	26	51	323	25	51	319	26	49
60	476	19	85	508	19	65	522	19	61	530	18	59	525	18	58
70	690	14	112	757	14	77	779	14	71	782	14	69	781	14	67

AppendixA 1 Measured I_{peak}, I_{dc} and TOF for unaged oil sample from transients

	First Measurement			Second Measurement			Third Measurement			Fourth Measurement			Fifth Measurement		
Time after filled in test cell (h)	3 to 10			27 to 34			51 to 58			75 to 82			99 to 106		
Voltage (V)	Peak Current (pA)	TOF (sec)	DC Current (pA)	Peak Current (pA)	TOF (sec)	DC Current (pA)	Peak Current (pA)	TOF (sec)	DC Current (pA)	Peak Current (pA)	TOF (sec)	DC Current (pA)	Peak Current (pA)	TOF (sec)	DC Current (pA)
30	729	102	644	1290	131	971	1560	144	1100	1760	154	1190	1910	156	1260
40	1180	75	984	1750	95	1320	2060	105	1480	2290	110	1590	2480	114	1680
50	1610	54	1300	2210	69	1670	2550	80	1840	2810	85	1980	3040	88	2100
60	1870	38	1480	2580	52	1930	2970	60	2150	3270	65	2310	3540	68	2450
70	1990	25	1560	2900	37	2130	3370	45	2410	3710	51	2600	4000	54	2750

AppendixA 2 Measured I_{peak}, I_{dc} and TOF for 2 days aged oil sample from transients

	First Measurement			Second Measurement			Third Measurement			Fourth Measurement			Fifth Measurement		
Time after filled in test cell (h)	3 to 10			27 to 34			51 to 58			75 to 82			99 to 106		
Voltage (V)	Peak Current (pA)	TOF (sec)	DC Current (pA)	Peak Current (pA)	TOF (sec)	DC Current (pA)	Peak Current (pA)	TOF (sec)	DC Current (pA)	Peak Current (pA)	TOF (sec)	DC Current (pA)	Peak Current (pA)	TOF (sec)	DC Current (pA)
30	1400	75	1280	2540	98	1890	3200	106	2240	3680	110	2510	4030	111	2700
40	2040	59	1800	3350	75	2520	4130	80	2930	4740	82	3260	5150	83	3480
50	2740	49	2350	4190	59	3160	5060	64	3610	5770	65	4000	6240	66	4280
60	3080	35	2650	4840	47	3680	5890	51	4220	6740	53	4690	7280	54	4980
70	3210	21	2780	5400	38	4110	6700	42	4780	7710	44	5340	8360	44	5700

AppendixA 3 Measured I_{peak}, I_{dc} and TOF for 4 days aged oil sample from transients

	First Measurement			Second Measurement			Third Measurement			Fourth Measurement			Fifth Measurement		
Time after filled in test cell (h)	3 to 10			27 to 34			51 to 58			75 to 82			99 to 106		
Voltage (V)	Peak Current (pA)	TOF (sec)	DC Current (pA)	Peak Current (pA)	TOF (sec)	DC Current (pA)	Peak Current (pA)	TOF (sec)	DC Current (pA)	Peak Current (pA)	TOF (sec)	DC Current (pA)	Peak Current (pA)	TOF (sec)	DC Current (pA)
30	4770	60	4270	7750	69	5960	9190	73	6790	10000	76	7280	10800	77	7730
40	7290	46	6190	10500	52	7950	12100	55	8890	13200	57	9490	14100	57	10000
50	9940	36	8110	13200	41	9940	15200	43	11000	16400	44	11700	17700	46	12400
60	11300	29	9350	15500	33	11700	17800	35	13000	19300	36	13800	20600	37	14500
70	11700	22	10000	17300	27	13100	20200	29	14700	22000	30	15600	23600	31	16500

AppendixA 4 Measured I_{peak}, I_{dc} and TOF for 8 days aged oil sample from transients

	First Measurement			Second Measurement			Third Measurement			Fourth Measurement			Fifth Measurement		
Time after filled in test cell (h)	3 to 10			27 to 34			51 to 58			75 to 82			99 to 106		
Voltage (V)	Peak Current (nA)	TOF (sec)	DC Current (nA)	Peak Current (nA)	TOF (sec)	DC Current (nA)	Peak Current (nA)	TOF (sec)	DC Current (nA)	Peak Current (nA)	TOF (sec)	DC Current (nA)	Peak Current (nA)	TOF (sec)	DC Current (nA)
30	2.57	94	1.37	2.57	95	1.39	2.51	93	1.42	2.47	90	1.42	2.39	88	1.40
40	3.30	71	1.53	3.31	71	1.55	3.20	70	1.56	3.18	67	1.57	3.07	66	1.55
50	4.28	53	1.76	4.13	55	1.69	4.00	53	1.71	3.95	52	1.70	3.84	51	1.68
60	4.99	44	1.80	5.07	43	1.81	4.93	42	1.83	4.89	40	1.85	4.76	39	1.82
70	5.93	35	1.93	6.08	34	1.92	6.00	33	1.98	5.92	32	1.98	5.76	31	1.96

AppendixA 5 Measured I_{peak}, I_{dc} and TOF for unaged oil sample with EFH1 Nanoparticles added post ageing (0.03-0.15g/L)

	First Measurement			Second Measurement			Third Measurement			Fourth Measurement			Fifth Measurement		
Time after filled in test cell (h)	3 to 10			27 to 34			51 to 58			75 to 82			99 to 106		
Voltage (V)	Peak Current (nA)	TOF (sec)	DC Current (nA)	Peak Current (nA)	TOF (sec)	DC Current (nA)	Peak Current (nA)	TOF (sec)	DC Current (nA)	Peak Current (nA)	TOF (sec)	DC Current (nA)	Peak Current (nA)	TOF (sec)	DC Current (nA)
30	4.96	20	3.94	4.22	25	3.21	3.99	28	3.00	3.85	29	2.89	3.79	30	2.83
40	6.21	15	4.45	5.51	18	3.82	5.23	20	3.59	5.05	21	3.47	4.97	21	3.40
50	7.57	11	4.93	6.84	14	4.37	6.51	15	4.14	6.31	16	4.00	6.20	16	3.92
60	9.47	7	5.77	8.42	10	5.01	8.02	12	4.74	7.75	12	4.56	7.61	12	4.49
70	1.19	5	6.80	1.03	5	5.71	9.67	6	5.33	9.32	6	5.13	9.11	6	5.02

AppendixA 6 Measured I_{peak}, I_{dc} and TOF for 2 day aged oil sample with EFH1 nanoparticles added post ageing (0.03-0.15g/L)

	First Measurement			Second Measurement			Third Measurement			Fourth Measurement			Fifth Measurement		
Time after filled in test cell (h)	3 to 10			27 to 34			51 to 58			75 to 82			99 to 106		
Voltage (V)	Peak Current (nA)	TOF (sec)	DC Current (nA)	Peak Current (nA)	TOF (sec)	DC Current (nA)	Peak Current (nA)	TOF (sec)	DC Current (nA)	Peak Current (nA)	TOF (sec)	DC Current (nA)	Peak Current (nA)	TOF (sec)	DC Current (nA)
30	13.3	15	10.7	12.8	22	97.3	12.4	26	9.33	12.3	27	9.11	12.1	28	8.95
40	17.3	12	12.7	16.7	17	11.8	16.3	19	11.3	16.1	21	11.0	15.0	21	10.8
50	21.5	10	14.5	20.7	14	13.5	20.2	15	13.0	19.9	16	12.7	197	17	12.5
60	26.1	8	16.6	25.1	11	15.4	24.5	12	14.8	24.1	13	14.4	2.39	14	14.2
70	31.4	6	19.0	29.8	8	17.3	29.0	10	16.5	28.5	11	16.1	28.2	12	15.9

AppendixA 7 Measured I_{peak}, I_{dc} and TOF for 4 day aged oil sample with EFH1 nanoparticles added post ageing (0.03-0.15g/L)

	First Measurement			Second Measurement			Third Measurement			Fourth Measurement			Fifth Measurement		
Time after filled in test cell (h)	3 to 10			27 to 34			51 to 58			75 to 82			99 to 106		
Voltage (V)	Peak Current (nA)	TOF (sec)	DC Current (nA)	Peak Current (nA)	TOF (sec)	DC Current (nA)	Peak Current (nA)	TOF (sec)	DC Current (nA)	Peak Current (nA)	TOF (sec)	DC Current (nA)	Peak Current (nA)	TOF (sec)	DC Current (nA)
30	26.9	16	23.9	26.2	21	23.2	25.7	23	22.5	24.0	29	20.8	23.6	30	20.5
40	34.4	12	30.2	34.2	15	29.2	33.5	16	28.4	31.5	20	26.4	31.0	20	25.9
50	43.6	9	36.9	42.1	11	35.2	41.3	12	34.2	38.9	15	31.7	38.1	14	31.1
60	52.2	7	43.3	50.7	9	41.5	49.7	10	40.4	46.6	11	37.2	45.8	11	36.5
70	60.7	6	49.2	59.8	7	48.1	58.4	8	46.5	54.4	9	42.6	53.6	9	42.1

AppendixA 8 Measured I_{peak}, I_{dc} and TOF for 8 day aged oil sample with EFH1 nanoparticles added post ageing (0.03-0.15g/L)

	First Measurement			Second Measurement			Third Measurement			Fourth Measurement			Fifth Measurement		
Time after filled in test cell (h)	3 to 10			27 to 34			51 to 58			75 to 82			99 to 106		
Voltage (V)	Peak Current (pA)	TOF (sec)	DC Current (pA)	Peak Current (pA)	TOF (sec)	DC Current (pA)	Peak Current (pA)	TOF (sec)	DC Current (pA)	Peak Current (pA)	TOF (sec)	DC Current (pA)	Peak Current (pA)	TOF (sec)	DC Current (pA)
30	114	78	63.9	119	68	45.3	115	70	39.7	110	64	38.3	106	64	37.2
40	197	40	71.1	206	37	48.4	203	36	43.9	200	37	43.5	200	37	42.6
50	323	24	73.3	340	24	52.0	338	24	48.4	337	24	50.2	342	24	48.9
60	472	17	84.4	526	17	58.3	523	17	54.3	519	17	56.2	523	17	54.2
70	597	13	102	767	13	66.2	760	13	60.3	745	13	63.7	747	13	59.8

AppendixA 9 Measured I_{peak}, I_{dc} and TOF for unaged oil sample with Sigma nanoparticles

	First Measurement			Second Measurement			Third Measurement			Fourth Measurement			Fifth Measurement		
Time after filled in test cell (h)	3 to 10			27 to 34			51 to 58			75 to 82			99 to 106		
Voltage (V)	Peak Current (nA)	TOF (sec)	DC Current (nA)	Peak Current (nA)	TOF (sec)	DC Current (nA)	Peak Current (nA)	TOF (sec)	DC Current (nA)	Peak Current (nA)	TOF (sec)	DC Current (nA)	Peak Current (nA)	TOF (sec)	DC Current (nA)
30	1.32	88	1.08	2.90	100	2.09	3.58	114	2.47	4.14	119	2.80	4.65	122	3.11
40	2.07	68	1.69	3.82	80	2.79	4.66	89	3.25	5.39	92	3.68	6.04	94	4.08
50	2.98	56	2.38	4.77	65	3.48	5.73	72	4.02	6.60	74	4.54	7.40	76	5.02
60	3.23	43	2.60	5.48	51	4.03	6.62	58	4.66	7.62	61	5.27	8.56	62	5.85
70	3.08	30	2.50	6.06	42	4.45	7.38	48	5.22	8.50	51	5.90	9.57	52	6.55

AppendixA 10 Measured I_{peak}, I_{dc} and TOF for 2 day aged oil sample with Sigma nanoparticles

	First Measurement			Second Measurement			Third Measurement			Fourth Measurement			Fifth Measurement		
Time after filled in test cell (h)	3 to 10			27 to 34			51 to 58			75 to 82			99 to 106		
Voltage (V)	Peak Current (nA)	TOF (sec)	DC Current (nA)	Peak Current (nA)	TOF (sec)	DC Current (nA)	Peak Current (nA)	TOF (sec)	DC Current (nA)	Peak Current (nA)	TOF (sec)	DC Current (nA)	Peak Current (nA)	TOF (sec)	DC Current (nA)
30	3.08	63	2.49	7.19	75	5.02	9.61	79	6.50	11.4	82	7.05	12.9	84	8.36
40	4.95	48	3.82	9.77	55	6.80	12.8	59	8.57	12.7	53	7.28	16.8	63	10.7
50	7.02	38	5.28	12.4	43	8.63	15.9	46	10.6	12.5	65	7.76	20.7	50	13.2
60	7.80	30	5.94	14.4	34	10.0	18.5	37	12.5	15.6	50	9.67	24.1	41	15.4
70	7.68	22	6.05	15.8	27	11.1	20.7	31	14.1	21.9	35	13.3	27.6	34	17.7

AppendixA 11 Measured I_{peak}, I_{dc} and TOF for 4 day aged oil sample with Sigma nanoparticles

	First Measurement			Second Measurement			Third Measurement			Fourth Measurement			Fifth Measurement		
Time after filled in test cell (h)	3 to 10			27 to 34			51 to 58			75 to 82			99 to 106		
Voltage (V)	Peak Current (nA)	TOF (sec)	DC Current (nA)	Peak Current (nA)	TOF (sec)	DC Current (nA)	Peak Current (nA)	TOF (sec)	DC Current (nA)	Peak Current (nA)	TOF (sec)	DC Current (nA)	Peak Current (nA)	TOF (sec)	DC Current (nA)
30	8.22	47	7.28	11.7	49	9.47	13.7	50	10.8	15.1	50	11.7	16.6	49	12.6
40	11.8	34	10.2	15.8	35	12.6	18.3	37	14.2	20.1	36	15.4	22.0	36	16.6
50	15.6	25	13.1	20.0	27	15.8	22.9	27	17.7	25.2	28	19.1	27.5	28	20.5
60	18.2	19	15.3	23.6	21	18.6	27.1	22	20.7	29.8	22	22.4	32.5	22	24.1
70	19.7	14	16.8	26.8	17	21.0	31.1	17	23.6	34.2	18	25.5	37.3	18	27.4

AppendixA 12 Measured I_{peak}, I_{dc} and TOF for 8 day aged oil sample with Sigma nanoparticles

	First Measurement			Second Measurement			Third Measurement			Fourth Measurement			Fifth Measurement		
Time after filled in test cell (h)	3 to 10			27 to 34			51 to 58			75 to 82			99 to 106		
Voltage (V)	Peak Current (pA)	TOF (sec)	DC Current (nA)	Peak Current (nA)	TOF (sec)	DC Current (nA)	Peak Current (nA)	TOF (sec)	DC Current (nA)	Peak Current (nA)	TOF (sec)	DC Current (nA)	Peak Current (nA)	TOF (sec)	DC Current (nA)
30	721	80	464	698	90	3.19	647	101	289	603	106	269	560	105	253
40	885	39	439	917	53	3.44	860	52	309	806	53	287	758	54	273
50	1210	25	445	1230	26	3.63	1170	25	328	1120	24	306	1090	24	290
60	1650	17	503	1720	18	4.03	1670	18	362	1610	17	332	1560	18	314
70	2170	12	604	2370	14	454	2310	14	399	2230	14	366	2150	14	341

AppendixA 13 Measured I_{peak}, I_{dc} and TOF for unaged oil sample with high-concentration of Sigma nanoparticles

APPENDIX B: SCHOTTKY PLOTS OF DATA

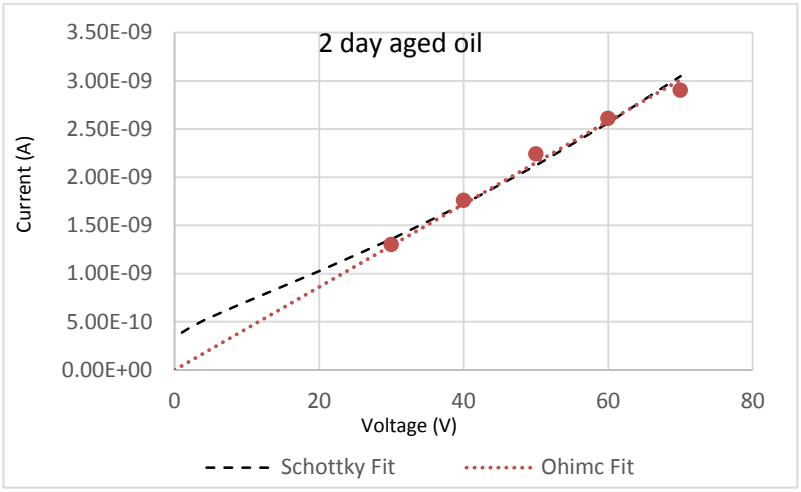

Appendix B: 1 Schottky fit for 2 day aged pure oil

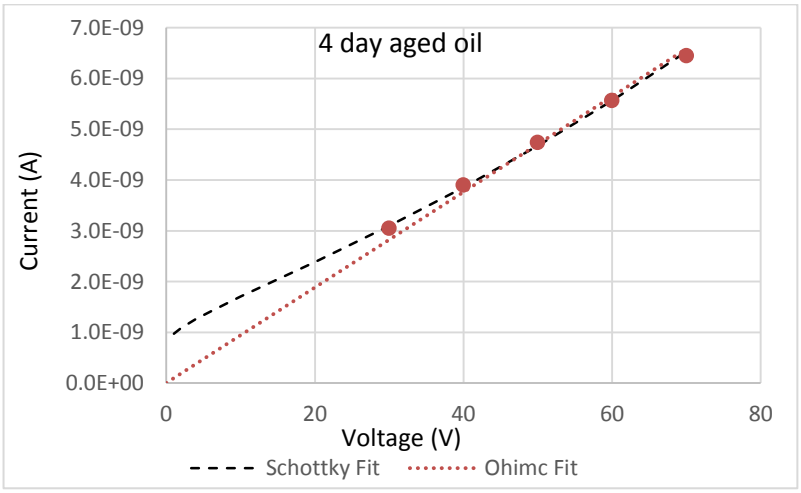

Appendix B: 2 Schottky fit for 4 day aged pure oil

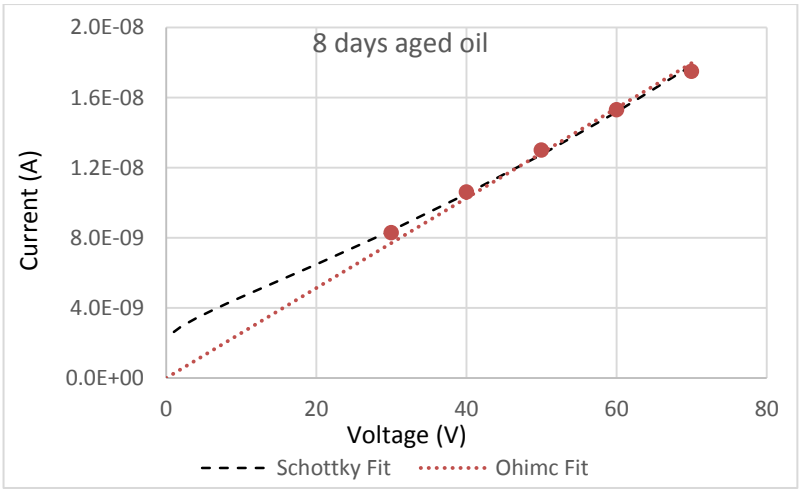

Appendix B: 3 Schottky fit for 8 day aged pure oil

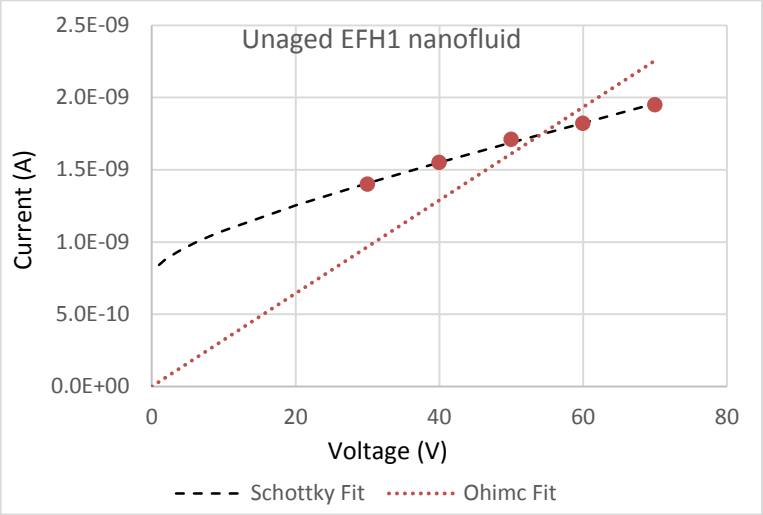

Appendix B: 4 Schottky fit for unaged EFH1 nanofluid

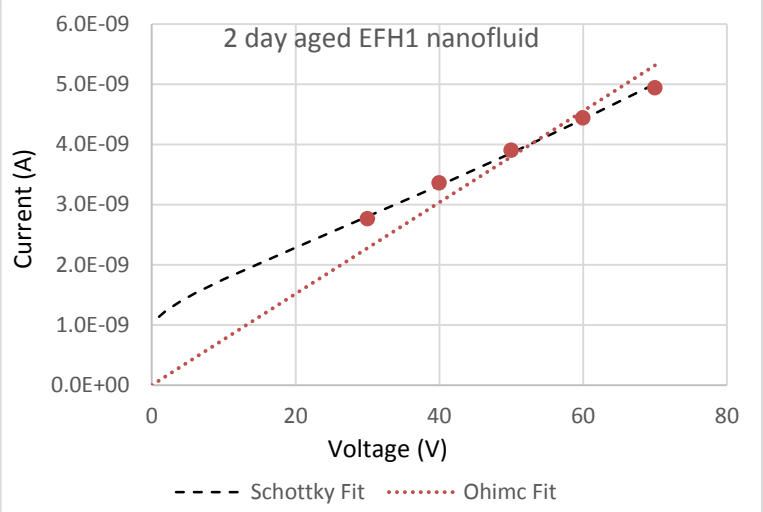

Appendix B: 5 Schottky fit for 2 day aged EFH1 nanofluid

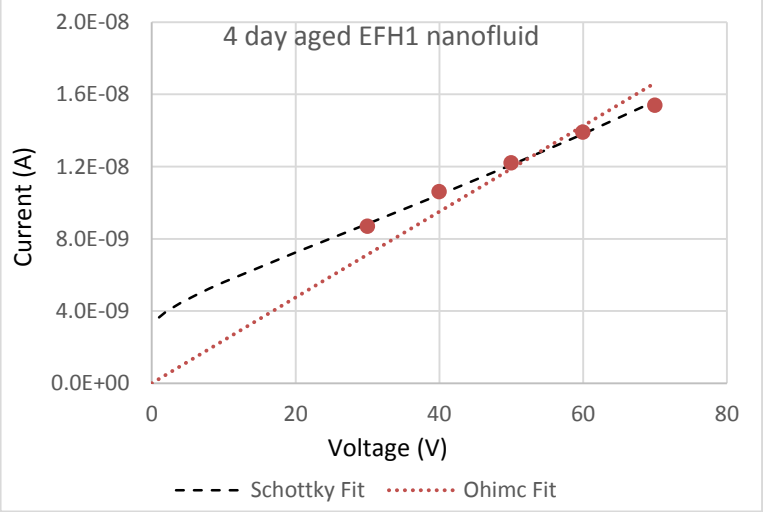

Appendix B: 6 Schottky fit for 4 day aged EFH1 nanofluid

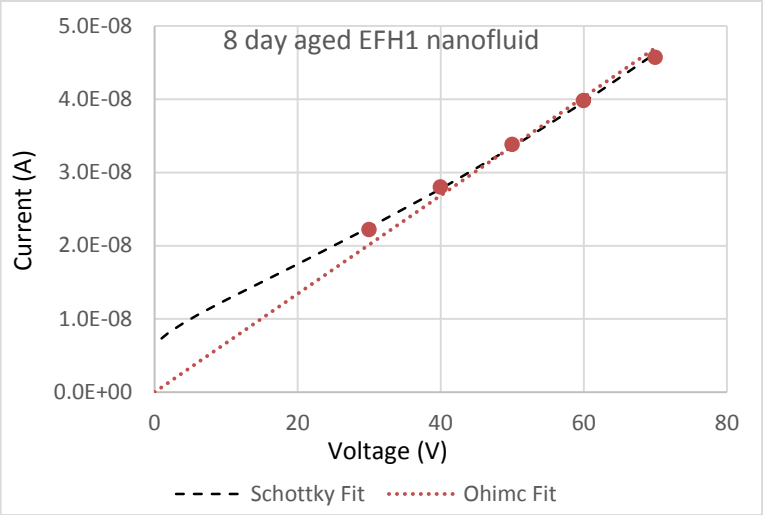

Appendix B: 7 Schottky fit for 8 day aged EFH1 nanofluid

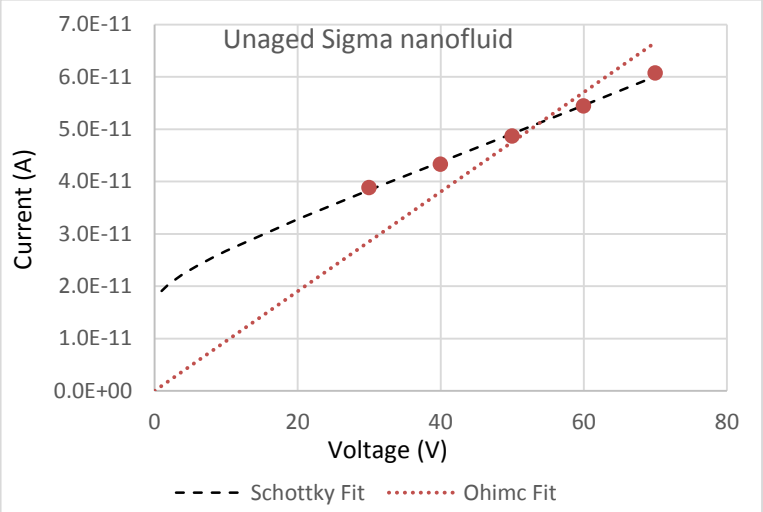

Appendix B: 8 Schottky fit for unaged Sigma nanofluid

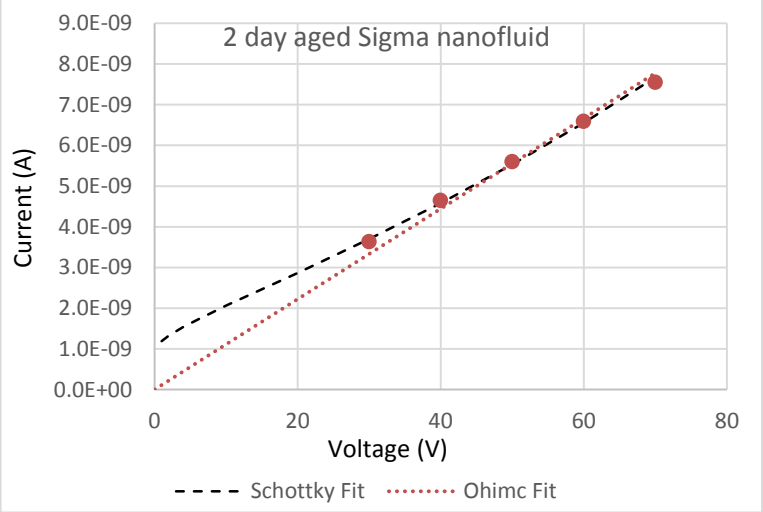

Appendix B: 9 Schottky fit for 2 day aged Sigma nanofluid

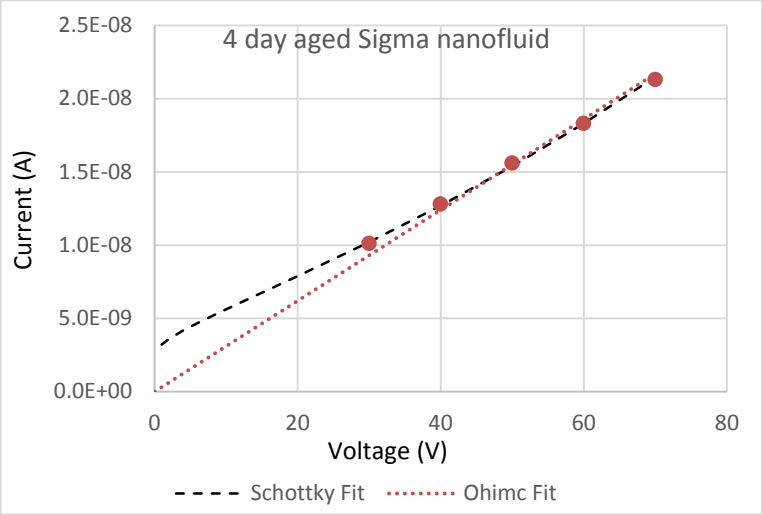

Appendix B: 10 Schottky fit for 4 day aged Sigma nanofluid

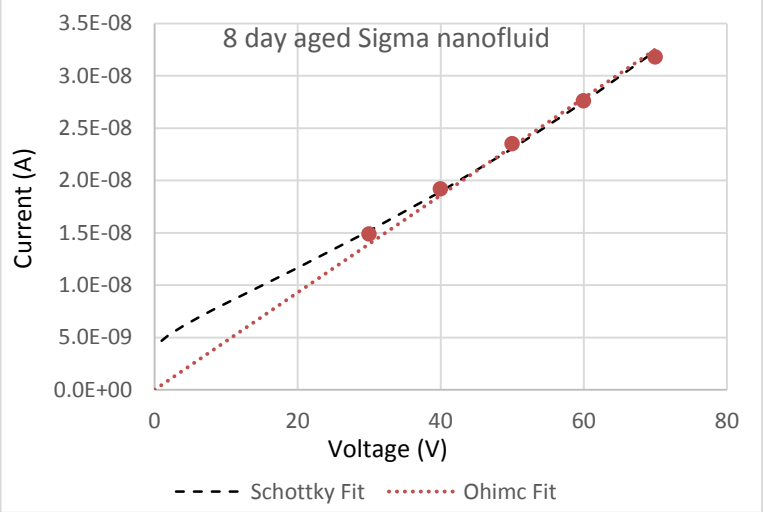

Appendix B: 11 Schottky fit for 8 day aged Sigma nanofluid